BEHAVIOUR OF REINFORCED CONCRETE STRUCTURAL WALLS AND ITS IMPLICATION FOR ULTIMATE LIMIT STATE DESIGN

by

Ioannis Lefas
Dipl(Eng), M.Sc., D.I.C.

February, 1988.

A thesis submitted for the degree of
Doctor of Philosophy of the
University of London

Department of Civil Engineering
Imperial College of Science and Technology

To my parents

ABSTRACT

A review of past analytical and experimental work on the behaviour of reinforced concrete structural walls under static and cyclic loading conditions, together with post earthquake field studies of the performance of buildings with such walls is presented and discussed. The review showed that the influence of a number of important parameters on the behaviour of walls is not yet fully understood and that current provisions for earthquake resistant design do not always yield safe design solutions.

Analytical work based on the use of a non-linear finite element programme and a series of experiments on large scale walls have been carried out to study the influence of a number of parameters generally considered to be related with the causes of the observed behaviour and the deformational and strength characteristics of walls subjected to a combination of loads increasing to complete destruction. Amongst the parameters investigated were the concrete strength, the wall height to width ratio, the arrangement and amount of longitudinal and horizontal reinforcement, the axial load and the detailing of the edge members of the wall. It was found that (a) wall resistance is associated with the strength of concrete in the compressive zone in the region where the maximum moment develops and not, as widely believed, in the region of the wall below the neutral axis and that (b) strengthening of the compressive zone can lead to a significant increase in wall capacity, in spite of the reduction of horizontal reinforcement.

The results of a series of tests on walls with height to width ratio of 2 subjected to a number of post-yield displacement cycles are also presented and discussed. It is shown that monotonically and cyclically tested specimens exhibited similar strength and deformation characteristics.

The recently introduced concept of compressive force path appears to provide a realistic description of the causes of the observed structural wall behaviour and is used in order to develop a physical model which can form a basis for the development of a simple and rational design method for structural walls.

The conclusions drawn from the analytical and experimental part of the work are used to identify and explain the causes of observed damage to structural walls in R.C. buildings of Kalamata (Greece) during the earthquake of 1986.

ACKNOWLEDGEMENTS

The work described in this thesis was carried out in the Civil Engineering Department of Imperial College under the supervision of Professor N.N. Ambraseys, Head of the Engineering Seismology and Earthquake Engineering Section and Dr. M.D. Kotsovos, Lecturer in Concrete Section.

The author would like to express his profound gratitude to Professor N.N. Ambraseys not only for his constant help and encouragement but also for his valuable comments and criticisms throughout the project. The author also wishes to express his sincere thanks to Dr. M.D. Kotsovos for his inestimable assistance, guidance and advice during all the steps of the present work. His willingness to discuss and clarify all the aspects of the work, his painstaking reading of the manuscript and his kindness and understanding will always be remembered.

Acknowledgements are also due to Professor J.W. Dougill for his help during the early stages of the project and Professor T.P. Tassios (President of CEB), who introduced the author to the field of Earthquake Engineering and contributed with many helpful discussions towards my better understanding of the behaviour of structural concrete. Thanks are also due to the other academic staff of Earthquake Engineering and Engineering Seismology and Concrete Sections for their co-operation in many ways and to past and present colleagues for their assistance and friendship.

The author would like to extend his thanks to the technical staff of the Concrete Laboratories for their readiness to help and their assistance in the experimental work; thanks are due to P. Jellis, A. Boxell, M. Rouse, J. Turner, B. Bobinski, R. Wilson, K. Mitchell and L. Clark.

Others have also contributed in no small way. Acknowledgements are made to Richard Packer and Andrew Chipling for the photography, Miss Patricia O'Connell for typing the whole thesis, Julian Bommer for proof-reading the manuscript and to Mrs. K. Crooks and Miss J. Underhill for their assistance in the library.

My deepest gratitude goes to my family and friends who have always encouraged and supported me throughout my education.

My wife, Teta, helped in a great number of ways, whilst carrying out her own research. Her love and devotion made it all possible.

TABLE OF CONTENTS

	Page
ABSTRACT	iii
ACKNOWLEDGEMENTS	iv
TABLE OF CONTENTS	v
LIST OF FIGURES	xv
LIST OF TABLES	xxvii
PRINCIPAL NOTATION	xxx
ABBREVIATIONS	xxxiv

PART I

CHAPTER 1 INTRODUCTION

1.1.	General Considerations	1
1.2.	Scope and Objectives of the Research	1
1.3.	Outline of the Thesis	2

CHAPTER 2 REVIEW OF LITERATURE ON THE BEHAVIOUR OF REINFORCED CONCRETE WALLS

2.1.	Introduction	4
2.2.	Analytical Research on Structural Walls	4
	2.2.1. General Remarks	4
	2.2.2. Simplified Models	4
	2.2.3. Detailed Models	7

Page

2.3. Experimental Research on Structural Walls 10

2.3.1. General Remarks 10
2.3.2. Tests on Isolated Walls with Height to Width Ratio Less than or Equal to One. 11
2.3.3. Tests on Isolated Walls with Height to Width Ratio Greater than One. 15
2.3.4. Tests on both Low Rise and High Rise Structural Walls. 20

2.4. Field Surveys of the Performance of Structural Walls during Earthquakes. 22

2.4.1. General Remarks 22
2.4.2. Case Histories 23

2.5. General Discussion 29

Figures 33

PART II

CHAPTER 3 NON-LINEAR FINITE ELEMENT PROGRAMME

3.1. Introduction 45

3.2. Non-Linear Finite Element Analysis Programme 45

3.2.1. Description of the Non-Linear Element System 45
3.2.2. Material Non-Linearity 47
3.2.3. Numerical Modelling of Cracking 48
3.2.4. Material and Procedural Factors Influencing Non-Linear Predictions 49

3.3. Analytical Modelling of Reinforced Concrete Walls 51

Page

3.4. Validation of the Non-Linear System 52

3.4.1. Introduction 52
3.4.2. Details of the Case Studies 53
3.4.3. Presentation of Results and Discussion 54

3.5. General Remarks and Conclusions 60

Tables 62

Figures 65

CHAPTER 4 PARAMETRIC STUDY

4.1. Introduction 75

4.2. Design Procedures of Current Codes 75

4.2.1. Determination of Flexural Strength 76
4.2.2. Determination of Shear Strength 77

4.3. Parameters Investigated 81

4.4. Layout of the Parametric Study 82

4.5. Presentation and Discussion of the Analytical Results 82

4.5.1. Effect of Distributed Flexural Reinforcement and Height to Width Wall Ratio 82
4.5.2. Walls with Height to Width Ratio of Two 85

Page

4.5.2.1. Effect of Horizontal Reinforcement and Reinforcing Details 86
4.5.2.2. Effect of Vertical Loading 88

4.5.3. Walls with Height to Width Ratio of One 89

4.5.3.1. Effect of Horizontal Reinforcement and Reinforcing Details 89
4.5.3.2. Effect of Vertical Loading 91
4.5.3.3. Effect of Concrete Strength 92

4.5.4. Walls with Height to Width Ratio of a Half 93

4.5.4.1. Effect of Horizontal Reinforcement 94
4.5.4.2. Effect of Vertical Loading 95

4.6. Conclusions 96

Figures 98

PART III

CHAPTER 5 DETAILS OF EXPERIMENTAL WORK

5.1. Introduction 111

5.2. Details of the Specimens 111

5.2.1. Geometry 111
5.2.2. Reinforcement 111
5.2.3. Concrete 112

Page

5.2.4. Mould, Casting Procedure and Curing Regime 113

5.3. Loading and Instrumentation Details 113

5.3.1. Test Rig and Loading Machines 113
5.3.2. Measurement of Displacements 115
5.3.3. Measurement of Steel Strains 115
5.3.4. Data Retrieval 116

5.4. Testing Procedure and Loading Sequence 117

Tables 119

Figures 122

CHAPTER 6 EXPERIMENTAL INVESTIGATION OF THE BEHAVIOUR OF TYPE I WALLS UNDER MONOTONIC LOADING

6.1. Introduction 130

6.2. Wall Details 130

6.3. Presentation of Results 131

6.4. Discussion of Results 133

6.4.1. Validation of the Experimental Set-up 133
6.4.2. Load Carrying Capacity and Deformational Response 135
6.4.3. Stiffness Characteristics 137
6.4.4. Fracture Processes and Failure Modes 139
6.4.5. Causes of Wall Resistance and Failure Mechanism 141

6.5. Conclusions 142

Page

Tables 144

Figures 150

CHAPTER 7 EXPERIMENTAL INVESTIGATION OF THE BEHAVIOUR OF TYPE II WALLS UNDER MONOTONIC LOADING

7.1. Introduction 166

7.2. Wall Details 166

7.3. Presentation of Results 167

7.4. Discussion of Results 168

7.4.1. Validation of the Experimental Set-up 168
7.4.2. Strength Characteristics and Deformational Response 169
7.4.3. Strain Measurements on Longitudinal Reinforcement 172
7.4.4. Stiffness Characteristics 174
7.4.5. Fracture Processes and Failure Modes 175
7.4.6. Causes of Wall Resistance and Failure Mechanism 178

7.5. Conclusions 179

Tables 181

Figures 187

CHAPTER 8 EXPERIMENTAL INVESTIGATION OF THE BEHAVIOUR OF TYPE II WALLS UNDER CYCLIC LOADING

8.1. Introduction 203

Page

8.2. Wall Details and Loading Conditions 203

8.3. Parameters of Structural Deterioration Investigated 204

8.3.1. Stiffness Degradation 204
8.3.2. Energy Dissipation and Equivalent Viscous Damping 205

8.4. Presentation of Results 206

8.5. Discussion of Results 207

8.5.1. Validation of the Experimental Set-up 207
8.5.2. Strength and Deformational Response 209
8.5.3. Stiffness Characteristics 211
8.5.4. Energy Dissipation and Damping Measurements 212
8.5.5. Strain Measurements on Longitudinal Reinforcement 213
8.5.6. Failure Characteristics 215

8.5.6.1. Mode of Failure 215
8.5.6.2. Failure Mechanism 217

8.6. Comparison with Monotonic Test Results 217

8.7. Conclusions 219

Tables 221

Figures 229

PART IV

Page

CHAPTER 9 COMPARISON OF EXPERIMENTAL AND ANALYTICAL WALL RESPONSES

9.1. Introduction 241

9.2. Analytical Modelling 241

9.3. Walls of type I 242

9.4. Walls of type II 246

9.5. Conclusions 248

Tables 249

Figures 251

CHAPTER 10 DESIGN IMPLICATIONS

10.1. Introduction 262

10.2. Evaluation of Code Predictions 262

10.3. Analytical and Experimental Supporting Evidence 265

10.4. Compressive Force Path 267

10.5. Physical Models 268

10.6. Failure Criteria 270

10.7. Provision of Horizontal Reinforcement 273

10.8. Conclusions 274

Page

Tables 276

Figures 280

CHAPTER 11 BEHAVIOUR OF STRUCTURAL WALLS DURING THE KALAMATA (GREECE) EARTHQUAKE OF 1986

11.1. Introduction 285

11.2. Earthquake Source Characteristics 285

11.3. Damage Observations in the Epicentral Area 286

11.4. Behaviour of Reinforced Concrete Structural Walls 289

11.5. Case Study : Wall Failures in the 18th Primary School of Kalamata 292

11.5.1. Description of the Building 293
11.5.2. Damage to the Building 294
11.5.3. Analytical Results and Discussion 296

11.6. Conclusions 298

Figures 300

CHAPTER 12 PRINCIPAL CONCLUSIONS AND RECOMMENDATIONS FOR FUTURE WORK

12.1. Principal Conclusions 308

12.2. Recommendations for Future Work 312

Page

REFERENCES 314

APPENDIX A ANALYTICAL PREDICTIONS OF WALL STIFFNESS CHARACTERISTICS AT THE UNCRACKED PHASE

A.1. Description of Wall Element Stiffness 326

A.2. Analytical Values of Wall Rigidities in the Uncracked Phase 327

A.3. Analytical Displacement Values 327

Tables 328

Figures 330

LIST OF FIGURES

Page

2.1. Typical inelastic beam model for structural wall systems (a) connecting beam, (b) wall member. 33

2.2. The reinforced concrete wall model of Kabeyasawa et al (1982) (a) wall member, (b) axial stiffness hysteresis model and (c) origin-oriented hysteresis model. 34

2.3. The analytical model of Vulcano and Bertero (1984). 34

2.4. The truss analogy model of Hiraishi (1984). 35

2.5. The wide-column analogy model of Smith et al (1984) (a) braced wide-column analogy and (b) braced wide-column module. 36

2.6. The braced frame analogy model of Smith et al (1984) (a) symmetric form and (b) asymmetric form. 36

2.7. Truss model for wall element. 37

2.8. Tie and strut model for structural wall (after Aoyama et al 1986). 37

2.9. Loading scheme (indicating sign convention) adopted for tests carried out by Paulay and Goodsir (1985). 38

2.10. Earthquake simulator used by Rothe (1986). 38

2.11. Mt. McKinley Building (a) damage on the facade walls (b) wall failure at the third storey level. 39

Page

2.12. 1200 L Street Building
(a) damage on the facade walls
(b) wall failure at the first storey level. 40

2.13. Collapse of the Four Seasons Apartment complex. 41

2.14. The Plaza One building - Caracas. 41

2.15. The Banco Central building
(a) typical plan (b) elevation. 42

2.16. The Banco de America building
(a) plan view (b) elevation. 42

2.17. The Imperial County Services building - California
(a) view of the building
(b) failure of the ground storey east columns. 43

2.18. Wall failure of the fifteen storey Acapulco building. 43

2.19. South and west facades of the Direccion General de Administra de Personal building. 44

3.1. Effect of cracking process on deformational response of concrete. 65

3.2. Constitutive relationships for steel bars. 65

3.3. (a) Testing set-up for the experiments of Oesterle et al (1980).
(b) Finite element mesh adopted for the analysis. 66

3.4. Finite element analysis predictions
(a) horizontal load - horizontal displacement curve of wall B4 and
(b) deformed shape and crack pattern at the ultimate load level. 67

Page

3.5. Tests by Cardenas et al (1980)
(a) nominal dimensions, (b) reinforcement details and (c) photographs after testing of specimens SW8 and SW9. 68

3.6. Magnified deformed shape of wall SW9 at
(a) crack initiation, (b) significant inclined cracking formation, (c) maximum sustained load. 69

3.7. Crack pattern and deflected shape of walls (a) SW8 and (b) SW9 at the maximum horizontal load level. 70

3.8. Horizontal load-horizontal displacement curve of wall SW9. 71

3.9. Crack pattern and deformed shape of wall S4 tested by Maier et al (1985) at the ultimate load level
(a) obtained experimentally and (b) predicted analytically. 72

3.10. Wall B1-1 tested by Barda et al (1977)
(a) details of the test specimen
(b) horizontal cross-section
(c) finite element mesh, loading and boundary conditions. 73

3.11. Predicted deformational response and crack pattern at various load levels, and mode of failure established by experiment. 74

4.1. Calculation of the ultimate wall flexural capacity. 98

4.2. Variation of the wall shear capacity with the amount of horizontal reinforcement. 98

Page

4.3. Variation of the ultimate horizontal load of R.C. walls, without horizontal reinforcement, with the amount of uniformly distributed vertical reinforcement. 99

4.4. Variation of the ratio of wall horizontal load capacity to flexural capacity with the wall height to width ratio. 100

4.5. Effect of horizontal reinforcement on the ultimate capacity of walls with height to width ratio of two. 101

4.6. Variation of wall horizontal load capacity (in terms of stresses) with normalized vertical stresses. 102

4.7. Effect of horizontal reinforcement on horizontal load carrying capacity of walls with height to width ratio of one
(a) ρ_v = 3% (b) ρ_v = 1.5% and 1.0%. 103

4.8. Variation of wall horizontal load capacity with amount of horizontal reinforcement for various levels of normalized axial load (ρ_v = 3% at the edges). 104

4.9. Variation of wall horizontal load capacity with amount of horizontal reinforcement for various levels of normalized axial load (ρ_v = 1.5% at the edges + 0.44% wall web). 105

4.10. Variation of wall horizontal load capacity with amount of horizontal reinforcement for various levels of normalized axial load (ρ_v = 1% at the edges + 0.44% wall web). 106

4.11. Ultimate shear stress - normalized compressive axial stress interaction diagram for a typical wall with height to width ratio of one. 107

Page

4.12. Effect of concrete cylinder strength on
(a) wall shear strength
(b) normalized wall shear strength with respect to either the concrete strength or the square root of the concrete strength. 108

4.13. Variation of ultimate wall capacity with amount of horizontal reinforcement for walls with height to width ratio of a half. 109

4.14. The effect of vertical loading on ultimate strength of walls with height to width ratio of a half. 110

5.1. Structural wall specimens (a) type I and (b) type II. 122

5.2. Typical stress-strain relationships of the high yield steel bars. 123

5.3. (a) Types of reinforcing bars used
(b) Details of the fracture zone of the bars after the tensile test. 124

5.4. Mould and reinforcement details of type I wall prior to casting. 126

5.5. Schematic representation of the test rig
(a) elevation and (b) plan view. 128

5.6. Arrangement of the linear voltage displacement transducers (LVDT's) and displacement sign convention. 129

6.1. Geometry and reinforcement details of type I walls. 150

Page

6.2. Horizontal load-displacement curves of specimen SW11 constructed by using measurements of (a) horizontal displacement, (b) vertical displacement and (c) out of plane displacement. 151

6.3. Horizontal load-displacement curves of specimen SW12 constructed by using measurements of (a) horizontal displacement, (b) vertical displacement and (c) out of plane displacement. 152

6.4. Horizontal load-displacement curves of specimen SW13 constructed by using measurements of (a) horizontal displacement, (b) vertical displacement and (c) out of plane displacement. 153

6.5. Horizontal load-displacement curves of specimen SW14 constructed by using measurements of (a) horizontal displacement, (b) vertical displacement and (c) out of plane displacement. 154

6.6. Horizontal load-displacement curves of specimen SW15 constructed by using measurements of (a) horizontal displacement, (b) vertical displacement and (c) out of plane displacement. 155

6.7. Horizontal load-displacement curves of specimen SW16 constructed by using measurements of (a) horizontal displacement, (b) vertical displacement and (c) out of plane displacement. 156

6.8. Variation of secant stiffness with horizontal load expressed in terms of both force and stress units for type I walls. 157

Page

6.9. Significant levels of cracking process exhibited by type I walls.
(a) Initiation of flexural cracking, (b) initiation of inclined cracking and (c) crack pattern prior to failure. 158

6.10. Modes of failure of type I walls subjected to normalized axial load (a) $\nu = 0$, (b) $\nu = 0.1$ and (c) $\nu = 0.2$. 160

6.11. Schematic representation of the failure mechanism of type I walls. 162

6.12. Variation of horizontal load with base vertical displacement of type I walls. 163

6.13. Horizontal load versus top horizontal displacement curves for all type I walls tested. 163

6.14. Bending moment - axial force interaction diagram. 164

6.15. Typical failure envelope of concrete under axi-symmetric triaxial state of stresses. 165

7.1. Geometry and reinforcement details of type II walls. 187

7.2. Horizontal load-displacement curves of specimen SW21 constructed by using measurements of (a) horizontal displacement, (b) vertical displacement and (c) out of plane displacement. 188

7.3. Horizontal load-displacement curves of specimen SW22 constructed by using measurements of (a) horizontal displacement, (b) vertical displacement and (c) out of plane displacement. 189

Page

7.4. Horizontal load-displacement curves of specimen SW23 constructed by using measurements of (a) horizontal displacement, (b) vertical displacement and (c) out of plane displacement. 190

7.5. Horizontal load-displacement curves of specimen SW24 constructed by using measurements of (a) horizontal displacement, (b) vertical displacement and (c) out of plane displacement. 191

7.6. Horizontal load-displacement curves of specimen SW25 constructed by using measurements of (a) horizontal displacement, (b) vertical displacement and (c) out of plane displacement. 192

7.7. Horizontal load-displacement curves of specimen SW26 constructed by using measurements of (a) horizontal displacement, (b) vertical displacement and (c) out of plane displacement. 193

7.8. Variation of the average strain of the longitudinal reinforcement with varying horizontal load for specimens (a) SW22, (b) SW23, (c) SW25 and (d) SW26. 194

7.9. Variation of secant stiffness with horizontal load expressed in terms of both force and stress units for type II walls. 195

7.10. Significant levels of cracking process exhibited by type II walls.
(a) Initiation of flexural cracking, (b) initiation of inclined cracking and (c) ultimate horizontal load. 196

7.11. Lower compressive failure zone of type II walls subjected to normalized axial load (a) $\nu = 0$, (b) $\nu = 0.1$ and (c) $\nu = 0.2$. 198

Page

7.12. Schematic representation of the failure mechanism of type II walls. 200

7.13. Variation of horizontal load with base vertical displacement for type II walls. 201

7.14. Axial strain distribution along the lower wall cross-section for specimen SW26 under various levels of increasing horizontal load. 202

8.1. Geometry and reinforcement details of type II walls subjected to cyclic loading. 229

8.2. Schematic representation of the loading history adopted for the cyclic tests in terms of (a) horizontal load and (b) top horizontal displacement. 230

8.3. Typical horizontal load-horizontal displacement curve and definition of the energy components and secant stiffness. 231

8.4. Variation with horizontal load of (a) top out of plane displacement and (b) vertical displacement of the foundation beam. 232

8.5. Horizontal load-displacement curves of specimen SW31 constructed by using measurements of (a) top horizontal displacement and (b) vertical displacement of the wall edges. 233

8.6. Horizontal load-displacement curves of specimen SW32 constructed by using measurements of (a) top horizontal displacement and (b) vertical displacement of the wall edges. 234

Page

8.7. Horizontal load-displacement curves of specimen SW33 constructed by using measurements of (a) top horizontal displacement and (b) vertical displacement of the wall edges. 235

8.8. Variation of secant stiffness with increasing horizontal load for type II walls subjected to cyclic loading. 236

8.9. Variation of the average strain of the longitudinal reinforcement with horizontal load for the specimen SW32. 237

8.10. Variation of the average strain of the longitudinal reinforcement with horizontal load for the specimen SW33. 238

8.11. Significant stages of the cracking process for type II walls subjected to cyclic loading. (a) At displacement ductility ratio of 1, (b) at displacement ductility ratio of 2 and (c) at ultimate horizontal load level. 239

9.1. Finite element mesh adopted for the analysis of (a) type I and (b) type II walls. 251

9.2. Experimental and analytical horizontal load-top horizontal displacement curves for wall specimens (a) SW15 and (b) SW16. 252

9.3. Comparison of experimentally obtained and analytically predicted crack patterns for specimen SW11 at (a) initiation of flexural cracking, (b) initiation of inclined cracking, (c) yielding of tensile reinforcement and (d) ultimate state. 253

Page

9.4. Analytical crack patterns and deformed shape plots for wall specimen SW15 (a) one load step prior to failure and (b) at the ultimate load step. 255

9.5. Analytical crack patterns and deformed shape plots for wall specimen SW16 (a) one load step prior to failure and (b) at the ultimate load step. 256

9.6. Predicted and experimental horizontal load-top horizontal displacement curve for wall specimen SW21. 257

9.7. Comparison of analytical and experimental cracking process for wall specimen SW22 at (a) initiation of significant flexural cracking, (b) initiation of inclined cracking and (c) prior to failure load. 258

9.8. Crack pattern and deformed shape plot for wall specimen SW32 at a load level corresponding to (a) ductility ratio $\mu = 1$ and (b) ductility ratio $\mu = 2$. 260

9.9. Typical analytically predicted modes of failure for type II walls subjected to a normalized axial load of (a) $\nu = 0$, (b) $\nu = 0.1$ and (c) $\nu = 0.2$. 261

10.1. Compressive force path. 280

10.2. Proposed "comb-like" model for R.C. beam. 280

10.3. Proposed physical model for R.C. wall. 281

10.4. Design equation for type II behaviour. 282

10.5. Validation of Eq. 10.2 with values obtained from FE Analysis for walls without horizontal reinforcement and with height to width ratio of (a) one and (b) two. 283

Page

10.6. Effect of horizontal reinforcement on proposed model in the region where path changes direction. 284

11.1. Typical failures suffered by structural walls during the Kalamata earthquake
(a) Severely cracked core wall unit
(b) Failure of the wall at the construction joint
(c) Early shear wall failure
(d) Failure of the lower compressive zone of the wall. 300

11.2. Analytically predicted deformed shape and mode of failure of walls with height to width ratio of (a) one and (b) two. 302

11.3. Plan view of the 18th Primary School of Kalamata. 303

11.4. Cracking suffered by walls A_1 and B_1 in 18th Primary School during the Kalamata earthquake. 304

11.5. Analytically predicted horizontal load-top horizontal displacement curve for walls A_1 and B_1. 306

11.6. Analytically predicted crack pattern and deformed shape for walls A_1 and B_1 at the ultimate horizontal load level of wall B_1. 307

A.1. Force-displacement relationship for one dimensional cantilevel element. 330

LIST OF TABLES

		Page
3.1.	Material properties and geometric characteristics for the wall specimens analysed by the non-linear finite element system.	62
3.2.	Measured and predicted values of ultimate horizontal load of the walls investigated in the validation study.	64
5.1.	Properties of reinforcement bars.	119
5.2.	Concrete mix proportion by weight.	119
5.3.	Characteristics of linear voltage differential transducers.	120
5.4.	Characteristics of strain gauges.	121
6.1.	Experimental data for type I walls.	144
6.2.	Concrete strength characteristics of type I walls.	145
6.3.	Principal results for type I walls at various loading levels.	146
6.4.	Shear stress values for type I walls at various loading levels.	147
6.5.	Stress conditions causing failure of type I wall specimens.	148
7.1.	Concrete strength characteristics of type II walls.	181

Page

7.2. Experimental data for type II walls. 182

7.3. Principal results for type II walls at various loading levels. 183

7.4. Shear stress values for type II walls at various loading levels. 184

7.5. Stress conditions causing failure of type II wall specimens. 185

8.1. Experimental data for type II walls subjected to cyclic loading. 221

8.2. Concrete strength characteristics of type II walls subjected to cyclic loading. 222

8.3. Principal results for type II walls at various cyclic loading levels. 223

8.4. Shear stress values for type II walls subjected to cyclic loading. 224

8.5. Experimental and analytical values of wall horizontal load relaxation with increasing number of cycles to a maximum displacement. 225

8.6. Experimental values of secant stiffness reduction with the number of cycles for various values of the ductility ratio. 226

8.7. Energy dissipation per cycle for wall specimens subjected to cyclic loading. 227

8.8. Analytical and experimental values of equivalent viscous damping for wall specimens subjected to cyclic loading. 228

Page

9.1. Analytical predictions and experimental values of ultimate horizontal load for type I walls. 249

9.2. Analytical predictions and experimental values of ultimate horizontal load for type II walls. 250

10.1. Code predictions and measured values of ultimate horizontal load for type I walls. 276

10.2. Code predictions and measured values of ultimate horizontal load for type II walls. 277

10.3. Assessment of flexural strength of two typical reinforced concrete walls. 278

10.4. Measured and predicted values of wall strength for walls without horizontal reinforcement. 279

A.1. Analytical values of wall parameters EI, GA_v and EA. 328

A.2. Analytical and experimental values of top horizontal displacement of the uncracked wall phase. 328

A.3. Analytical and experimental values of wall axial shortening. 329

PRINCIPAL NOTATION

A - cross-sectional area of the wall

A_h - total area of wall horizontal reinforcement

A_s - total area of uniformly distributed wall vertical reinforcement

$A_{s,col}$ - cross-sectional steel area in the wall's edge element

A_v - effective shear area

a_{vx} - M_{ax}/V_{ax}

a'_{vx} - $(l/l').a_{vx}$

b - wall thickness

C_c - compressive force of concrete

C_s - compressive force of steel

c - depth of neutral axis

d - effective depth of wall cross-section

E_i - energy dissipation per cycle

E_s, E - modulus of elasticity of steel

EA - axial wall rigidity

EI - flexural wall rigidity

F_H - horizontal load

F_v - vertical load

f_{cyl}, f'_c - uniaxial compressive cylinder strength of concrete

f_{cu} - uniaxial compressive cube strength of concrete

f_{sy}, f_y - yield tensile strength of steel

f_{su} - ultimate tensile strength of steel

G - shear modulus of rigidity of concrete

GA_v - shear wall rigidity

g - gravity acceleration

h - wall height

I - moment of inertia

K - secant stiffness

l - wall width

l' - the distance of horizontal load resultant to the extreme compressive fibre of the wall

M - bending moment

M_{ax} - applied bending moment at a given section x

M_{cx} - moment corresponding to "shear" failure

M_{fx} - flexural capacity

M_s - earthquake magnitude

M_{ult} - ultimate wall flexural capacity

N - axial (vertical) load (positive for compression)

T_1, T_2 - tensile force of steel bars

t - half depth of the loading beam

V, V_H - shear force

V_{ax} - applied shear force at a given section x

V_i - input voltage of the bridge circuit at the time of reading

V_o - output voltage of the bridge circuit at the time of reading

v - shear stress

v_c - shear stress contribution of concrete

v_{cr} - shear stress corresponding to initiation of wall flexural cracking

v_{ic} - shear stress corresponding to initiation of wall inclined cracking

v_s - shear stress contribution of wall horizontal reinforcement

v_{sf} - shear stress corresponding to significant wall flexural cracking

v_y - shear stress corresponding to first yielding of tensile reinforcement

v_{ult} - wall shear stress capacity

W_D - energy dissipated per cycle

W_i - input voltage of the bridge circuit when the steel bar was unstressed

W_o - output voltage of the bridge circuit when the steel bar was unstressed

W_s - strain energy per quarter cycle of a linear system with the equivalent secant stiffness of the non-linear loop

W_1 - damage energy

W_2 - damping energy

W_3 - recoverable energy

z - level arm

β_1 - reduction factor

γ - drift index

Δ - vertical displacement

$\Delta\sigma$ - stress differences at Gauss points

δ - displacement

ϵ - bond degradation parameter

ϵ_{cu} - ultimate strain of concrete

ϵ_{sy} - yield strain of reinforcing bars

ϵ_u - ultimate strain

ζ - equivalent hysteretic damping ratio

θ - rotation

μ - ductility ratio

ν - normalized vertical (axial) stress ratio or Poisson's ratio

π - 3.14159, the ratio of the circumference of a circle to its diameter

ρ - the ratio of the area of the tensile reinforcement of the concealed wall column to the gross concrete wall area

ρ_{fl}, ρ_{flex} - ratio of main flexural reinforcement to gross concrete area of wall edge element

ρ_{hor} - ratio of horizontal reinforcement to gross concrete area of vertical section of wall web

ρ_n - percentage of vertical reinforcement of the wall boundary member

ρ_s - ratio of effective volume of confinement reinforcement to the volume of the core

ρ_v - percentage of wall vertical reinforcement

$\rho_v * f_{su}$ - vertical reinforcement index

ρ_{ver} - ratio of vertical web reinforcement to gross concrete area of horizontal section of wall web

σ - stress at Gauss point

σ_o - normal octahedral stress

$\sigma_x, \sigma_y, \sigma_z$ - average concrete stresses in the x, y, z direction

σ_1 - principal longitudinal stress

σ_2, σ_3 - principal transverse stresses

τ_o - normal octahedral stress

τ_{xy} - stress due to shear

ω_t - volumetric percentage of confinement reinforcement

ABBREVIATIONS

ACI - American Concrete Institute
ASCE - American Society of Civil Engineering
ATC - Applied Technology Council
AUL - Analytical Ultimate Load

BS - British Standards

CEB - Comite Euro-International du Beton

EEFIT - Earthquake Engineering Field Investigation Team
EERI - Earthquake Engineering Research Institute
EUL - Experimental Ultimate Load
ersg - electrical resistance strain gauge

FE - finite element
FINEL - linear finite element package
FIP - Federation Internationale de la Precontrainte

LVDT - Linear Voltage Differential Transducer

OSFP - onset of stable fracture propagation
OUFP - onset of unstable fracture propagation

PCA - Portland Cement Association

RC - Reinforced Concrete

UBC - Uniform Building Code

CHAPTER 1

INTRODUCTION

1.1. GENERAL CONSIDERATIONS

Reinforced concrete structural walls are widely considered to provide an efficient economic bracing system, not only for high-rise, but also for low-rise buildings in areas of high or moderate seismicity. Over the past two decades major advances have been made in the understanding of the behaviour of reinforced concrete structural walls, particularly with regard to the role of the variables affecting their flexural strength.

Designers have a range of tools at their disposal, but those currently used to design reinforced concrete walls are based on (a) theoretical concepts and assumptions which, in many cases, are incompatible with fundamental concrete properties and (b) empirical formulae derived originally for beam analysis. It is clear that design procedures based on a fundamental understanding of wall behaviour at the ultimate limit state would be preferable to the present methods. Such procedures would be invaluable in extending present experience to new circumstances and optimising design in a more rational way. Furthermore, the need for a simple and rational design method is becoming more pronounced for the analysis of structures expected to be subjected to strong earthquake motions, where the requirement for a safe and economic design is deemed essential.

1.2. SCOPE AND OBJECTIVES OF THE RESEARCH

The intention of the present thesis has been to encompass both analytical and experimental studies of the behaviour of reinforced concrete walls at the ultimate limit state, which will complement each other. The main objectives of the research are as follows:

(a) The use of a reliable non-linear finite element package for the modelling of concrete structures in order to provide considerable insight into the general question of failure of structural walls and to identify the governing parameters of wall resistance.

(b) The investigation in the laboratory of the behaviour of selected large scale wall models under monotonic and cyclic loading, and the comparison between the measured and the analytically predicted behaviour.

(c) The development, on the basis of analytical and experimental results, of a design model that will provide rational, safe and economic design solutions.

1.3. OUTLINE OF THE THESIS

The present work has concentrated, therefore, on the following four main areas:

Part I reviews previously published analytical and experimental work on walls subjected to combined monotonic and cyclic loading and assesses their relevance to the behaviour of concrete walls at the ultimate limit state. The survey is extended to the valuation of field observations on the performance of concrete walls during recent earthquakes.

Part II is concerned with the analytical investigations carried out to develop a better understanding of structural wall behaviour and to study the influence of a number of parameters on the response of walls subjected to combinations of loads increasing to complete destruction. The non-linear finite element analysis programme used is outlined and validated by using already available experimental information. An extensive parametric study of the variables that affect wall behaviour follows and the results of the analytical investigation are used to identify and quantify shortcomings of current Code procedures.

Part III deals with a comprehensive experimental investigation of the behaviour of walls with constant thickness and a height to width ratio varying between one and two. Such walls are considered to represent the critical storey element of a structural wall system. Attention is paid to the causes and mechanisms of failure and to the effect of varying vertical force on the strength, stiffness and deformational characteristics of walls subjected to monotonically increasing horizontal load. Structural deterioration characteristics of walls with height to width ratio of two, subjected to cyclic loading, are also established experimentally and compared with behaviour under monotonic loading.

Part IV is initially concerned with a comparative study of the experimental results with the analytical predictions obtained by using the finite element programme. The underlying causes of wall behaviour at the ultimate limit state, identified in Parts II and III, form the basis for a reappraisal of current Code predictions and the development of simple and rational design method. These interpretations are also compatible with the performance of buildings incorporating walls during the Kalamata (Greece) earthquake of 1986.

CHAPTER 2

REVIEW OF LITERATURE ON THE BEHAVIOUR OF REINFORCED CONCRETE WALLS

2.1. INTRODUCTION

This chapter contains a comprehensive literature survey of analytical and experimental investigations carried out to date on the behaviour of reinforced concrete structural walls under monotonic and cyclic loading. The survey also includes a discussion of field observations of the performance of the above structural members during recent earthquakes.

2.2. ANALYTICAL RESEARCH ON STRUCTURAL WALLS

2.2.1. GENERAL REMARKS

Predicting the structural response involves the two interrelated tasks of how the load is shared among the elements of the structure and how each element responds to its applied loads. Many analytical models have been proposed to predict the non-linear response of reinforced concrete structural walls. They can be classified into two main categories : (a) simplified models used to predict the overall behaviour of reinforced concrete structural systems incorporating structural walls (i.e. coupled wall system, frame-wall system), and (b) detailed models used to study the local behaviour of a wall element, especially under post yield deformations (derived on the basis of first principles of the mechanics of solids).

2.2.2. SIMPLIFIED MODELS

For the non-linear analysis of a reinforced concrete structural system, it is very important to choose a suitable idealized element model to represent the non-linear behaviour of the reinforced concrete member components. A wide range of models which take into account material and geometric non-linearities have been reported to date.

(a) Laminae Model

The basic feature of the model is that the discrete system of connecting beams between the walls or the wall and the column is replaced by a continuous connecting medium of equivalent stiffness. The model either in its original version or modified was used in the early 1960's by a number of investigators who tried to analyze coupled structural walls or frame–wall systems under lateral loads. Close examination of the model reveals that the following major points have not been considered :

(a) the lengthening and shortening of the extreme vertical sides of the system;

(b) the stress concentrations at the corner junctions of the beams and the walls;

(c) the local distortions of the surfaces of the walls caused by moments and forces exerted by the connecting beams.

(b) Inelastic Beam Models

In these models (for frame–wall or coupled wall systems) a connecting beam is presented by a flexural line element while the structural wall is considered as a beam located at the axis of symmetry of the wall and connected by rigid line elements to the frame beams, as Figure 2.1 depicts. Some of the more successful models are the one, two and four component models, the equivalent spring model, the flexibility distribution model, the two cantilever beam models with non–linear springs, the divided element beam model and the multiple spring beam element. The main limitation of a beam model depends on the assumption that rotations occur around points lying on the centroidal axis of the wall; hence, important features of the experimentally observed structural behaviour like the translation of the neutral axis of the wall cross–section, rocking of the wall and interaction with the frame surrounding the wall, are disregarded.

Recently, Kabeyasawa et al (1982) developed a mathematical model which takes into consideration the above features. As shown in Figure 2.2(a), the wall member was idealised as a three vertical line elements with two infinitely rigid beams at the top and bottom floor levels. Two outside truss elements provide the axial stiffness of the boundary edges of the wall, while the central element was a beam–model with vertical, horizontal and rotational springs concentrated at the base. The axial stiffness hysteresis model shown in Figure 2.2(b) was used to describe the axial force–deformation relationship of the three vertical line elements, while the

origin-oriented hysteresis model shown in Figure 2.2(c) was used for both the rotational and horizontal springs.

Vulcano and Bertero (1984) incorporated into Kabeyasawa's wall model, an analytical model idealizing the hysteretic behaviour of a reinforced concrete column member under axial load reversals. As shown in Figure 2.3, the model comprises two axial elements in series with one-component representing the axial stiffness of the column segments, where bond still exists, and another component representing the axial stiffness of the remaining (almost unbonded) segments of steel and concrete. Even though the wall model is able to simulate satisfactorily the hysteretic behaviour of reinforced concrete structural walls, uncertainties about the choice of the hysteretic properties of the model elements remain, since the model proved to be very sensitive to the choice of several parameters like the bond degradation parameter, ϵ, and the yield shear value assumed for the horizontal spring.

(c) Equivalent Truss Model

The versatility of this model is that it can account for stress redistribution caused by the inclined cracks of the wall. As shown in Figure 2.4, in the analytical technique proposed by Hiraishi (1984) the structural wall is represented as a truss system having a non-prismatic truss member whose cross-sectional area is determined accounting for the stress along the height of the edge member of the wall under tension. The main object of the analysis is the assessment of deformations at the first storey, hence truss members above the first storey are assumed to be rigid. The basic drawback of the method is that difficulties arise in defining both geometric and material properties of the equivalent truss system. Another difficulty arises from the changes of the structural topology depending on the crack propagation during the loading history.

(d) Analogous Frame Models

Two types of such models were proposed by Smith and Girgis (1984). They were especially developed for the stress analysis of structural walls and they are applicable to walls that can be subdivided into a mesh of rectangular modules. As indicated in Figure 2.5, one of them is similar to the widely used wide-column analogous frame, except for the addition of diagonal braces in each module. The braces prevent the interference of bending and shear stiffnesses and therefore allow the more accurate presentation of structural walls with high shear to moment ratio. The second analogous frame also includes horizontally rigid arms and braces but the

central column is omitted and replaced by a column on one vertical edge and a hinged link on the other, as shown in Figure 2.6. A standard frame analysis programme is used to analyze the frames.

(e) Two and Three Dimensional Plane Stress Finite Element Models

Such models are used for the analysis of the overall behaviour of multistorey building incorporating structural walls under monotonic or cyclic lateral loads. However, the use of unsuitable models of the behaviour of concrete under generalised stresses and the cost of the analysis due to the large number of finite elements used, have significantly limited the application of this method.

2.2.3. DETAILED MODELS

Although the simplified models discussed in Section 2.2.2 are useful tools for the study of the behaviour of reinforced concrete structural systems, no realistic prediction of the global behaviour can be achieved without taking into account the behaviour of the constituents of the system.

A series of analytical studies to investigate flexural strength, stiffness and ductility properties of slender structural walls were carried out by Salse and Fintel (1974). The mathematical model used for the development of interaction diagrams of wall sections was based on the non-linear beam theory. The model simulated only the response of slender walls to monotonic loading. The basic assumptions of the theory were that strains vary linearly across the section, while the stresses in both concrete and reinforcement vary non-linearly according to their actual stress-strain relationship. Stress-strain relationships available in the literature were used for the steel reinforcement, while a complex equation based on tests was used for the stress-strain characteristics of concrete. Two principal sections were investigated : a rectangular section with uniformly distributed reinforcement and reinforcement bunched at the ends and an I-section with concentrations of reinforcement in the flanges. In addition, the effect of confinement was considered. The results indicated that the available ductility in a wall depends on the arrangement of reinforcement, geometry of the section, axial load and confinement of the concrete.

The most common model used for the analysis of wall elements not governed by a flexural mode of failure is the truss analogy model. The analogy assumes that the wall acts as a statically determinate truss. As shown in Figure 2.7.,

flexural reinforcement in the tensile region is assumed to act as the tension chord. Compression is assumed to be carried by concrete and steel in the compressive edge of the wall. Horizontal reinforcement and concrete between inclined cracks form the tensile ties and compressive struts respectively. To determine the ultimate capacity of the wall, failure criteria are incorporated into the truss analogy model.

For two decades the only failure criterion used was the yielding of the horizontal reinforcement. Recent experimental work showed that an important limit on wall strength is the "crushing" of concrete in the compressive zone of the wall. Based on these observations, Oesterle et al (1984) proposed a failure criterion based on the average compressive strength of concrete struts. They believed that concrete "crushing" is dependent on the magnitude of shear stress and the level of deformation. Therefore, they considered a relationship between shear deformations and lateral drift within the hinging region of the wall and the truss analogy to develop a relationship between "crushing" strength and lateral drift.

Hsu and Mo (1985) presented a truss model theory based on equilibrium and compatibility conditions as well as a new stress–strain relationship for softened concrete to predict the behaviour of reinforced concrete structural walls with low height to width ratio which incorporate boundary elements. The theoretical predictions were found to correlate closely with test results for twenty three walls throughout the loading history. Since the iterative procedure used to assess the load–deflection relationship of the wall is not suitable for design purposes, Mau and Hsu (1986) proposed a direct solution to obtain the load–deflection relationship of the wall. Furthermore, they showed that, depending on the relative contribution of the longitudinal reinforcement to that of the concrete, different failure modes can be identified.

Vecchio and Collins (1986) presented the modified compression–field theory in order to predict the response of reinforced concrete elements like the structural walls to in–plane shear and axial stresses. In their model, equilibrium, compatibility and stress–strain relationships are formulated in terms of average stresses and average strains. Cracked concrete is treated as a new material with its own stress–strain characteristics. While the original compression–field theory ignored tension in the cracked concrete, this model takes into account tensile stresses in the concrete between the cracks. The stress–strain relationship for the cracked concrete was determined by testing reinforced concrete panels under a variety of uniform biaxial stresses.

Another approach to estimate the ultimate strength of reinforced concrete

structural walls is the theory of plasticity. Plastic theory was extensively investigated in the 1970's to rationalize the shear design of reinforced concrete members. However, the analysis adopted in the CEB/FIP Code (1978) could not account for the parameters (such as height to width ratio, axial load) affecting the ultimate strength of the element. Some efforts were made in the 1980's, mainly in Japan, to take these effects into consideration. Aoyama and Shiohara (1986) proposed a mathematical model using the truss model and the theory of plasticity. The lower bound theorem of the limit analysis is used to assess the ultimate resistance of structural walls subjected to lateral loading. The assessment is based on the selection of a permissible stress field, such as that shown in Figure 2.8 for a structural wall with clear height h_w, wall width l_w and uniform thickness t_w, which satisfies the boundary conditions and does not violate the failure criterion anywhere within the structure.

Gurley (1987) showed that there are a number of possible plastic collapse mechanisms which satisfy the static and kinematic conditions and correlate reasonably well with experimentally observed crack patterns. Thürlimann (1987) also applied the theory of plasticity to describe the results of a series of ten tests on reinforced concrete structural walls with height to width ratio of one.

The main difficulty in the case of plastic plane stress problems is the ability to conceive and visualize realistic collapse mechanisms. Furthermore, despite the fact that the method leads to solutions which satisfy local or global equilibrium conditions, compatibility equations are not satisfied. Another difficulty arises from the fact that usually concrete is treated as a simple rigid–plastic material having some definite uniaxial compressive strength and zero tensile strength. Experimental investigations at both material and structural level indicate that these assumptions are gross simplifications.

Non–linear effects related to modelling of the material behaviour, like concrete cracking, bond–slip behaviour between reinforcement and concrete, stress transfer between cracks and dowel action of the reinforcing bars, have not been answered uniquely yet. Attempts to model inelastic effects have been carried out by many investigators, but it is felt that the application of simple and effective models to a finite element formulation has met so far with limited success. However, Shirai and Sato (1981) investigated the non–linear behaviour of reinforced concrete structural walls under monotonic and cyclic loading by an analysis based on the use of models describing fundamental material behaviour. They presented a new concept of bond behaviour and they modelled aggregate interlock and dowel action with the concept of equivalent shear moduli by introducing crack spacing and width.

The incremental self-correcting approach was used as a numerical procedure and its application was valuable since it reduced the computational time. The analytical results appear to correlate closely with experimental data irrespective of whether or not bond, aggregate interlock and dowel action are considered in the analysis. It should be mentioned that the whole programme is rather overloaded and impractical. Therefore, justified improvements and simplifications as well as a more realistic description of the material behaviour in terms of both microcracking and macrocracking is required in order to develop a reliable finite element package for the modelling of reinforced concrete structural elements.

2.3. EXPERIMENTAL RESEARCH ON STRUCTURAL WALLS

2.3.1. GENERAL REMARKS

Laboratory tests of structural walls can be characterized by the type of applied loadings. Two general types of loading have been used, (a) static and (b) dynamic.

Static Monotonic Load Tests are carried out by incrementally applying load or deflection until the specimen is destroyed. The primary advantage of these tests is that they are simple and relatively inexpensive. They also represent, to some extent, a "control" or "reference" point for the other types of test. However, monotonic response is not sufficient to describe the response of structures for earthquake type loading.

Static Cyclic Load Tests are carried out using load or deflection control. With the cyclic load test, the specimen is subjected to a predefined series of load cycles so that the sequence from elastic behaviour through inelastic behaviour to destruction of the specimen can be monitored. This type of loading, though not as realistic as dynamic base motions, permits detailed evaluation of the hysteretic behaviour of the structure tested.

Following this type of load test, complete control of the loading sequence is possible. Since the test can be stopped at any stage, decisions about subsequent loading can be made based on the then current status of the test specimen. It is also possible to observe closely overall behaviour, crack patterns and the physical condition of the specimen at any time during the test. Useful information regarding the hysteretic response of the structure can be obtained from the test. For example, based on measured force-displacement curves, changes in the stiffness

and energy dissipation characteristics of the specimen can be determined.

Since loads are applied slowly, characteristics sensitive to the rate of loading are neglected. Furthermore, the application of loads does not completely simulate the inertia forces on the structure. But the primary disadvantage of the reversing load test is related to the selection of the applied loading history. The common method of testing has been to subject the specimen to gradually increasing levels of force or deformation. Another approach has been to select a specific prototype structure and to model it in the laboratory. Then the loading history can be based on dynamic response analysis of the prototype. But, above all, the major question that exists is whether hysteretic response based on static cyclic load tests can be generalised.

Dynamic Earthquake Simulator Tests require an earthquake simulator consisting of a servo-equipped hydraulic system, a power supply, a test platform, an electronic control and monitoring equipment. Specimens attached to the test platform are subjected to base motions simulating real or artificial earthquake records or any kind of simple harmonic pulses.

A significant advantage of the earthquake simulator test is that the test specimen responds to base motion rather than an attached loading system. The primary drawbacks of these tests are the cost of the test facility, both initial and life cycle costs, limitations on the size of test specimens, as well as secondary testing procedure effects (e.g. scale effects, radiation, high rates of loading etc.).

Experimental investigations of isolated structural walls to date will be presented and discussed in the following sections. Experimental programmes on walls with height to width ratio less than or equal to one and higher than one will be covered by Sections 2.3.2 and 2.3.3 respectively, while Section 2.3.4 will deal with test series on walls covering a variety of height to width ratios.

2.3.2. TESTS ON ISOLATED WALLS WITH HEIGHT TO WIDTH RATIO LESS THAN OR EQUAL TO ONE

Walls with height to width ratio less than or equal to one are usually called low-rise walls in the United States or squat walls in New Zealand. This ratio however may not be the best indicator, since wall behaviour also depends on loading conditions, section geometry and section reinforcement. A more important design consideration for low-rise walls is that the shear capacity rather than the

flexural capacity of the wall may govern.

Prior to the mid 1960's the most significant experimental investigation on the behaviour of structural walls was that carried out by Benjamin and Williams (1957), (1958) and (1960) at Stanford University and Galletly (1952) at Massachusetts Institute of Technology. Their work consisted primarily of monotonic load tests of one-storey reinforced concrete structural walls with edge members. Tests by Antebi et al (1960) included dynamic loads to evaluate the blast resistance of structural walls.

Subsequent to 1966, interest in structural walls as earthquake resistant elements has increased in the United States, Japan and New Zealand. This interest has stemmed primarily from the generally satisfactory performance of buildings incorporating walls in recent earthquakes.

At the Portland Cement Association (P.C.A.), at Skokie, Illinois, Barda (1977) tested eight low-rise walls with flanged edge members. The test programme was designed so as to determine the effect of load reversals on wall behaviour. Also, one specimen was repaired and retested. The principal variables of the investigation included the amount of flexural reinforcement, the amount of vertical and horizontal wall reinforcement and the height to width ratio. Loads were applied to the wall through the top slab. Results indicated that current design procedures underestimate the strength of low-rise structural walls, even when the walls are subjected to load reversals. Specimens subjected to load reversals had a shear strength about 10% less than similar specimens subjected to monotonic loading. Also, it was found that horizontal wall reinforcement did not contribute to shear strength for specimens with height to width ratio of $\frac{1}{2}$ and less, while vertical wall reinforcement was effective as shear reinforcement in these specimens. Shear strength of specimens with height to width ratio of $\frac{1}{2}$ was not affected by differences in the amount of flexural reinforcement. In all cases the frame action of the boundary elements provided a gradual mode of failure.

Shiga et al (1973) have tested low-rise walls with column boundary elements. Their tests were similar to Barda's, but they also provided for the application of vertical loads. The results of the study showed that deflection at the cracking load and ultimate load were not much influenced by the reinforcement ratio and the level of axial load. The stiffness of the wall reduced as the number of loading cycles increased. The bigger the amplitude of loading, the more pronounced the trend. The damping capacity was scarcely influenced by the level of deflection, the axial load and the wall reinforcement ratio.

A series of seven tests on low-rise rectangular walls with height to width ratio of one were carried out at P.C.A. by Cardenas et al (1980). This series included one wall subjected to load reversals. Among the variables were amount and distribution of vertical and horizontal reinforcement. Vertical reinforcement was either distributed uniformly over the width or concentrated near the ends, while horizontal reinforcement, when provided, was uniformly distributed along the wall height. The main findings of this investigation were that (a) the shear design provisions of the 1977 ACI Building Code provided a satisfactory lower bound value even when reversed loads were applied (b) the strength of a wall subjected to monotonic loading was approximately 7 percent greater than that for a similar wall subjected to reversals of high shear forces.

To study the behaviour of squat structural walls and the effects of both flexural (vertical) and shear (horizontal) reinforcement on the failure mode and the ductility, tests have been carried out at the University of Canterbury by Beekhuis (1971), on square 150 mm thick cantilever structural walls. The walls were subjected to a load in such a way that the shear force was distributed along the top edge. Tests indicated that sliding shear may limit the wall capacity. For a wall with a flexural capacity corresponding to a low level of shear stress, the full flexural strength was developed under lateral load reversals. The wall contained shear reinforcement greater than that required to develop the flexural capacity.

At McMaster University, Alexander et al (1973) investigated the effect of axial (vertical) load on low-rise rectangular walls. The results indicated that compressive axial stress increases the horizontal load carrying capacity of the wall, reduces the rate of deterioration in stiffness and reduces attainable ductility.

Four wall units with height to width ratio of $\frac{1}{2}$ were tested under cyclic loading at the University of Canterbury by Synge (1980), and Paulay et al (1982). Two of these had rectangular cross-section with a beam at the top to introduce shear forces into the free end of the cantilever walls. The other two units included small flanges. To reduce excessive sliding displacements at the base of the wall immediately above the foundation beams, diagonal reinforcement was provided for two of the four test units. The existence of crossed diagonal reinforcement was found to improve the response of the wall to reversed loading, even when as little as 30 percent of the applied shear was resisted by such reinforcement. However, the above special diagonal reinforcement was insufficient to prevent slip. When the diagonal bars yielded due to slip displacements, significant energy dissipation resulted, additional to that due to yielding of the flexural reinforcement.

Maier and Thürlimann (1985) carried out a series of tests on ten square large scale walls with the main objective being the investigation of strength and behaviour of reinforced concrete wall elements loaded by vertical and horizontal forces. The vertical force remained constant during the test while the horizontal force was increased monotonically or cyclically until failure occurred. The following quantities were chosen as test parameters : shape of the extreme vertical edges of the specimens (i.e. walls with and without flanges), arrangement and amount of reinforcement, level of the vertical load and opening in the compression zone. Test results showed the following features :

(a) horizontal resistance is a function of the cross-sectional geometry, percentage of vertical reinforcement and vertical force. The addition of flanges to the vertical edges improved the strength;

(b) the influence of horizontal reinforcement on the maximum load was negligible. Percentage of horizontal reinforcement influenced only the deformational capacity of the wall;

(c) failure occurred in the compression corner of the specimen due to vertical splitting of the concrete. The depth of the fractured zone was found to increase with the level of vertical load;

(d) under cyclic loading, the wall sustained a maximum horizontal load similar to that sustained under monotonic loading;

(e) walls with an opening adjacent to the compression flange at the lower edge of the wall sustained a load 25% lower than that of a similar wall without opening. Openings placed adjacent to the tension flange of the wall had no effect on strength.

Wiradinata and Saatcioglu (1986) carried out an experimental programme including tests of large scale structural walls with height to width ratio of $\frac{1}{2}$ and $\frac{1}{4}$ under inelastic load reversals. Results of the study showed that the failure mode of the walls is affected by the height to width ratio of the wall. Walls with low height to width ratios may fail in sliding shear prior to flexural or compressive failures. The other main finding of the study is that vertical reinforcement is highly effective in resisting shear and that the wall specimen with height to width ratio of $\frac{1}{2}$, even though it contained only a minimum amount of horizontal reinforcement, showed a characteristically ductile behaviour.

2.3.3. TESTS ON ISOLATED WALLS WITH HEIGHT TO WIDTH RATIO GREATER THAN ONE

Probably the first series of tests on structural walls with height to width ratio greater than one was carried out by Cardenas (1973) at P.C.A. The investigation considered the walls as horizontal cantilever beams. Six rectangular structural wall specimens were tested under static combinations of axial load, bending and shear. All specimens had a thickness of 76 mm and a width of 1900 mm. Four of the six walls had a height of 6400 mm, the other two were 4090 mm high. The main variable was the amount and distribution of the vertical reinforcement. Horizontal reinforcement equal to 0.27 percent of the concrete cross-sectional area was provided in all specimens. The results showed that the strength of tall rectangular walls subjected to monotonic loading is generally governed by flexure rather than shear. Concentration of vertical reinforcement near the ends of the wall resulted in a higher moment capacity and a greater ultimate curvature. Axial compression on the walls increased the moment capacity, but reduced the ultimate curvature.

Since monotonic tests do not yield useful information related to the hysteretic behaviour of the walls, major experimental programmes related to the evaluation of the behaviour of structural walls under cyclic loading were carried out at the University of California, Berkeley and at the P.C.A. in the mid-1970's.

A series of 8 specimens were constructed, tested, repaired and retested in Berkeley, resulting in a total of 18 tests presented in three reports by Wang et al (1975), Vallenas et al (1979) and Iliya et al (1980). All specimens were $^1/_3$ scale sub-assemblages of the first three stories of a number of 7 to 10-storey single solid walls. Specimens had a first storey height of 1219 mm and subsequent storey heights of 914 mm each. Six tests were carried out with column boundary elements. Four of them were tested with spiral reinforcement in the boundary elements, while the other two had closely spaced square ties.

The specimens were initially loaded with equal axial forces on each of the edge columns representing the gravity forces. Although the total axial force was kept constant throughout the experiment, the relative values were varied to simulate the overturning moment effects. The overturning moment was itself varied in accordance with the variation of lateral load in such a manner that the moment to shear ratio was maintained constant. The main parameters of these studies included (a) loading history, (b) cross-section geometry, (c) amount and arrangement of wall reinforcement, (d) magnitude of nominal shear stress, (e) methods of

confining the edge columns, (f) construction joints and splices and (g) effectiveness of repair and retrofitting techniques.

All specimens failed under high horizontal forces after attaining various levels of post-yielding deformations despite the fact that the design of the walls against shear did not satisfy current Code requirements. For the same type of horizontal wall reinforcement arrangement, the larger the amount and the closer the spacing, the better the behaviour of the wall. However, the degree of improvement is not directly proportional to the amount of horizontal wall reinforcement. Specimens incorporating only half the horizontal reinforcement of the comparable specimens, resisted 90 percent of the horizontal force resisted by the much more heavily reinforced ones. In fact Code expressions predicted that these walls would resist only 58 percent of the horizontal force. Other results of the investigation were : (a) wall strength under combined axial load and bending moment was significantly higher than that predicted by Code provisions, (b) diagonal arrangement of the reinforcement resulted in better behaviour than the vertical and horizontal reinforcing bar arrangement, (c) the techniques used for the repair and strengthening of the specimens, while permitting them to develop a comparable lateral load resistance to that observed in the virgin specimens, did not restore the stiffness and the ductility of the specimen; significantly more brittle failure was observed, (d) carefully cast construction joints behaved very well.

A series of sixteen large structural walls have been tested by Oesterle et al (1980), at P.C.A. laboratories. The specimens were 1910 mm wide, 4570 mm high and 102 mm thick cantilevers with no intermediate beams or slabs, representing a $^1/_3$ scale model of an element of a structural wall system. The specimens were loaded horizontally by a concentrated force at the top. Monotonic and two different cyclic loading histories were applied during the tests. Cyclic loading was effected through the top slab while the base block was clamped to the test floor. Constant vertical column loads were applied to seven of the specimens, while no axial load was applied to the rest. The variables studied included (a) cross-section geometry, (b) amount of main flexural reinforcement of the edge members, (c) amount of confining reinforcement of the edge members, (d) amount of horizontal (shear) wall reinforcement, (e) axial forces, (f) concrete strength, (g) loading history and (h) construction joints.

Failure of walls subjected to cyclic boundary shear stresses smaller than 0.3 times the square root of the uniaxial compressive concrete strength (f'_c) in MPa, occurred due to either yielding or buckling of the main vertical reinforcement. Buckling was accompanied by spalling of the concrete cover. Confinement hoops

around the main vertical reinforcement delayed bar buckling and provided efficient confinement to the core concrete. In one rectangular wall, large out-of-plane displacements of the compression zone of the wall were observed as the specimen was subjected to cyclic loading in the inelastic range.

Failure of walls subjected to cyclic boundary shear stresses greater than 0.6 $\sqrt{f'_c}$ MPa occurred due to "crushing" of concrete in the compressive zone of the wall. The cyclic loading resulted in a system of inclined cracks that criss-crossed the web of the wall forming relatively symmetrical compression strut systems for each direction of loading. Loss of load carrying capacity of the wall due to "crushing" was usually sudden. Tests indicated that axial compressive stress corresponding to approximately (0.1)* f'_c increased ductility prior to "crushing". Also, a significant increase in the amount of horizontal reinforcement has only a small effect on ductility prior to "crushing". Other results pointed out that (a) the deformation mode usually associated with shear deformations within the hinging region of a wall was coupled to flexural rotations, (b) use of confining reinforcement in the vertical edge elements within the hinging region significantly improves inelastic behaviour and (c) stiff boundary elements help to limit shear deformations and construction joint slip.

In order to investigate the behaviour of reinforced concrete structural walls Shirai and Sato (1981) conducted cyclic tests on eighteen 1/5 scale wall specimens with I-shaped cross-section. The walls had three stories and one bay and simulated the lower portion of buildings. The failure mode of the walls was characterized by buckling of main reinforcement and concrete "crushing" at the compressive corner of the wall.

With the primary objective being the investigation of the validity of current Code provisions for the prevention of premature inelastic instability and the effect of confining reinforcement in regions subjected to large compression strains, Paulay and Goodsir (1985) tested four ¼ full size reinforced concrete structural wall models. Three walls with rectangular sections and one with a T section, were tested under a fully reversing cyclic lateral load simulating seismic actions and variable axial compression. When the compression zone of the wall had "softened" after a previous loading history a significant compression load in addition to that due to flexure was applied. The above loading scheme is shown in Figure 2.9. While all units exhibited good energy dissipation properties, failure in the majority of cases occurred suddenly when concrete compression strains became excessive. Only one unit could be identified to have failed because of lateral instability. The important feature of this buckling failure was that it occurred under a relatively small

horizontal load, after the buckled region had been subjected to cyclic loading causing large inelastic tensile strains.

Hiraishi et al (1985) carried out static tests on three storey structural walls with vertical edge members in order to investigate the seismic behaviour of flexural type walls. The two test specimens were half scale models of structural wall-beam assemblies of the lower three stories of the full-scale seven storey building. Each specimen consisted of wall, connecting beams with half length and slabs. The main parameter investigated was the amount of reinforcement provided to the wall. Both test specimens showed a stable load-deflection hysteresis curve . The deformation of the walls was largely governed by the stretching of the tension side column at the first storey. Failure of the test units occurred due to "crushing" of concrete at the base of the column. For the less reinforced specimen, fracture of the longitudinal wall reinforcement also took place.

Morgan et al (1985) tested an isolated wall representing the first five levels of a seven level wall-frame specimen. The specimen duplicated the wall portion of the wall-frame structure except that it did not have slab stubs. The isolated wall was loaded laterally with a single force applied at the top (or fifth storey level) of the specimen. The boundary elements of the wall were also loaded vertically. Three cycles of lateral load were applied to the wall. The lateral displacement was increased for each cycle until the specimen reached the point when it could no longer maintain a load level for a given imposed ductility. First yield occurred in the reinforcement at the base of the boundary element at 83 percent of maximum lateral load, while almost all tensile reinforcement at the base of the wall had yielded at 93 percent of maximum load. The specimen exhibited ductile flexural behaviour during hinge formation and beyond. The boundary shear stress applied to the walls was moderate.

The two latest investigations were part of the U.S.-Japan Cooperative Earthquake Research Programme Utilizing Large-Scale Testing Facilities.

Daniel et al (1986) tested two nominally identical wall specimens one with and the other without openings. Specimens were $^1/_3$ scale representations of six-storey walls with short stubs simulating floor slabs at each storey level. Openings represented window areas located in the centre of the wall at each storey level. Specimens were loaded as vertical cantilevers with forces applied through the top slab. No external axial loads were applied to the specimen. Reinforcement arrangement in both specimens was identical with the exception of details around openings. Reinforcement interrupted by openings was moved in equal amounts to

each side of the opening. Based on test results, the following conclusions were drawn :

(a) load–deformation relationships of the two wall specimens were similar;

(b) stress concentrations around the openings did not affect the overall behaviour of the specimen;

(c) no yielding of reinforcement in the lintels was observed, even after vertical wall reinforcement yielded;

(d) both specimens exhibited large deformation and energy dissipation capacities while the shear strength of each specimen was reached after large inelastic deformations had occurred in the boundary elements;

(e) the measured boundary shear strengths were approximately 50 percent greater than the shear strengths predicted by A.C.I. Code.

At the beginning of 1980's dynamic earthquake simulator tests have been conducted on structural walls with boundary frames and coupled walls, as well as isolated walls, in order to obtain fundamental information on their earthquake resistant capabilities.

Araki and Shimazu (1986) tested $^1/_{16}$ scale models of four, eight and sixteen storey isolated walls. Each test structure was subjected to a series of sinusoidal base motions so as to cause resonance at each input level. Each test series consists of several resonance experiments. In each resonance experiment amplitudes of base motion with constant frequency were increased up to the occurrence of stiffness degradation of the test structure. Beforehand free vibration tests were carried out in order to establish the initial frequency of structures in each test series. Acceleration and displacement time histories were measured at several stories. Cracks were observed to be distributed along the lower portion of the isolated walls. The lateral displacement distributions measured along the height of the wall were found to be nearly linear even in the post–yielding range. It was concluded that taller structures are much more dangerous, as far as the sinusoidal type of earthquake motion is concerned, than lower ones.

Eight structural walls with height to width ratio of 1.5 are being tested by Rothe (1986) on a one–dimensional earthquake simulator. The main parameters of the investigation include the amount of horizontal and vertical reinforcement,

cross-section characteristics and axial force. The horizontal load is transferred to both sides of the wall by means of a mass which is "fork" hinged to the top of the wall, as shown in Figure 2.10. The top of the wall can move and rotate freely. An external axial force is introduced by prestressing steel bars mounted on both sides of the wall. In order to reduce the change in axial force due to the upward movement of the wall a spring is placed between the top of the wall and the anchors of the steel bars. From the various existing earthquake records the El Centro 1940 NS and SSE2 have been chosen. The preliminary results of the first two tests indicate that:

(a) wall stiffness is reduced considerably after exceeding the tensile strength of concrete. The ratio of initial stiffness to stiffness at failure is about 10;

(b) calculation of the energy dissipation after cracking showed that the equivalent viscous damping is about 4 percent;

(c) both walls had stable hysteresis curves.

2.3.4. TESTS ON BOTH LOW-RISE AND HIGH RISE STRUCTURAL WALLS

Endo et al (1980) carried out twenty experiments on structural wall models with vertical edge elements and with or without intermediate horizontal beams. Main parameters of the investigation were (a) the overall height of the wall, 2000 and 3000 mm; (b) the thickness of the wall, 50 and 100 mm, (c) the amount of longitudinal reinforcement in the boundary elements, (d) the amount of confining reinforcement in the boundary elements and (e) the amount of vertical and horizontal reinforcement in the wall. Three specimens were subjected to monotonic loading, while the rest were subjected to cyclic loading. Lateral loading was incrementally applied through the top beam, while a constant axial force was applied through the boundary elements. The basic conclusion of the experimental research indicated that the ductility of the wall subjected to monotonic loading is different from that subjected to cyclic loading. The load-horizontal displacement curves of the former have long flat parts and then suddenly drop, while the load-displacement curves of the latter proceed to lower load values gradually as higher displacement values are reached. It was also found that confining reinforcement at the boundary elements causes plastic behaviour after the peak horizontal load level is reached.

The research programme of Hernandez and Zermeno (1980) dealt with the

hysteretic behaviour of concrete walls and included the testing of 22 models at $\frac{1}{8}$ scale and one full scale wall under reversing lateral load. They studied the effect on strength and inelastic behaviour, when "shear" governs the failure, of several variables such as : height to width ratio, concrete strength, amount and distribution of reinforcement, axial load, the presence of intermediate slabs along the height of the wall and of boundary elements as columns or transverse walls. The main conclusions of the study were :

(a) structural walls with shear failure have an inadequate hysteretic behaviour due to progressive deterioration in strength under repetition of loads;

(b) the efficiency of boundary elements on improving behaviour is low;

(c) intermediate slabs increase initial rigidity of the walls and improve deformation capacity at failure but they do not affect wall strength;

(d) the principle variables influencing wall strength are height to width ratio, concrete strength, wall reinforcement, axial load and the presence of boundary elements while the main variables influencing deformation capacity at failure are height to width ratio and reinforcement percentages.

Tomii and Esaki (1984), in an attempt to develop a design method for reinforced concrete monolithic structural walls with boundary elements, tested 8 specimens of two-bay one-storey walls assumed to be $^1/_{10}$ scale models of a two-bay multistorey structural wall. The results indicated that failure was due to slip failure of the panel wall and that the damage can be easily repaired. The boundary elements, which did not fail, could carry the vertical loads when the bearing capacity of the crushed panel wall was significantly reduced.

Jianjun (1986) investigated the behaviour of partially prestressed rectangular concrete structural walls. Six large scale post-tensioned specimens with height to width ratio of 1.72 and sixteen pre-tensioned $\frac{1}{4}$ scale models with height to width ratio varying from 0.9 to 2.0 were subjected to low cycle horizontal reversing loads. The effects of prestressing degree, height to width ratio and ways of reinforcing were studied. Test results showed that prestressing can increase the shear stength of the walls but does not greatly affect the ductility of the walls, while it improves their ability of energy absorption and control of displacement between storeys. The effect of height to width ratio on shear strength of walls cannot be ignored. The role of wall reinforcement is also affected by the above ratio, since projection of inclined crack length is difficult for different height to width ratios.

2.4. FIELD SURVEYS OF THE PERFORMANCE OF STRUCTURAL WALLS DURING EARTHQUAKES

2.4.1. GENERAL REMARKS

Many researchers and most professionals working in the field of earthquake engineering feel that design and construction of earthquake resistant structures is still an art and not a science. Therefore, the critical ingredient in design and construction should be engineering judgement. Field surveys of the performance of reinforced concrete structural systems during earthquakes and the back-analyses of the observed damages might be the best way to develop such judgement. Field observations and back-analyses provide invaluable information about the effectiveness of current Code provisions for aseismic design and of the available analytical models.

Usually a post-earthquake inspection programme on damage of buildings aims to:

(a) identify the reasons for the damage and assess the reliability of various analytical models and techniques used to predict structural response to earthquake ground motions;

(b) assess the possible improvements in design and construction which might minimize the damage in future earthquakes;

(c) assess the efficiency of existing structures to sustain a strong future ground motion without severe structural and non-structural damage;

(d) investigate the efficiency of present methods of repairing and strengthening structures damaged during earthquakes.

The following section presents a review of post-earthquake investigations on the behaviour of reinforced concrete structures incorporating structural walls during past earthquakes. Information related to structural behaviour during earthquakes up to 1980 is reported by Fintel (1974) and Bertero et al (1980).

2.4.2. CASE HISTORIES

The Skopje, Yugoslavia, Earthquake of 1963.

Many of the residential buildings in Skopje up to 10 stories high had two structural walls, all across the width flanking the central stairway. The walls were usually non-reinforced and of poor concrete quality. Nevertheless, the rigidity of the walls did not permit interstorey distortions and therefore prevented severe damage. Slip of the cold joints between successive storey lifts was observed in some cases. The ten-storey Quay Tower, the fourteen-storey Karpos Tower and the fourteen-storey Party Headquarters were reported to have absolutely no damage. The fourteen-storey Trade Union Building was reported to have insignificant structural damage. A number of medium-height reinforced concrete structures not equipped with walls, were extensively damaged or collapsed during the earthquake.

The Anchorage, Alaska, Earthquake of 1964.

One of the largest earthquakes in modern times occurred in Alaska. Anchorage, Alaska, although located some 125 km from the epicentre suffered considerable damage. A significant number of buildings incorporating structural walls were built during 1950-1960 and were extensively damaged during the earthquake.

The eight-storey Hill Building, which had two reinforced concrete central core units connected by beams and a steel frame, survived with relatively less extensive damage. The stiffer core units were damaged at the foundation level and a local shear failure between the first and second floor was observed along a weak plane caused by irregular openings. Connecting beams at the 2nd and 3rd floors were damaged, while the damage was less extensive to beams and core of the upper stories. Severe damage was attributed to a substandard layer of concrete at the foundation level of the stiffer core units.

Mt. McKinley and 1200 L Street 14-storey Apartment Buildings were identical with respect to construction, orientation and damage. Both buildings had central core units and facade structural walls with openings along the peripheries. Significant damage was observed on the facade walls as indicated in Figures 2.11 and 2.12. The connecting beams suffered diagonal shear failure up to the 12th floor. On the narrower sides, both structures had two stiff walls on each side of a flexible wall, all connected by deep beams. One of the stiffer walls had a complete fracture at a low storey level, while no visible damage was observed on

the other wall as shown in Figures 2.11 and 2.12. The wall damage was attributed to the existence of improper construction joints in the locations of damage and to the small amount of vertical and horizontal reinforcement.

The Penney Building was a five-storey structure nearly square on plan with predominant lateral stiffness along one side only. The structural walls of the building varied in amount and distribution along the height of the structure. As a consequence stress concentrations due to torsional effects caused wall damage at the second floor level.

The Four Seasons Apartment complex, a six-storey structure completed just before the earthquake but not occupied, collapsed completely. The structure had two interior cores and peripheral steel columns. Post-tensioned prestressed lift slabs were also used. The collapse of the building was due to failure of the cores which was attributed to the poor splicing of the main bars at the first-storey level. Figure 2.13 shows the results.

The Caracas, Venezuela, Earthquake of 1967

Of a significant number of structures which were extensively damaged, several had a central core made of reinforced concrete wall units. The ten-storey Palace Corvin Building, which had a concrete core wall unit accounting for less than 15 percent of the lateral stiffness, collapsed. The ten-storey H-shaped apartment building Amalfi had a central core unit, on the side of which a vertical crack through the height of the structure appeared after the earthquake. The corner columns of the structure were also damaged. Both the eight-storey Atlantic Oil Building and the twelve-storey Bahia del Mar building incorporated a reinforced concrete central core unit which was terminated at the fifth floor. Extensive damage was observed in the vicinity of this floor. The twelve-storey Plaza One building consisting of two separate towers with reinforced concrete structural walls in both directions had no structural or non-structural damage, while the surrounding structures suffered severe damage and a ten-storey building collapsed, as shown in Figure 2.14.

The San Fernando, California, Earthquake of 1971.

A significant number of strong motion records were obtained from this earthquake enabling a realistic appraisal of the induced forces. A number of damaged structures incorporated walls. Several tall structures with structural walls had no damage despite significant recorded acceleration magnitudes.

The Indian Hills Medical Centre was a seven storey structure with reinforced concrete frames. Four structural walls were used in each direction of the building for lateral strength. Some of the walls were damaged by cracks along the construction joints at floorlines. In addition to the inclined wall cracking, at the first floor the edge member was separated from the wall at the base of this floor. More damage involving slabs and frame members was also observed.

At the seven-storey Holy Cross Hospital, the lateral resistance was provided by structural walls and four core units distributed within the building. Some of the walls terminated below the second floor. The building suffered extensive damage. The damage consisted of severe diaphragm cracking at the discontinuities of the walls along the height of the building as well as several modes of wall failure. Most of the walls had serious damage over the doors which perforated the walls, since insufficient shear reinforcement was provided above the door openings. Walls below the fourth floor level had extensive criss-cross cracking, with reinforcing bars exposed at numerous locations.

The Certified Life Building, built according to the 1964 Los Angeles Code Provisions, was a fourteen-storey reinforced concrete building with walls running in one direction of the building and a central core unit continuous throughout the height of the structure. There was no structural damage while minor non-structural damage was repaired with little cost, despite the fact that analytically obtained shear forces and overturning moments were roughly twice the values estimated by the Codes.

The Managua, Nicaragua Earthquake of 1972.

Detailed damage appraisals showed that none of the structures incorporating walls had more than moderate damage, while many moment resisting frame structures exhibited severe damage and some collapsed.

The ENALUF building with basement, ground floor and six additional floors, had two central reinforced concrete core wall units and a frame for lateral resistance. Splitting of concrete occurred locally at one corner of the core at the foundation level where the cross-section was weakened by large indentations on both sides of the core, made for telephone ducts, metal boxes and piping. Diaphragm cracking as well as some inclined cracking on the cores were observed. The analysis showed that drifts exceeded twice the elastic limit during the earthquake.

The Banco Central building, a fifteen-storey reinforced concrete frame structure

had four elevator shafts enclosed by concrete walls, eccentrically located in the west end of the building as illustrated in Figure 2.15. The walls suffered cracking, spalling of concrete and buckling of the reinforcement in the fourth and fifth floors. There was evidence of yielding at some junctions between the columns and the beams, however the structure has enough ductility to sustain the large distortions. In contrast, the building across the corner, the eighteen–storey Banco De America was a coupled structural wall building, square in plan with two axes of symmetry. The primary lateral force resisting system was 4 L–shaped wall cores symmetrically coupled by pairs of girders at the floor levels as depicted in Figure 2.16. These were T–shaped facade columns along the periphery, connected to the cores by a flat slab. The core walls suffered only hairline inclined cracks between floor levels. The connecting beams appeared to have yielded at the wall connections while slight non–structural damage was observed. It might be concluded that the healthy system of walls incorporated in the latter building, restricted the interstorey distortions providing damage control.

The Guatemala City Earthquake of 1976.

Moderate to insignificant damage was observed to structural systems incorporating structural walls. The fifteen–storey Camara de Industria Building with four core wall units at each corner and the eleven–storey Edificio Medico Building with two rigid central core units, suffered widespread cracking to beams and joists connecting the core units but no damage was observed to the cores. The thirteen–storey Condominio Reforma Building was square and symmetric in plan and had four external concrete walls and an internal core. Hairline inclined cracks were observed on the walls, while coupling beams and non–structural masonry walls suffered slight cracking. The fifteen–storey Condominium Convista Building, the Bomcode Guatemala and Edificio El Cortijo, all relying on structural walls or a structural wall core system for lateral resistance, were reported to have exhibited excellent performance during the earthquake.

The Miyagi–Ken–Oki, Japan, Earthquake of June 1978.

The eighteen–storey Sunimoto Life Insurance Building was a steel frame building with a central reinforced concrete core unit and transverse reinforced concrete structural walls at the exterior four corners. The building was instrumented, thus the maximum recorded acceleration at the ground floor was 0.26g where $g = 9.8\ m/s^2$, with the corresponding acceleration at the 18th floor of 0.56g. No damage was reported except some minor cracking in the interior core as well as along some construction joints.

Another instrumented structure was the engineering faculty building of Tohoku University, a nine-storey reinforced concrete frame building with structural walls. Peak ground acceleration of 0.24g was recorded while the peak value on the 9th floor was 1.0g. The duration of intense response in excess of 0.25g was approximately 20 seconds. The damage consisted of minor structural wall cracking and broken windows, which is a great success considering the intensity of ground excitations. A number of structures not incorporating structural walls suffered excessive damage.

The Imperial Valley, California Earthquake of 1979.

Singularly, the most interesting aspect of this earthquake was the damage of the Imperial County Services Building in El Centro. For this modern six-storey building lateral resistance was provided by moment resisting frames in the longitudinal E-W direction and structural walls in the transverse N-S direction. Structural walls in the upper five stories were provided for the full width of the building on its east and west faces but they were not extended below the first floor slab. Four considerably narrower walls were asymmetrically placed in the first storey. Damage to the building consisted of the failure of the four columns along the east side at the ground floor, spalling of concrete cover and buckling of longitudinal steel in other columns of the ground floor and cracking in slabs, beams, columns and walls throughout the building. Figure 2.17 shows the results.

The Chile Earthquake of 1985.

The majority of rigid reinforced concrete structural walls performed very well in the Chilean Earthquake as reported by Dowrick (1985), Connor (1985) and the U.S. Reconnaissance EERI Team (1986). However, in buildings incorporating structural walls designed around 1967, brittle modes of failures were observed. Two cases of sliding shear, five cases of extensive inclined cracking and three cases of bending compression failure were reported. Damaged walls appear to have contained amounts of horizontal (shear) reinforcement smaller than those recommended as nominal.

In a number of cases the cause of damage may be due to poor structural configuration. For an example, one building in Villa Olympia Complex failed with total collapse of the last two bays of the structure both of which were open in the first floor. The end wall of this building was a solid reinforced concrete wall 200 to 250 mm thick, down to the second floor where it was supported on two columns. The failure occurred at the top of the columns where they meet the

wall. In another complex of residential buildings in Villa Portales distress at the top of the column supporting the discontinuous structural wall, as well as inclined cracks on the walls or failure of the wall adjacent to service opening were reported.

The fifteen storey Acapulco Building, located in Vina del Mar, consisted of structural walls, slabs and connecting beams; several of the walls suffered distress in construction joints and crushing and spalling at the boundaries. The most dramatic wall failure is shown in Figure 2.18. The fifteen-storey Hanga Roa Building is located immediately north of the Acapulco. The building is of reinforced concrete with a substantial structural wall system providing lateral support. Walls were reinforced with 8 mm bars at 250 mm centres at both faces of the wall. The most spectacular distress in the Hanga Roa was a vertical crack in walls between doors on the north side. Less spectacular cracking was observed on the south side. There was also universal spalling of the lintels at the west end of the building. The location of cracks suggests a non-uniform distribution of mass in the building and an interaction of the various wall elements of the building in an attempt to evenly distribute forces and moments.

Minor cracking of walls mainly at the ground floor, spalling in shallow beams between walls, cracking and spalling at horizontal construction joints were reported in a number of 15 to 23 storeys reinforced concrete buildings in Vina del Mar.

The Mexico City Earthquake of 1985.

Reinforced concrete structural walls as the principal means of resistance to lateral loads were scarcely found in Mexico. As reported by the EEFIT team (1986), the Direccion General de Administra de Personal was a twelve storey building originally of moment frame construction which had been damaged by the 1981 earthquake. External concrete structural walls had subsequently been added to strengthen the building. Figure 2.19 shows the south and west facades of the building after the earthquake. Part of the glazing had broken and the wall on the south face had settled about 200 mm. Three moment frame buildings, which had concrete structural wall cores, and one moment frame building, which had an isolated structural wall along part of one end, appeared to have major cracks in the walls while the damage to the frame structure was slight to negligible.

The ACI Concrete International team (1986) reported that where structural walls were used in buildings damage to non-structural elements was minimal. At the sixteen-storey El Presidente Hotel in Ixtapa, near the epicentre, structural walls

saved the building from major non-structural damage. Nearby moment frame buildings with masonry infill panels suffered severe non-structural damage.

The San Salvador Earthquake of 1986.

As reported by Bommer and Ledbetter (1987), reinforced concrete structural walls were rarely used in El Salvador, but where they were adopted they generally performed well. An example of this was the ten-storey Benjamin Bloom Children's Hospital constructed in 1969, which comprises a massive central lift wall core unit and a pair of structural walls at either end. No damage was observed to the structural walls but unreinforced masonry panels located between the walls failed at every storey. The three-storey wing of the Hospital consisted of three structurally separate units built into sloping ground and incorporating no walls. Ground floor columns of different height were used along one façade. The block with the longest columns failed completely, while another one suffered partial collapse.

2.5. GENERAL DISCUSSION

The foregoing presentation of analytical and experimental work on the non-linear behaviour of reinforced concrete structural walls shows that despite major advances that have been made over the past two decades in the understanding of wall behaviour, there are still several problems requiring further study.

The analytical work discussed in Section 2.2 indicates that there is a lack of a relatively simple and reasonably accurate wall model to be used in the non-linear analysis of structural systems incorporating structural walls.

Even though current simplified wall models are able to describe important features of the experimental or field observed behaviour of structural walls, uncertainties related to the hysteretic properties of model elements remain. Especially when walls are subjected to high shear stresses, the accurate idealisation of the hysteretic wall behaviour is difficult to achieve since many parameters, and hence many uncertainties, are involved. In addition, all analytical models at present suffer from poor modelling of the cracking process. It is worth noting that a lot of simplified models ignore basic features of wall behaviour or utilize a number of oversimplified assumptions. Following these procedures they succeed in predicting satisfactory results for a small number but not for the majority of wall case studies.

As far as detailed models are concerned the lack of a realistic model for the behaviour of concrete into well-established numerical techniques and the complexities involved in a detailed solution appear to be the reason for the unsatisfactory attempts of recent models to predict the non-linear behaviour of structural walls at the ultimate limit state. For years uniaxial strength characteristics of concrete formed the basis of analytical modelling, while critical wall areas are under biaxial or triaxial conditions, as the experimentally observed wall behaviour indicates. Furthermore, it was proved by non-linear finite element analysis and also shown experimentally that the concept of truss analogy used by the majority of the investigators either to model the inelastic effects of the wall behaviour or to use it together with the theory of plasticity to predict wall strength, does not offer a suitable basis for the analysis of the wall behaviour. It was shown that the influence of inelastic effects like bond, aggregate interlock and dowel action to load carrying capacity is small (Shirai et al, 1987).

The literature survey shows that the behaviour of walls under different loading histories has recently been extensively studied by experiment. However, while the effect of some parameters on the observed behaviour is clear, uncertainties related to the influence of others remain.

A brief discussion of some of the uncertainties follows:

(a) It was illustrated experimentally that walls with low height to width ratio tend to fail under high levels of horizontal load. However, the extent of the role of horizontal (shear) reinforcement in safeguarding against shear is an unknown. Despite the vast experimental work carried out worldwide, a proper evaluation of the effect of horizontal reinforcement on the behaviour of walls with varying height to width ratio is still lacking. In a number of experimental investigations it was concluded that a minimum amount of horizontal reinforcement can be enough in some cases, while the degree of improvement with increasing levels of horizontal reinforcement is not in direct proportion to the amount of horizontal reinforcement, but is significantly smaller.

(b) Another unclear point is related to the problem of how the amount of vertical reinforcement provided to the walls, mainly to cope with axial-flexural demands, affects the shear strength capacity of the wall. It was shown that as the height to width ratio of the wall drops, vertical reinforcement becomes more effective in resisting shear. Furthermore, when higher amounts of vertical reinforcement are accommodated at wall vertical ends, mainly in walls with barbell-section, higher resistance in shear was observed, despite the fact

that the amount of wall reinforcement remained unchanged.

(c) Axial force significantly affects stiffness, strength, ductility and energy dissipation characteristics of the walls. But again, experimental results differ on whether the presence of certain amounts of axial compression is lightly or highly beneficial. To the author's knowledge, nothing has been said on whether the presence of axial load can change the failure mode of the walls. There is still a lack of interaction diagrams of walls with varying height to width ratio when flexure or shear failure dominates. It is likely that axial force affects differently these two possible failure modes and that for certain amounts of axial load there is an interplay between the two modes.

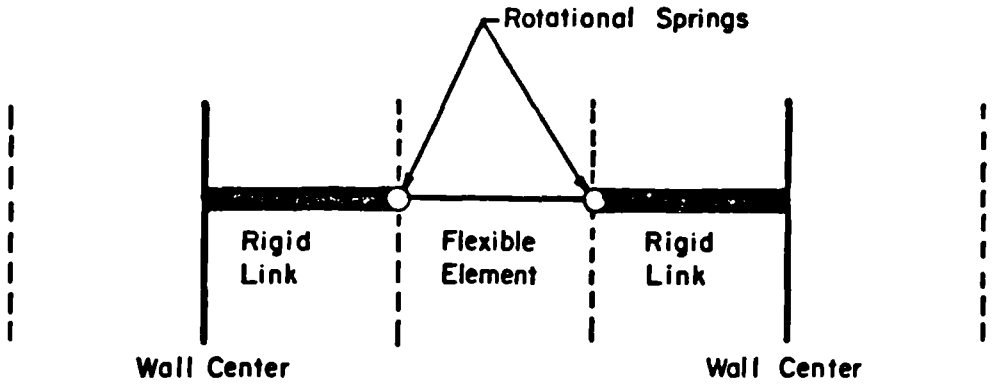
(d) Experimental information related to the effect of openings on the ultimate behaviour of structural walls has indicated that ultimate strength characteristics of the wall are affected only when the opening penetrated the bottom compressive zone area of the wall. Openings in the middle or near the tensile edge of the wall do not decrease the wall strength. Such information is in conflict with mechanisms of shear resistance based on classical continuum mechanics and truss analogy concept. The image of the actual failure mechanism of walls subjected to high shear stresses appears to be vague.

A wide range of damage on structural walls varying from complete collapse to insignificant minor damage was recorded during the field observations following major past earthquakes.

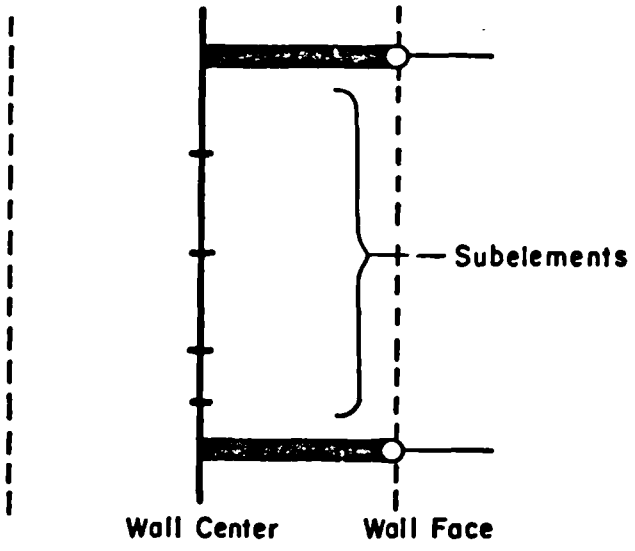
In the case of major structural damage either gross design and detailing errors or poor construction and/or poor quality control of materials were the basic sources of imperfection. Since the latter has mostly to do with inspection deficiencies and poor standards of workmanship during construction, the former merits some discussion as far as wall behaviour is concerned.

Walls were proved to be superior than concrete frame with or without masonry, reinforced or unreinforced, infill panels to resist lateral forces. But since they are the most rigid elements in the structure they attract most of the lateral load. Therefore proper selection of the structural layout is essential, while symmetry and avoidance of discontinuities in mass, stiffness, strength and deformability are crucial. Most of the damages on buildings with walls were due to the conceptually inappropriate presence of walls in the plan view of the building. Furthermore, excessive confidence on the strength capacity of a structural system incorporating walls, led in a number of cases to improperly dimensioned and

inadequately detailed R.C. walls. A part of the below par performance of buildings incorporating walls under strong ground excitations should be attributed to Current Code provisions. Back-analyses have shown that the axial-flexural capacity of walls under combined loading can be as much as 2 to 4 times the Code predictions. Despite the reduction factors that present codes utilized for the calculation of the shear strength of structural walls, and despite limitations imposed on the maximum permissible horizontal load applied to the walls, undesirable premature shear failure modes were observed. It should be noted that Code provisions for shear design are empirical expressions based on a broad scatter of test results. Therefore, these defects hamper a proper understanding and judgement of wall behaviour under high levels of horizontal load since the existence of a theory which could provide a realistic description of the underlying causes of shear failure in walls is lacking.

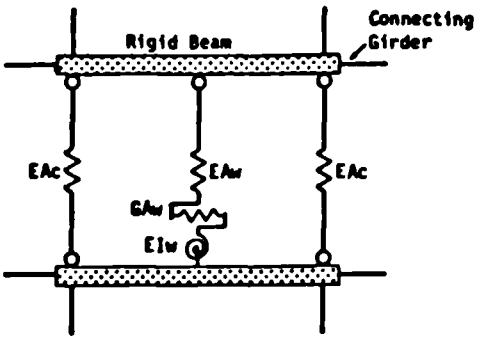


(a) Connecting Beam Model

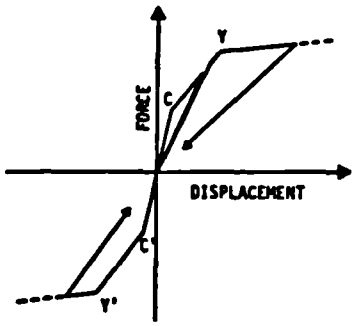


(b) Wall Member Model

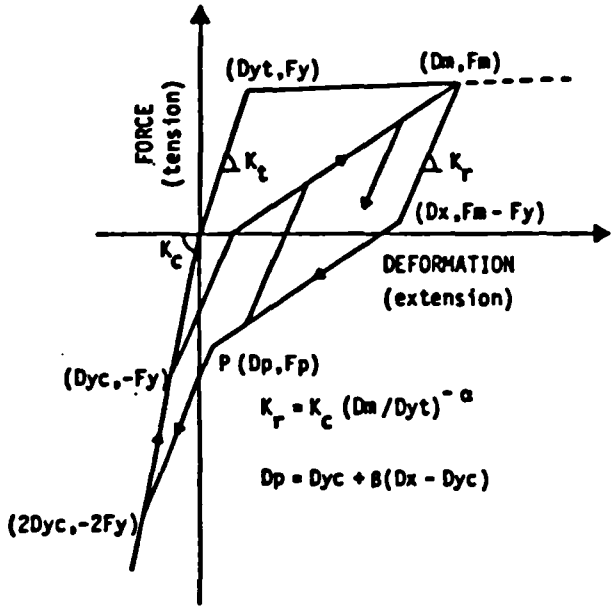
Fig. 2.1. Typical inelastic beam model for structural wall systems (a) connecting beam, (b) wall member.



(a) R/C Wall Model

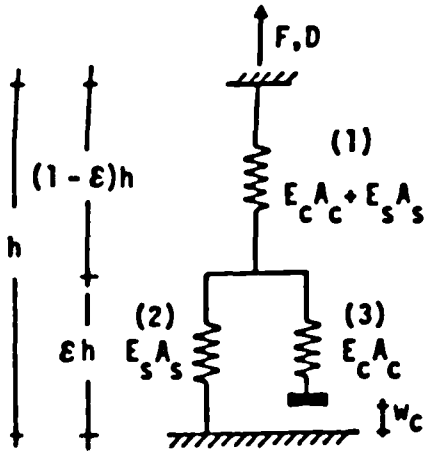


(c) Origin-Oriented Hysteresis Model



(b) Axial-Stiffness Hysteresis Model

Fig. 2.2. The reinforced concrete wall model of Kabeyasawa et al (1982)
(a) wall member, (b) axial stiffness hysteresis model and (c) origin-oriented hysteresis model.



Two-element-in-series Model

Fig. 2.3. The analytical model of Vulcano and Bertero (1984).

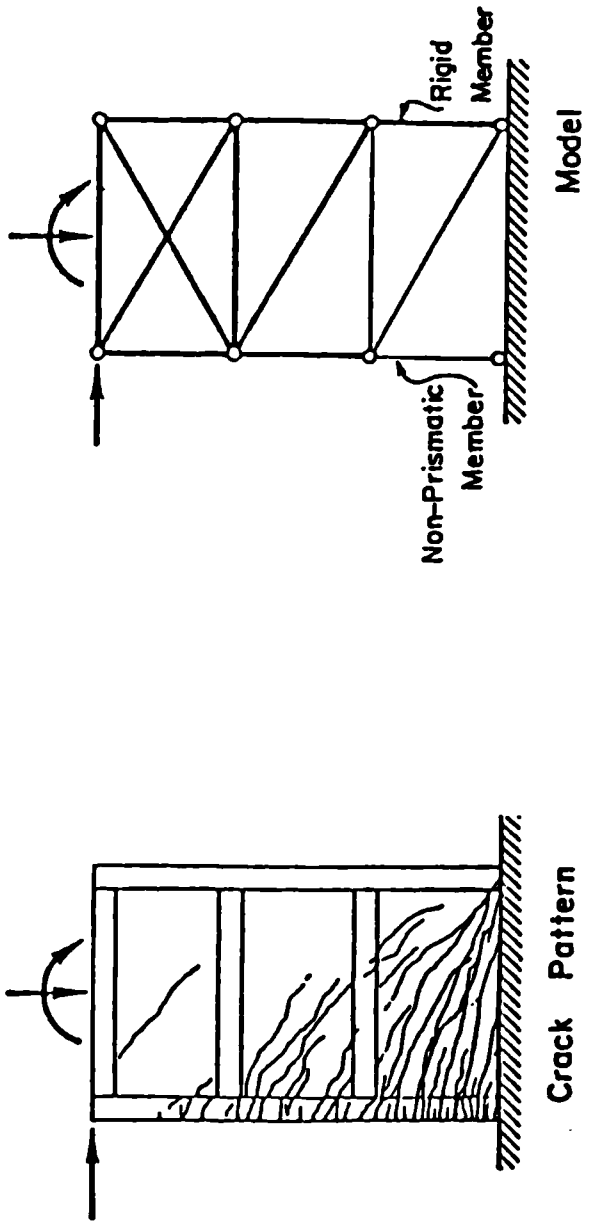


Fig. 2.4. The truss analogy model of Hiraishi (1984).

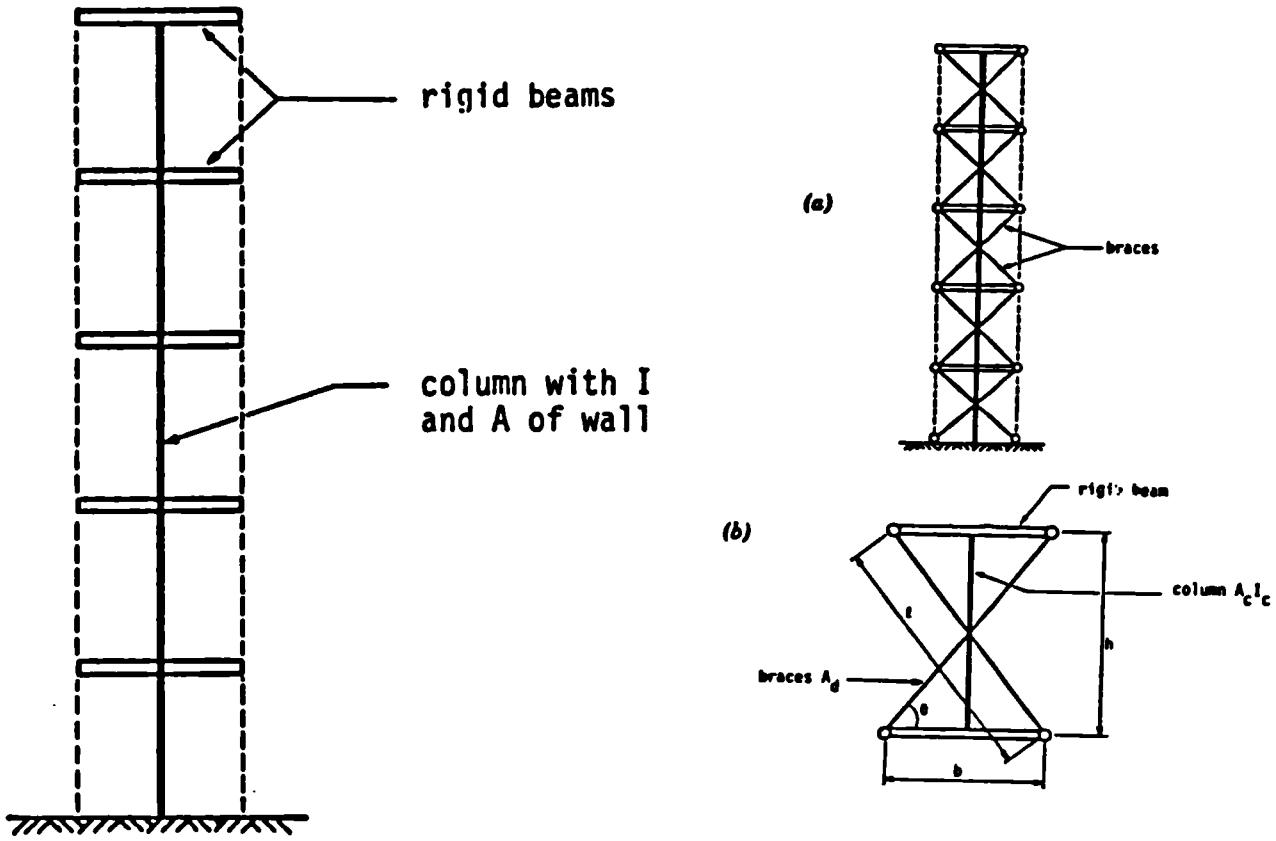


Fig. 2.5. The wide-column analogy model of Smith et al (1984) (a) braced wide-column analogy and (b) braced wide-column module.

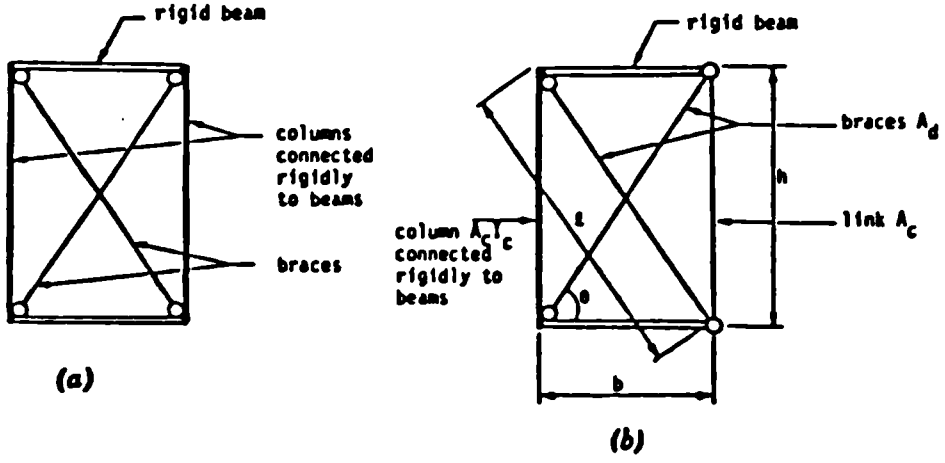


Fig. 2.6. The braced frame analogy model of Smith et al (1984) (a) symmetric form and (b) asymmetric form.

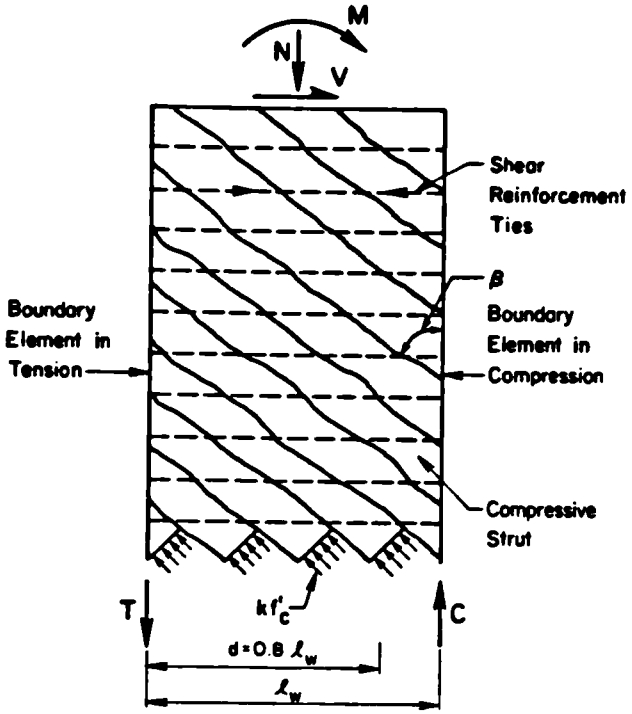


Fig. 2.7. Truss model for wall element.

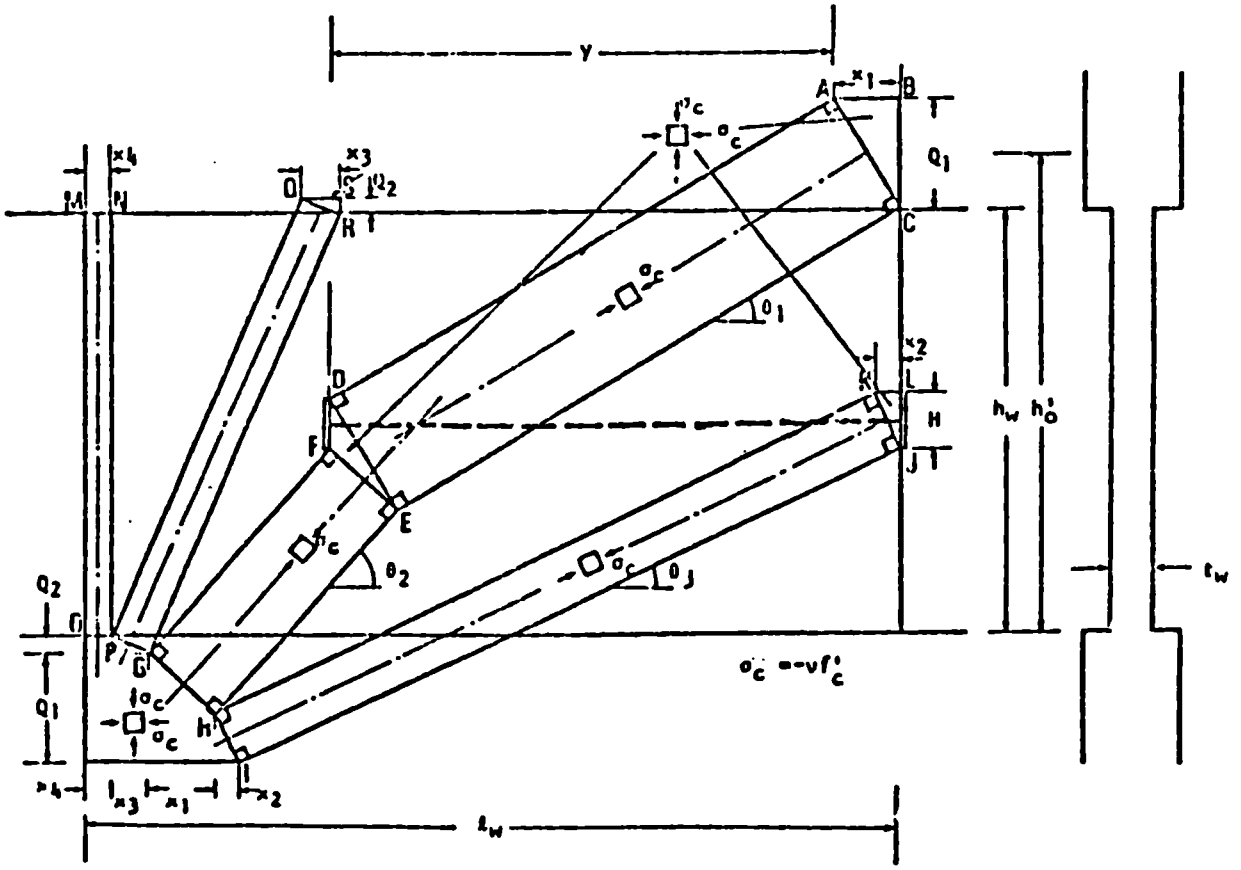


Fig. 2.8. Tie and strut model for structural wall (after Aoyama et al 1986).

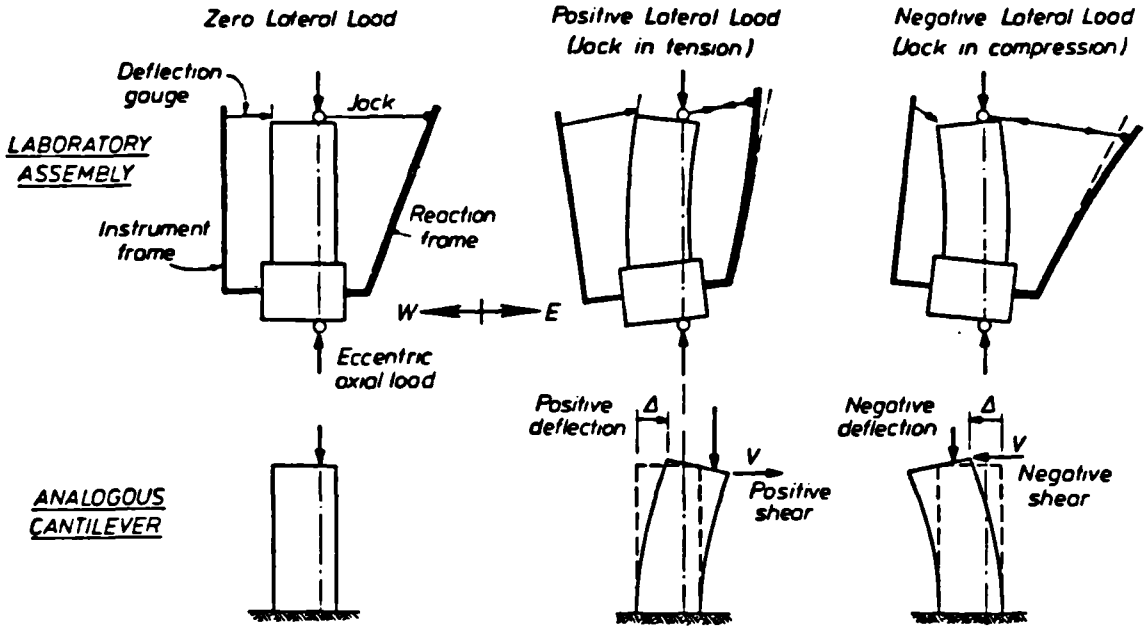


Fig. 2.9. Loading scheme (indicating sign convention) adopted for tests carried out by Paulay and Goodsir (1985).

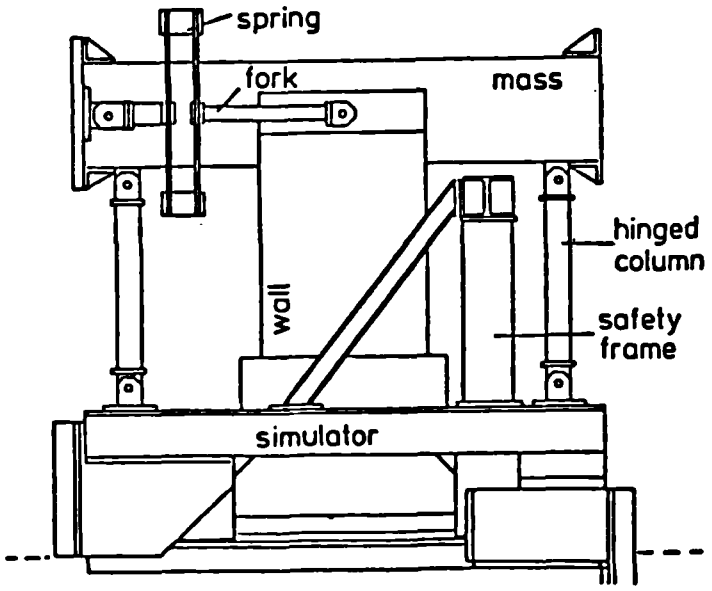
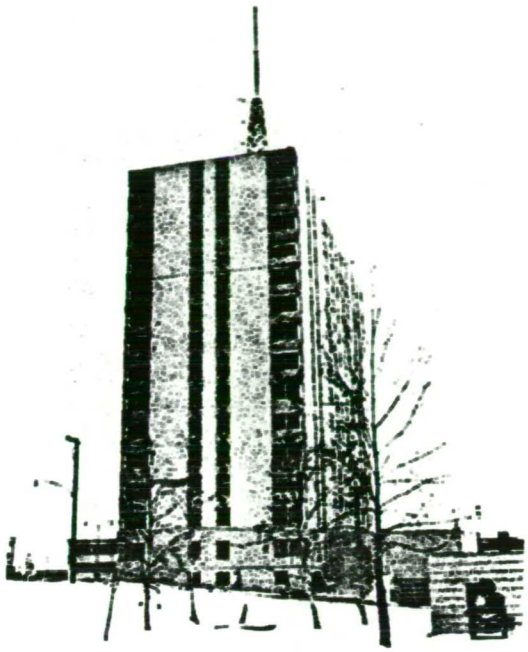
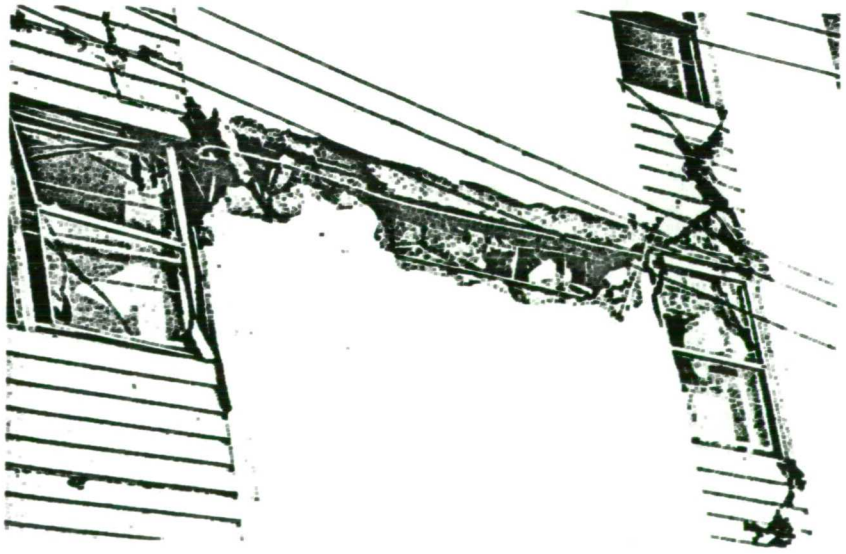


Fig. 2.10. Earthquake simulator used by Rothe (1986).



(a)



(b)

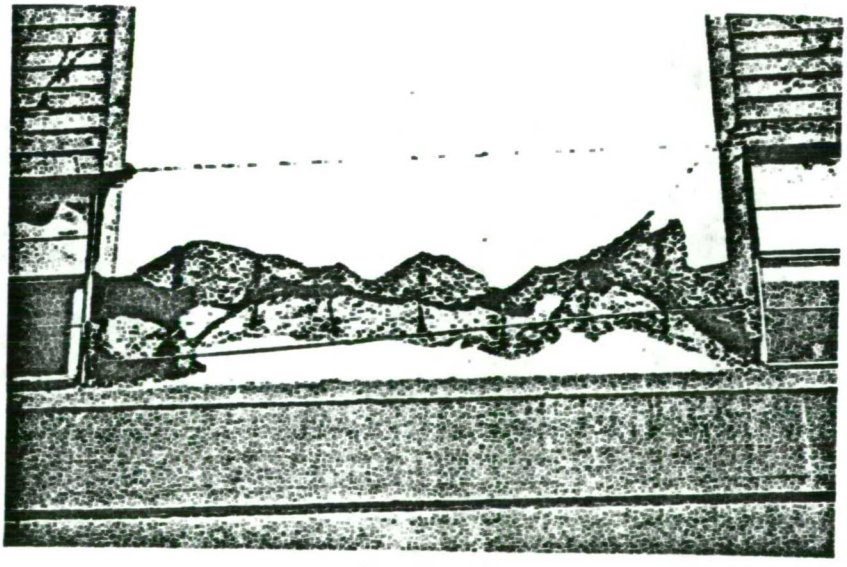
Fig. 2.11. Mt. McKinley Building

(a) damage on the facade walls

(b) wall failure at the third storey level.



(a)



(b)

Fig. 2.12. 1200 L Street Building

(a) damage on the facade walls

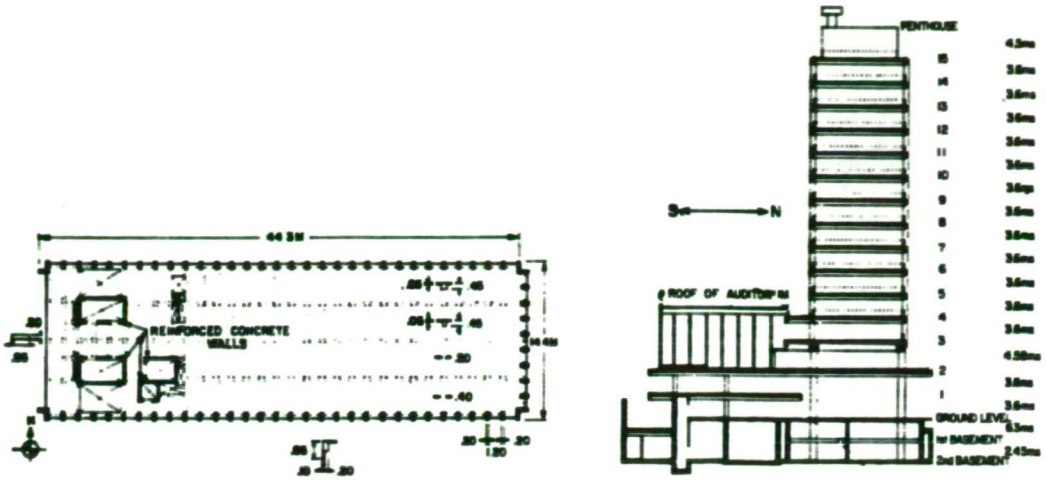
(b) wall failure at the first storey level.



Fig. 2.13. Collapse of the Four Seasons Apartment complex.

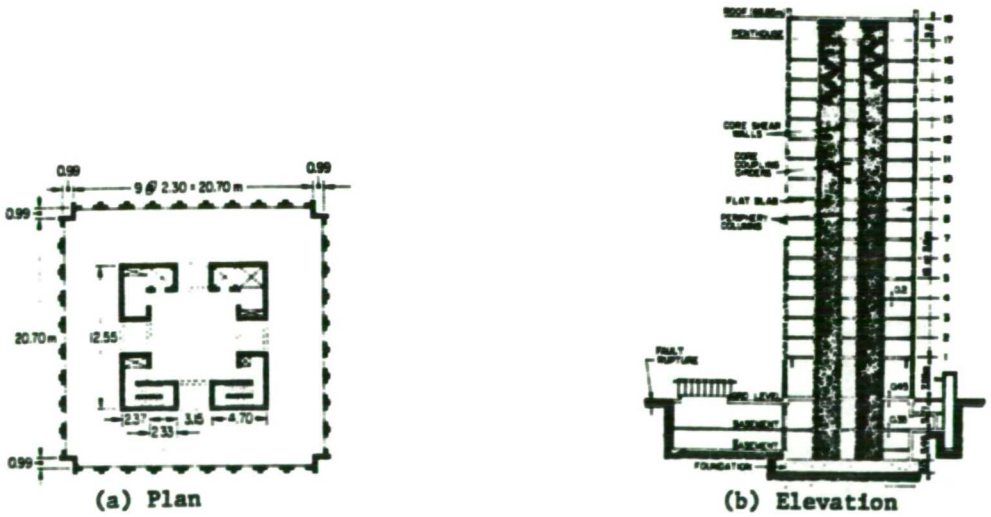


Fig. 2.14. The Plaza One building - Caracas.



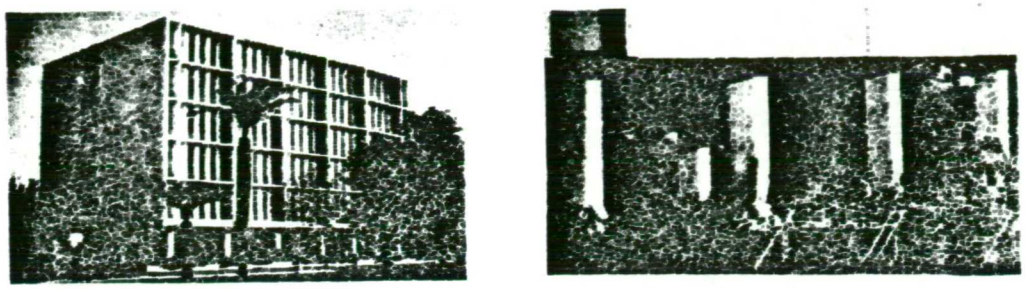
(a) Typical Plan of Upper Stories (b) Elevation

Fig. 2.15. The Banco Central building
(a) typical plan (b) elevation.



(a) Plan (b) Elevation

Fig. 2.16. The Banco de America building
(a) plan view (b) elevation.



(a) (b)

Fig. 2.17. The Imperial County Services building - California
(a) view of the building
(b) failure of the ground storey east columns.

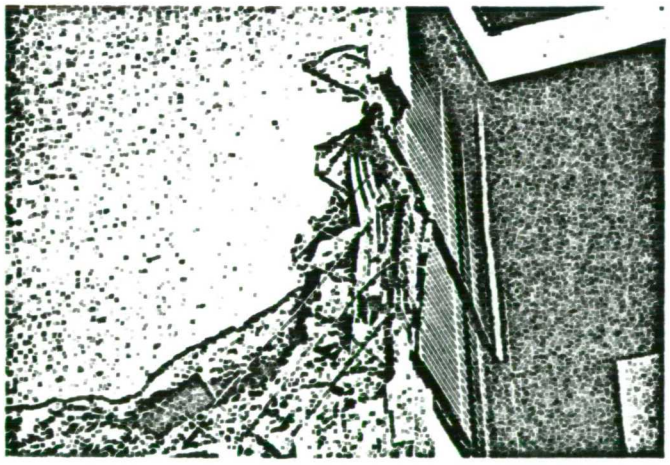


Fig. 2.18. Wall failure of the fifteen storey Acapulco building.

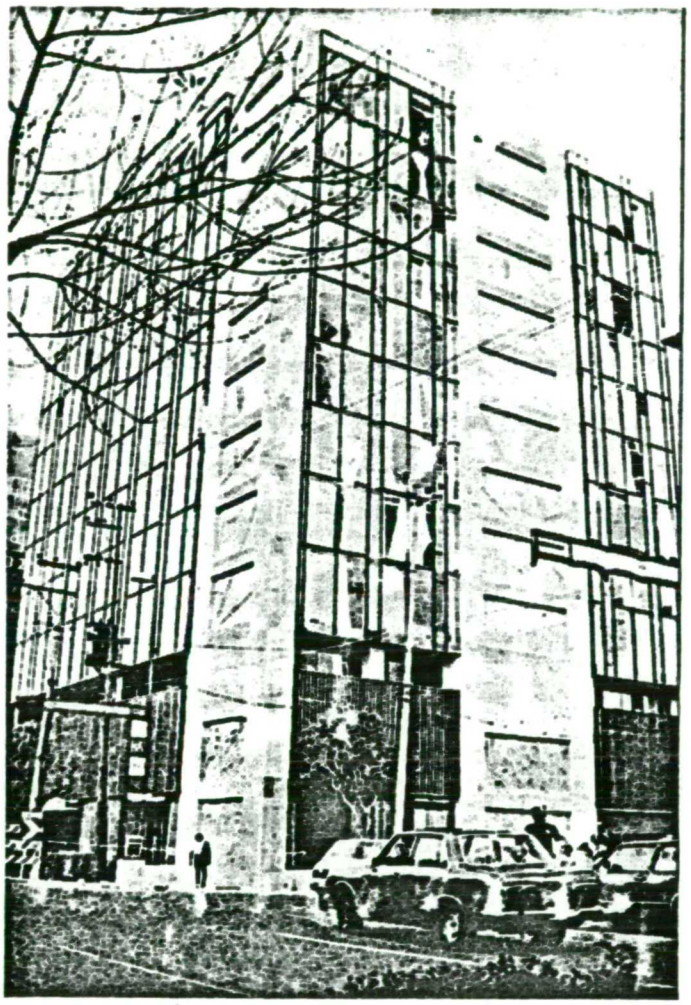


Fig. 2.19. South and west facades of the Direccion General de Administra de Personal building.

CHAPTER 3

NON-LINEAR FINITE ELEMENT PROGRAMME

3.1. INTRODUCTION

This chapter describes aspects of the finite element package used for the non-linear analysis of reinforced concrete structural walls. The concrete model adopted into the package and the factors affecting the non-linear predictions of the programme are presented. Results of past experimental investigations were used to validate the programme and to illustrate its capacity for realistic, simple and accurate predictions of structural behaviour for a wide variety of reinforced concrete structural walls.

3.2. NON-LINEAR FINITE ELEMENT ANALYSIS PROGRAMME

3.2.1. DESCRIPTION OF THE NON-LINEAR FINITE ELEMENT SYSTEM

A linear finite element analysis package called FINEL, developed in the Department of Aeronautics at Imperial College (Hitchings, 1981), was adopted as the finite element analysis framework. It is a flexible programme which provides a reliable package for structural analysis and can be easily extended to include additional facilities (e.g. new types of elements, material properties, non-linear techniques etc.). The "standard" version of FINEL provides the user with the possibility of performing several types of analysis using an extensive choice of elements. It basically consists of a set of routines (modules) and a large data storage device (database). The execution of the whole programme is controlled by a main routine which first reads the input data, then brings into operation each module in turn. Data can be easily transferred to or from the database by a "shuttle" routine, accessible by any routine, from any module, at any stage of the execution process.

Finite Element Mesh

The modelling of most reinforced concrete structures, which can be reduced to a two-dimensional problem of plane stress or an axisymmetric case, may be achieved by means of an 8-node isoparametric element for concrete and a 3-node

bar element for reinforcing steel. The 8-node isoparametric element, is a well-tested element which can exhibit parabolic distortions along its edges, thus ensuring realistic modes of deformation in flexure. The only restriction related to its use is that the ratio of the longer side to the shorter side should not exceed 3. The 3-node bar element can only exhibit either longitudinal stiffness in plane stress applications or biaxial in-plane stiffness in axisymmetric analysis. Since it deforms following the same pattern as the 8-node isoparametric element, it ensures compatibility of deformation between steel and concrete. The only prerequisite which has to be followed is that all the 3-node bar elements must lie on the boundaries of existing 8-node isoparametric elements. This implies that the generation of the steel mesh should follow the generation of the concrete mesh.

Non-Linear Strategy

The non-linear strategy of the system involves an iterative procedure based on a linear solution technique. In this way, the previously described linear finite element analysis system (FINEL) was combined with the modified Newton-Raphson method and the residual forces concept.

The modified Newton-Raphson method adopted is an iterative scheme which incorporates a reformulation or update of the stiffness matrix only periodically (Phillips and Zienkiewicz, 1976). This proved to be a method which represents a good compromise between high convergence rates and low computing cost.

Some of the essential features of the non-linear programme in which it differs from the original linear programme are as follows:

(a) A 2 x 2 integration rule was adopted in the non-linear version since it resulted in considerable cost savings without affecting accuracy.

(b) Additional storage necessary to follow the structural response at each load level was introduced in terms of extra storage facilities. The need for such a facility is even more apparent when an incremental procedure is incorporated.

In order to maintain overall equilibrium between successive iterations while satisfying at the same time the correspondence between stresses and strains dictated by constitutive relationships, a set of residual forces is computed at the end of each iteration and stored internally as a vector of nodal forces. The calculation of residual forces also includes stress differences arising from cracking of concrete and/or yield of reinforcement bars.

Convergence criteria try to keep the stress differences generated from the constitutive relationships and equilibrium within limits. They are expressed in terms of stress differences $\Delta\sigma$. The adopted double criterion is as follows:

$$|\Delta\sigma| \leq 0.1 \text{ MPa and } |\frac{\Delta\sigma}{\sigma}| \times 100 \leq 1.$$

When the convergence criteria are eventually satisfied at a given iteration, an increment of external loading can be added to the vector of the nodal forces, in an attempt to find an acceptable solution at a higher load level. By alternating iterations and incrementations of external load, it becomes possible to follow a monotonic load path up to the overall failure of the structure.

3.2.2. MATERIAL NON-LINEARITY

An extensive concrete testing programme concerned with uniaxial, biaxial and axisymmetric triaxial stress states was the base of the constitutive relationships for concrete. They are valid for concretes over a range of uniaxial cylinder compressive strength (f_c') from 15 to 65 MPa and can predict concrete response under both loading and unloading conditions. They include analytical descriptions of the deformational behaviour and of the variation of ultimate strength level of concrete in stress space.

The formulation of the analytical expressions has been based on two fundamental observations which were made during the above testing programme. The first concerns the stress–strain behaviour of concrete. It was shown experimentally (Kotsovos, 1974) that only the branch of the stress–strain relationship of concrete up to a level of stress close to, but not beyond, ultimate strength describes material behaviour. The descending branch appears to merely represent secondary testing procedure effects arising from the interaction between the concrete specimen and the testing platens. Experiments (Kotsovos, 1983a) show that as these effects are reduced the descending branch becomes steeper and if they are eliminated a complete and immediate loss of load–carrying capacity takes place.

The second observation is associated with the fracture processes which the concrete undergoes under increasing load. This internal fracture process was identified to be responsible for the non–linear behaviour of concrete under increasing stress. Non–linear behaviour is mainly dictated by structural changes which occur in the form of crack initiation and propagation processes which have the following effects on the material deformation:

Effect A : cracking causes a reduction of the high, predominantly tensile stress concentrations existing near the crack tips. This reduction can be assumed equivalent to the application of an effective compressive stress which tends to reduce the volume of concrete.

Effect B : cracking produces voids which tend to increase the volume of the material.

The combination of effects A and B results in the 3 stages of cracking process summarized in Figure 3.1. The figure also illustrates that the tensile strain (orthogonal to compressive stress) increases at a much higher rate than the compressive strain when the stress exceeds a level close to the ultimate strength. This stress level corresponds to the minimum volume level and has been observed to mark the onset of unstable fracture propagation (OUFP).

The deformational response of the concrete is therefore resolved into a linear elastic component (recoverable during unloading) and a non-linear permanent component representing the effect of the fracture processes occurring at the microscopic level under increasing stress. The constitutive model used for concrete is described in detail elsewhere (Kotsovos, 1980).

Another important material non-linearity is the postyield behaviour exhibited by steel bars. As for concrete, the constitutive relationships describing the strength and deformational behaviour of steel were introduced in a specific routine. The constitutive relationships which were adopted for the steel bars were based on the British Code of Practice (1985) and are illustrated in Figure 3.2.

3.2.3. NUMERICAL MODELLING OF CRACKING

The numerical treatment of concrete cracking, as expected, is the most influential non-linear aspect in the numerical modelling of concrete structures. The numerical representation of cracking adopted by the programme is the "smeared" crack approach. This method allows for the change in geometry and structure stiffness through a description of the effect of macrocracking on the stress conditions in the region where macrocracks occur. The other alternative was the use of the "discrete" crack approach, which requires the use of a criterion for crack extension dependent on the geometry of the crack tip and the material characteristics in the vicinity of the crack tip. Since both these items were difficult to establish, the smeared crack approach was used in view of the

availability of a criterion for cracking derived from the available experimental information, the generality in its application and the relative simplicity of implementation.

The common criticism to the adopted method is that it leads to predictions which are dependent on the finite element size. However, it was found by Bédard (1983), that provided the smallest finite element size implemented in the analysis of concrete structures is greater than 2 to 3 times the maximum size of aggregate used in the concrete mix, this dependence is negligible.

Before the appearance of any crack, the state of stress is isotropic. By the onset of cracking, the state of stress is assumed to change from biaxial to uniaxial since a crack is considered to form in the direction of the maximum principal compressive stress (i.e. orthogonal to the maximum principal tensile stress). An anisotropic state of stress now exists and is described in terms of stress and strain components which act across and along the crack. Up to now, cracking has been associated with loss of stiffness in one direction only. Under increasing load, a second crack can occur i.e. the failure criterion is fulfilled for a second time. This results in the complete loss of the load-carrying capacity of concrete and is treated numerically by equalling the material property matrix to zero. It should be noted that local failure represents only a material failure at one integration point, and does not also mark structural failure.

Since the smeared crack approach spreads the effect of cracking over a region which exceeds the localized region where bond slip actually occurs, the assumption of perfect bond is considered to describe sufficiently the interaction between concrete and steel. Furthermore, the experimental work of Labib and Edwards (1978) indicates that tensile strength of concrete is smaller than bond strength. Numerical examples carried out by Bédard (1983), also demonstrate the validity of the above assumption.

3.2.4. MATERIAL AND PROCEDURAL FACTORS INFLUENCING NON-LINEAR PREDICTIONS

The previous sections dealt with the general description of the non-linear finite element system, the material non-linearities involved and aspects of the numerical modelling of cracking. A number of additional factors affecting the non-linear predictions will be discussed herein.

An important feature of the modelling of the fracture process in concrete lies in the numerical procedure associated with the rate of crack propagation. The criteria for cracking are usually fulfilled at more than one Gauss point location during a particular iteration. The non-linear programme used by the author follows two numerical procedures to deal with crack propagation. They are termed total crack procedure and single crack procedure. The total crack procedure proved to be suitable for any type of plain concrete structural form. It comprises the occurrence of a crack at all locations where the criteria for the onset of cracking are satisfied during a particular iteration. An update of the global stiffness matrix is carried out after each iteration during which cracking occurs. After the last cracks have formed, one update followed by four iterations and one further update are automatically imposed.

In reinforced concrete structures, the presence of embedded reinforcing bars significantly retards the crack propagation process. The single crack procedure proved suitable in this case. It allows the occurrence of only one crack at the Gauss point where the stress conditions are the most critical during a particular iteration. An update of the global stiffness matrix is imposed after four cracks have occurred consecutively. After the last crack has formed at a given load level, three iterations and one update are imposed to ensure that the stiffness matrix reflects the actual state of cracking and that convergence is reached before adding load.

After cracking has occurred at a Gauss point, the orientation of the principal stresses does not in general coincide with the orientation of the existing crack. Therefore, some transfer of the force across the crack surfaces is required. The transfer of the shear component of this force through "cracked" concrete is accounted for by multiplying the shear modulus of the "uncracked" concrete by a factor α. The value of this factor cannot be zero since this would create unrealistic displacements orthogonal to the crack. Neither can it be one since this assumes that the shear stiffness is unaffected by cracking. A value of 0.1 was adopted in the validation examples and parametric study since (a) at the time of cracking significant friction cannot exist along the crack faces since the crack is aligned in the direction of principal compressive stress and (b) under monotonically increasing load, cracks should open up reducing any possibility of friction between crack faces.

Many investigators use a finer finite element mesh in zones of the structure where localized effects take place. In this way, they can sometimes achieve a more accurate prediction of experimental results. However, their numerical

solution usually lacks generality, since it is successful for a certain structural form subjected to certain loading conditions. In addition no mathematical criteria exist which can determine in advance the size of a finite element mesh necessary to achieve a given level of accuracy. Therefore, the use of a regular grid over all the structural forms becomes the most appropriate proposal for defining the finite element mesh emphasizing, at the same time, the role of engineering judgement in the final assessment. Such a coarse finite element mesh will be used for the numerical examples of the following section and the parametric study of the next chapter.

Another procedural factor affecting non-linear predictions is the load path dependency. Previous runs with the programme have pointed out that load step size has not appeared to influence the quality of predictions produced by the analysis. It is apparent that smaller load step sizes tend to slow down the rate of crack propagation and larger load step sizes may destabilize the numerical solution, but the effect on the predicted ultimate load appears to be small for practical purposes. For the sake of simplicity and consistency, a load increment equal to approximately 5 percent of the ultimate load was undertaken per load step in each run before the structural wall had reached its ultimate loading stage, both in the validation case studies and the parametric study.

3.3. ANALYTICAL MODELLING OF REINFORCED CONCRETE WALLS

The procedure adopted for the analysis of R.C. structural walls subjected to combined vertical and horizontal loading assumes plane stress conditions and homogeneous material behaviour.

The finite element mesh adopted to represent the structural walls is a simplified grid of 7 x 7 concrete elements with steel bar elements lumped at discrete locations corresponding to the boundaries of the concrete elements. Therefore, even if the original structure had a denser arrangement of reinforcement mesh, the equivalent steel area of the flexural reinforcement and confinement of the edge members was placed at the boundaries of the two extreme columns of concrete elements, while the appropriate area of steel corresponding to the horizontal and vertical web reinforcement was arranged at the boundaries of the intermediate concrete elements. Base fixity boundary conditions were achieved by fixing the degrees of freedom of the nodes of the corresponding mesh.

In all the experiments a top beam or a top slab acted as the distributor of

the applied vertical and horizontal loading. Therefore, the edge pressure load type was selected from the FINEL load library. It applies a uniformly distributed edge pressure or traction to a series of elements. In the particular case of the analytical study of the behaviour of R.C. structural walls, constant traction simulated the constant applied vertical load, and/or the weight of the heavy top slab or beam, and edge pressure simulated the incrementally applied horizontal load on the wall up to failure. The choice of the horizontal load-step size was based on the accuracy required to predict the maximum horizontal load carrying capacity of the structural wall. For the structural walls investigated, between 15 and 20 load steps were undertaken in each run before the wall had reached its ultimate lateral load.

The non-linear finite element system is also equipped with an automatic post-processing plotting package which stores the displacement components of the nodes per load step as well as information on the patterns of concrete cracking and steel yielding. Cracking is indicated by short straight lines oriented along the direction of the crack and centred at the relevant Gauss point where the criterion for the onset of cracking is met. A single line indicates a crack that occurred at a previous load stage, while two closely spaced parallel lines indicate a crack that occurred at the current load stage. Intersecting lines indicate a complete loss of load carrying of the concrete at the location of a given Gauss point. Steel yielding is indicated by black dots at the Gauss points of the steel elements.

3.4. VALIDATION OF THE NON-LINEAR SYSTEM

3.4.1. INTRODUCTION

The reliability of the non-linear finite element program, briefly described in Section 3.2, has been illustrated by means of twenty case studies (Kotsovos, 1984 and 1986; Kotsovos et al. 1985; Bédard et al. 1985 and 1986) involving both plain and reinforced concrete structures for which the experimental behaviour was known. The procedure was found to yield close predictions of strength, deformation and cracking process of the structural forms analysed. The investigations included cases studied using either plane stress analysis or axisymetric analysis such as the response of reinforced concrete beams in shear and flexure, reinforced concrete deep beams with and without web openings and web reinforcement, reinforced concrete shear panels, plain concrete hollow sphere under hydrostatic pressure, eccentrically loaded plain concrete prisms, reinforced concrete slabs and other applications.

The case studies presented in this section have been chosen in order to

validate the performance of the non-linear finite element system on twelve reinforced concrete structural walls with various geometric and material properties subjected to combined loading conditions. Analyses has been carried out for typical reinforced concrete structural walls representing the critical storey element of a structural wall system and for which adequate experimental information is available.

3.4.2. DETAILS OF THE CASE STUDIES

The following experimental information is necessary for the analysis; geometric properties, the uniaxial compressive concrete cylinder strength, the strength characteristics of the reinforcement, the arrangement and amount of the reinforcement, the loading conditions and the boundary conditions.

The walls investigated had rectangular, barbell or flanged cross-section, height to width ratio varying from 0.25 to 2.4 and thickness to width ratio varying from 0.04 to 0.10. The ultimate strength of the reinforcement varied from 510 to 765 MPa, while the uniaxial compressive cylinder strength of concrete varied from 28 to 55 MPa. The experimental data were the results of tests on walls carried out at the Portland Cement Association, Skokie, Illinois, at the Institut für Baustatic und Konstruction, Zürich, Switzerland and at the Structures Laboratory of the University of Toronto, Canada.

Table 3.1 summarizes the geometric and material properties of the test specimens analysed using the non-linear finite element program, together with information related to the amount and arrangement of reinforcement and the presence of any vertical load.

The correlation between predicted and experimental values is based on the following aspects of structural behaviour :

(a) the maximum horizontal load carrying capacity of the structural walls;

(b) the crack pattern up to the above level;

(c) the horizontal load-top horizontal displacement curve from zero to ultimate load.

No attempt has been made to correlate analytical values with values which were not measured in the experiments. The above three aspects of experimental evidence are selected since they are derived from direct measurements, descriptions of the observed behaviour and photographs at ultimate load stage incorporated in the references.

It should be noted that the analytical equivalent to the ultimate load measured experimentally, is the maximum load level for which the numerical solution stabilizes (i.e. convergence criteria mentioned in Section 3.2.1) and for which realistic deformed shape plots can be obtained.

As already mentioned the adopted 'smeared crack' representation will model discrete physical cracks by spreading their effect over part of a concrete element related to a given integration point. Therefore each crack represented on the plots stands for fissures covering one quarter of each 8-node isoparametric element. Consequently, such cracks cannot possibly be compared to single experimental cracks. However, crack patterns are expected to compare to each other, although crack patterns predicted analytically are usually more extensive than their experimental counterparts.

Differences between analytical and experimental load-displacement curves are also expected, especially in the recording of displacement after yielding of the vertical bars of the tensile part of the wall since cracking, and thus displacements, are time-dependent phenomena. In the analytical procedure, the numerical system is stable and the displacement value is unique.

Table 3.2 includes the measured ultimate strength values of the walls together with the corresponding values predicted by the present numerical scheme.

3.4.3. PRESENTATION OF RESULTS AND DISCUSSION

Behaviour of Structural Walls with Height to Width Ratio of 2.4

The examples of reinforced concrete structural walls with height to width ratio greater or equal to two are the structural walls B2, B4 and B5 tested by Oesterle et al, 1980, at PCA. As Table 3.1 illustrates wall B4 has less vertical flexural and horizontal reinforcement from the other two and is the only one tested under monotonic loading. The experimental results for wall B4 are used in order to validate the finite element model.

Figure 3.3 shows the testing set-up for this series of experiments and the finite element mesh adopted for the numerical scheme. The size of each load step was equal to 28.65 KN. Up to load step 4 (114.6 KN) no crack had formed, but then the first horizontal cracks appeared at the bottom tensile area of the wall. At load step 6, (171.9 KN) inclined cracking appeared leading to a more pronounced drop of stiffness as shown in Figure 3.4(a), which depicts the analytical horizontal load versus top horizontal displacement curve. The tensile reinforcement started to yield when the horizontal load reached 286.5 KN (load step 10), while at load step 13 (372.5 KN) a number of steel bars yielded, concrete lost its load-carrying capacity in the region of the deepest macrocracks adjacent to the tension reinforcement and at one point the steel bar reached its ultimate strength in tension. Figure 3.4(b) illustrates the deformed shape (displacements magnified by 20) and crack pattern at the ultimate horizontal load predicted by the analytical scheme. The correlation in terms of ultimate load with the experimental value of 345 KN is excellent. The observed behaviour and cracking pattern of the tested wall, described in the relevant reference is also accurately predicted by the model.

Walls B2 and B5 were also analysed using the numerical scheme, despite the knowledge that they were experimentally subjected to cyclic loading. Due to higher amounts of flexural reinforcement both walls were subjected to higher shear stresses which led to different experimental failure mode than the one observed in the former wall. Capacity of the specimens was limited in this case by "crushing" of the concrete in the compressive zone. As described in the literature review (Chapter 2) monotonic loading offers an upper bound for the ultimate horizontal load level attained by the wall when subjected to cyclic loading. Since analytical predictions are based on monotonic loading of R.C. structural forms, they are expected to be a fraction higher. Nevertheless, they may give an indication of the reliability of the predicted load-carrying capacity of walls with same geometric properties but different reinforcement percentages (see Table 3.2). The pattern of cracks and the subsequent failure mode, as well as the maximum horizontal load predicted by the analysis, were in good agreement with the experimental observations.

Behaviour of Structural Walls with Height to Width Ratio of One

The validation examples of reinforced concrete structural walls with height to width ratio of one include the behaviour of walls tested in two different experimental programmes. Walls SW7, SW8 and SW9 are three of the specimens tested in Portland Cement Association by Cardenas et al (1980), while walls S4, S9, S10 are three of the walls tested in the Structural Laboratory of the University of

Zürich by Maier et al (1985). All tests describe the behaviour of structural walls under monotonic loading. Table 3.1 includes all information with respect to data needed as input to the analytical procedure. It should be noted that the experiments in Zürich included the additional parameter of the constant vertical load applied before horizontal loading. Despite the differences in the arrangement of the reinforcement between the above walls and those discussed previously, the same simplified finite element mesh of 7 x 7 concrete elements was used in both cases.

With respect to the specimens selected from the PCA experimental investigation, specimens SW7 and SW8 contained close to the minimum amount of horizontal reinforcement specified by the ACI code (1983), while for specimen SW9 the amount of horizontal reinforcement was equal to 1%. Vertical reinforcement was distributed uniformly, in all specimens except SW7, in which one-third of total vertical reinforcement was concentrated within a distance equal to one tenth of the wall width from either extremity of the cross-section.

Figure 3.5 shows the nominal dimensions and reinforcement details of the test specimens together with photographs of the specimens after testing. Figure 3.6 contains representations of the magnified deformed shape of the wall SW9 (displacement magnification factor is 20) at

(a) crack initiation (Load step 2 : 83.8 KN);

(b) significant inclined cracking formation (Load step 6 : 251.4 KN);

(c) one load step before the ultimate load level (Load step 15 : 628.7 KN).

Figure 3.6(a) exhibits the initiation of typical flexural cracking of walls at low load levels. The early inclined cracking and the extensive flexural and inclined cracking of the wall are shown in Figures 3.6(b) and 3.6(c) respectively.

Figure 3.7 shows the typical macrocrack pattern and deflected shape at the maximum horizontal load sustained by walls SW8 and SW9. The figure indicates that wall SW8 suffered extensive inclined cracking and yielding of some of the horizontal reinforcement. A characteristic feature of the failure mode of this wall is the complete loss of load carrying capacity of the concrete at a point in the region of the tensile zone. A comparative look at Figures 3.6(c) and 3.7 shows that failure of wall SW9 occurred due to extension of the macrocracking into the compressive zone and near vertical splitting of this zone in the region of the wall base. A similar splitting is also noticeable in the final analytical loading step of

wall SW8 which incorporates nominal horizontal reinforcement. In all the photographs in Figure 3.5 almost vertical splitting of the lowest part of compressive zone is evident. However, the almost minimum percentage of horizontal reinforcement should be considered responsible for the further post-failure widening and propagation of the inclined crack in walls SW7 and SW8, while in wall SW9 splitting zone extended on a horizontal plane near the base of the wall, as shown in Figure 3.5, since the higher amount of horizontal reinforcement prevented the crushing from propagating to the wall's web. A similar macrocrack pattern at maximum horizontal load to SW9, was also observed in wall SW13 which was subjected to horizontal load reversals. Cardenas et al (1980) report that load reversals had not affected the ultimate behaviour of the wall and only resulted in a 7 percent drop in ultimate horizontal load capacity.

Figure 3.8 presents both the experimental and analytical horizontal load - top horizontal displacement curve of wall SW9. The correlation in terms of ultimate horizontal load is excellent, while the figure also indicates realistic displacement predictions. A source of difference between experiment and analysis in the recording of displacement should be due to the time dependent displacement of the experimental structural element (also termed "second order" displacement) as well as the inherent microcracking of the test specimen due to shrinkage. The combination of both might have resulted in less stiff response by the specimen and in higher levels of experimental displacement compared with the analytical predictions. Table 3.2 points out the very good agreement between measured and predicted values in terms of ultimate horizontal load carrying capacity of the above walls.

Wall specimens S4, S9, S10 of the experimental investigation carried out in Zürich, all had rectangular cross-section and were subjected to monotonic loading up to failure. In particular, specimen S9 incorporated no horizontal reinforcement to carry any of the shear stresses induced in the specimen and walls S4 and S10 maintained the same amount of horizontal reinforcement while the amount of flexural reinforcement concentrated in the edges of the wall varied considerably.

The measured ultimate strength values of 342 and 393 KN for walls S9 and S4 respectively correlate closely with the analytically predicted values and indicate that not only is an element without horizontal reinforcement capable of withstanding a much higher horizontal load than that predicted by any current Code, but also that the influence of the horizontal reinforcement on the maximum horizontal load is minimal and by no means follows the truss analogy formula. The amount of horizontal reinforcement appears to only affect the deformational response of the

specimens. The experimental crack pattern for wall S4 at ultimate horizontal load stage in Figure 3.9(a) can be readily compared with the predicted ones in Figure 3.9(b) to show essentially the same pattern of cracks and the initiation of crushing of the compression edge corner due to the near-vertical extension of the deepest inclined crack. It should be noted that the analytical crack pattern is more extensive than the experimental one in the top corner of the compressive edge of the wall. The main reason is that the criteria for tensile concrete cracking incorporated by the analysis has already been exceeded in these points, but the crack width is not sufficiently big to make the crack visible in the experimental ultimate load level. Another reason for this minor difference in crack pattern might be accrued to the assumption of uniformly distributed horizontal load followed by the analysis. In fact, from the experimental point of view neither a top beam nor a slab can transmit the horizontal load to the wall as uniformly as is assumed in the analysis. Usually stress concentrations are higher the nearer the wall specimen is placed to load cell.

The main difference between walls S4 and S10 is the much higher amount of vertical (flexural) reinforcement in the edges of wall S10. Wall S10 was observed to withstand higher levels of horizontal load before its incipient failure resulting in a more extensive inclined crack pattern. However, the mode of failure observed in this wall follows the previously discussed principles. The predicted ultimate horizontal load value underestimates the experimentally established by 10 percent (see Table 3.2).

Behaviour of Structural Walls with Height to Width Ratio Less than One

The validation study on structural walls with height to width ratio less than one included a monotonic loading test carried out at PCA by Barda et al (1977) and two cyclic loading tests conducted at the Structures Laboratory of University of Toronto by Wiradinata et al (1986). The former wall incorporated a flanged cross-section and a height to width ratio of $\frac{1}{2}$. Two squat walls with rectangular cross-section and height to width ratio of $\frac{1}{2}$ and $\frac{1}{4}$ were the test specimens of the latter experimental programme. Table 3.1 provides all the necessary information related to geometric and material properties as well as the reinforcement percentage details of the analytically studied walls.

Figure 3.10(a) shows details of the test specimen B1-1 of the PCA investigation, while Figure 3.10(b) illustrates a representative horizontal cross-section of the test series. A simple 7 x 7 concrete element mesh was adopted for the analytical procedure as shown together with loading and boundaries conditions in

Figure 3.10(c). The two extreme rows of concrete elements represented the two flanges with their corresponding thicknesses, while the equivalent amount of vertical and horizontal reinforcement was placed at the boundaries of the concrete elements. The centre grid of 5 x 7 concrete elements represented the geometric and material detailing of the walls' web. The weight of the heavy top slab was simulated as a constant vertical load at the top of the wall. The higher stiffness characteristics of the slab compared to that of the wall were taken into account by increasing the amount of the top horizontal reinforcement.

The first observed crack occurred in the lower portion of the wall closest to the applied load at about 278 KN, and at the higher applied load level of about 506 KN several long inclined cracks suddenly covered most of the wall's web. Figure 3.11(a) and (b) show the response of the wall at load step 3 (257.2 KN) and load step 4 (342.9 KN) of the analytical run and indicate how close the predicted crack pattern is to the observed crack behaviour. The reported horizontal load level of 965 KN and 1086 KN as the yield load of the vertical and horizontal wall bars respectively also correlate closely with the corresponding analytically predicted values of 943 KN and 1028.3 KN. The predicted ultimate horizontal load level is within 9% of the experimental value for wall B1-1, as summarized in Table 3.2. Figures 3.11(c) and 3.11(d) illustrate the deformed shape representation of the wall and a photograph of the specimen respectively, at the ultimate load, indicating a close agreement of the crack pattern and the failure mode exhibited by the wall.

The wall-1 with height to width ratio of $\frac{1}{2}$, tested in Toronto, exhibited similar characteristics to the previous wall, reached a peak horizontal load of 575 KN and a corresponding top displacement of 10 mm, and showed a ductile behaviour up to this load stage. Both load and displacement measured values are in very good agreement with the corresponding analytically predicted values of 570 KN and 11.9 mm. It should be noted that despite the low level of distributed flexural reinforcement and minimum amount of horizontal reinforcement, the wall was found to be highly effective in resisting high levels of shear stresses. This might point out the need for a re-appraisal of current views of causes of failure in structural walls.

The wall-2 with height to width ratio of $\frac{1}{4}$, also tested in Toronto was reported to exhibit its first inclined crack at a horizontal load level of 233 KN, which correlated closely with the analytical value of 245 KN. At a horizontal load of 680 KN a major crack formed along the construction joint at the wall base, indicating the inability of the wall to develop its flexural strength due to excessive

sliding. The premature failure of the wall, perhaps due to out of plane instability, explains the 23% overestimate of the ultimate predicted horizontal load by the numerical scheme, since plane stress conditions were assumed by the analytical procedure.

3.5. GENERAL REMARKS AND CONCLUSIONS

The non-linear finite element system used in the analysis blends an iterative procedure, which incorporates a linear solution technique, with realistic descriptions of material characteristics such as failure criteria and deformational properties of concrete and steel, fracture processes of concrete and concrete-steel interaction. The system had already been successfully used to correlate theoretically predicted to experimentally observed behaviour of over twenty reinforced concrete structural forms.

A simple finite element mesh was adopted for the modelling of reinforced concrete structural walls. The numerical representation of cracking was based on the "smeared crack" approach, while the single crack procedure was selected to treat the rate of crack propagation in the walls.

The non-linear finite element system has been validated by comparing analytical predictions with published information obtained experimentally for a wide range of reinforced concrete structural walls. A satisfactory correlation between analysis and experiment was demonstrated for all aspects of structural behaviour investigated i.e. load-carrying capacity, deformational characteristics, crack patterns and mode of failure. The successful application of the numerical scheme to all cases investigated to date is attributed to the constitutive model of concrete behaviour which the system incorporates.

Despite the minimum percentage of horizontal reinforcement incorporated in a number of walls, both experimental and analytical results indicate that these walls can resist high levels of horizontal load without failing. The above conclusion points out the need for re-appraisal of the code provisions dealing with the ultimate load-carrying capacity of walls.

The predicted mode of failure is characterised by longitudinal cracking within the compressive zone near the base of the wall where the flexural moment attains its maximum value. Similar cracking was observed in a number of photographs showing the analysed test specimens at the ultimate horizontal load stage.

It is apparent that the discussed non-linear finite element programme may be used to carry out a comprehensive analytical investigation of structural wall behaviour.

SPECIMEN	REFERENCE	HORIZONTAL CROSS SECTION	$\frac{h}{l}$	$\frac{b}{l}$	AXIAL LOAD (KN)	f_c' (MPa)	fsy (MPa)		REINFORCEMENT PERCENTAGE %			
							VERTICAL BARS	HORIZ. BARS	Pflex	Phor	Pver	Ps
B2*	Oesterle et al (1980)	barbell	2.4	0.053	none	53.6	410.3	no inform.	3.67	0.63	0.29	—
B4		barbell	2.4	0.053	none	45.0	450.2	no inform.	1.11	0.31	0.29	1.28
B5*		barbell	2.4	0.053	none	45.3	444.0	no inform.	3.67	0.63	0.29	1.35
SW7	Cardenas et al (1980)	rectang.	1.0	0.04	none	43.0	448.2	413.7	8.28	0.27	1.04	0.27
SW8		rectang.	1.0	0.04	none	42.5	448.2	465.0	4.2	0.27	2.6	0.27
SW9		rectang.	1.0	0.04	none	43.0	448.2	413.7	4.2	1.00	2.6	1.00
S4	Maier et al (1985)	rectang.	1.0	0.085	262	32.9	574.0	574.0	1.05	1.05	1.05	1.05
S9		rectang.	1.0	0.085	260	29.2	560.0	—	0.99	—	0.99	—
S10		rectang.	1.0	0.085	262	31.0	496.0	496.0	5.71	0.98	1.00	0.98
B1—1	Barda et al (1977)	flanged	0.5	0.053	heavy top slab=11KN	29.0	543.3	495.8	1.80	0.50	0.50	0.80
WALL1*	Wirandinata et al (1986)	rectang.	0.5	0.05	heavy top slab=8.25KN	25.0	435.2	424.0	0.80	0.25	0.80	0.25
WALL2*		rectang.	0.25	0.05	heavy top slab=8.25KN	22.0	435.2	424.0	0.80	0.25	0.80	0.25

*cyclic tests

Table 3.1. Material properties and geometric characteristics for the wall specimens analysed by the non-linear finite element system.

Table 3.1 Cont'd

NOTATION

fc' :cylinder strength

fsy : yield strength

Pflex :ratio of main flexural reinforcement to gross concrete area of edge element

Phor : ratio of horizontal reinforcement to gross concrete area of vertical section of wall web

pver : ratio of vertical web reinforcement to gross concrete area of horizontal section of wall web

ps : ratio of effective volume of confinement reinforcement to the volume of the core

SPECIMEN	ULTIMATE LOAD (KN)		PREDICTED / MEASURED
	MEASURED	PREDICTED	
B2*	688.0	802.0	1.17
B4	345.0	372.5	1.08
B5*	763.0	916.0	1.20
SW7	518.7	544.8	1.05
SW8	569.4	586.7	1.03
SW9	678.8	670.6	0.99
S4	392.0	424.8	1.08
S9	342.0	339.8	0.99
S10	670.0	604.2	0.90
B1—1	1218.7	1114.4	0.91
WALL1*	575.0	570.0	0.99
WALL2*	680.0	840.0	1.23
			MEAN=1.05
			ST.DEVIAT.=0.10

*cyclic loading test

Table 3.2. Measured and predicted values of ultimate horizontal load of the walls investigated in the validation study.

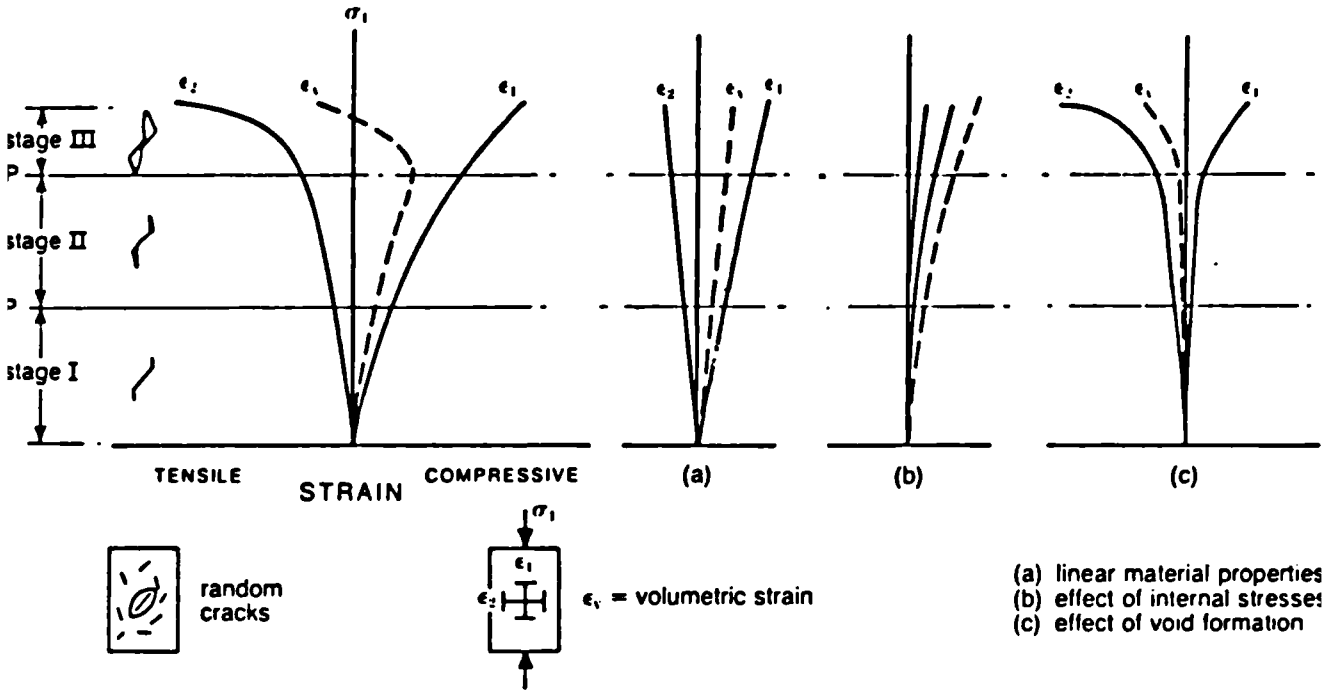


Fig. 3.1. Effect of cracking process on deformational response of concrete.

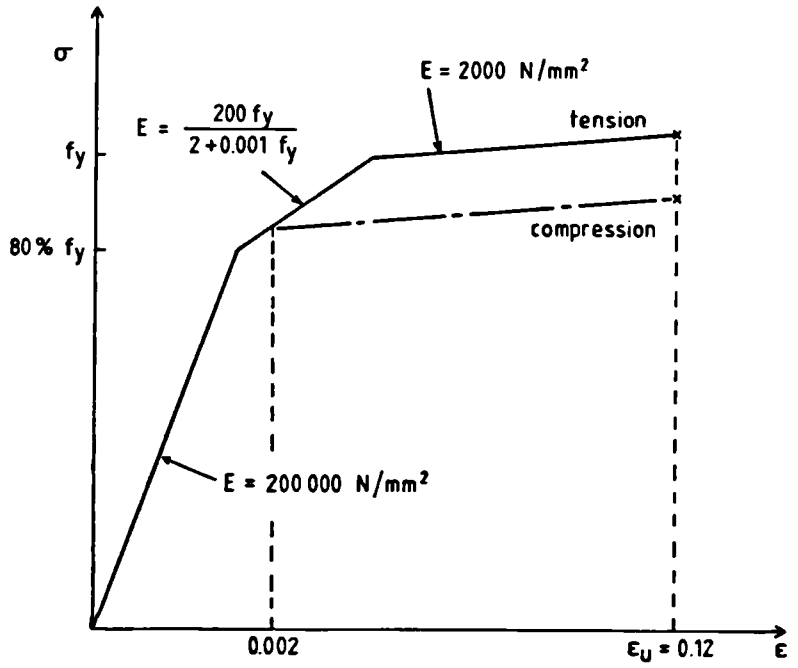
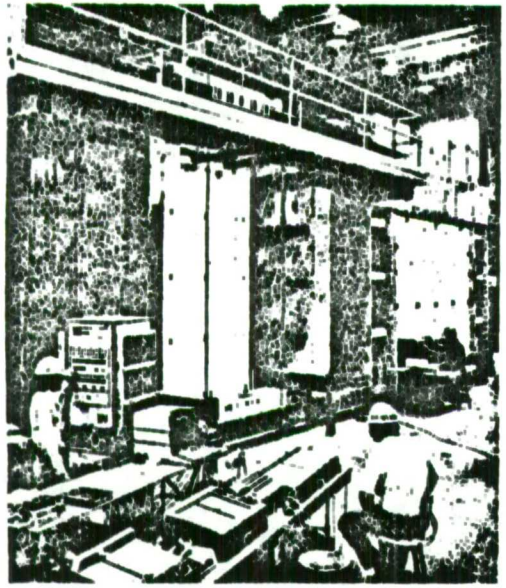


Fig. 3.2. Constitutive relationships for steel bars.

(a)



(b)

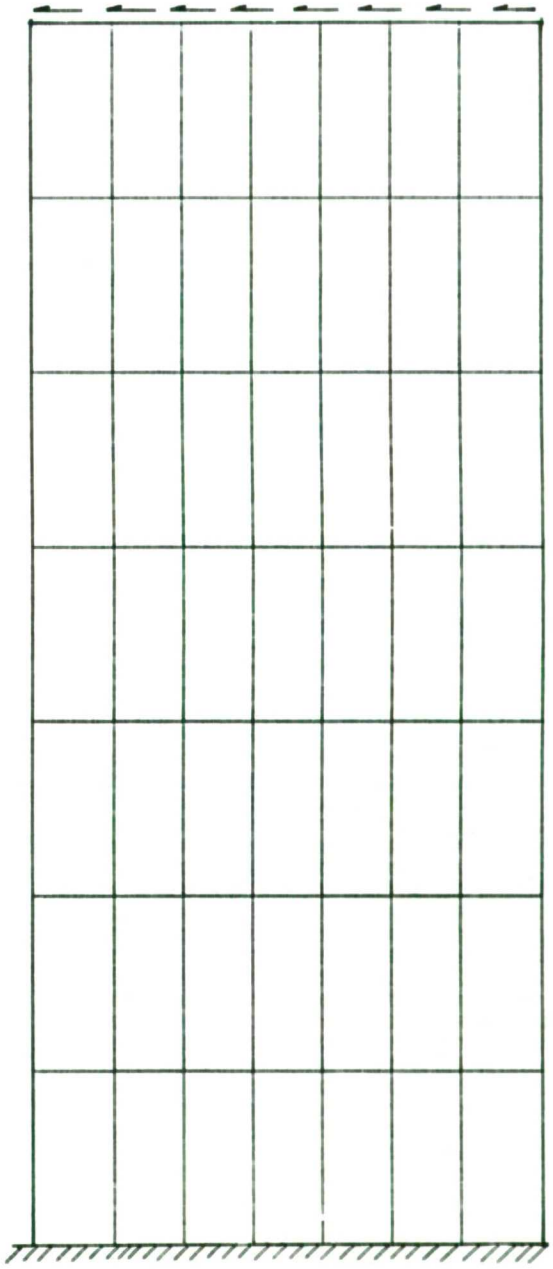


Fig. 3.3. (a) Testing set-up for the experiments of Oesterle et al (1980).
(b) Finite element mesh adopted for the analysis.

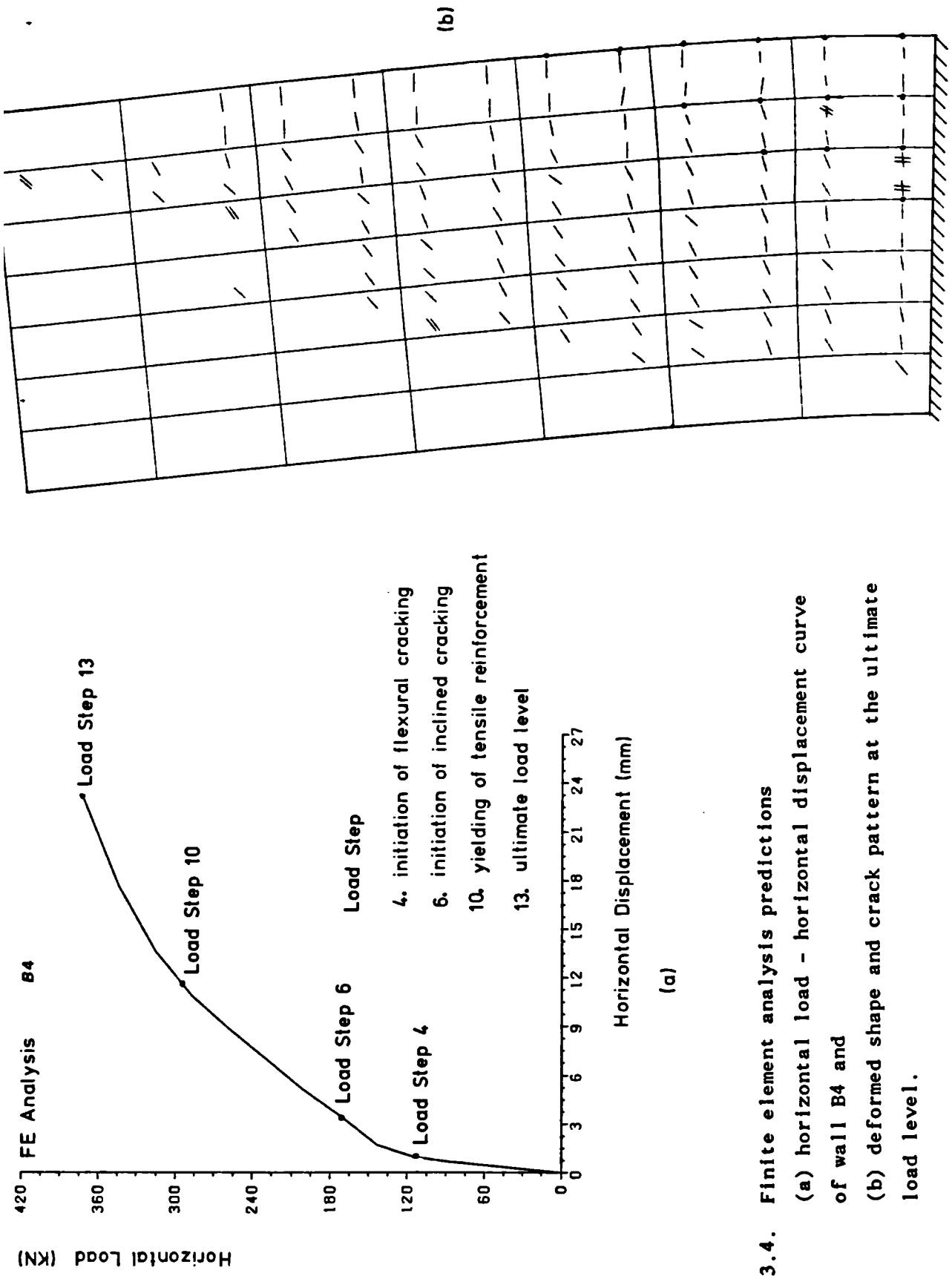
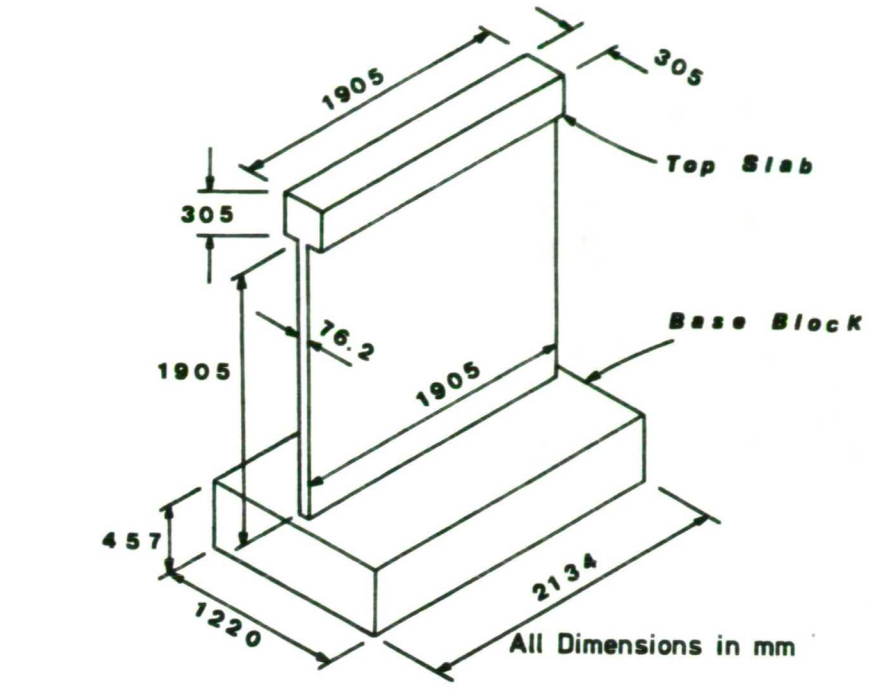
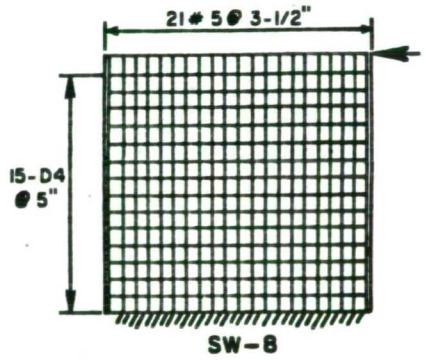


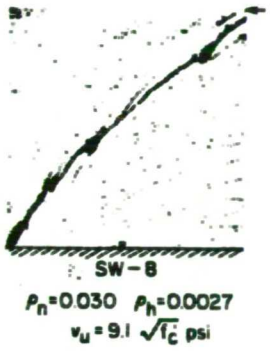
Fig. 3.4. Finite element analysis predictions
(a) horizontal load - horizontal displacement curve of wall B4 and
(b) deformed shape and crack pattern at the ultimate load level.



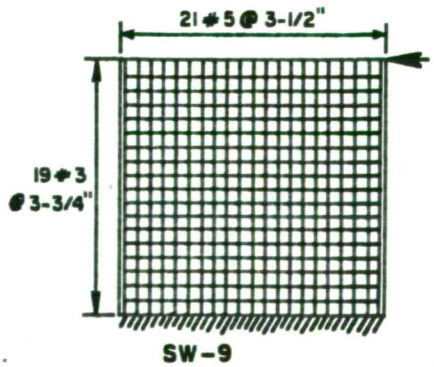
(a)



(b)



(c)



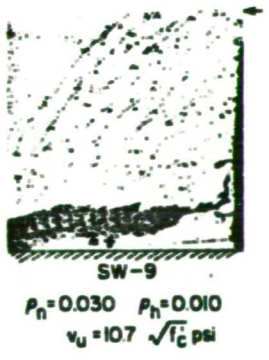


Fig. 3.5. Tests by Cardenas et al (1980)
(a) nominal dimensions, (b) reinforcement details and (c) photographs after testing of specimens SW8 and SW9.

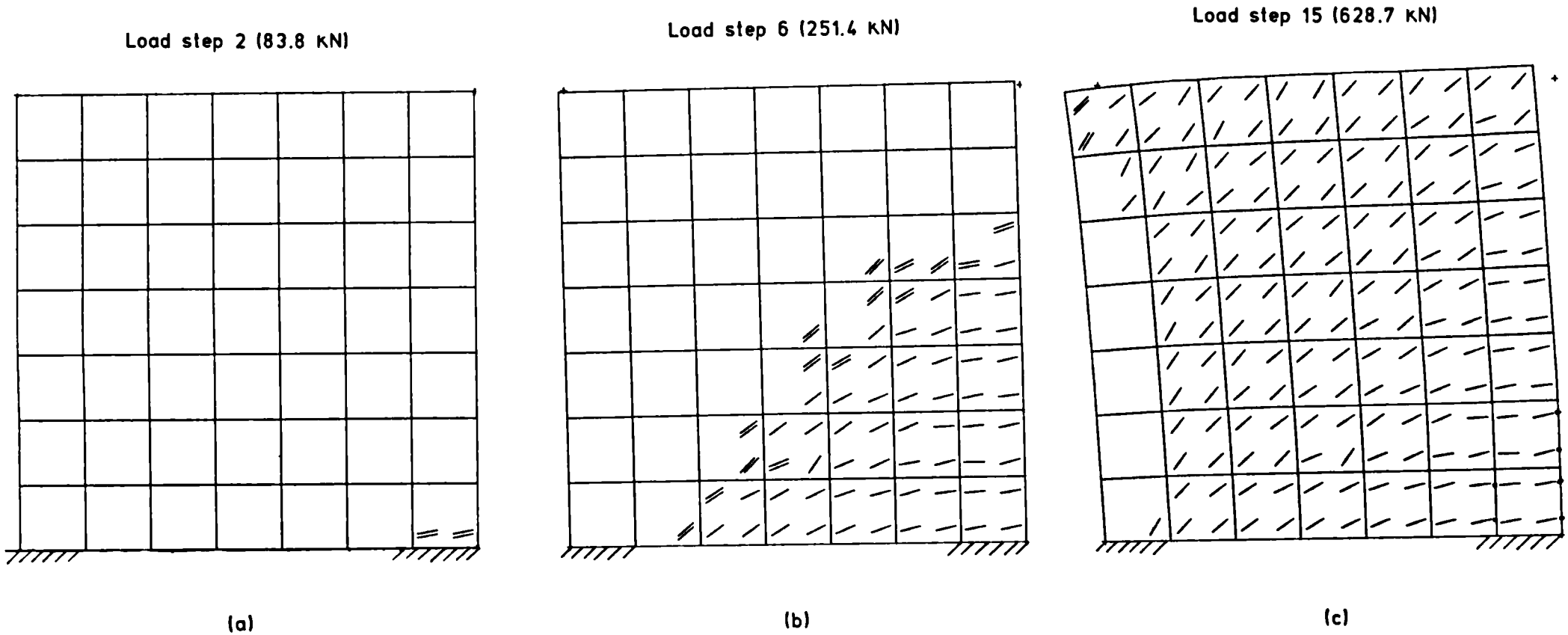


Fig. 3.6. Magnified deformed shape of wall SW9 at (a) crack initiation, (b) significant inclined cracking formation, (c) maximum sustained load.

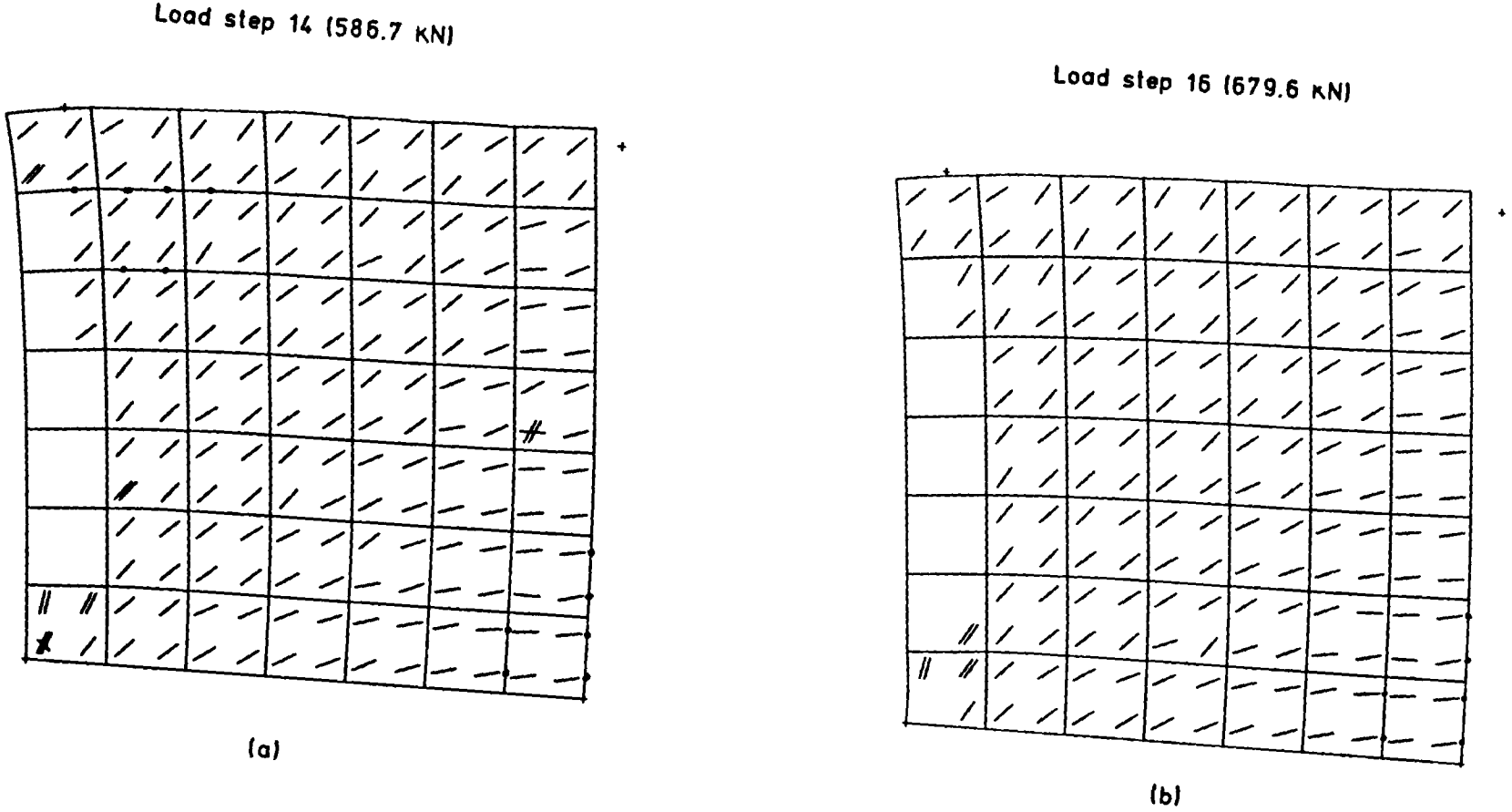


Fig. 3.7. Crack pattern and deflected shape of walls (a) SW8 and (b) SW9 at the maximum horizontal load level.

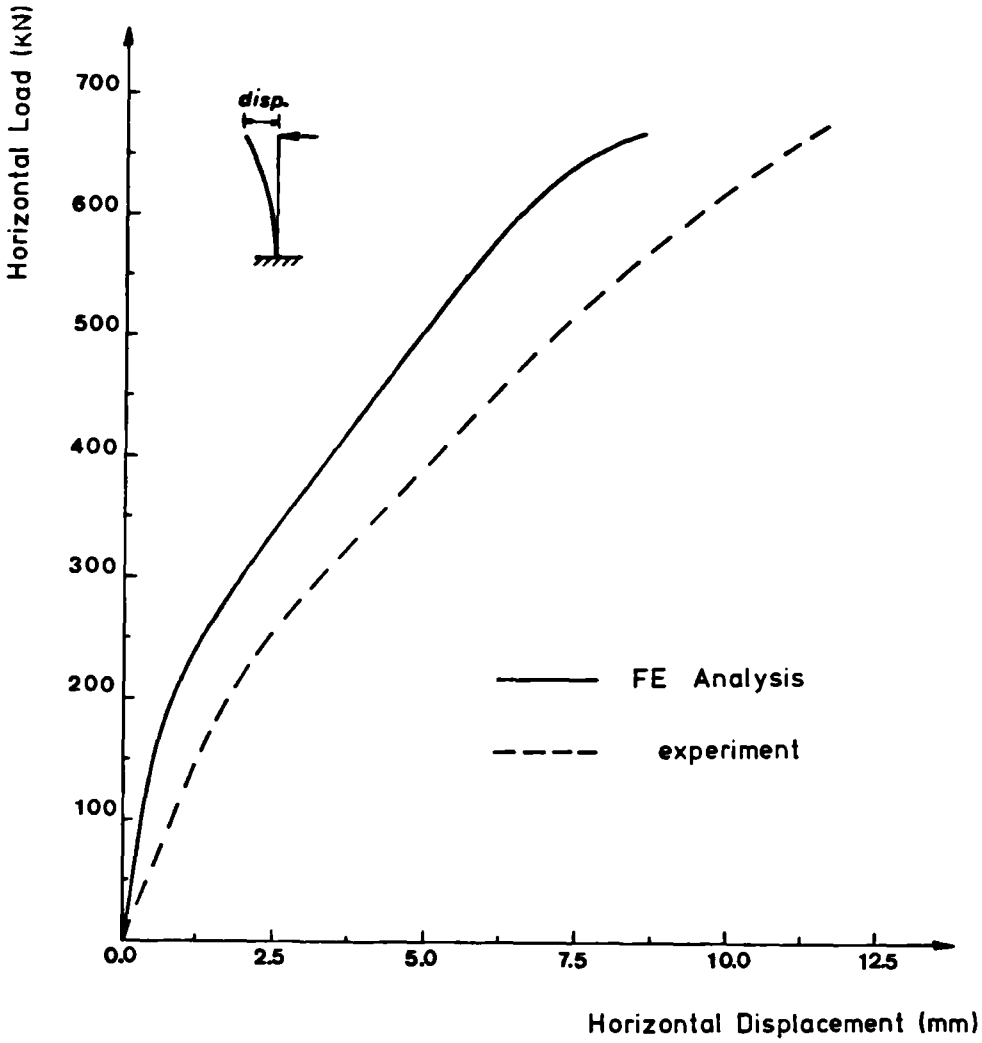


Fig. 3.8. Horizontal load-horizontal displacement curve of wall SW9.

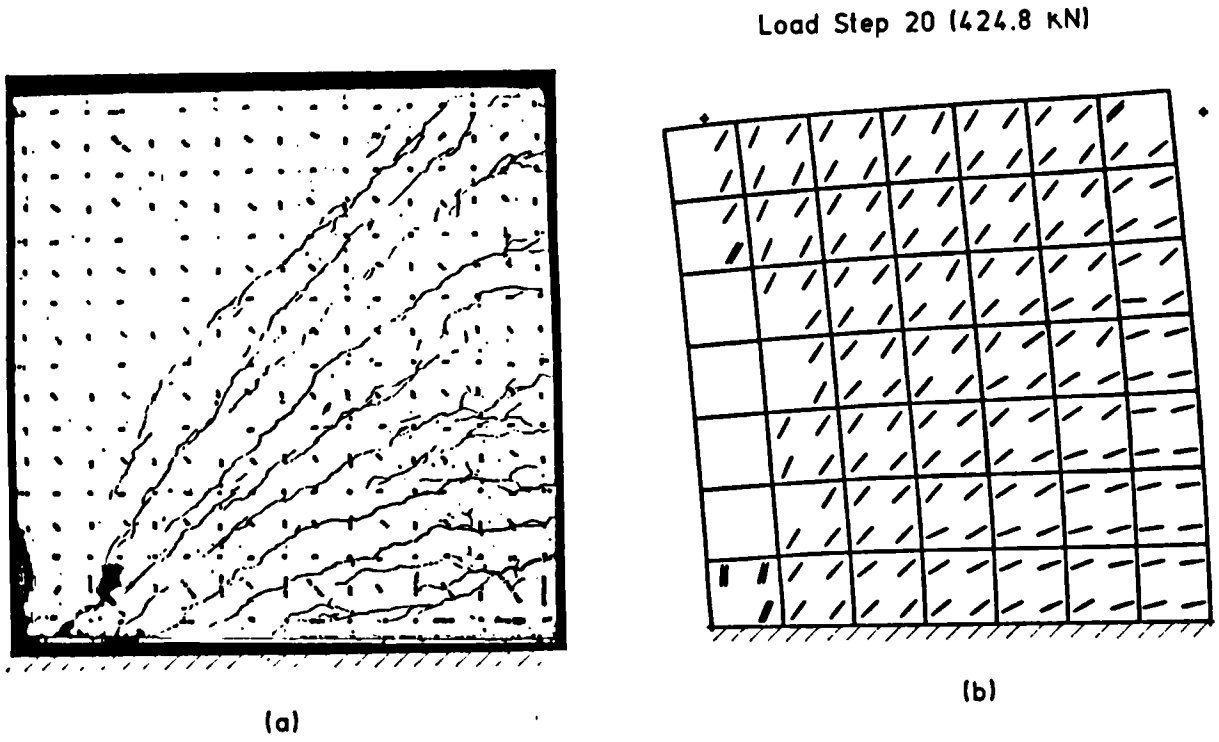


Fig. 3.9. Crack pattern and deformed shape of wall S4 tested by Maier et al (1985) at the ultimate load level (a) obtained experimentally and (b) predicted analytically.

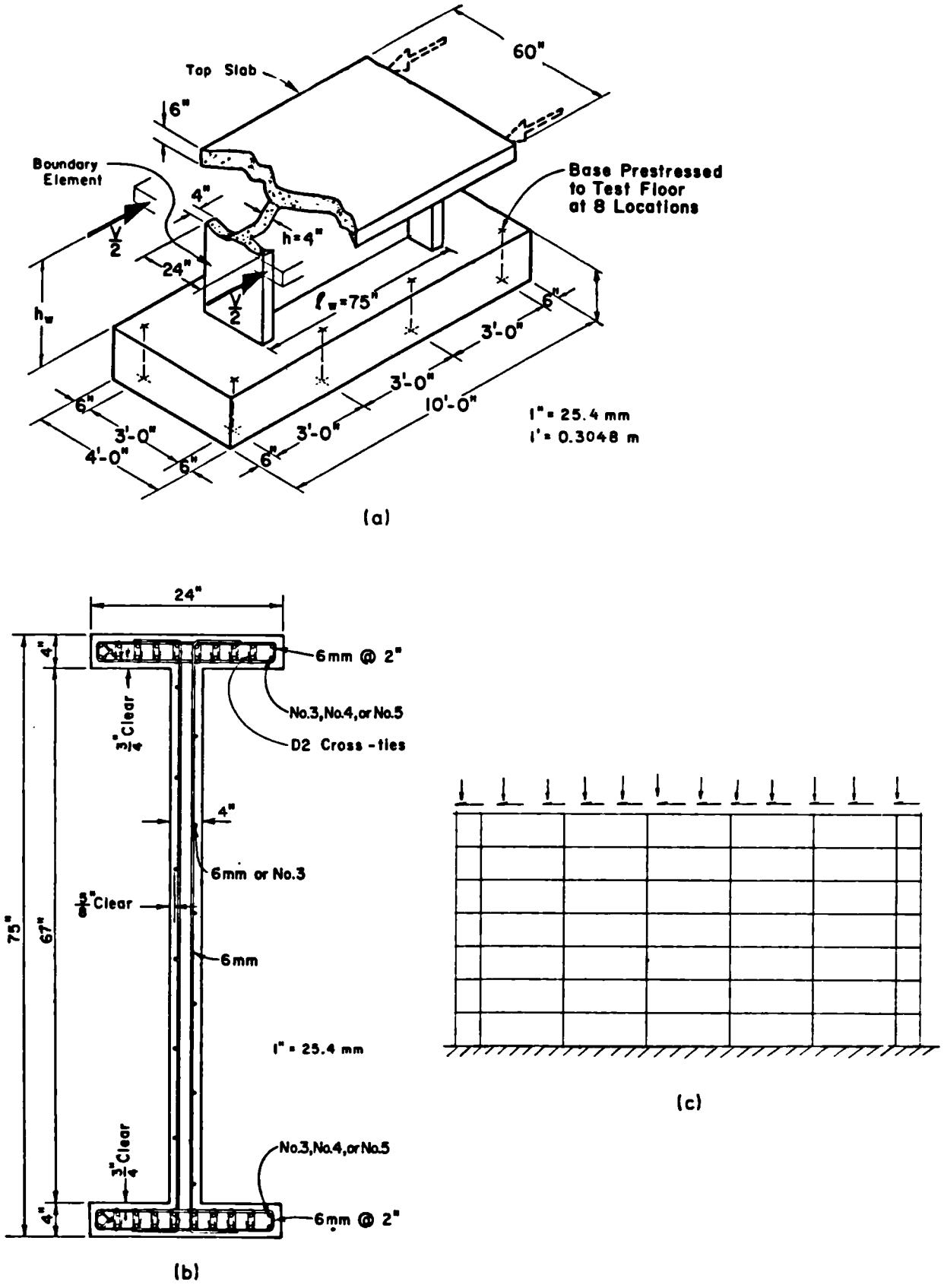
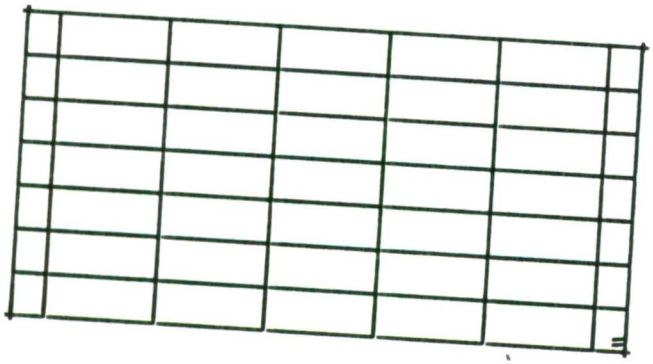
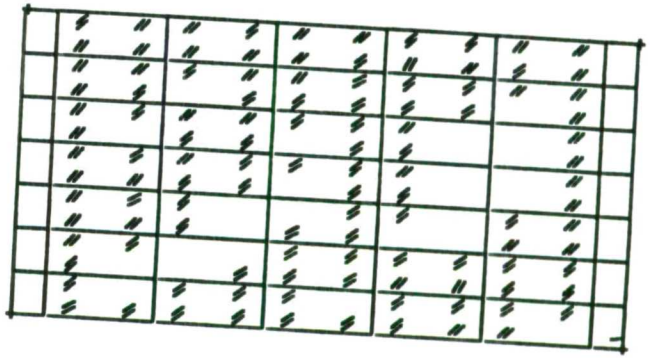


Fig. 3.10. Wall B1-1 tested by Barda et al (1977)
(a) details of the test specimen
(b) horizontal cross-section
(c) finite element mesh, loading and boundary conditions.

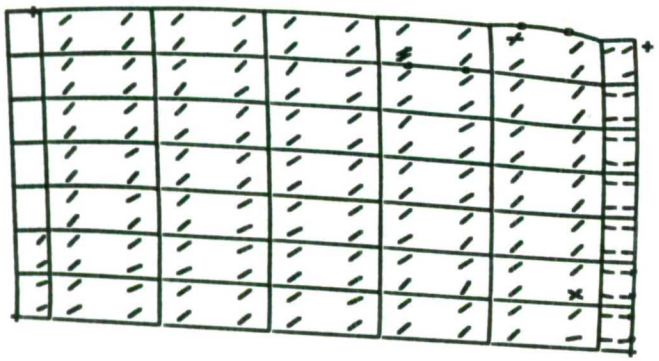
(a) Load Step 3 (257.2KN)



(b) Load Step 4 (342.9KN)



(c) Load Step 13 (1114.4KN)



(d) Mode of failure

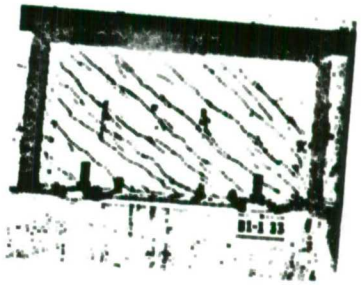


Fig. 3.11. Predicted deformational response and crack pattern at various load levels, and mode of failure established by experiment.

CHAPTER 4

PARAMETRIC STUDY

4.1. INTRODUCTION

It appears from the preceding chapters that, in order to develop a better understanding of the fundamental causes of the observed behaviour of reinforced concrete structural walls subjected to combined vertical and horizontal loading, it is essential to carry out an extensive parametric study of the variables that affect the behaviour of these walls. This chapter describes an attempt to achieve this objective by using the non-linear finite element programme discussed and validated in Chapter 3, for the analysis of a wide range of reinforced concrete structural walls. Not only is the effect of a number of variables (selected as described later) on the behaviour of the walls up to incipient failure presented and discussed, but also seismic resistant design procedures of current Codes are evaluated. Results of the analytical investigation were used to identify and quantify possible shortcomings in these procedures.

4.2. DESIGN PROCEDURES OF CURRENT CODES

Since the evaluation of the axial-flexural and shear design procedures of current Codes by means of integrated analytical studies is one of the main objectives of this chapter, it is helpful to delve a little on the main principles underlying the Code design proceedings. Therefore, this section presents an overview of the seismic resistant provisions for ultimate limit state design of reinforced concrete structural walls. The description will be focused on how unfactored axial-flexural and shear strengths are determined by Code provisions. It should be noted that as stated by Paulay, (1981), the desirable seismic resistant design philosophy for structural systems incorporating reinforced concrete walls is to assure that axial-flexural yielding controls the seismic response at ultimate limit state and that shear modes are suppressed until sufficient energy is dissipated through flexural yielding at the critical regions of the different elements of the structural system.

4.2.1. DETERMINATION OF FLEXURAL STRENGTH

Current Code (UBC 1982, ACI 1983) provisions for the design of structural members cross-section, subject to flexural or axial loads or to combined flexure and axial loads have been derived on the basis of the following assumptions:

(a) strains in reinforcement and concrete are directly proportional to the distance from the neutral axis;

(b) failure occurs when the strain at the extreme concrete compression fiber attains a limiting value (equal to 0.003 for ACI, 1983 or 0.0035 for BS 8110, 1985);

(c) below specified yield strength f_{sy}, the behaviour of reinforcement is linear and completely defined by the modulus of elasticity E_s. For strains greater than that corresponding to f_{sy}, stress in reinforcement is independent of strain and equal to f_{sy};

(d) tensile strength of concrete is neglected in flexural calculations of reinforced concrete;

(e) the behaviour of concrete in compression is defined by an idealised stress-strain relationship which defines completely the compressive stress distribution usually expressed in the form of an equivalent rectangular stress block.

As Figure 4.1 indicates, the dimensions of the rectangular stress block, adopted by the ACI Code provisions, are: (a) an equivalent concrete stress of $0.85 * f'_c$ uniformly distributed over the compression zone and (b) a portion of the depth of neutral axis $\beta_1 * c$, where β_1 a reduction factor varying from 0.65 to 0.85 according to the concrete cylinder strength f'_c. Similar design provisions can be found in all Codes.

On the basis of the above assumptions, the ultimate flexural capacity of a cantilever structural wall of rectangular cross-section and uniformly distributed vertical reinforcement, subjected to combined vertical load, bending moment and horizontal load can be approximately calculated by the expression:

$$M_{ult} = 0.5 * A_s * f_{sy} * l * (1 - \frac{c}{l}) * (1 + \frac{N}{A_s . f_{sy}}) \qquad \text{(Eq. 4.1)}$$

where A_s : the total uniformly distributed wall steel
N : the vertical (axial) load, taken as positive for compression
l : the width of the wall

The other terms have already been defined above. Figure 4.1 summarizes the main intermediate steps leading to the expression of the ultimate flexural capacity of the wall adopted by the Codes.

If most of the vertical reinforcement is concentrated at the wall edge elements then the flexural capacity of structural walls may be given by the simplified expression:

$$M_{ult} = (A_{s_{col}} * f_{sy} + N/2) * d \qquad \text{(Eq. 4.2)}$$

where $A_{s_{col}}$: Cross-sectional steel area in the wall's edge element
d : effective depth of cross-section, assumed to be the centre to centre distance between the wall's edge elements.

4.2.2. DETERMINATION OF SHEAR STRENGTH

Horizontal forces are applied to structural walls through floor slabs or beams, which distribute the shear along the side of the wall. It is generally considered and adopted by Code provisions that shear is resisted by the structural wall acting as a truss. The tensile and horizontal web reinforcements of the wall form the tensile members of the truss, while the concrete (a) in the compressive zone and (b) between the inclined cracks, forms the compression members. The truss is designed not to fail before flexural failure of the wall occurs.

On the basis of the above, the ultimate horizontal load sustained by the wall when plotted against the percentage of the amount of horizontal web reinforcement should follow a bilinear relation. The intercept of the first part of the line corresponds to the contribution of concrete to shear resistance, the inclined part of the line represents the contribution of the yielded horizontal web reinforcement, while the horizontal part of the line represents a limiting value for the shear capacity dictated by the concrete strength of the inclined struts (see Figure 4.2).

The nominal shear stress capacity of the critical cross-section of the structural wall can be determined by using the expression:

$$v_{ult} = v_c + v_s \qquad \text{(Eq. 4.3)}$$

where v_c : the shear stress contribution from the concrete
v_s : the shear stress contribution from the horizontal reinforcement

The term v_c is considered to represent the contribution to shear resistance of three separate components:

(a) shear resistance of the uncracked concrete within the compressive zone;

(b) shear resistance due to aggregate interlock developing across the inclined crack surfaces, and

(c) shear resistance due to dowel action of the longitudinal reinforcement.

With (b) and (c) assumed to provide more than 70 percent of the v_c, the value of v_c in a structural wall with horizontal web reinforcement is usually considered equal to the shear stress which causes diagonal tension failure in an identical wall without horizontal steel bars.

Both UBC (1982) and ATC 3-06 (1978) regulations incorporate a concrete shear stress contribution of $0.166\sqrt{f'_c}$ (in MPa) in which f'_c is the uniaxial concrete cylinder compressive strength in MPa. The ACI (1983) Code expressions incorporate a concrete shear stress contribution which varies linearly from $0.25\sqrt{f'_c}$ (in MPa) for wall height to width ratio of 1.5 to $0.166\sqrt{f'_c}$ (in MPa) for wall height to width ratio of 2.0.

A number of semi-rational, more detailed expressions have been developed to predict the flexural-shear cracking load of reinforced concrete structural members. The best known is the ACI Code equation for reinforced concrete developed by ACI-ASCE Committee 326, (1962).

$$v_c = 0.16\sqrt{f'_c} + 17.2\,\rho_v \frac{V.1}{M} \leq 0.29\sqrt{f'_c} \text{ (in MPa)}$$

where M and V are the moment and shear, respectively, at the point under consideration, and
ρ_v is the percentage of vertical reinforcement.

Note that as Table 4.1 below indicates, the values for v_c adopted by the ACI 1983 Code expressions form an upper bound limit to the value suggested by the above expression. Therefore, only the values given by the simplified version of v_c will be considered in the following sections of the parametric study.

$100\ \rho_v$	v_c (MPa)	
	$h/l = 2$	$\frac{1}{2} \leq h/l \leq 1$
0.5	$0.161\ \sqrt{f'_c}$	$0.175\ \sqrt{f'_c}$
1.0	$0.162\ \sqrt{f'_c}$	$0.189\ \sqrt{f'_c}$
2.0	$0.163\ \sqrt{f'_c}$	$0.218\ \sqrt{f'_c}$
3.0	$0.164\ \sqrt{f'_c}$	$0.247\ \sqrt{f'_c}$
4.0	$0.166\ \sqrt{f'_c}$	$0.276\ \sqrt{f'_c}$

Table 4.1.

The contribution of the horizontal wall reinforcement to nominal ultimate shear stress is evaluated using the expression

$$v_s = \frac{A_h}{b * s} * f_{sy} \quad \text{(in MPa)} \qquad \text{(Eq. 4.4)}$$

where A_h : the area of horizontal reinforcement (in mm^2) within a vertical distance s (in mm)
b : the thickness of the wall web (in mm)
f_{sy}: the yield stress of the reinforcement (in MPa)

The design provisions require a minimum amount of horizontal reinforcement. This amount should not be less than 0.25% of the concrete area. In walls with overall height to width ratio less than 0.5, the ACI 318-83 Code requires vertical reinforcement of the wall's web, ρ_v, equal to the amount of horizontal

reinforcement.

It should be mentioned that, since ACI 318 (1983) regulations define the effective nominal shear area as b * l (where b and l the thickness and width of the wall respectively), rather than (0.8)*b * l like UBC (1982) and ATC 3-06, they yield 25% higher shear strength.

Allowance is also made in the Codes for the contribution of axial compression in boosting the share of the concrete shear resisting mechanism, as measured by the nominal shear stress, v_c. If the effect of axial compression is taken into account in design then a term equal to (0.25) * (N/(b * l)) (in MPa, where N is the maximum applied axial load) is added to the previous expressions concerning the calculation of v_c. Codes point out that the adverse effect of vertical accelerations induced by earthquakes should also be considered. Therefore, Code expressions suggest the omission of axial compression in zones of high seismicity. In cases, where yielding of the flexural reinforcement bars is possible in both faces of the base of the wall, it is suggested that the contribution of concrete towards the shear strength should be neglected when the axial compressive stress on the gross wall area is less than 0.2 * f'_c, since this small compression might possibly be offset by vertical acceleration causing tension. This implies that horizontal reinforcement should be provided to carry the whole of the shear force over the length of the plastic hinge at the base of the wall.

The only expressions which take into account the contribution of boundary edge members of the wall in predicting their shear strength are the ones incorporated in the Japanese Code, AIJ (1980). Structural walls designed in Japan generally consist of a boundary frame with a panel wall cast in place, frequently after the frame members are built. The cracking shear for such a wall is given by

$$v_c = 0.74 + 0.015 * f'_c \quad \text{for} \quad 20.7 \text{ MPa} < f'_c < 34.5 \text{ MPa} \qquad \text{(Eq. 4.5)}$$

while the ultimate shear stress is expressed by

$$v_{ult} = v_s + \tfrac{7}{8}\, b*d\, [1.5 * v_c + 0.5 * f_{sy} * (\rho_n - 0.002)] \qquad \text{(Eq. 4.6)}$$

where b, d, f_{sy} and ρ_n refer to dimensions and reinforcement properties of the boundary edge member and v_s and v_c are given by expressions (Eq. 4.4) and (Eq. 4.5) respectively.

An important feature of the design provisions for shear strength of UBC, ACI and ATC 3-06 is that the shear stress assigned to any wall should not exceed $0.83\sqrt{f'_c}$ (in MPa), considered to represent failure due to crushing of concrete "struts".

It is worth noting that all these provisions are empirical lower bounds to a broad scatter of test results on reinforced concrete beams, sometimes ranging up to more than twice code values, particularly when no shear reinforcement is provided. These drawbacks have been recognised by researchers and by committees such as the ACI-ASCE Committee 426, (1973), but no rational explanation or theory has been developed to date.

4.3. PARAMETERS INVESTIGATED

The parametric study dealt with the investigation of the behaviour of reinforced concrete structural walls with rectangular cross-section representing the critical storey element of a structural wall system. The walls were subjected to a constant level of vertical (axial) force (simulating the dead and live gravity loads of a structural system) and to monotonically increasing horizontal (lateral) load to incipient failure. The objective was the study of the behaviour and strength characteristics of such walls at their ultimate limit state.

It was pointed out in Chapter 2, where the analytical and experimental investigations carried out to date on wall behaviour were reviewed, that the role of a number of parameters affecting the wall behaviour at the ultimate limit state is unclear. A similar conclusion is drawn from the discussion of the design procedures presented in Section 4.2. Therefore, the choice for the variables of the parametric study was based on the review of the design procedures and the uncertainties governing the axial-flexural and shear strength expressions adopted by current Code provisions.

The main variables of the analytical investigation of the behaviour of reinforced concrete walls were:

(a) the height to width ratio of the critical storey of the wall elements;

(b) the level of constant vertical compressive stress applied to the wall cross-section normalized with respect to the uniaxial cylinder compressive strength of concrete;

(c) the amount of flexural and confinement reinforcement of the edge members of the wall;

(d) the amount of vertical and horizontal reinforcement of the wall web;

(e) the concrete strength.

4.4. LAYOUT OF THE PARAMETRIC STUDY

Although reinforced concrete structural walls without horizontal reinforcement is the exception rather than the rule in current structural practice, it was thought that basic features concerning the behaviour and strength of rectangular structural walls without horizontal reinforcement should have been established for a wide range of walls, prior to considering the effect of additional parameters. Hence, as a preliminary analysis, non-linear finite element runs were carried out to study the effect of uniformly distributed vertical reinforcement on reinforced concrete walls with various height to width ratio subjected only to monotonically increasing horizontal load up to ultimate. The results of this study will be presented and discussed in Section 4.5.1. Since horizontal reinforcement was not provided in these walls, Code design procedures for flexural strength and for concrete contribution to shear strength were evaluated.

Having evaluated the adequacy of Code provisions in predicting modes of failure and ultimate horizontal load capacity of walls without horizontal reinforcement, further analytical investigations were carried out. They comprised the study of the effect of the amount of horizontal reinforcement, the level of constant vertical load, the reinforcing details (concealed columns) and the concrete strength on the horizontal load carrying capacity of walls with various height to width ratios. The analytical results of the investigation on walls with critical storey height to width ratio of two, one and a half are presented and discussed in Sections 4.5.2, 4.5.3 and 4.5.4 respectively.

4.5. PRESENTATION AND DISCUSSION OF THE ANALYTICAL RESULTS

4.5.1. EFFECT OF DISTRIBUTED FLEXURAL REINFORCEMENT AND HEIGHT TO WIDTH WALL RATIO

The uniaxial cylinder compressive strength for concrete (f'_c) and the ultimate

tensile strength of vertical bars (f_{su}) chosen for the analysis were 35 MPa and 560 MPa respectively. Of the parameters investigated, those discussed in this section are:

(a) the height to width ratio of the wall, ($^{h}/_{l}$);

(b) the amount of uniformly distributed vertical wall reinforcement (ρ_v) or the vertical reinforcement index $\rho_v * f_{su}$.

The influence of ρ_v or $\rho_v * f_{su}$ on the ultimate horizontal load carrying capacity of rectangular reinforced concrete structural walls without horizontal reinforcement may be seen in Figure 4.3. The figure shows the predicted ultimate horizontal load in terms of stress (i.e. horizontal load divided by the wall cross-section) for various amounts of vertical reinforcement for walls with height to width ratio of two, one and half, respectively. This figure also includes flexural and shear strength values assessed by using Code provisions. The flexural capacity was calculated by using either Eq. 4.1 or the general ultimate limit state method recommended in BS 8110, (1985). The calculation of the shear capacity of the wall was based on the concrete shear stress contribution predicted by Codes.

Case (a) of Figure 4.3 indicates that for walls with height to width ratio of two, the analytically predicted wall capacity is higher than the Codes flexural capacity for most of the values of the amount of vertical reinforcement. Only when the amount of vertical reinforcement exceeds 4 percent, the wall capacity predicted by the non-linear finite element analysis becomes smaller than the wall strength corresponding to flexural capacity of the wall as predicted by the ultimate limit state method, indicating a shear failure. It is interesting to note that according to Code design procedures, walls with height to width ratio of two without horizontal reinforcement fail in shear when amounts of vertical reinforcement higher than 0.5 percent are supplied to the walls. If a flexural failure were desirable, usually horizontal reinforcement in excess of the nominal should have been provided. This would have resulted in a conservative and uneconomical design. Another point stressed by the study is that even for low amounts of vertical reinforcement the analytically predicted flexural capacity of the wall is higher than the relevant Code prediction as far as ultimate limit state design procedure is concerned. The reason for this is partly the strain hardening characteristics of the reinforcing steel bars and partly the simplicity of the assumptions made by the ultimate limit state method.

Attention should also be paid to the fact that Eq. 4.1 may not predict

accurately the ultimate flexural capacity of the wall. A comparison between the predictions of Eq. 4.1 (using either the yield stress of steel, f_{sy}, or the higher steel stress, f_{su}, due to hardening) and the relevant results of the general ultimate limit state indicate that the two versions of Eq. 4.1 work as an upper and lower bound to the values of wall flexural capacity suggested by the ultimate limit state method. The assumption made during the derivation of Eq. 4.1 presented in Figure 4.1, that enough reinforcement has yielded (or reached its ultimate strength) when maximum compressive stress of concrete has developed, is mainly responsible for these discrepancies. In fact, Figure 4.3 (case (a)) indicates that for low amounts of vertical reinforcement ($0.5\% \leq \rho_v < 2.0\%$) the wall was so proportioned that the stresses in steel reached their maximum value before maximum compressive stress was reached in the concrete ("underreinforced" wall cross-section). For higher amounts of ρ_v ($2\% \leq \rho_v < 4\%$), enough wall vertical reinforcement had yielded before the maximum compressive stress of concrete was developed (balanced wall cross-section). When ρ_v exceeded 4 percent the comparative study, between provisions by Eq. 4.1 and ultimate limit state theory, shows that more vertical reinforcement than that required to develop the concrete strength was present ("overreinforced" wall cross-section). .

Cases (b) and (c) of Figure 4.3 indicate that the analytically predicted wall capacity is lower than the flexural wall capacity (based on ultimate limit state theory) when structural walls without horizontal reinforcement and height to width ratio of one and a half, are reinforced with amounts of vertical steel higher than 1.3 and 1 percent, respectively. Even when the results of the analytical non-linear runs show that wall capacity is higher than the wall flexural capacity (due to pure bending), code design procedures predict that the wall shear capacity should have been exceeded. Hence, Code provisions suggest what amounts of horizontal reinforcement are required, if a ductile flexural failure is desired.

A further look at the cases composing Figure 4.3 shows that distributed vertical reinforcement is more effective in resisting shear as the wall height to width ratio decreases. The above remark is in compliance with experimental findings of Barda et al (1977) which point out that vertical wall reinforcement is more effective as "shear" reinforcement in specimens with height to width ratio of $\frac{1}{2}$, compared to specimens with height to width ratio of 1.

As the results of the non-linear analysis have already shown, shear failure preceding flexural failure depends on both the geometric and the material properties of the structural wall. Therefore, it is important to compare the analytically predicted ultimate horizontal load capacity of structural walls with varying height to

width ratio and amount of distributed vertical reinforcement with the theoretically obtained flexural capacity, especially for structural walls reinforced for shear. This is portrayed in Figure 4.4 where the ratio of wall horizontal load capacity to that corresponding to ultimate flexural capacity is plotted against the wall height to width ratio for various indices of uniformly distributed vertical reinforcement. This concept was first applied by Kani, 1966, for the shear failure of reinforced concrete beams. The figure shows that, for a constant cross-section and a certain index of vertical wall reinforcement, the increase of the wall height to width ratio results in a decrease of the likelihood of a shear failure. It also shows that a reduction of vertical reinforcement tends to reduce the value of height to width ratio which marks the transition from a flexural to a "shear" failure.

It is clear from the previous discussion that the effect of height to width ratio and the amount of vertical wall reinforcement are not adequately accounted for in the current Codes. Expressions describing the concrete shear stress contribution, not only prove to be conservative but also they do not provide an indication of the type of failure the structural wall is prone to exhibit at the ultimate limit state. Furthermore, it was demonstrated that the mode of failure of the wall is primarily dependent on the height to width ratio of the wall. The amount of vertical reinforcement affects considerably the load level at which a particular mode of failure occurs, rather than the mode of failure itself.

4.5.2. WALLS WITH HEIGHT TO WIDTH RATIO OF TWO

Having discussed how the amount of vertical reinforcement affects the ultimate behaviour of walls with height to width ratio of two ($h/l = 2$) and without horizontal reinforcement, the effect of additional parameters on walls with $h/l = 2$ and given amount of vertical reinforcement will be presented and discussed in this section. The parameters investigated comprised the horizontal reinforcement, the reinforcing details and the vertical loading.

Material characteristics have been assumed constant throughout the numerical tests described in this section, unless stated. The ultimate cylinder compressive strength was equal to 35 MPa, while the ultimate tensile strengths of vertical and horizontal reinforcing bars were equal to 560 and 517 MPa, respectively. The exact dimensions of the rectangular wall cross-section do not matter, since the numerical test results and the theoretically predicted ultimate wall strength will be presented in terms of stresses, i.e. ultimate horizontal load divided by the cross-sectional area of the wall.

4.5.2.1. EFFECT OF HORIZONTAL REINFORCEMENT AND REINFORCING DETAILS

The numerical results included in Figure 4.3 (case (a)) indicate that walls with height to width ratio of two, uniformly distributed vertical reinforcement and without horizontal reinforcement mainly fail in flexure. Walls with 1.5 and 3.0 percent of distributed reinforcement were selected to study the influence of the amount of uniformly distributed horizontal reinforcement; they represent walls with an underreinforced and a balanced cross-section, respectively. Two more cases were investigated in which walls with vertical reinforcement percentage of 3 and 4.7 percent had half the total vertical reinforcement concentrated within a distance of 0.15 l from either extremity of the cross-section, where l is the width of the wall.

In Figure 4.5 the numerical results for all four cases are shown for different amounts of horizontal reinforcement and are compared with the flexural and shear strength of the wall obtained from the ultimate limit state theory of BS 8110, (1985) and the equation 4.3 respectively. The intersection of the theoretical lines of flexural and shear capacity of the wall, gives a measure of the required amount of horizontal reinforcement recommended by Codes, if ductile flexural failure is to occur.

The results indicate that, for given uniformly distributed vertical reinforcement, the "underreinforced" (see Section 4.5.1) wall exhibits a flexural failure under a load 17% higher than that theoretically predicted. It can be seen that this load is not affected by the variation in the amount of horizontal reinforcement. For the case of the "balanced" wall, the results show a slight enhancement in the ultimate load-carrying capacity of the wall with the increase of the amount of horizontal reinforcement. This enhancement appears to be related with the strengthening of the compressive zone of the wall, since the additional amount of horizontal reinforcement gives rise to triaxial conditions in the compressive edge of the wall, permitting more tensile reinforcement bars to reach their hardening stress level before the incipient flexural failure. It is worth noting that the concept of truss analogy, on which most Codes base their shear strength calculations, seems not to predict realistically the ultimate wall behaviour. Code provisions predict that walls with 3.0 and 1.5 percent of distributed vertical reinforcement require 0.45 and 0.20 percent of distributed horizontal reinforcement, respectively, in order to attain their flexural capacity. The numerical results show that, even without any horizontal reinforcement, the horizontal load carrying capacity of the walls is higher than their flexural capacity as predicted by the ultimate limit state theory.

When 3.0 percent of vertical reinforcement was concentrated at the wall edges instead of being distributed, a higher flexural wall capacity is predicted by the ultimate limit state theory. The analytical runs of this particular case with varying amounts of horizontal reinforcement show two interesting features. Firstly, when the amount of horizontal reinforcement supplied to the wall was less than 0.2 percent the wall horizontal load carrying capacity, predicted by the analysis, was less than its theoretically predicted flexural capacity. Secondly, the analytical results show that, for an amount of horizontal reinforcement equal to 0.88 percent, the ultimate horizontal load is 16 percent higher than the theoretically obtained flexural capacity compared with just a 6 percent enhancement observed in the case of uniformly distributed vertical reinforcement. Bearing in mind that for both cases the failure predicted by the analysis was caused by vertical splitting of the compressive zone, it appears that the provision of additional vertical reinforcing bars and horizontal reinforcement within the lower part of the compressive zone of the wall increases the confinement conditions of this region and results in a higher flexural wall capacity.

When the amount of concentrated vertical reinforcement was increased to 4.7 percent, which is unrealistic for practical applications but necessary for research purposes, the following features were observed: (a) the ultimate horizontal load carrying capacity of the wall is smaller than the theoretical flexural capacity of the wall and (b) the Code provisions for shear strength are conservative for percentages of horizontal reinforcement less than 0.7, while they become unsafe for higher values. This observation shows that the shear capacity of the walls cannot be explained by the "truss analogy" concept.

For the particular case in which 4.7 percent vertical reinforcement was concentrated at the wall edges, two more analytical runs were carried out after modification of the horizontal reinforcement details. The modification involved strengthening the compressive zone by increasing the amount of confinement reinforcement (in the form of stirrups) at the wall edges, while an amount of 0.45 percent of horizontal reinforcement was supplied to the wall's web. Confinement levels of 0.66 and 0.88 percent resulted in the same ultimate horizontal load carrying capacity and behavioural characteristics for the wall as the analytical runs with 0.66 and 0.88 percent horizontal reinforcement throughout the cross-section of the wall. This indicates that if a minimum amount of horizontal reinforcement is placed in the wall web to cope with the tensile stresses, enhancement in strength and ducility can only be achieved by strengthening the lower compressive zone of the wall.

4.5.2.2. EFFECT OF VERTICAL LOADING

A group of three structural walls subjected to normalized vertical stress ratio (ν) of 0, 0.1 and 0.2 were analysed, where ν is the ratio of the initially applied constant vertical stress to the uniaxial cylinder compressive concrete strength. The walls were only reinforced with various amounts of uniformly distributed vertical reinforcement. No horizontal reinforcement was supplied to the walls. The percentages of vertical wall reinforcement were equal to 0.86, 1.50 and 3.0 and the corresponding ultimate tensile steel strengths were 690 MPa, 560 MPa and 560 MPa, respectively. Therefore, cases with vertical reinforcement indices of 5.9, 8.4 and 16.8 were investigated.

Figure 4.6 presents the variation of horizontal load carrying capacity of the walls, in terms of stresses, with normalized vertical stresses predicted by the analysis, together with the values of flexural and shear wall strength predicted by BS 8110, (1985) and ACI 318, (1983) respectively.

The figure indicates that Code provisions significantly underestimate the wall strength. In particular for walls supplied with low vertical reinforcement indices and subjected to normalized vertical stress ratios up to 0.1, Code design procedures predict a shear failure under a horizontal load about 50% lower than the numerically obtained ultimate horizontal load. The difference between analysis and Code predictions decreases with increasing vertical force. When the normalized vertical stress is equal to 0.2, Codes also predict a flexural mode of failure, occurring at a slightly lower load level than that predicted by the analysis. It should be noted, that if the recommendation of the Codes for the omission of the vertical force term in the calculations of v_c (see Section 4.2.2) were followed, unnecessary amounts of horizontal reinforcement would have been required for the walls to reach their flexural capacity.

The numerical results of the case where distributed vertical reinforcement of 3 percent was supplied to the wall, indicate that as the level of applied vertical force increases, slight enhancement in ultimate horizontal load capacity of the wall can be achieved. The non-linear finite element analysis showed that the incipient failure of these walls commenced with almost vertical splitting of the compressive edge of the wall near the support. Such splitting destroyed the high shear resistance of this region since it eliminated the triaxial compression stress conditions existing there. The presence of high vertical stresses resulted in an increase of the depth of neutral axis and thus in an enhancement of the area of the compressive zone which in turn increased the "shear capacity" of the compressive zone. However,

the rate of increase of shear strength does not follow the sharp trend suggested by the Codes, for cases where "shear" wall failure dominates.

4.5.3. WALLS WITH HEIGHT TO WIDTH RATIO OF ONE

It was shown in Sections 4.5.1 and 4.5.2 that structural walls with height to width ratio of two (i.e. slender walls) are likely to fail in shear only when they are over-reinforced. It was also pointed out that current Code provisions for flexural design, although conservative, yield rational and simple design solutions. The discussion of the numerical results presented in case (b) of Figure 4.3 and described in Section 4.5.1, indicates that when the vertical reinforcement index exceeds 7 MPa, the ultimate horizontal load attained by walls with height to width ratio of one is lower than the flexural wall capacity predicted by BS 8110, (1985). What remains to be seen is how parameters, such as the amount of horizontal reinforcement, the constant vertical stress, the concrete strength and the reinforcement detailing can influence the mode of failure and the strength of these elements. The ability of current Code provisions for shear design to provide a realistic description of the causes of shear failure will be also discussed.

The material characteristics of the walls analysed were 560 and 517 MPa for the ultimate tensile strength of vertical and horizontal reinforcement respectively, and 35 MPa for the uniaxial cylinder compressive concrete strength, unless stated.

4.5.3.1. EFFECT OF HORIZONTAL REINFORCEMENT AND REINFORCING DETAILS

For the first two cases analysed the amount of vertical reinforcement incorporated into the wall was 3 percent. The cases differ in the sense that vertical reinforcement was either uniformly distributed throughout the width of the wall or concentrated into the extremes of the wall within a distance of 0.15 of the wall width. The relevant theoretical horizontal load wall capacities due to pure bending expressed in terms of the horizontal load divided by the wall cross-sectional area were 5.44 and 6.37 MPa respectively. These predictions were based on the ultimate limit state theory. The analytical values of the ultimate horizontal load capacity attained by these walls with respect to various amounts of uniformly distributed horizontal reinforcement are presented in Figure 4.7(a). The figure also includes the wall "shear" strength predictions of the ACI, (1983) Code. The results of the analytical runs show that the wall capacity was lower than the

corresponding flexural wall capacity for all the cases investigated.

They also point out that for the case of the distributed vertical reinforcement, Code predictions are conservative for the lower range of values of the percentage horizontal reinforcement, while for the upper range of these values they overestimate considerably the wall capacity. Another feature illustrated in Figure 4.7(a) is that when the vertical reinforcement is concentrated in the wall edges, the numerically obtained ultimate wall capacity is higher than the corresponding strength of the wall which incorporated the same amount of vertical reinforcement but distributed along its width. In addition, the rate of increase in wall strength, with increasing amount of horizontal reinforcement, is higher when the same amount of vertical reinforcement is concentrated at the wall edges rather than uniformly distributed. In the particular cases investigated, 26 and 13 percent enhancement of the wall capacity was observed, respectively, for an increase in the amount of horizontal reinforcement from 0 to 0.88 percent. A likely explanation is that, when there is no vertical reinforcement in the wall web, only the horizontal reinforcement bars sustain the tensile stresses developed for equilibrium purposes at the web of the wall.

The concentration of vertical reinforcement at the walls extremes cannot alter the "shear" capacity of the wall if Equation 4.3 is considered. Therefore design procedures based on the truss analogy concept cannot effectively predict the wall shear capacity, since (a) concrete strength and the contribution of vertical reinforcement are not well accounted for in the v_c term, and (b) the contribution of horizontal reinforcement to "shear" resistance is smaller than that provided by the v_s term.

The influence of the amount of horizontal reinforcement on the ultimate wall capacity was also investigated for walls incorporating amounts of vertical reinforcement equal to 1.5 and 1.0 percent of the wall cross-sectional area, concentrated in the wall extremes and detailed as before. An additional amount of uniformly distributed vertical reinforcement equal to 0.44 percent was supplied to the wall web in both cases. The numerical results of these cases are presented in Figure 4.7(b). The relevant theoretical horizontal load wall capacity in flexure expressed in terms of horizontal load divided by wall cross-section was 4.05 and 2.98 MPa respectively. Current design procedures consider that if a ductile flexural failure is desirable, amounts of horizontal reinforcement equal to 0.6 and 0.35 percent respectively should have been provided to the walls.

The results of this study confirm that horizontal reinforcement does not play

the role suggested by the Codes. In the former case (ρ_v = 1.5% at the wall edges), ultimate strength values obtained from the non-linear finite element analysis indicate that for amounts of horizontal reinforcement lower than 0.5 percent, the predicted values are smaller than the flexural capacity, but higher than "shear" capacity predicted by Codes. However, for the upper range of values of the percentage of horizontal reinforcement the Code predictions for shear overestimate the wall capacity. In the latter case, (ρ_v = 1.0 at the wall edges) the analytically obtained wall capacities are higher than the corresponding theoretical flexural capacity of the wall. Despite the fact that the flexural mode of failure is dominant, a slight enhancement in the ultimate wall capacity is observed with the increase in the amount of horizontal reinforcement. This implies that horizontal reinforcement in the form of confinement assists the development of triaxial compressive stress conditions in the compressive zone of the wall near the foundation level, prior to the incipient failure.

4.5.3.2. EFFECT OF VERTICAL LOADING

The parametric study of the influence of constant levels of applied vertical force on structural walls with and without horizontal reinforcement was conducted on walls incorporating three different amounts of vertical reinforcement. The vertical reinforcement provided was 3, 1.5 and 1.0 percent of the wall, covering the extreme edges within a distance of 0.15 of the wall's width. In the latter two cases an additional amount of 0.44 percent of uniformly distributed vertical reinforcement was supplied to the wall's web.

The numerical results of the three case studies investigated are presented in Figures 4.8, 4.9 and 4.10 respectively. The figures illustrate the variation of ultimate horizontal load capacity with the amount of horizontal reinforcement for given levels of normalized axial compressive stress. The figures also include information with regard to theoretically calculated flexural and shear capacities of the wall.

It appears from the results that the presence of axial compressive force does not change the effectiveness of horizontal reinforcement. Code provisions for shear are still conservative for the lower range of horizontal reinforcement percentages, but they overestimate wall strength for the upper range of horizontal reinforcement percentages. This is particularly the case for wall with low amounts of vertical reinforcement (ρ_v = 1.5%) subjected to low levels of compressive stresses as shown in Figure 4.9. A comparative study of the cases included in Figures 4.8 (ρ_v =

3%) and 4.9 (ρ_v = 1.5%) show that for given normalized axial stress, horizontal reinforcement is more effective when higher amounts of vertical reinforcement are incorporated into the walls. Analytical results included in Figure 4.10 indicate that despite theoretical predictions walls reinforced with low amounts of vertical reinforcement (ρ_v = 1.0%) do not require excessive amounts of horizontal reinforcement to fail under horizontal load corresponding to their flexural capacity, particularly when low normalized axial stresses ($\nu \leq 0.1$) are applied to the walls.

Figure 4.11 portrays the ultimate shear stress (i.e. ultimate horizontal load divided by wall cross-section) against normalized compressive axial stress interaction diagram for a typical wall reinforced with given amount of horizontal reinforcement but with varying amounts of vertical reinforcement. The material and geometric properties of the case are included in the figure together with the theoretical predictions for wall strength in flexure and in shear (in terms of stresses). Current design procedures suggest that shear failure occurs in all but one cases and that wall strength is not affected by the variations in the amount of vertical reinforcement. The numerical results point out that Code predictions are conservative in all but one cases. This particular wall incorporates a low percentage of vertical reinforcement and is subjected to high compressive stresses. Furthermore, the results (see Figure 4.11) show that, the higher the axial compressive force on the wall, the smaller the influence of the amount of vertical reinforcement on the increase of the ultimate "shear" strength of the wall.

4.5.3.3. EFFECT OF CONCRETE STRENGTH

A typical structural wall with height to width ratio of one was selected in order to estimate how changes in uniaxial concrete cylinder compressive strength affect the horizontal load carrying capacity of the wall. It incorporated an amount of vertical reinforcement equal to 1.5 percent of the wall cross-sectional area concentrated at the wall extremities and a uniformly distributed amount of vertical and horizontal reinforcement equal to 0.44 percent in the wall's web. A constant normalized vertical stress of 0.05 was also applied to the wall. Since the theoretical flexural capacity of the selected structural wall was higher than the corresponding shear strength predicted by Codes for all concrete strengths, the influence of concrete strength on the shear strength of walls was investigated.

The effect of concrete strength f'_c (varying between 25 and 60 MPa) on the shear strength of the particular wall is shown in Figure 4.12(a). The figure includes both the numerical results and the ACI predictions. The ultimate shear

strength of the wall increased as expected with increasing f'_c. However, the ACI predictions, while conservative for concrete strengths higher than 50 MPa, became unsafe for low to medium concrete strengths.

Figure 4.12(b) portrays the effect of concrete strength on the shear strength of the wall normalized with respect to either concrete strength or the square root of the concrete strength. For the typical wall analyzed, the ratio of v_{ult}/f'_c decreased 31 percent as f'_c increased from 25 to 60 MPa, while the ratio of $v_{ult}/\sqrt{f'_c}$ increased 18 percent for the same increase in f'_c. Oesterle et al, (1984) recognised the unsafe design solutions which current Codes yield for walls with concrete compressive strength less than 34.5 MPa subjected to low vertical (axial) stress and suggested a simplified equation, based on the truss analogy, in order to overcome the problem. The predicted strength values using their expression are also presented in Figure 4.12(b). It appears from the figure that while the expression suggested by PCA yields better predictions than the relevant expression of ACI for lower concrete strengths, it is less safe for medium to high concrete strengths. In fact, the PCA expression was validated with experimental data for concrete strengths from 20.7 to 41.4 MPa. Therefore the numerical results illustrate that neither f'_c nor $\sqrt{f'_c}$ can be used as effective normalizing factors for the ultimate shear strength of the wall, since neither shear strength nor uniaxial compressive strength express realistically the stress conditions arising at the compressive zone of the wall near the support prior to failure.

It is clear from the discussion that the effect of concrete strength is not adequately accounted for in current design methods. It should also be mentioned that tests providing the basic data for these expressions were conducted on structural members, mainly beams, with concrete strength below 45 MPa. Although it appears to be unwise to extrapolate these expressions for higher concrete strengths, there is nothing in the Codes to prohibit such an extrapolation.

4.5.4. WALLS WITH HEIGHT TO WIDTH RATIO OF A HALF

Case (c) of Figure 4.3 illustrated that squat structural walls without horizontal reinforcement subjected to combined bending and shear fail predominantly in shear, even if they incorporate low levels of vertical reinforcement. Three levels of distributed vertical reinforcement were considered in order to study the influence of the amount of horizontal reinforcement and the applied vertical stress on the strength characteristics of such walls. Amounts equal to 0.5, 1 and 2 percent of the total cross-sectional wall area were selected, since they cover the whole

transition zone from flexural to shear behaviour (as shown in Figure 4.3, case (c)). Material characteristics have been assumed constant throughout the study; the adopted values were the same as in the preceding section.

4.5.4.1. EFFECT OF HORIZONTAL REINFORCEMENT

The theoretically calculated ultimate horizontal load carrying capacity of walls incorporating 0.5, 1 and 2 percent of distributed vertical reinforcement due to pure bending is, in terms of stresses, (i.e. horizontal load divided by wall cross-section) 2.52, 4.32 and 7.71 MPa respectively. These values imply that if the flexural capacity of the walls is to be attained, 0.25, 0.69 and 0.83 percent of horizontal reinforcement should have been provided to the wall's web, bearing in mind that concrete shear contribution can offer only 1.48 MPa.

The variation of ultimate wall capacity with the amount of horizontal reinforcement supplied to the wall is illustrated in Figure 4.13. The figure includes the non-linear finite element predictions as well as shear and flexural strength Code predictions. It appears from the figure that for low vertical reinforcement levels flexural failure is dominant, while the amount of horizontal (shear) reinforcement required according to the Codes does not appear to be justifiable. Nevertheless, as the amount of horizontal reinforcement increased from zero to one percent, an 18 percent enhancement of the ultimate strength was observed for the wall incorporating 1% of vertical reinforcement. This appears to be associated with the beneficial effect the horizontal reinforcement provides in confining the compressive zone of the wall and permitting more and more vertical reinforcement to yield prior to wall failure. When only 0.5 percent of vertical reinforcement was supplied to the wall, the ultimate horizontal load wall capacity predicted by the finite element analysis was 45 percent higher than the theoretically calculated ultimate wall capacity due to pure bending, indicating that Code provisions for flexure can also be conservative in cases where very low amounts of vertical reinforcement are supplied to the wall. It also supports the belief of some engineers that the concept of flexural capacity does not make sense for squat walls, since a squat wall does not behave like a beam in flexure. Hence the assumptions of flexural strength underlined in Section 4.2.1 are not applicable for squat walls.

It should be mentioned that the provision of horizontal reinforcement in such cases can only slightly enhance the wall strength. Hence if the designer, in compliance with any of the present codes, uses a factor of safety greater than one

in the calculations of flexural strength and then employs this strength as a measure to reinforce the wall with horizontal reinforcement against shear, the design will be uneconomical. These remarks are in compliance with the experimental data obtained by Wiradinata et al, (1986) on wall specimens with height to width ratio of ½. A wall specimen with 0.8% vertical reinforcement showed ductile behaviour, even though it contained only a minimum amount of horizontal reinforcement (0.25 percent).

If the "truss analogy" model were effective, squat walls with high levels of vertical reinforcement and without horizontal reinforcement should provide low horizontal load capacity while their capacity should improve rapidly with the increase of the amount of horizontal reinforcement provided to them. However, the numerical results show that walls reinforced with small amounts of horizontal reinforcement present higher horizontal load carrying capacity than that predicted by the "truss analogy" model. Furthermore it can be observed that the rate of increase of wall strength with the increase of the amount of horizontal reinforcement is far smaller than that predicted by the Codes. The non-linear runs of a wall incorporating two percent of vertical reinforcement show that only a 9 percent increase can be achieved by increasing the amount of horizontal reinforcement from zero to one percent. The numerical tests indicate that the primary role of horizontal reinforcement is the restriction of the width of inclined cracks and hence the control of top horizontal wall displacement at failure.

4.5.4.2. EFFECT OF VERTICAL LOADING

A parametric study of the influence of the initial application of a constant normalized axial stress was conducted on walls reinforced with varying amounts of uniformly distributed vertical reinforcement, but without incorporating any horizontal reinforcement.

Figure 4.14 illustrates in an interaction diagram the variation of the ultimate horizontal load capacity in terms of stresses attained by walls with 0.5, 1 and 2 percent of vertical reinforcement, with respect to the normalized axial stress ratio. The shear and flexural strength Code predictions of these particular walls are also included in the figure. Current Code predictions suggest for all three cases the walls will fail in shear long before their flexural capacity is attained. As shown in Figure 4.14 the numerical tests suggest that the use of shear strength design equation 4.3 leads to overconservative design even for low percentages of vertical reinforcement. Furthermore, the numerical results point out that under high axial

forces, even walls which failed in flexure, when subjected to very low amounts of axial force, fail under low horizontal loads before reaching their theoretically calculated flexural capacity.

4.6. CONCLUSIONS

The main conclusions of the parametric study of the behaviour of reinforced concrete walls with rectangular cross-section at the ultimate limit state may be summarised as follows:

(a) The influence of either distributed or concentrated vertical reinforcement on the ultimate horizontal load carrying capacity of walls without horizontal reinforcement, is not properly taken into consideration in current Code provisions. For walls with height to width ratio of two, Code design procedures predict a shear failure for percentages of vertical reinforcement higher than 0.5. The analysis shows that even for low amounts of vertical reinforcement the wall fails in flexure subjected to a horizontal load higher than the flexural wall strength predicted by Codes. For walls with height to width ratio less than or equal to one, the analytically predicted wall capacity is lower than the flexural wall capacity (based on ultimate limit state theory), when the amount of vertical steel supplied to the wall is higher than 1%. Even for these cases the wall shear capacity predicted by Codes is significantly less than the analytically predicted wall strength. Therefore, the likelihood of shear failure preceding flexural failure is dependent on both the geometric and the material properties of the structural wall. The wall shear strength is not a simple function of concrete strength as the Code provisions suggest.

(b) The equation for ultimate flexural wall capacity proposed by the ACI Code assumes that enough vertical reinforcement has yielded when maximum compressive stress of concrete develops ("balanced" wall cross-section). The analytical results show that depending on the percentage of vertical reinforcement, the wall cross-section can be "under-reinforced", "balanced" or "overreinforced" and that equation 4.1 describes crudely the flexural capacity of the wall.

(c) For walls failing at an ultimate horizontal load higher than their flexural capacity, a slight enhancement in the wall capacity with the increase of the amount of horizontal reinforcement was observed. Horizontal reinforcement in the above cases gives rise to triaxial conditions in the lower compressive edge

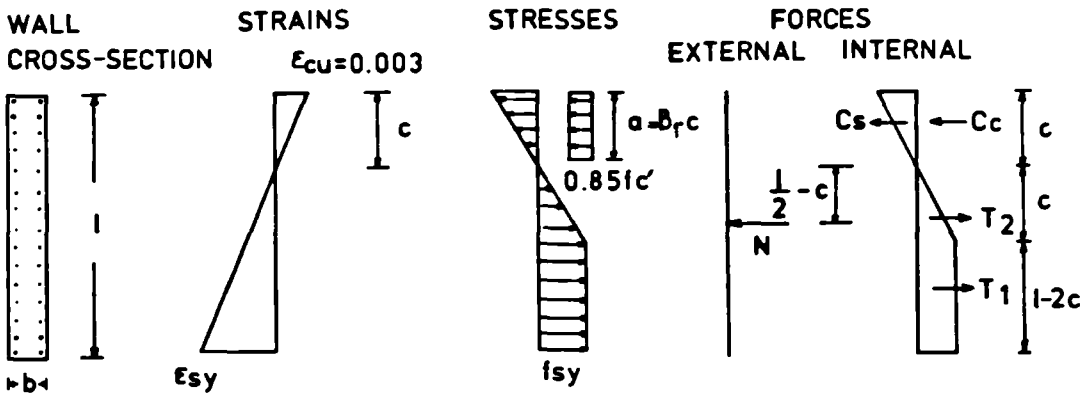
of the wall, increasing therefore the wall resistance.

(d) For walls failing at an ultimate horizontal load below their flexural capacity the analytical results of the parametric study indicate that the role of horizontal reinforcement in increasing wall strength is different from that suggested by current Codes. Code provisions suggest a linear increase of wall shear capacity with increasing percentage of horizontal reinforcement, from a lower level representing the contribution of concrete to shear resistance, to an upper level corresponding to "crushing" of the concrete struts of the "truss" model. Beyond this level, it predicts that shear capacity remains constant. The analytical results pointed out that while Code predictions are conservative for the lower range of values of the percentage of horizontal reinforcement they overestimate considerably the wall capacity for the upper range of these values. Furthermore the inclusion, near the extreme compression and tension fibres, of additional reinforcement in both the compression and tension zones of the wall results in a significant increase of wall load–carrying capacity; this happens in spite of the considerable reduction of horizontal reinforcement to near nominal levels.

(e) It appears from the numerical results that the presence of axial compressive force does not improve the effectiveness of horizontal reinforcement. It should be also noted that the Code recommendation for omission of the vertical force term in the calculation of concrete shear stress contribution, might lead to excessive unrequired amounts of horizontal reinforcement if it were desired to reach the wall flexural capacity. The analytical tests indicate that, for walls subjected to axial load, the overconservativeness of Code provisions for shear increases with the decrease of the wall height to width ratio and with the increase of the amount of vertical reinforcement supplied to the wall.

(f) The ultimate shear strength of the wall was found to increase, as expected, with increasing cylinder compressive strength of concrete, f'_c. However, the numerical results illustrate that neither f'_c nor $\sqrt{f'_c}$ can be used as effective normalizing factors of the wall ultimate shear strength. Wall shear capacity and uniaxial strength of concrete cannot realistically express the stress conditions arising at the lower compressive zone of the wall prior to failure.

(g) The analytically predicted mode of failure of walls was characterised by longitudinal cracking within the compressive zone near the base of the wall where the flexural moment attains its maximum value.



. EQUILIBRIUM OF FORCES

$$\left\{\begin{matrix}\text{external} & - & \text{internal} \\ \text{forces} & & \text{forces}\end{matrix}\right\}$$

$$N = C_c + C_s - T_1 - T_2 \quad (1)$$

where

$$\left\{\begin{matrix} T_1 = \frac{1 - 2c}{l} * A_s * f_y \\ T_2 = \frac{c}{l} * A_s * f_y - C_s \\ C_c = \beta_1 * c * b * 0.85 * f'_c \end{matrix}\right\}$$

. MOMENT EQUILIBRIUM ABOUT K

$$\left\{\begin{matrix}\text{external} & - & \text{internal} \\ \text{moments} & & \text{moments}\end{matrix}\right\} \quad (2)$$

$$M_{ext} = V * h - N * (\frac{1}{2} - c)$$

where

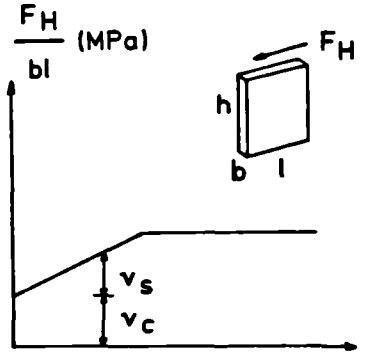
$$\left\{\begin{matrix} h = \text{height of the wall} \\ V = \text{horizontal load} \end{matrix}\right\}$$

$$M_{int} = T_1 * \frac{1}{2} + (T_2 + C_s) * \frac{2}{3} * c + C_s * \frac{c}{2}$$

. COMBINATION OF (1) AND (2) LEADS TO:

$$M_{ult} = V * h = \tfrac{1}{2} * A_s * f_y * l * (1 - \frac{c}{l}) * (1 + \frac{N}{A_s f_y})$$

Fig. 4.1. Calculation of the ultimate wall flexural capacity.



v_c : concrete contribution to shear

v_s : horizontal reinforcement contribution to shear

Fig. 4.2. Variation of the wall shear capacity with the amount of horizontal reinforcement.

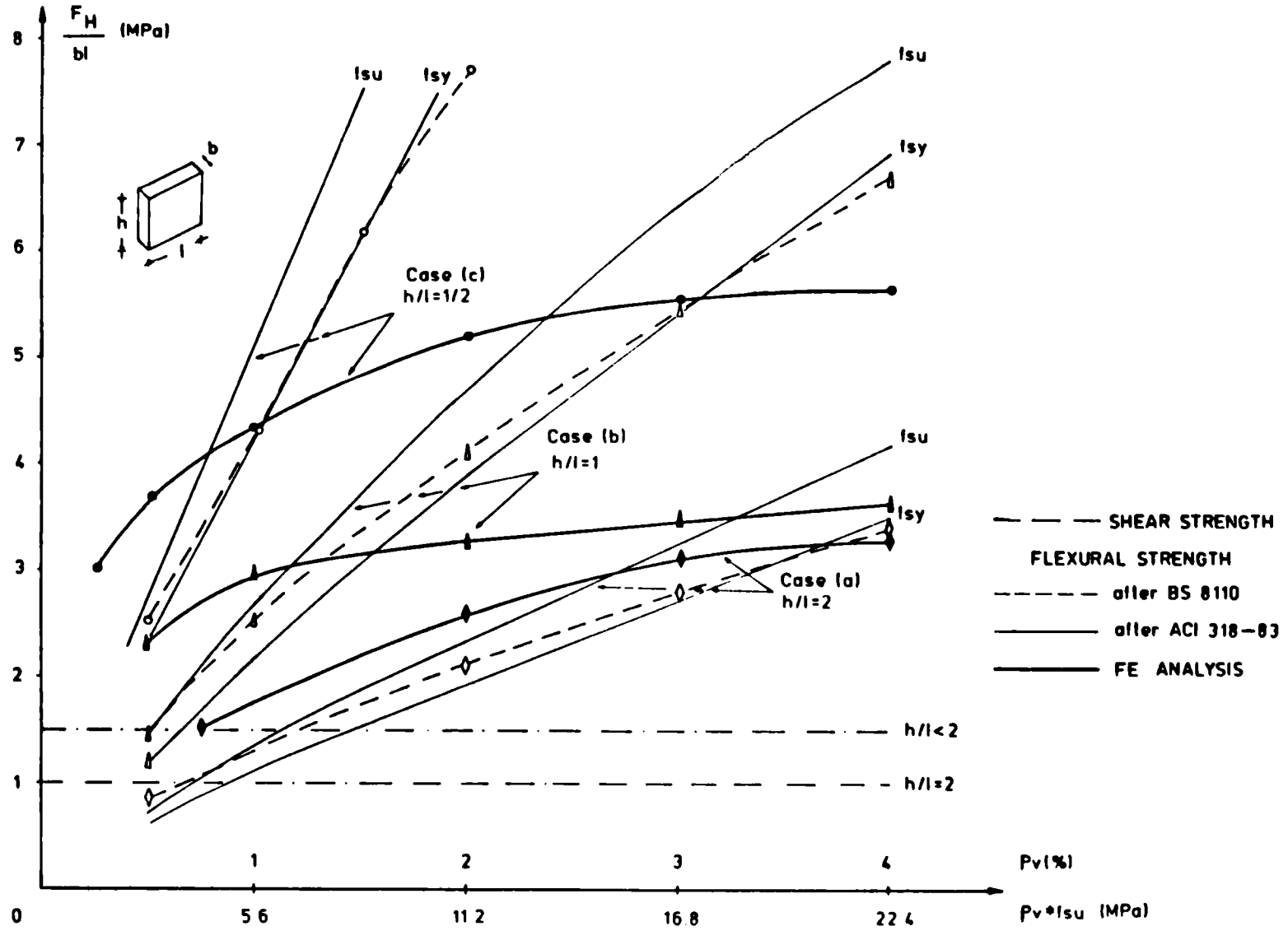


Fig.4.3. Variation of the ultimate horizontal load of R.C. walls, without horizontal reinforcement, with the amount of uniformly distributed vertical reinforcement.

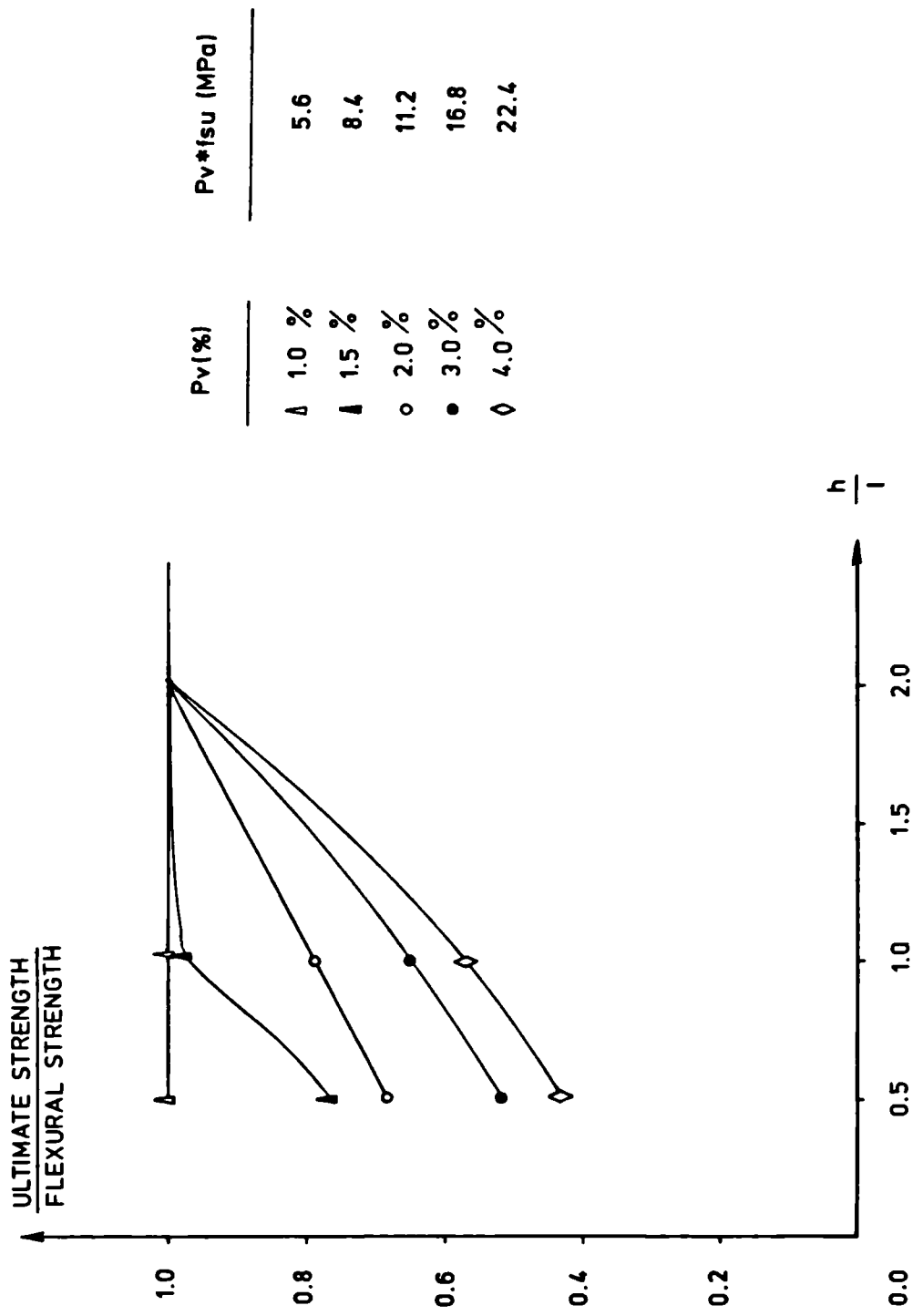


Fig. 4.4. Variation of the ratio of wall horizontal load capacity to flexural capacity with the wall height to width ratio.

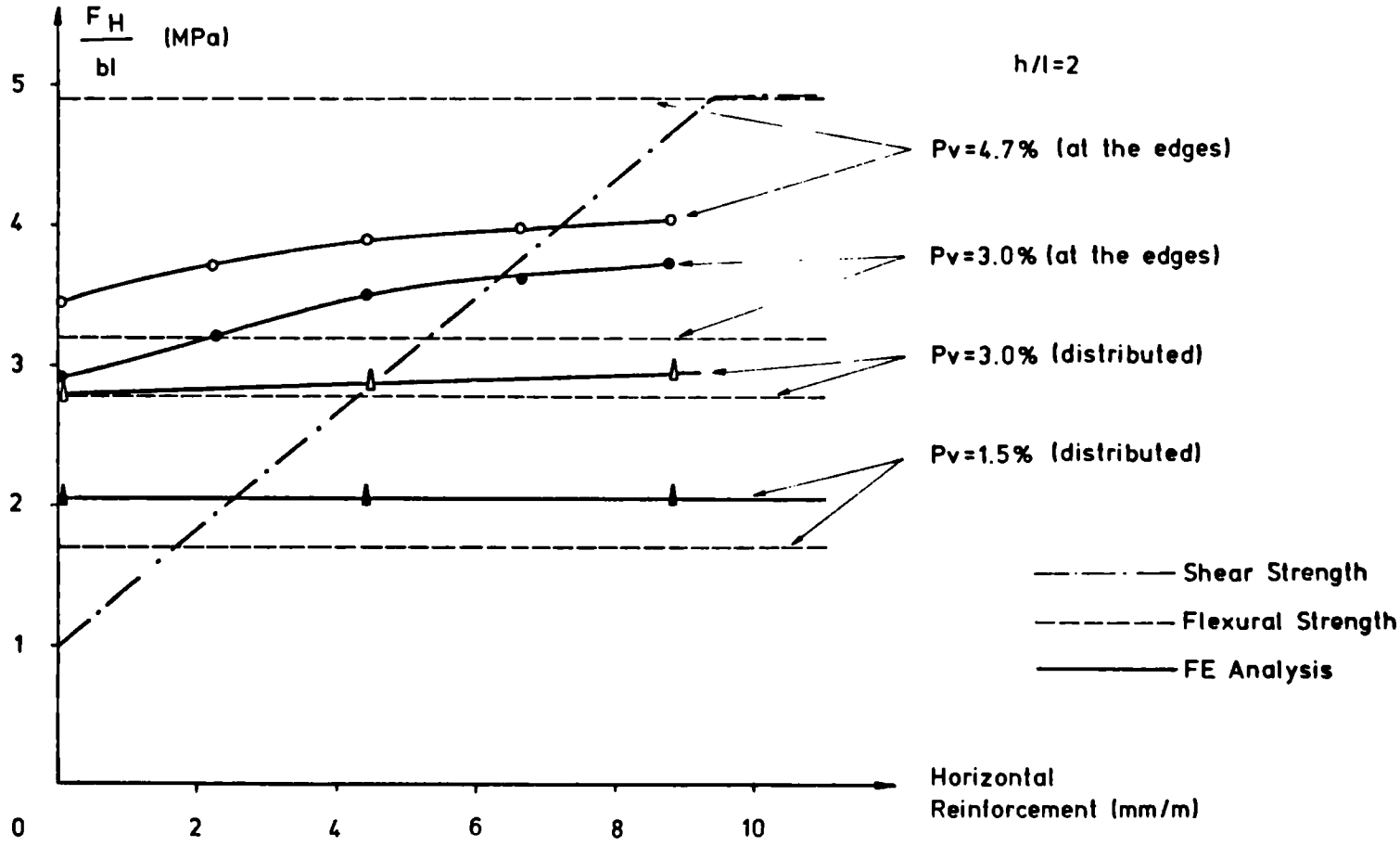


Fig. 4.5. Effect of horizontal reinforcement on the ultimate capacity of walls with height to width ratio of two.

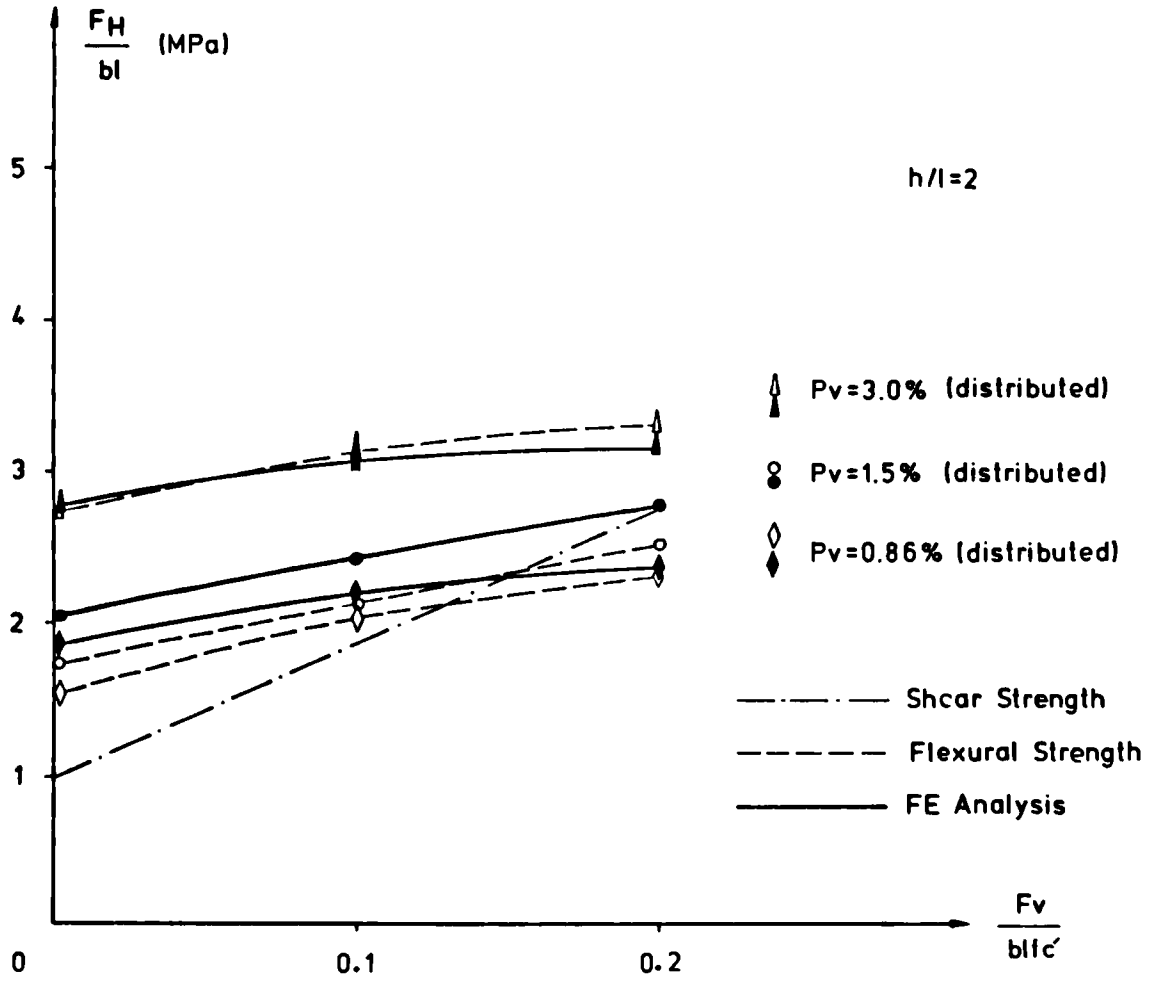
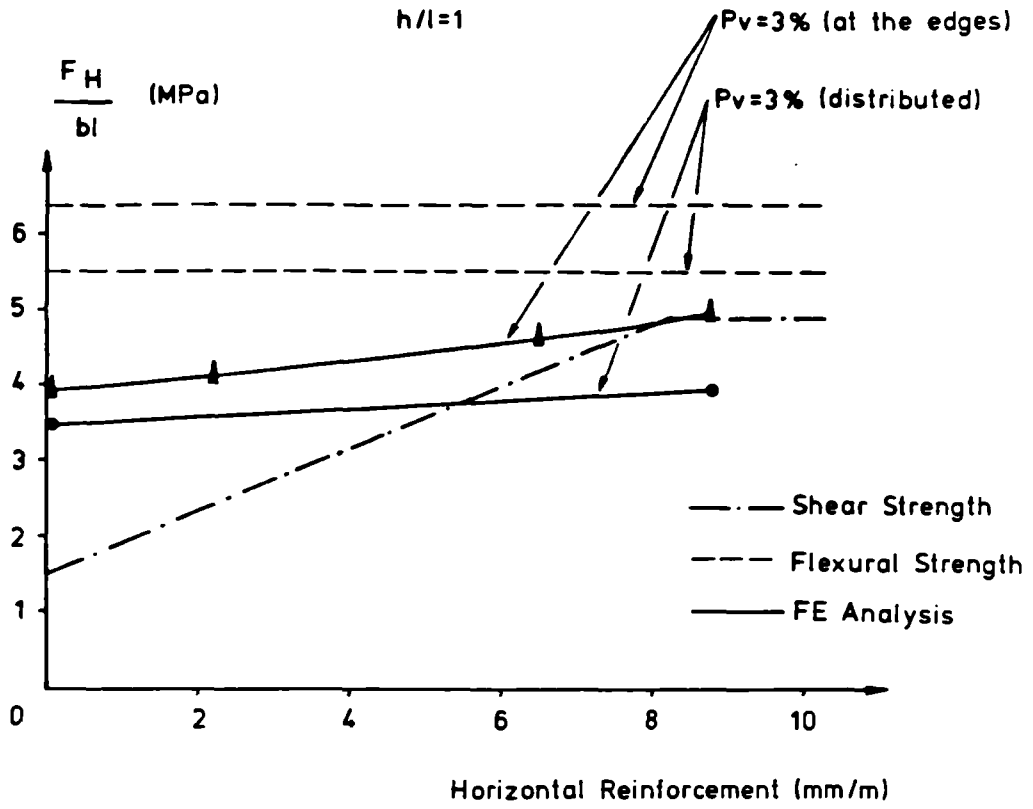
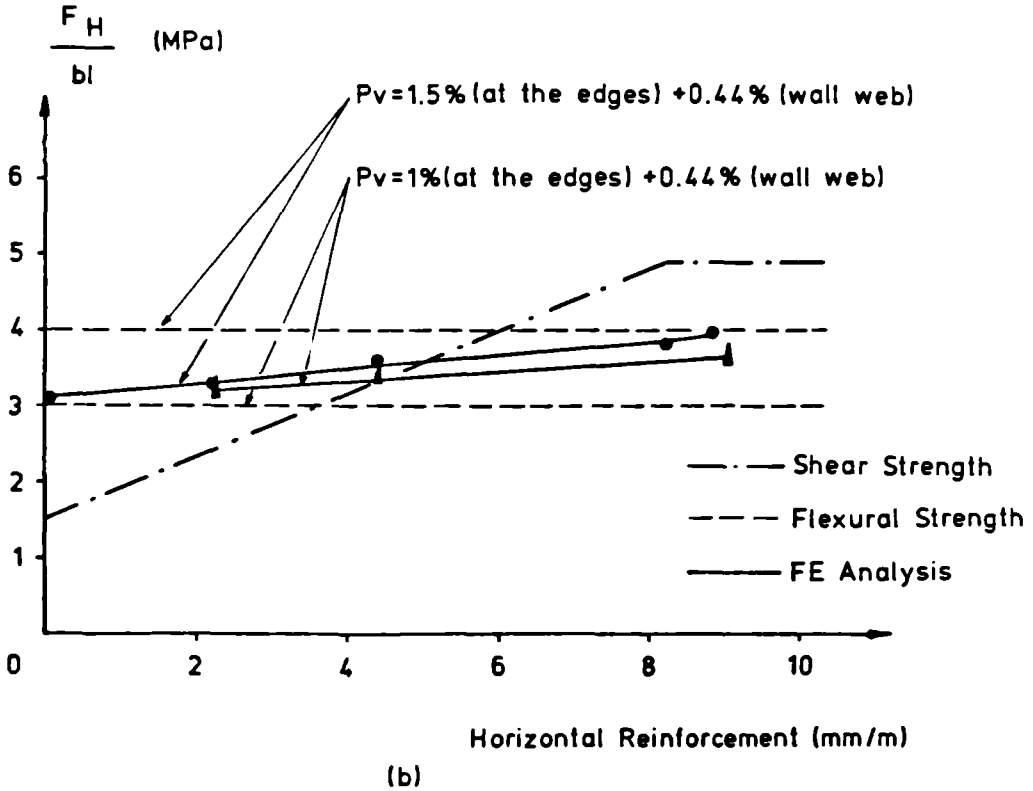


Fig. 4.6. Variation of wall horizontal load capacity (in terms of stresses) with normalized vertical stresses.



(a)



(b)

Fig. 4.7. Effect of horizontal reinforcement on horizontal load carrying capacity of walls with height to width ratio of one
(a) ρ_v = 3% (b) ρ_v = 1.5% and 1.0%.

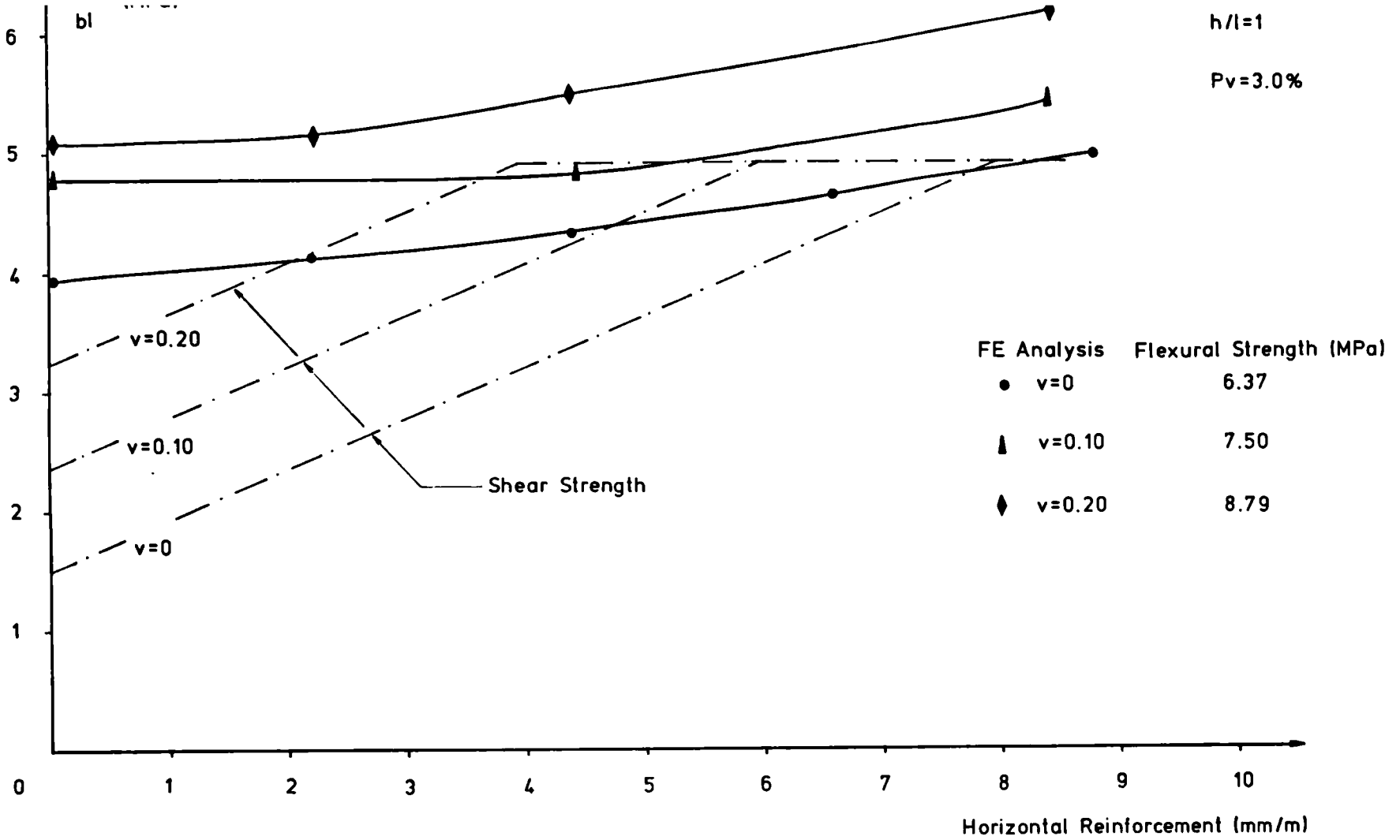


Fig. 4.8. Variation of wall horizontal load capacity with amount of horizontal reinforcement for various levels of normalized axial load (ρ_v = 3% at the edges).

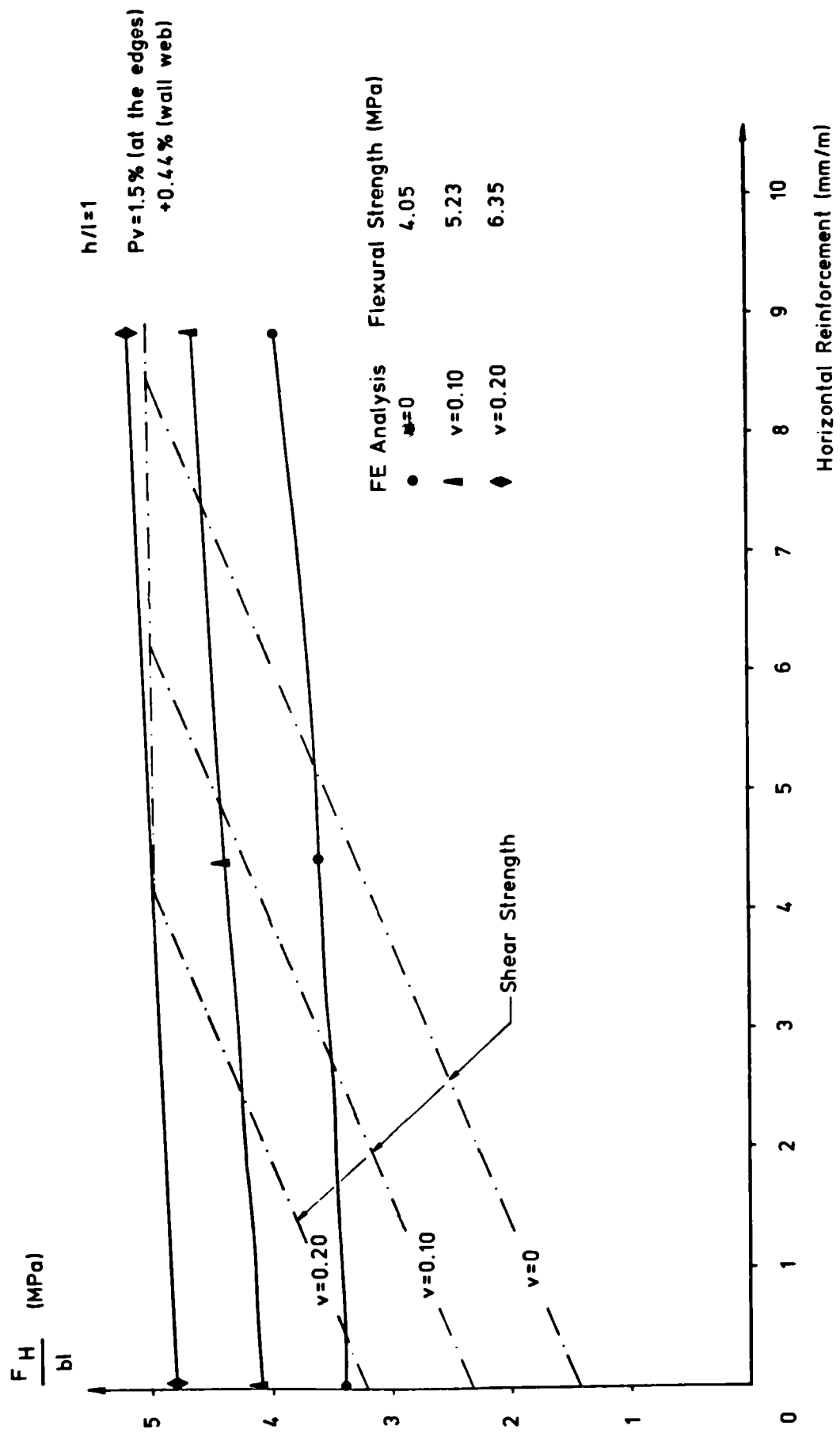


Fig. 4.9. Variation of wall horizontal load capacity with amount of horizontal reinforcement for various levels of normalized axial load (ρ_v = 1.5% at the edges + 0.44% wall web).

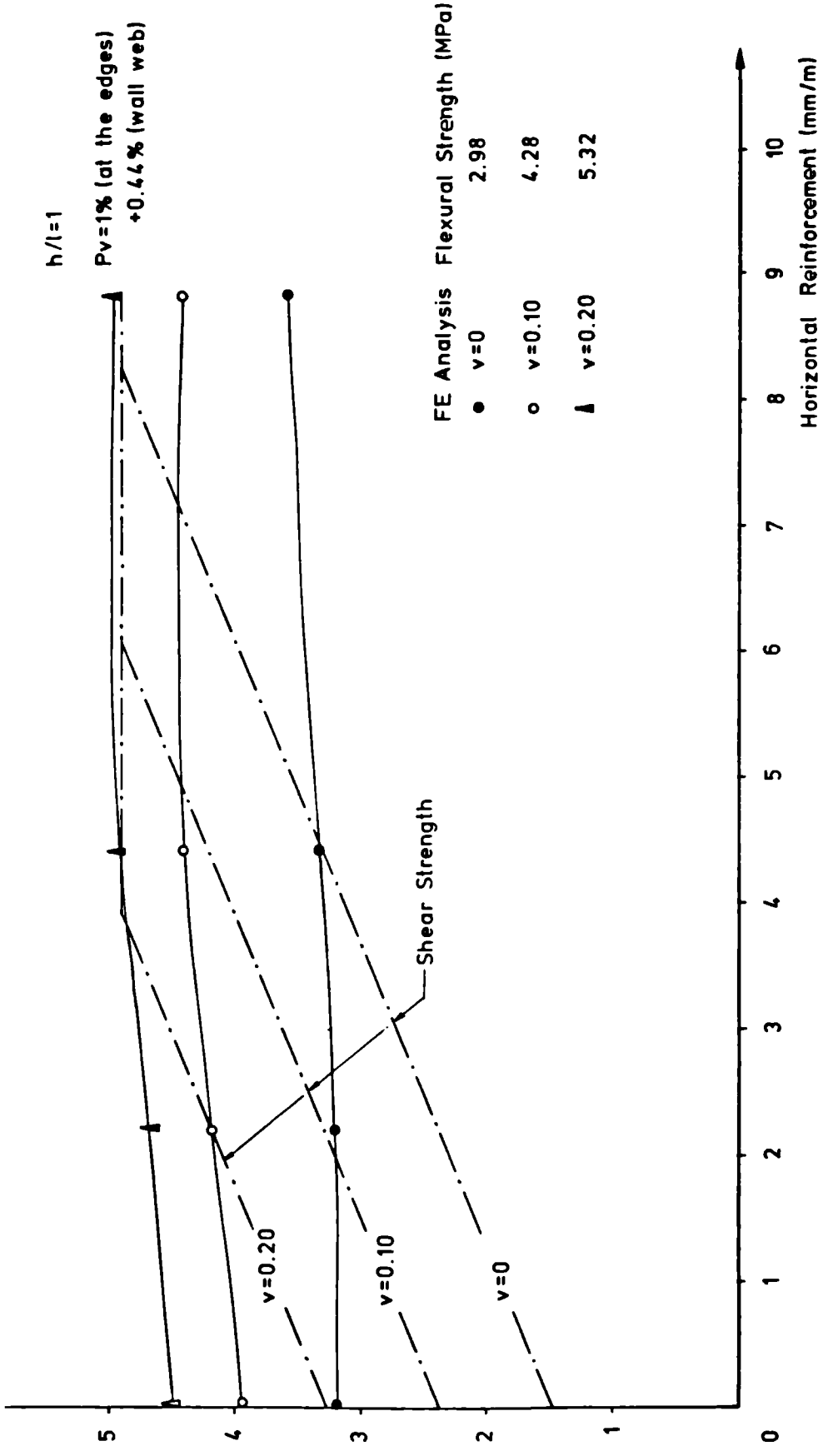


Fig. 4.10. Variation of wall horizontal load capacity with amount of horizontal reinforcement for various levels of normalized axial load (ρ_v = 1% at the edges + 0.44% wall web).

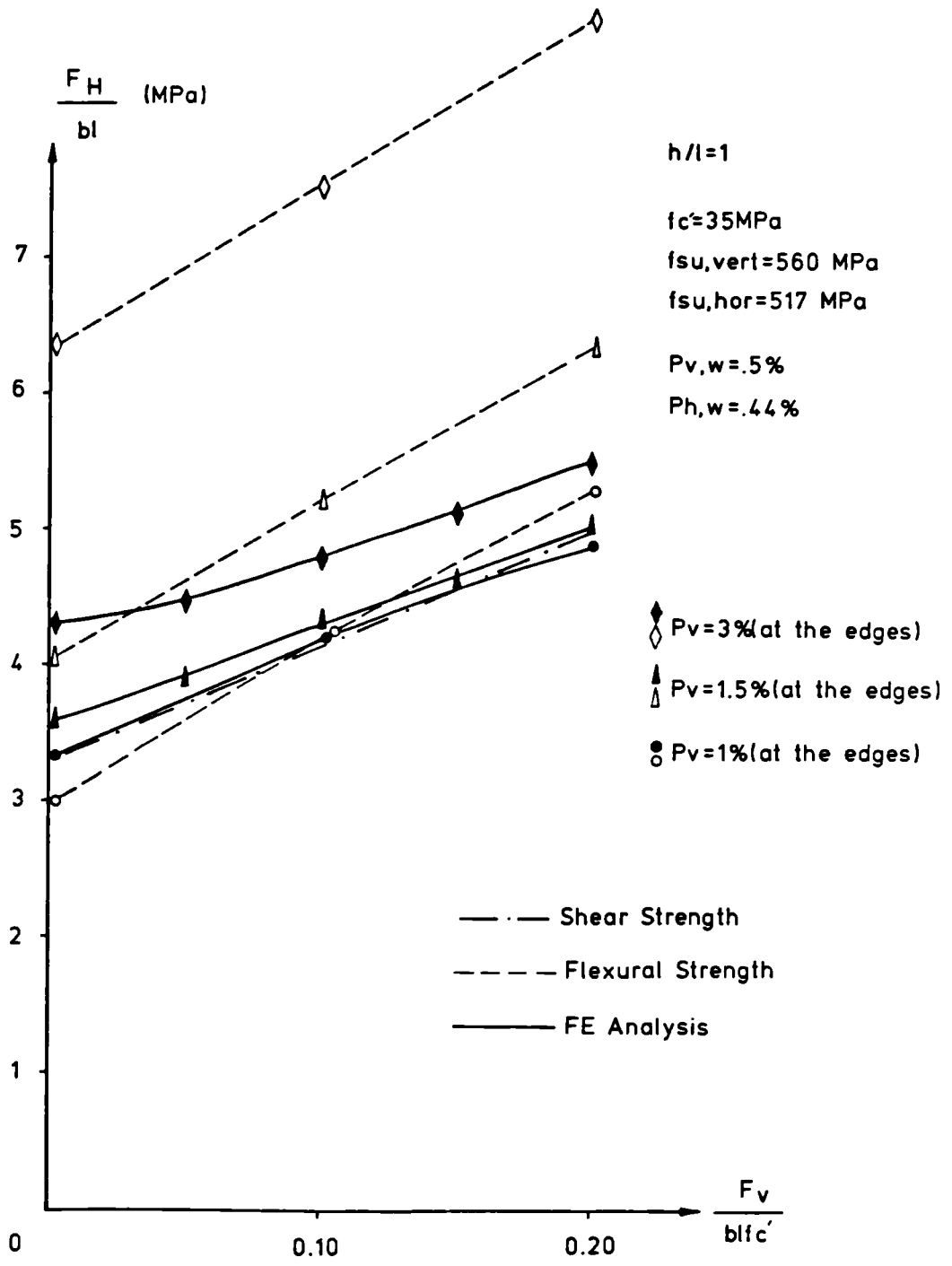


Fig. 4.11. Ultimate shear stress - normalized compressive axial stress interaction diagram for a typical wall with height to width ratio of one.

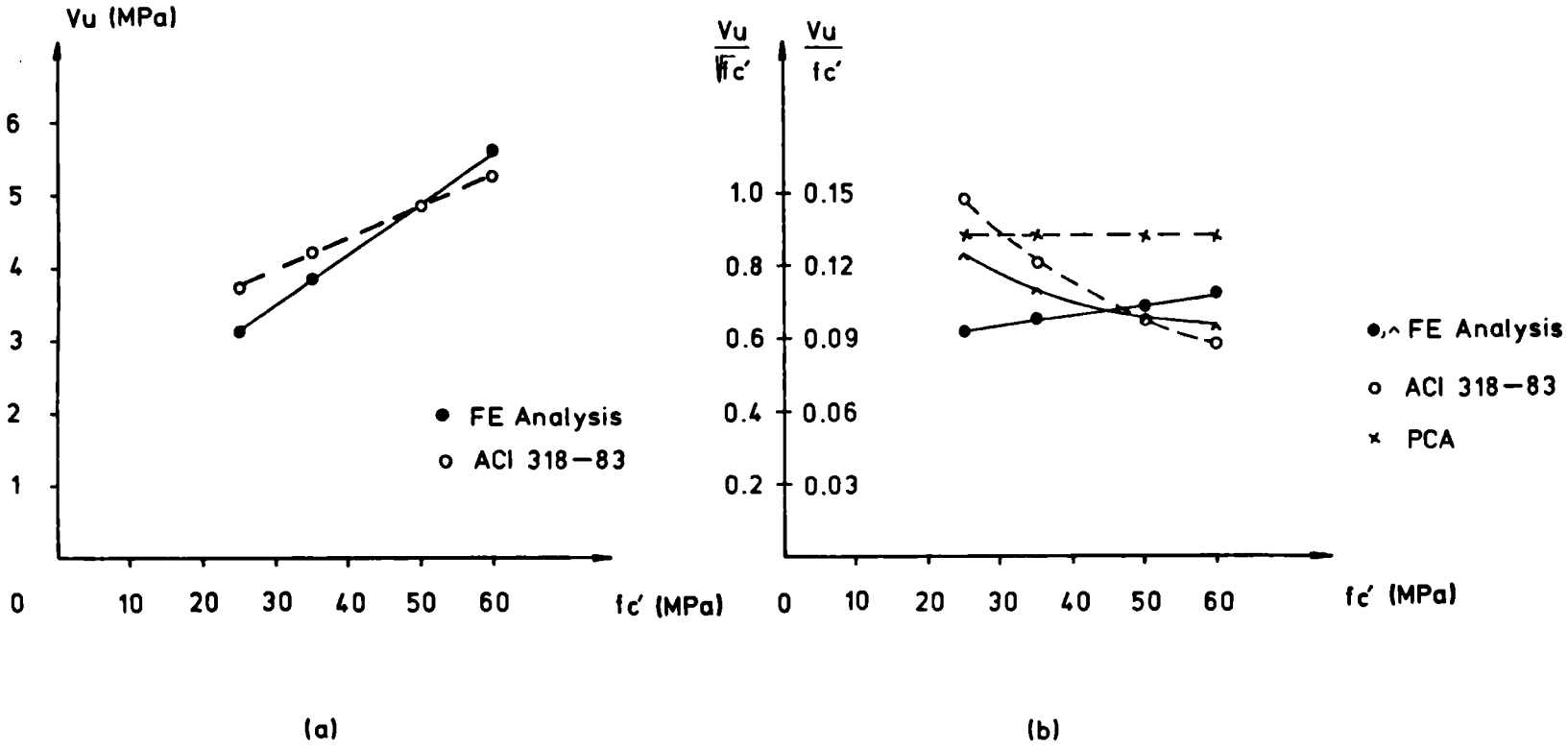


Fig. 4.12. Effect of concrete cylinder strength on
(a) wall shear strength
(b) normalized wall shear strength with respect to either the concrete strength or the square root of the concrete strength.

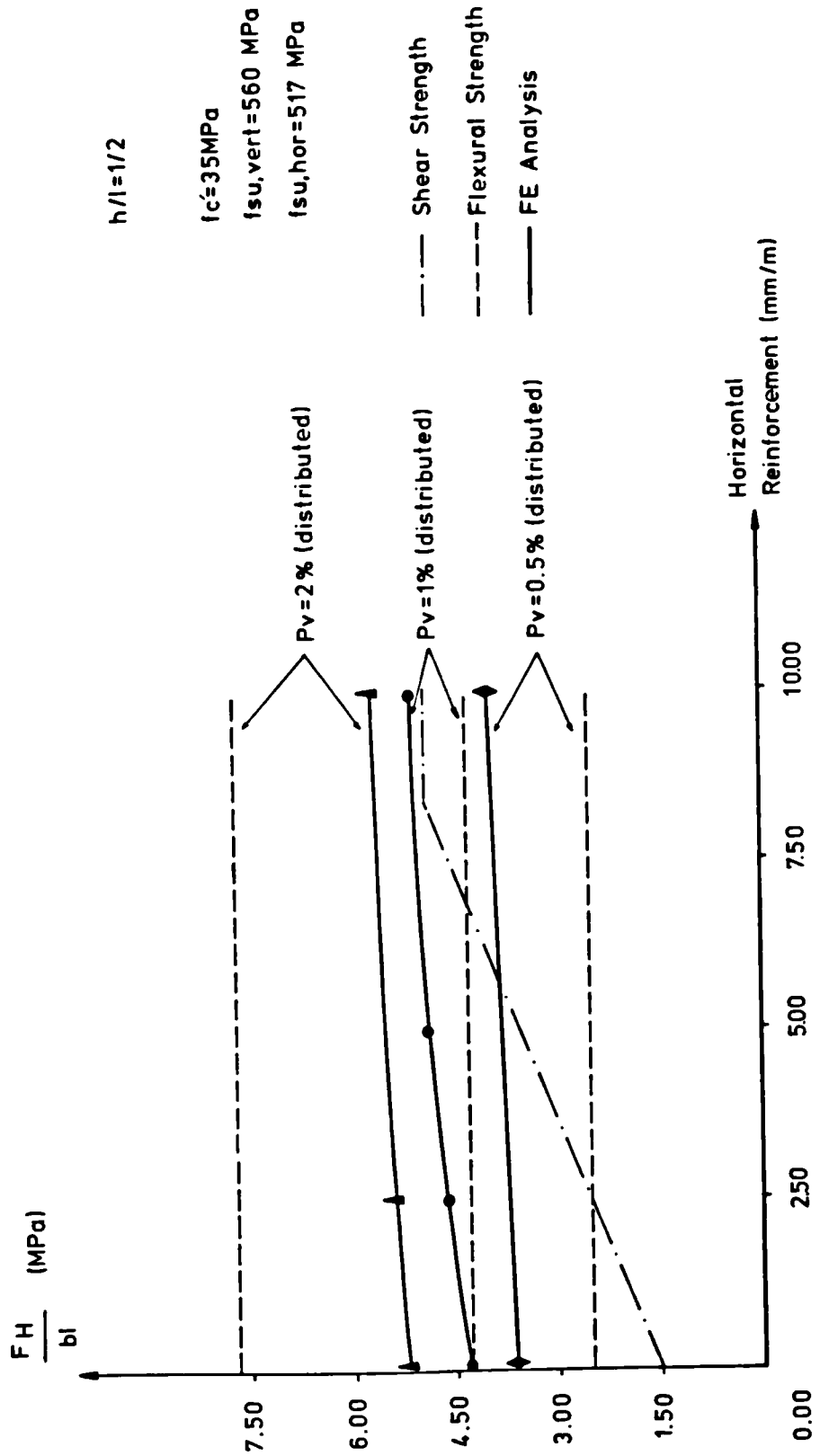


Fig. 4.13. Variation of ultimate wall capacity with amount of horizontal reinforcement for walls with height to width ratio of a half.

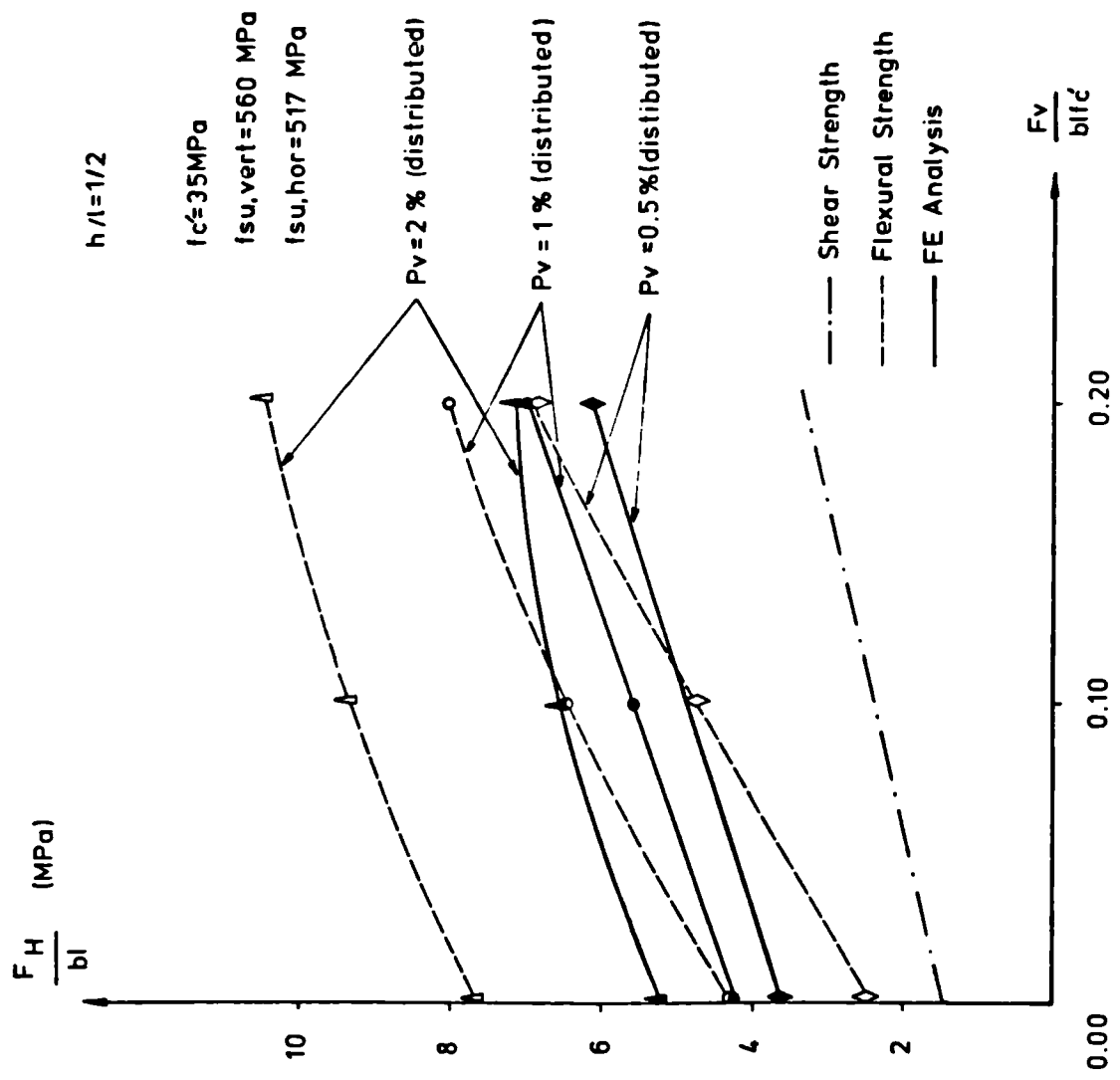


Fig. 4.14. The effect of vertical loading on ultimate strength of walls with height to width ratio of a half.

CHAPTER 5

DETAILS OF EXPERIMENTAL WORK

5.1. INTRODUCTION

This chapter describes the characteristics of the structural forms investigated, their loading and instrumentation details and the testing procedures followed. Since there is a repetition in the basic principles which governed the experimentation, most of the present chapter should be regarded as back-up material for the next two which follow.

5.2. DETAILS OF THE SPECIMENS

5.2.1. GEOMETRY

Two types of reinforced concrete structural walls, as shown in Figure 5.1, were tested. Type I walls were 750 mm wide, 750 mm high and 70 mm thick, whereas type II walls were 650 mm wide, 1300 mm high and 65 mm thick. Such specimens which are the $\frac{1}{4}$ and $^1/_{2.4}$ scale models of full size walls, with height to width ratio of 1 and 2 respectively, are considered to represent the critical storey element of a structural wall system with a rectangular cross-section.

In all cases, the walls were monolithically connected to an upper and lower beam. The upper beam, 1150 mm long, 150 mm deep and 200 mm thick, not only simulated a slab or a beam in an actual building, but also functioned both as the element through which vertical and horizontal loads were applied to the walls and as a cage for the proper anchorage of the longitudinal reinforcement of the walls. The lower beam, 1150 mm long, 300 mm high and 200 mm thick was utilized to clamp down the specimens to the laboratory test floor, simulating a rigid foundation.

5.2.2. REINFORCEMENT

The vertical and horizontal reinforcement of the walls comprised high tensile deformed steel bars of 8 and 6.25 mm diameter, respectively. Additional horizontal reinforcement was placed at the edges of the walls (concealed columns)

in the form of stirrups to provide confinement. Mild steel bars of 4 mm diameter were used for this purpose. Yield and ultimate strength was obtained by testing at least 6 bars in tension in a 10 ton (about 100 KN) Amsler machine. Table 5.1 summarizes these results.

Typical stress–strain curves for the high tensile reinforcement were obtained by averaging the results of two gauged bars of each type, such as those shown in Figure 5.2. Strain gauges were fixed on the circumference of the bar and during this process the cross–sectional area of the bar was slightly reduced, by the removal of the secondary ribs, at the position of the gauging. The reduction of the area results to an equivalent 10 percent reduction of the ultimate load for the 8 mm bars and a 7 precent reduction of the ultimate load for the 6.25 mm bars. It should also be noted that the strain gauge readings were outside the sensitivity range for load levels beyond 95 percent of the ultimate load.

The photographs in Figure 5.3 illustrate the different types of reinforcement used, as well as details of their fracture zone after the tensile test.

5.2.3. CONCRETE

In all but 2 specimens, the same concrete mix proportions were used. The design cube strength was 45 MPa in 28 days. Two other mixes designed for 28 day cube strengths of 30 MPa were used for the type II specimens. Details of the mix proportions used for the concrete of the specimens are given in Table 5.2.

For every test specimen manufactured, 8 control cubes (100 mm side) and 2 cylinders (100 mm x 250 mm) were cast, in standard steel moulds in accordance with the requirements of British standards. Two and three control cubes were crushed at 7 and 28 days respectively, while the remaining control specimens were crushed on the day of testing of the corresponding structural wall.

The mean (± standard deviation) cube strength achieved in 7 and 28 days were 33.6 (± 2.9) and 46.9 (± 4.1) respectively. Detailed tables of the test results of the controls can be found in Sections 6.2, 7.2 and 8.2.

5.2.4. MOULD, CASTING PROCEDURE AND CURING REGIME

Moulds were made from 19 mm thick plywood, the surface of which was made waterproof by the application of several coats of polyurethane sealant. The mould produced for the first series of walls with height to width ratio of 1, was also used after some amendments, in an elongated form, for the casting of the walls with height to width ratio of 2.

Before casting, the inside surfaces of the mould were lightly coated with a layer of releasing agent and the mesh of the appropriate reinforcement was placed in it. Figure 5.4 shows mould and reinforcement details prior to casting of a wall with height to width ratio of 1.

The constituents of each mix were carefully batched and mixed for a couple of minutes in a TEKA THZ 375 heavy duty mixer, with an input capacity of 375 litres, allowing casting of each wall and its control cubes and cylinders in one batch. Concrete was placed in the mould in two layers for the upper and lower part of the wall specimen and in one layer for the wall itself. A 1 inch diameter electrical pocket vibrator, capable of vibrating in two minutes a circular area of 4 inches in diameter per piercing of the mix, was used to vibrate each layer. Control cubes were cast in two layers and cylinders in three layers on the laboratory vibrating table.

All wall specimens were covered with wet hessian and polythene and cured for 7 days. Control specimens were demoulded 24 hours after casting and kept beside the wall specimens for the purpose of matching curing conditions. Care was taken to ensure that the hessians were kept wet during the first week. Thereafter wall specimens were demoulded and stored in an upright position, together with the controls, in the laboratory, at a constant temperature of 20°C and a relative humidity of 65 percent, until tested.

5.3. LOADING AND INSTRUMENTATION DETAILS

5.3.1. TEST RIG AND LOADING MACHINES

The test floor of the laboratory is designed to form the lower member of an internal reaction frame. Steel uprights and concrete reactions blocks are bolted to the floor and the test rig is completed by the fixing of a steel transom. The holding-down bolts in the floor are on a 3'00" (914 mm) square grid, and can be

post-tensioned up to 25 tons (about 250 kN) each. Thus, both the steel uprights and the concrete blocks were bolted to the floor by a 4 x 25 = 100 tons (about 1,000 KN) force.

The two uprights were placed at 3'00" (914 mm) centres. Their twin supports were braced at a height of approximately 4'6" (1372 mm) by a 17" x 8" (432 mm x 203 mm) deep steel box girder. The concrete reaction blocks had overall dimensions 1200 mm x 600 mm x 600 mm and were also placed at 3'00" (914 mm) centres in two piles. They were either 3 or 4 in a pile according to the type of the wall tested. A 4 m long, 400 mm x 200 mm rectangular hollow section steel transom with 12.5 mm thickness (bolted in the uprights by means of 12 bolts and fixed above the concrete blocks by means of a 30 ton clamp-down force) stiffened the whole rig and carried the vertical (axial) load system. A schematic representation of the test rig is shown in Figure 5.5.

The wall specimen was approximately positioned on a marked space, between the steel uprights and the concrete blocks, by the overhead crane. The specimen was then clamped to the floor by means of two transverse 1250 mm long steel box girders, with 200 mm x 100 mm cross-section and 10 mm thickness, and 4 holding-down bolts post-tensioned to 20 tons (≈ 200 KN) each. Auxiliary platens were positioned between the box sections and the lower beam of the specimen to ensure the even distribution of the load on the lower beam and to secure base fixity conditions. The loading system was designed to apply increased lateral (horizontal) load either from one side or both sides depending on the type of loading, and constant axial (vertical) load when the testing procedure required it. Provision was made to accommodate a 25 mm sway movement of the wall specimen. Two 50 tons ENERPAC RC-506T general purpose single acting load cylinders, with 159 mm stroke and 70.9 cm^2 cylinder effective area, were used for both load systems. One of them was always connected to a Walter and Baiag hydraulically operated cabinet, equipped with an internal pressure transducer, and the other one to either a 10,000 psi or a 5,000 psi Amsler testing machine. A Bell and Howell pressure transducer in the hydraulic supply line to the Amsler machine ram provided the means of accurate measurement of the applied load. Power to the transducers was supplied by a stable 10 V d.c. source. The output voltage was found to be a linear function of the applied load for loads up to 450 kN. Both transducers were calibrated against a standard 100 tons (≈ 1,000 kN) strut load cell. The calibration procedure was repeated before the commencement of each series of tests. The calibration factor was 70.6 kN/V for the transducer of the Walter and Baiag machine and 5960.9 kN/V for the Bell and Howell transducer connected to the 5,000 psi Amsler machine.

5.3.2. MEASUREMENT OF DISPLACEMENTS

Deformations were measured by a number of linear voltage differential transducers (LVDT's). The lateral displacement of the specimen was measured by four or five LVDT's depending on the type of the wall, positioned at different heights from the lower beam level. One LVDT, in the case of monotonic lateral loading, and two LVDT's, in the case of cyclic lateral loading, were placed against the foundation beam surface to measure the rotation of the beam. Two LVDT's were placed on top of the loading beam at the edges of the wall to measure the contraction and/or the extension of the edge members of the wall. A series of three LVDT's covered the bottom, middle and top areas of the web of the wall to monitor any out-of-plane movement of the specimen. Details of the LVDT's arrangement for different types of walls and loading are given in Figure 5.6. A specially designed rigid scaffolding, rigid stands based on the laboratory floor and the steel transom, ensured the fixity of the LVDT's throughout the testing procedure.

The LVDT's were calibrated against a screw micrometer in a purpose built calibration rig. Calibration was achieved for a displacement of the plunger of ± 25 mm or ± 50 mm about the LVDT zero voltage position. The output voltage was ascertained to be a linear function of the plunger displacement. Characteristics of the LVDT's are given in Table 5.3. Calibration of the LVDT's was carried out before each individual testing.

5.3.3. MEASUREMENT OF STEEL STRAINS

Electrical resistance strain gauges (ersg) for measuring steel strains on some bars of the longitudinal reinforcement were provided in a number of tests in order to determine first yielding. The strain gauges were positioned on locations adjacent to the analytically predicted failure zone of the specimen. The characteristics of the post-yield strain gauges are given in Table 5.4.

Prior to gauging, the reinforcement was especially prepared. The secondary ribs of the high tensile bars were taken off with a file at the position where the gauges were to be placed. The resulting section was rubbed with emery paper and cleaned with a water-based degreasing surface cleaner. The gauges were fixed to the surface of the bars using an epoxy adhesive. Once the epoxy hardened, the gauges were waterproofed.

The gauges were wired in series. Each gauge was connected to a quarter-bridge circuit and strains were calculated using the unbalanced bridge method. The expression used for the calculation of strains was

$$E = \frac{-4 \times \Delta V}{G \times (1 + 2|\Delta V|)}$$

where $\Delta V = {}^{V_o}/_{V_i} - {}^{W_o}/_{W_i}$

V_o, V_i : output and input voltages respectively, of the bridge at the time of reading, in Volts

W_o, W_i : output and input voltages respectively, of the bridge when the bar was unstressed (untensioned and uncompressed), in Volts

G : strain gauge factor

It should be underlined that a small number of gauges displayed unstable behaviour during testing. Possible cause might be the formation of "dry" joints for some connections. The thinner PLS-10 gauges showed better performance than the PL-10 gauges and were preferred for use for the type II walls.

5.3.4. DATA RETRIEVAL

The experimental data of applied load, displacement and strain gauge measurements were recorded by a Hewlett Packard data logging system. The system consisted of an HP-85 microcomputer, an HP3497A Data Acquisition/Control Unit and an HP 3456A Digital Voltmeter. The data recording was controlled by programming the microcomputer.

During the reading cycle, readings were taken of all the measurement devices and were printed out by the microcomputer printer. Readings were taken at regular intervals corresponding to the loading sequence adopted for the test. The voltmeter was set in auto-range, the measuring speed employed was just over 10 channels per second. Over the range of voltages employed, the resolution was 0.01 mV and the accuracy was ± 0.0138%. The data were then transferred in file form to the main frame computer to be further processed and used for the graphical presentation of the results.

5.4. TESTING PROCEDURE AND LOADING SEQUENCE

Each wall specimen was centrally placed on its final position and its base fixity was secured by means of the transverse beam device, one week before testing. After the South surface of the wall specimen was rubbed down with a carborundum stone, the positions of load platens and the measuring instruments were marked. The finite element mesh adopted for the analytical study of the behaviour of the wall was also lightly marked by chalk on the South face of the specimen. A couple of days before testing the LVDT's were securely positioned and adjusted so that their output voltages were approximately zero.

Since one of the variables studied in the experimental programme was the effect of constant vertical (axial) load on the strength and stiffness characteristics of wall specimens with varying height to width ratio, strong attention was paid to the proper application of such a load. The vertical (axial) load was applied through a spherical seating, consisted of a spherical bearing between two platens, and connected with four springs and a 815 mm x 130 mm x 50 mm spreader beam supported by loading platens and rollers kept apart at the distance of the centres of the edge members (concealed columns) of the wall specimens. A system of spirit levels and a plump bob assured that the load cylinders acted centrally on the loading beam. Concentricity of the vertical loading was also checked by comparing the readings obtained from the LVDT's placed on the loading beam. If values given by these LVDT's differed significantly, vertical load was removed and the position of the loading platens adjusted manually to correct the eccentricity.

The application and amount of axial load investigated in this programme was subjected to the following principles : The total axial force at the base of the critical storey of the wall can be replaced by two axial loads placed at the top of the edge members of the specimens. This type of axial force simulation differs from the actual one, in the sense that it induces some stress concentration in the upper part of the specimen. Since the combination of applied forces at the upper part of the wall is far from inducing critical stresses at this level, the stress concentration should not affect the overall performance of the wall.

After the total constant vertical force was applied, the wall specimen was incrementally loaded with the horizontal (lateral) load at a rate of approximately 0.04 kN/s. The horizontal load was applied to the loading beam through a bearing ball attached at the centre of a loading platen in order to secure the concentricity of the load. At each increment the load was maintained constant for at least two minutes in order to monitor load and deformation response of the wall,

mark the cracks, if any, and take photographs of the wall crack patterns. The initiation and development of cracking was observed with the unaided eye. Crack progress was monitored by marking the cracks with coloured pens and labelling them with the corresponding load. Photographs were taken at zero and peak horizontal load as well as at several interesting intermediate stages of crack propagation.

The cubes and cylinders were tested at the time of testing of the wall specimens. For specimens loaded with a constant vertical load crushing of controls preceded the testing of the specimen. A level of 85% of the mean, ultimate, uniaxial strength of cubes was used to define the level of vertical load which had to be applied to the specimen, since the normalized axial force to concrete strength was amongst the main parameters whose effects were investigated in the experimental programme.

Type	Yield strength f_{sy}(MPa)	Ultimate strength f_{su}(MPa)	Modulus of elasticity E_s(GPa)
8 mm high tensile bar	470	565	159
6.25 mm high tensile bar	520	610	150
4 mm mild steel bar	420	490	-

Table 5.1 : Properties of reinforcement bars

Proportions by weight	45 MPa mix	30 MPa mix (a)	(b)
10 mm aggregate	3.15	3.60	3.15
Coarse sand	2.00	2.30	2.00
Fine sand	0.89	1.03	0.89
Cement	1.00	1.00	1.00
Free water	0.68	0.78	0.74

Table 5.2 : Concrete mix proportion by weight

Type of LVDT	Rated stroke	Linearity	Sensitivity (load impedance of 20 kΩ)	Power input	Range of calibration factor	Accuracy of measurement
Sangamo Schlumberger DCR/25	± 25 mm	0.3%	17.12 mV/V/mm	10V d.c	11 to 13.5 mm/V	± 0.059 mm ± 14 $\mu\epsilon$
Sangamo Schlumberger DCR/50	± 50 mm	0.3%	6.36 mV/V/mm	10V d.c	13.5 to 14.5 mm/V	± 0.055 mm ± 12 $\mu\epsilon$

Table 5.3: Characteristics of LVDT's

Type	Gauge length	Gauge resistance	Range of gauge factors	Power input	Accuracy of measurement
PL-10	10 mm	120 ohms ± 0.3	2.10 to 2.13	2V d.c	± 3$\mu\epsilon$
PLS-10	10 mm	120 ohms ± 0.3	2.06 to 2.09	2V d.c	± 3 $\mu\epsilon$

Table 5.4: Characteristics of strain gauges

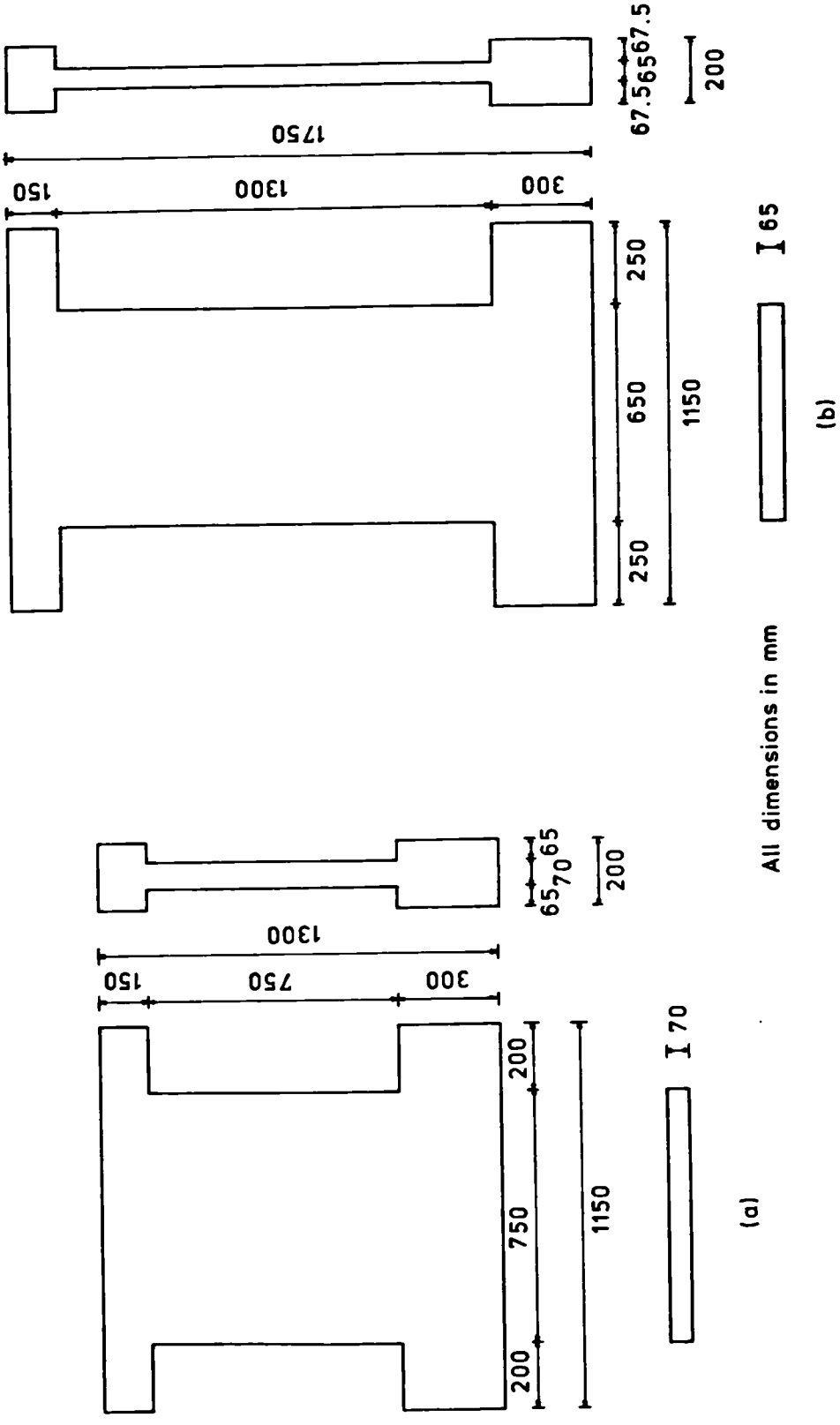


Fig. 5.1. Structural wall specimens (a) type I and (b) type II.

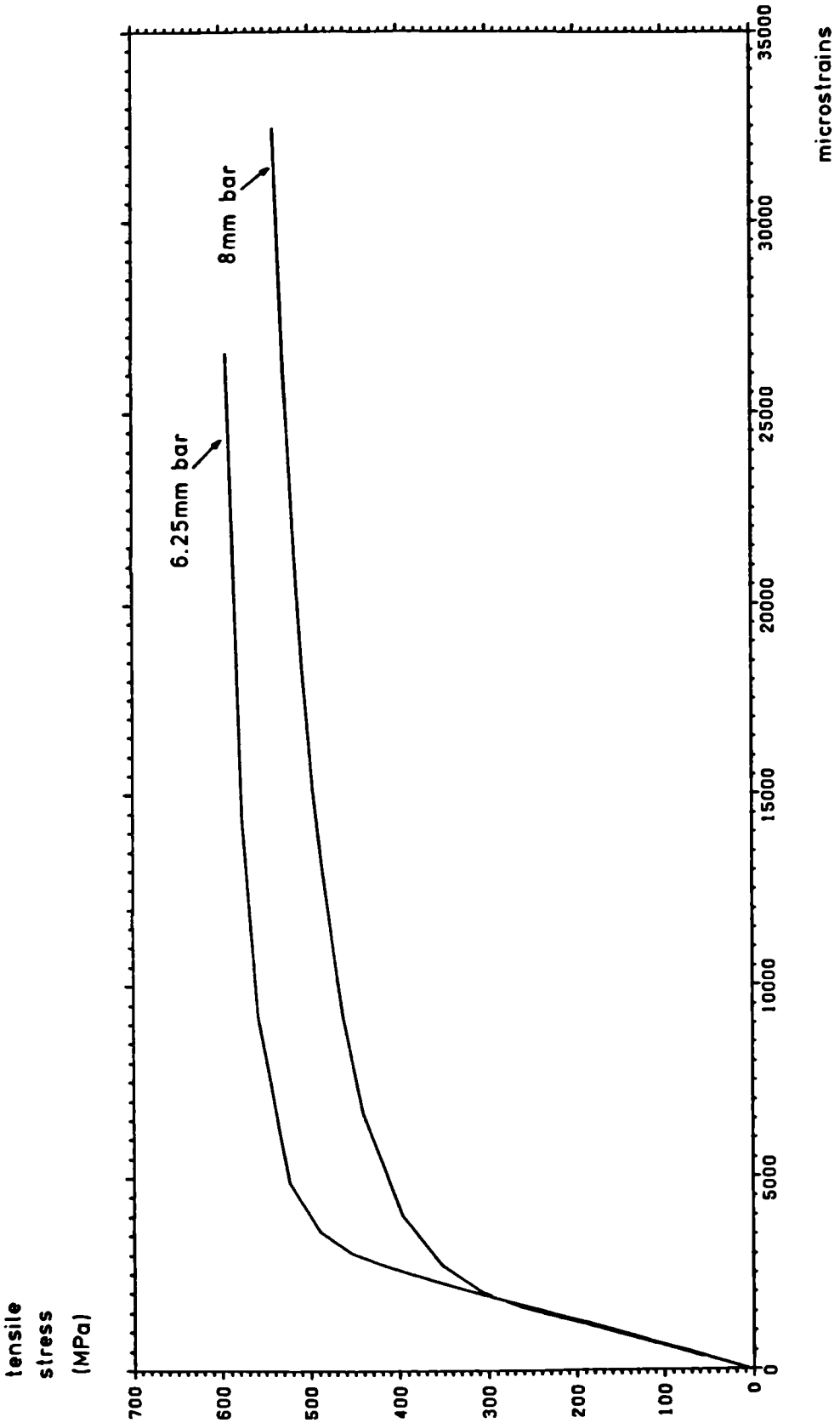


Fig. 5.2. Typical stress-strain relationships of the high yield steel bars.

Fig. 5.3. (a) Types of reinforcing bars used (upper plate),
(b) Details of the fracture zone of the bars
after the tensile test (lower plate).

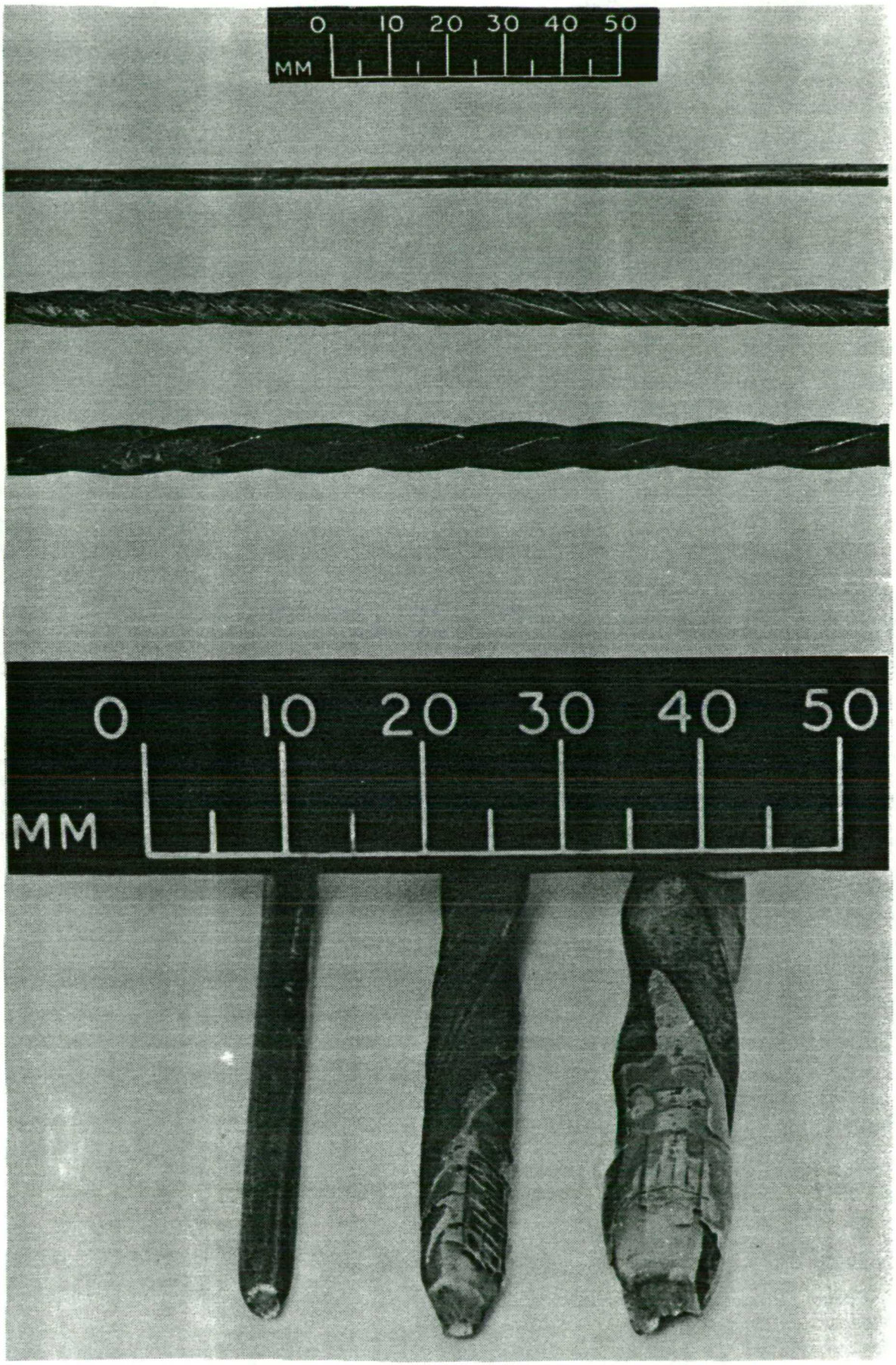
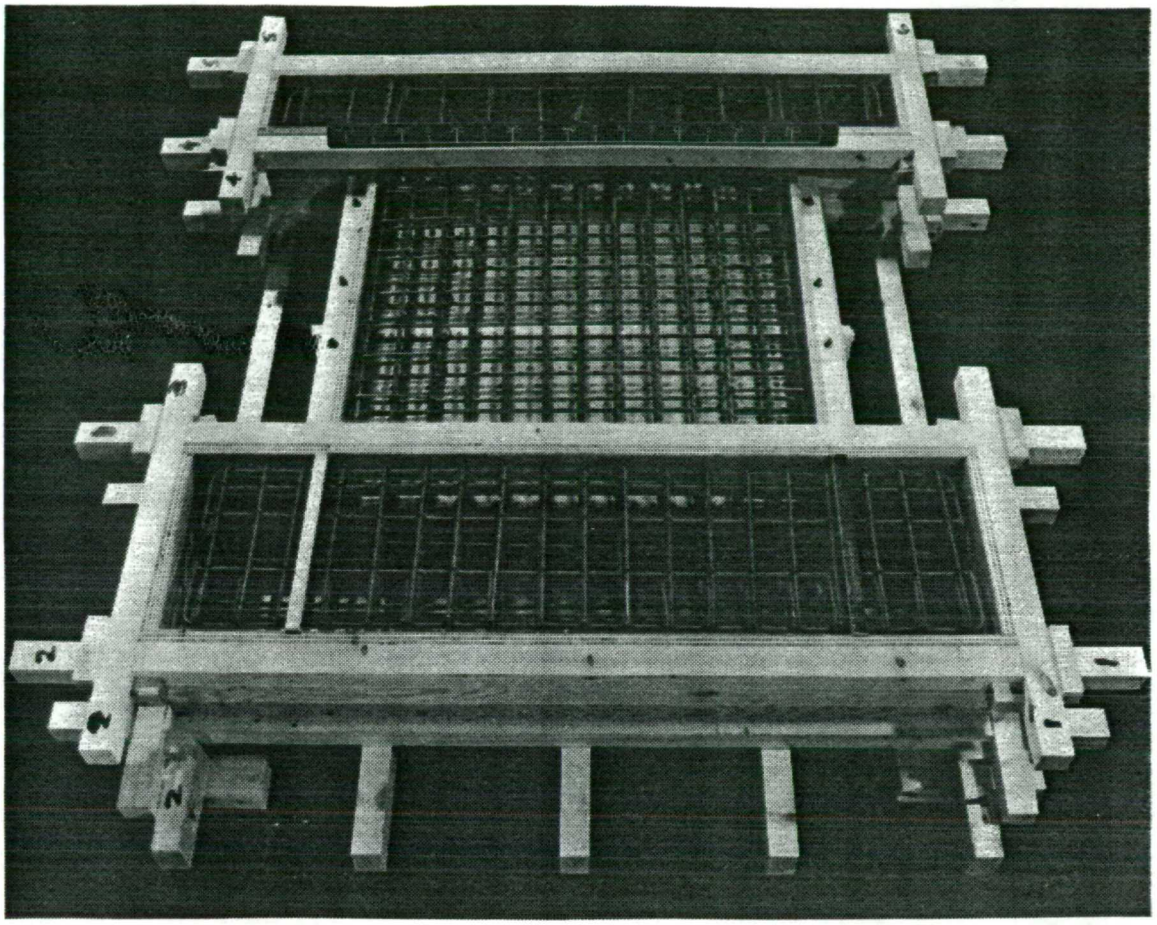

0 10 20 30 40 50
MM
0 10 20 30 40 50
MM

Fig. 5.4 Mould and reinforcement details of type I wall prior to casting.



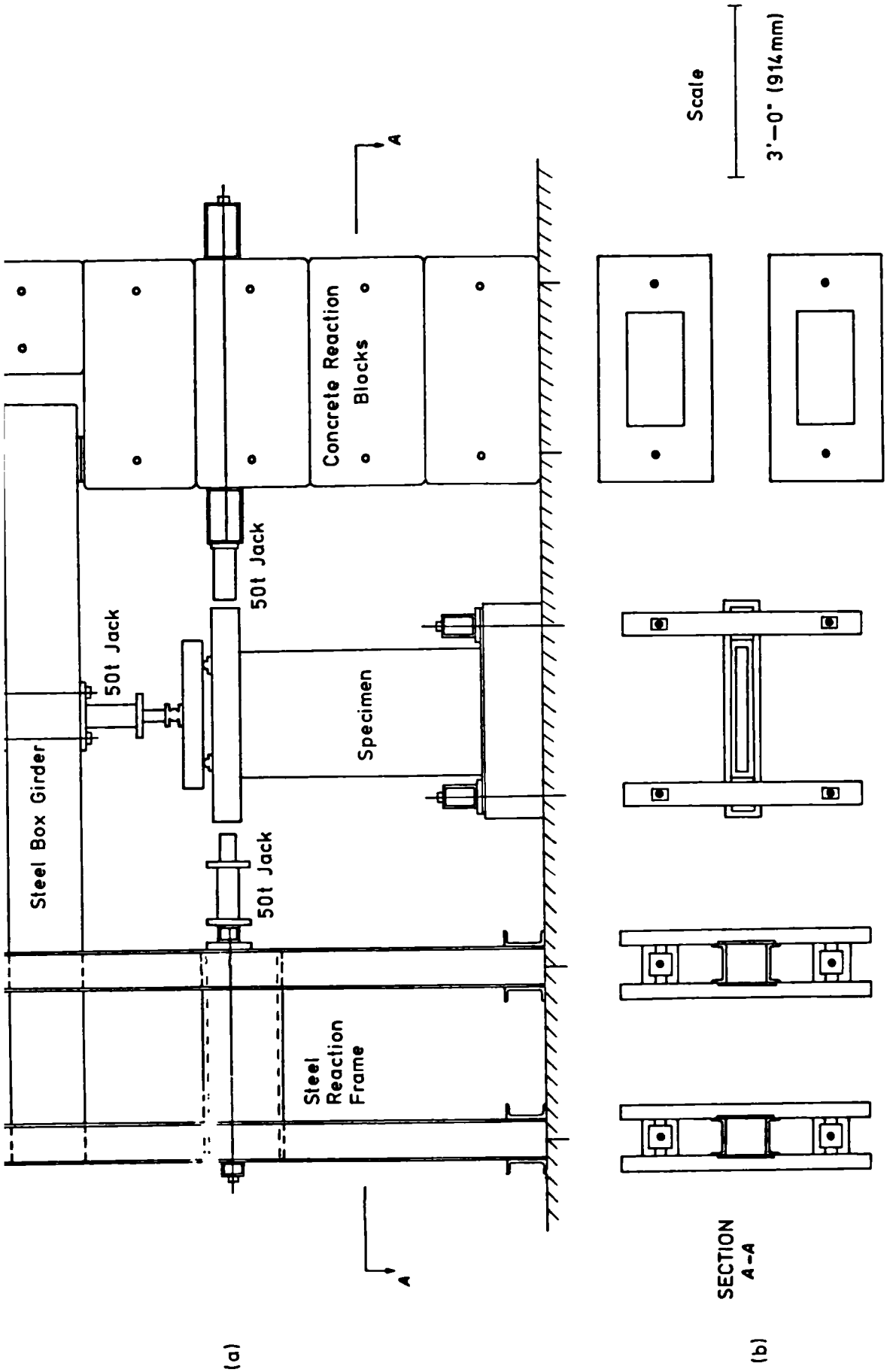


Fig. 5.5. Schematic representation of the test rig (a) elevation and (b) plan view.

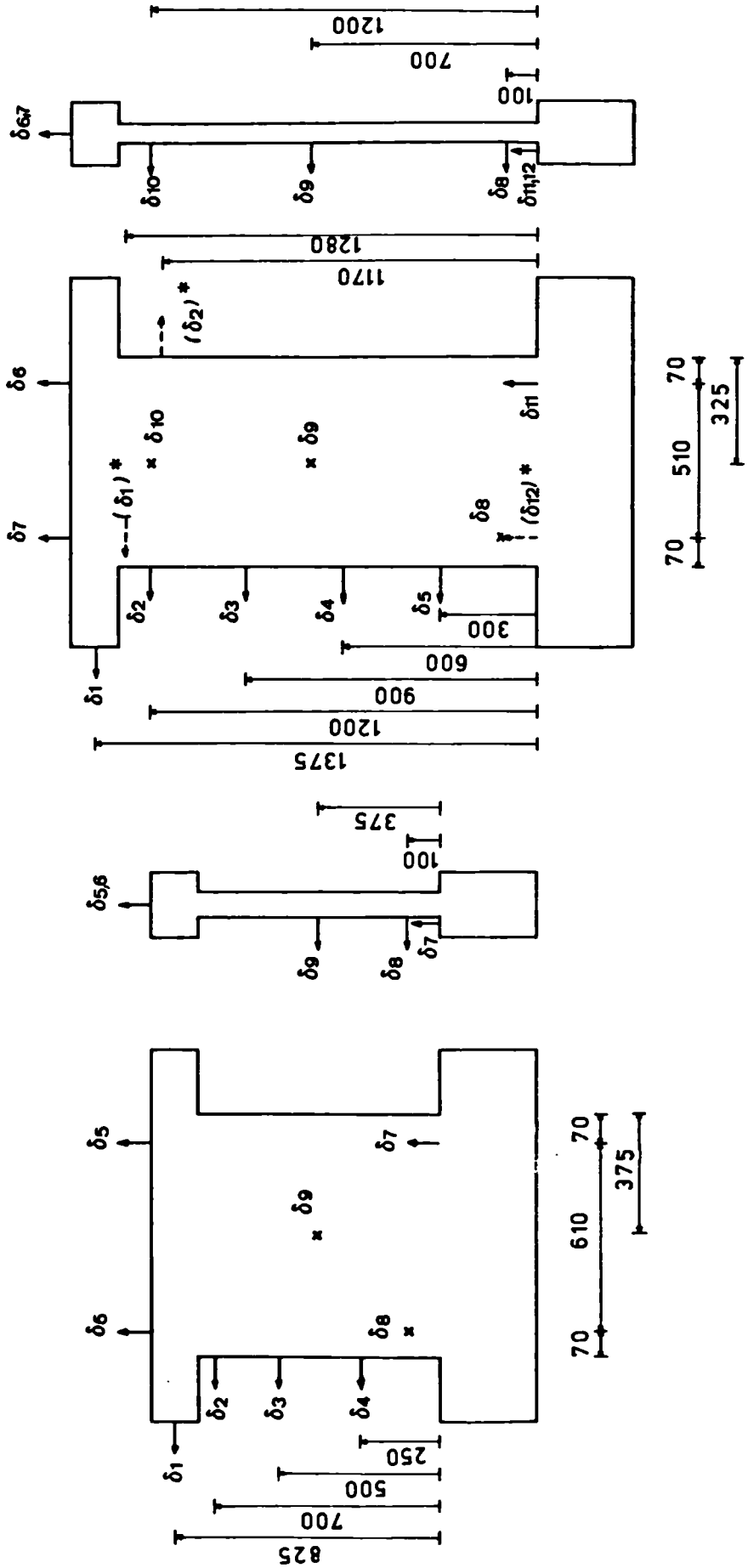


Fig. 5.6. Arrangement of the linear voltage displacement transducers (LVDT's) and displacement sign convention.

CHAPTER 6

EXPERIMENTAL INVESTIGATION OF THE BEHAVIOUR OF TYPE I WALLS UNDER MONOTONIC LOADING

6.1. INTRODUCTION

This chapter describes the results obtained from six tests on reinforced concrete walls with a height to width ratio of one, subjected to various combinations of constant vertical load and monotonically increasing horizontal load. In an attempt to identify the causes and mechanisms of failure, the aspects of wall behaviour investigated included the strength and deformation characteristics, fracture processes and modes of failure. The influence of parameters such as the vertical (axial) stress and concrete strength was also investigated.

6.2. WALL DETAILS

The main information referring to the properties of the materials used in the specimens is given in Section 5.2. Only additional data related to reinforced detailing and concrete strength characteristics will be presented here.

Figure 6.1 shows details of both cross-sectional characteristics and reinforcement arrangement of the wall with height to width ratio of one together with the design details of the upper and lower beams monolithically connected to it. The design of specimens SW11 to SW16 was based on the 1983 edition of the ACI code. As the main variable examined was the level of constant vertical load, it was decided that percentages of vertical and horizontal reinforcement in the wall could be kept constant throughout the experimental programme.

In all specimens, uniformly distributed horizontal reinforcement was placed in the 70 mm thick web. The vertical reinforcement consisted of uniformly distributed bars. In the extreme tensile and compressive zones of the wall, 4 mm transverse hoops were provided to enhance confinement of the concrete and to prevent the premature buckling of the vertical bars.

Table 6.1 includes information associated with the percentages of reinforcement used, the level of constant vertical load applied in each specimen in terms of both actual and normalized values, and the level of maximum horizontal load attained

during testing. Two walls were tested under the same level of normalized vertical load.

The design of the lower beam was governed by the requirement of carrying the clamping forces without cracking, while the main requirement in the design of the upper beam was the transmission of the applied forces to the wall.

Table 6.2 includes full details of the average uniaxial compressive strength of the concrete used in wall specimens of type I. Although the concrete used in all specimens had the same mix design, the strength of the concrete tested on the day of testing of the walls varied because the walls were tested at different concrete ages. It is believed, however, that in addition to the difference in ageing the discrepancies in the concrete strength values may be also attributed to the curing conditions. The control cubes were not cured in water but in the ambient laboratory conditions after 7 days curing with wetted hessians near the wall specimen. The 28–day compressive cube strength was close to the specified value of 45 MPa but at the time of testing the cube strength varied from 40.6 to 53.6 MPa. Since the ratio of cylinder–strength to cube–strength of the specimens had not been constant, cube strength was selected as the reference value. Therefore, the value of cylinder strength, f_c' (MPa), used in the discussion of the results and in the comparative study of the wall behaviour, was taken as being equal to 85% of the experimentally obtained average cube strength.

Three levels of normalized constant vertical load were adopted in the testing procedure. They corresponded to 0.0, 0.1 and 0.2 of the product of 85% of the unconfined compressive cube strength and the gross horizontal cross–sectional area of the specimen. These levels might be considered representative of the amount of axial load resulting from dead and live load at the base of the wall of a single storey, medium height and high rise building respectively.

6.3. PRESENTATION OF RESULTS

The main results of the experimental work on reinforced concrete structural walls with height to width ratio of one, together with information essential for a better understanding of their behaviour are presented in this section.

Results derived from the test measurements are given in the form of curves of horizontal load versus deflection in Figures 6.2 to 6.7. Each figure corresponds to one of the six specimens tested and comprises three subfigures which present

information related to

(a) the horizontal displacement of the specimen at different elevations;

(b) shortening of the compressive edge of the wall, elongation of the tensile edge of the wall and rotation of the lower foundation beam;

(c) detection of any out–of–plane movement of the specimens near the lower part of the compressive edge of the wall and at the mid–height level of the wall.

Table 6.3 contains information concerning the lateral load, the top lateral displacement, the stiffness and the drift index of type I walls at the following loading stages:

(a) initiation of flexural cracking;

(b) initiation of inclined cracking;

(c) first yield of the tensile reinforcement and

(d) the ultimate horizontal load.

The above loading stages are defined as follows :

Initiation of flexural cracking denotes the loading stage at which the monotonically increasing horizontal load produces the first flexural crack to the specimen. During testing the first crack was visually noted while the applied horizontal load was gradually increased. The actual first cracking load is always less than the value included in Table 6.3, since the crack must become visible before it can be detected. The horizontal load which produces the first inclined crack resulting from the combined action of moment and shear designates the initiation of the inclined cracking process. Knowledge concerning the yield of the tensile reinforcement is useful in the sense that it provides data for evaluating the inelastic behaviour of the wall. This basically refers to the computation of the ductility level of the wall. Yielding of both extreme bars in the tensile edge of the wall determines the loading stage assigned as first yield of tensile reinforcement. The experimental determination of the first yield load was based, either on the reading of the strain gauges attached to the extreme tensile bars, or on the level when the stiffness of the wall underwent significant change in cases where information from strain gauges (ersgs) was not available. When the strain measured by the gauges

exceeded 0.0025 the specimen was assumed to have reached its yielding phase. Ultimate horizontal load stage is the situation when the experimental value of horizontal load sustained by the wall suddenly drops and the wall fails.

Code provisions (UBC, 1982 and ACI, 1983) and recent investigations (Oesterle et al, 1984) relate the ultimate shear stress of the walls to either the uniaxial compressive cylinder strength of concrete f'_c or its square root $\sqrt{f'_c}$. Not only for comparison purposes, but also in order to check the validity of such considerations, Table 6.4 is produced. It presents shear stress values at different loading stages and normalized values of ultimate shear stress with respect to f'_c and $\sqrt{f'_c}$. Shear stress is defined as the ratio of the horizontal load to the gross horizontal cross-sectional area of the wall.

The initial stiffness characteristics as well as variations in stiffness with the level of deformation and load, are necessary for any non-linear static structural analysis. In the case of structures incorporating walls, predicting the wall stiffness characteristics is particularly important because the walls are generally substantially stiffer than the other components of the structure and their contribution would tend to dominate the stiffness of the whole system.

Figure 6.8 shows the pattern of the variation of secant stiffness with increasing horizontal load and/or shear stress, for the three levels of constant normalized vertical load adopted for the walls tested.

Significant stages of cracking process and behaviour up to incipient failure, exhibited by the type I walls, are shown in Figure 6.9. Typical modes of failure exhibited by the type I walls tested under different vertical load conditions are shown in Figure 6.10, whereas Figure 6.11 gives a schematic representation of the mechanism that leads to such modes of failure.

6.4. DISCUSSION OF RESULTS

6.4.1. VALIDATION OF THE EXPERIMENTAL SET-UP

The suitability of any testing procedure must be judged on whether or not it fulfils the initial requirements and assumptions of the test.

In order to examine how realistic were the assumptions of a plane stress analysis in the EW direction during the testing procedure, the out-of-plane

displacement history of potential buckling zones was of primary interest. Figures 6.2(c) to 6.7(c) indicate that for the majority of the cases the maximum out of plane displacement was only of the order of 0.03% of the height of the wall. Only for specimens SW12 and SW13 the level of maximum out-of-plane movement reached 0.13% of the height of the wall. However, such a displacement can only contribute secondary rotational moment about the EW axis and secondary torsional moment of the order of 0.3% of the rotational moment about the NS axis, which is the primary moment, and thus the plane stress conditions assumed in the analytical investigation are justified.

Another of the assumptions of the analytical work with respect to the boundary conditions of the wall element, was the base fixity. In all cases, except SW13 and SW14, the clamp force was transferred to the lower beam through two transverse steel girders in the NS direction, as indicated in Figure 5.5. The absence of the steel rods in specimen SW13 and SW14 led to comparatively higher values of base rotation which were still too small to affect the horizontal load carrying capacity of the walls. The actual horizontal load levels sustained by these specimens justify the assumption of base fixity. The levels of maximum base rotation observed during testing were 3% and 5% of a degree for specimens SW13 and SW14 respectively, while for the other specimens base fixity rotation values drop with the increase of the level of constant vertical load applied to them. Maximum values corresponding to 1%, 0.4% and 0.3% of a degree for walls subjected to normalized vertical stress levels of 0, 0.1 and 0.2 respectively, were measured. The pattern of the variation of horizontal load versus base vertical displacement can be seen in Figures 6.2(b) to 6.7(b), while Figure 6.12 illustrates the base fixity results of all specimens in enlarged base vertical displacement scale.

To check for repeatability the horizontal load versus top horizontal displacement curves of all specimens tested is presented in Figure 6.13. The results underline the almost identical load-displacement curves of specimens initially subjected to levels of normalized constant vertical stress equal to 0 and 0.1. Specimen SW16 subjected to precompression stress of 0.2 f_c' also follows the pattern of enhancement in stiffness as the level of axial load increases. The only exception might have been the load-displacement curve of Specimen SW13. The more flexible behaviour of this specimen compared to its companion SW16 is attributed to the damage (cracking and spalling of the concrete cover) suffered by the lower foundation beam during the clamping procedure. The higher values of out-of-plane movement and base rotation observed by this particular specimen during testing are also partially correlated to the above damage. It is interesting

to note, that besides this unexpected event, the ultimate horizontal load carrying capacity of SW13 was not affected. Differences in the measured horizontal load capacity of specimens subjected to the same vertical load history never exceeded ± 4% and can be attributed to concrete cube strength variations.

6.4.2. LOAD CARRYING CAPACITY AND DEFORMATIONAL RESPONSE

Evaluation of the effect of varying vertical load levels on the behaviour of structural walls with height to width ratio of one can be made by a comparative study of their load carrying capacities and deformational characteristics.

As Table 6.2 indicates the horizontal load carrying capacities of walls subjected to the same level of normalized vertical load, ν, are similar. A load carrying capacity enhancement of the order of 25% and 30% with respect to specimens subjected to no vertical load was observed in cases where ν was equal to 0.1 and 0.2 respectively. It is interesting to note that specimens with higher uniaxial compressive concrete strength exhibit only a slightly higher load carrying capacity, if subjected to the same level of normalized vertical stress. Specimens SW11 and SW14, which were not subjected to any vertical loading showed almost identical strength characteristics. These observations are also illustrated in the moment–axial force interaction diagram of Figure 6.14.

The deformational response of all walls is distinctly non–linear. Figures 6.2(a) to 6.7(a) indicate that even for high levels of constant vertical load some ductility was observed. A characteristic feature of the horizontal load–lateral displacement curves is the occurrence of some sudden increases in deflection under a constant horizontal load. These events appear to reflect the extension of flexural cracking into the web of the wall in a loading stage between the first appearance of flexural and inclined cracking, and the beginning of yielding of the vertical reinforcement of the web of the wall.

Axial compressive stress has been found to reduce the value of the top horizontal displacement at near ultimate horizontal load level as indicated in Table 6.3. A drop of the ductility ratio (i.e. the ratio of top horizontal displacement at ultimate to top horizontal displacement at first yielding) from 2.8 to 2.3 was observed only when axial stress level reached 0.2 f'_c. Top horizontal displacement attained by the specimen one load step prior to the ultimate horizontal load, was considered as the reference point for the calculation of the ductility ratio. The reason is that as the wall fails, its horizontal load carrying capacity drops

considerably and thus the recorded value of displacement may correspond to any load value.

Figures 6.2(b) to 6.7(b) show that axial stress level also affected the amount of shear distortion in the walls. As the horizontal load applied to the wall increases, one edge of the wall is elongated while the other is shortened. It is apparent that the higher the level of axial stress level applied to the wall, the smaller the elongation of the tensile edge of the wall. However, axial stress variations did not alter the level of shortening of the edge of the wall under compression. These observations lead to two implications. Firstly, the smaller the difference between the absolute values of elongation and shortening, the greater the depth of neutral axis of the wall. Secondly, an assessment of lateral displacement attributed to flexural and shear deformations can be carried out. The angle of rotation due to pure flexure is calculated as the sum of the absolute measured vertical displacements, cleared from any base fixity component, divided by the horizontal distance between them. The flexural deformation component at top lateral displacement level is calculated by multiplying the angle of rotation by the height between the foundation level and the position of the top displacement transducer. The shear deformation component is then estimated as the difference between the total top deformation and the calculated rotation component. As the test measurements indicate, flexural distortion was the primary deformation occurring at the top level of each wall. When normalized vertical load ν was equal to zero, the ultimate flexural distortion measured at the top was approximately 76% of the total displacement. When ν = 0.10, this value increased to 81% and reached 86% in the specimen SW16, where ν was equal to 0.2.

It should be noted that flexural deformation was responsible for almost all of the top lateral displacement before the development of significant inclined cracking in the walls and that levels of shear deformation were higher at the lower and intermediate height parts of the wall. Despite the lack of instruments measuring vertical displacements at intermediate heights along the wall, an approximate calculation based on the top vertical displacements and the assumption that plane sections remain plane shows that the contribution of flexural deformation at the lower part of the wall dropped to levels equal to 62%, 68% and 78% of the corresponding lateral displacement for walls subjected to 0, 0.1 and 0.2 normalized axial levels respectively.

Tables 6.3 and 6.4 indicate that with increasing level of constant vertical load, the level of horizontal load and shear stress corresponding to the various loading stages, described in Section 6.3, increased likewise. Nevertheless, normalizing these

values with respect to the ultimate capacity attained by each specimen, it is interesting to note that initial flexural cracking, first inclined cracking and first yielding of tensile longitudinal bars occur at about 15%, 40% and 70% of the ultimate limit state respectively. The same statement does not hold for the displacement and drift indices at various loading stages. The above deformational characteristics appear not to be consistently affected by the variation in the initial vertical stress.

The middle columns of Table 6.4 show that the values of measured shear stresses normalized with respect to the uniaxial cylinder compressive concrete strength, f'_c, for the same level of normalized axial stress present a scatter well outside the scatter of test results. In contrast, the normalization with respect to the square root of f'_c, leads to values with considerably less variation. This appears to indicate that the uniaxial strength characteristics of concrete is not an efficient factor for normalization purposes. The reason for this may be the fact that stress conditions in the failure zones of the specimens are complex and cannot be adequately represented by uniaxial stress conditions.

6.4.3. STIFFNESS CHARACTERISTICS

Table 6.3 and Figure 6.8 show that all of the specimens, except SW13, present an increase in secant stiffness values as the applied level of constant vertical stress increases. Section 6.4.1 deals extensively with the reasons for the more flexible response of wall SW13. Had specimen SW16 been considered as the most representative of the walls subjected to ν = 0.20, the values of secant stiffness in Table 6.3 indicate that values of 65 and 100 percent enhancement in stiffness were observed in almost all intermediate loading stages when specimens were subjected to ν = 0.1 and ν = 0.2 respectively. The ultimate secant stiffness values of all specimens was approximately equal to 25% of the stiffness value exhibited by the wall before the observation of any visible cracking.

Some characteristic features of the secant stiffness–horizontal load/shear stress curves, illustrated in Figure 6.8, are described below. Each curve can be subdivided in four parts. The first part and up to point (a) represents the uncracked response of the specimens and shows that for the first increments of horizontal loading stiffness values exhibit a large variability and cannot be trusted. After point (a), the initiation of flexural cracking is characterised by a sudden drop in stiffness with respect to the applied horizontal load. Before reaching point (b) most of flexural crack pattern has developed and the curve tends to become almost

horizontal. At point (b) significant inclined cracking commences and the stiffness values show again an abrupt change in direction. Point (c) denotes the first yielding of vertical reinforcement and it is near this point that the secant stiffness–horizontal load curve changes curvature. As more of the vertical bars yield, stiffness values quickly drop to their ultimate level. A common feature of the stiffness curves is that, as expected, when the level of constant vertical load applied to the wall is low, flexural cracking is responsible for most of the reduction in stiffness. High levels of normalized compression stresses result in a more balanced loss in secant stiffness characteristics between the loading stages.

The one–dimensional cantilever element force–displacement relations provided by structural analysis and adopted by Codes lead to a lateral displacement value equal to 3 x 10^{-6} mm/N. (See Appendix A for the theoretical calculations). If the horizontal load corresponding to first crack is considered representative to describe the uncracked behaviour of the wall, then the theoretical secant stiffness for the uncracked case is equal to 333.3 KN/mm independent of the level of vertical load.

The stiffness values included in Table 6.3 show that the level of vertical load is observed to influence strongly the secant stiffness values measured before cracking. The latter values vary from 30 to 60 percent of the theoretical nominal secant stiffness as the level of constant vertical stress increases from zero to 0.2 x f'_c. Therefore, the effect of vertical force on wall element secant stiffness, is apparent even at the uncracked serviceability limit state of response.

Greater disagreement with the standard analytical procedure was observed when analytically predicted values of axial displacement were compared with the measured axial displacement along the edge members, as different levels of vertical (axial) load were applied to the specimens. The analytical axial rigidity EA based on the gross cross–sectional area is approximately equal to 2000 x 10^6 N, while the experimentally measured value is almost 20 times less. Table A.3. illustrates the axial force (compression)–axial strain (shortening) relationship for the wall section examined, including both the analytical and the experimental values.

The main reason for the considerably smaller measured values of wall stiffness should be the cracking of concrete at the microscopic level. Many of these microcracks are either due to shrinkage or due to the heterogeneous nature of concrete; furthermore they exist within the concrete even before loading. They result in a much smaller effective modulus of elasticity of concrete at service level stresses compared with the value obtained from cylinder tests.

6.4.4. FRACTURE PROCESSES AND FAILURE MODES

Information regarding the fracture processes of low-rise structural walls will be presented for three pairs of specimens. Each pair was subjected to a certain level of normalized vertical (axial) stress.

Specimens SW11 and SW14

The first flexural cracks appeared near the bottom third part of the tensile edge of the specimens, after the application of 15% of the ultimate horizontal load. Their spacing varied from 100 to 150 mm. The flexural cracking continued to spread at a slight inclination towards the web of the wall, under increasing horizontal load (see Figure 6.9(a)). As the level of applied horizontal load reached 40% of its ultimate value, the first significant inclined crack appeared. It started from the upper tensile corner of the wall and extended at approximately 45° almost half-way through the lower compressive corner of the wall as shown in Figure 6.9(b). Further loading caused not only new flexural cracks to develop in between the first flexural cracks, but also inclined cracking which almost reached the compressive edge of the wall. When 80% of the ultimate horizontal load was reached, the spacing of the flexural cracks was reduced to 60 mm, the spacing of the inclined cracks was 90 mm, while the depth of the compressive zone covered approximately one-fifth of wall width as illustrated in Figure 6.9(c).

The macrocrack pattern remained unchanged for horizontal load increasing from 80 to 95% of the ultimate capacity of the wall. Further horizontal load increments resulted in splitting of the concrete cover of the extreme compressive edge of the wall, together with the propagation of the inclined crack closest to this region near-vertically towards the base of the wall. This finally led to the failure of the compressive zone of the wall and the sudden drop of horizontal load carrying capacity of the wall. (See Figure 6.10(a)). It should be noted that, (a) concrete cover splitting happened in a progressive manner with not a hint of strength drop being observed during this process and (b) the overall behaviour of the wall up to failure was that of a ductile flexural element.

Specimens SW12 and SW15

Both specimens were subjected to a normalized axial load level of 0.1. Their initial crack pattern was similar to that of the previous specimens. Although the values of horizontal load of the precompressed specimens at the initiation of flexural and inclined cracking had been noticeably higher than those of the specimens

discussed in the previous subsection, as a percentage of the ultimate horizontal load, they were similar. When a level of horizontal load equal to 80% of its ultimate value was reached, a number of distinct features of the fracture process of these specimens were observed. The distribution of horizontal flexural cracks was still uniform but with smaller spacing while the inclined cracking was less extensive, covered a smaller region and penetrated into a smaller area of the compressive zone of the wall.

Further horizontal load increments resulted in insignificant changes, up to the stage when progressive splitting of the concrete cover of the compressive edge of the wall and near-vertical propagation of the inclined crack closest to the lower part of the wall under compression were noted. Due to the presence of axial load the depth of the neutral axis was larger and the subsequent "crushing" band width was more extensive, as shown in Figure 6.10(b).

Specimens SW13 and SW16

The presence of higher levels of constant vertical load led to even less extensive crack formation. Fewer flexural cracks were formed at the tensile edge of the wall and diagonal cracking covered less of the web of the wall. Nevertheless, higher axial load levels only managed to delay but not prevent the extension of the inclined crack within the lower compressive edge of the wall. The consequent crushed compressive zone, as depicted in Figure 6.10(c), almost covered the entire horizontal width of the specimen. The extension of the crushing zone to nearly the whole of the wall width is attributed to the sudden unloading of the vertical load when no more horizontal load could be sustained by the specimen. In fact it was observed that the more synchronized was the unloading of the vertical load, with the drop of the horizontal load carrying capacity, the lesser the extent of the crushing zone.

Buckling of the horizontal reinforcement at the compressive edge of the wall in both directions could also be observed after removing the loose concrete pieces. The phenomenon was more pronounced when the specimen was also subjected to high levels of vertical load. Then buckling was extended to some of the longitudinal bars of the web of the wall. It should be recognized that in order for the reinforcement to buckle first the concrete cover must split at the level of all the longitudinal bars. Since no sign of such a sequence was observed, the concrete at the lowest compressive zone of the wall should have crushed first. As a consequence, reduction in concrete stiffness increased the load on longitudinal steel bars precipitating buckling.

6.4.5. CAUSES OF WALL RESISTANCE AND FAILURE MECHANISM

As Figure 6.10 indicates, the collapse of all the wall specimens occurred due to failure of the compressive zone. The presence of vertical load delays the occurrence of failure and thus further increases the horizontal load carrying capacity of the walls. One load stage before failure, the width of the major flexural cracks became considerable. It should be expected, for the crack width of 0.5 mm, that the aggregate interlock is negligible. A negligible aggregate interlock action should result in an insignificant shear resistance of the concrete region of the wall below the neutral axis, since the shear resistance of this region could be provided mainly by aggregate interlock.

Figure 6.10 shows that in all walls tested the inclined crack reduces the depth of the compressive zone to a small value equal to 0.12, 0.17 and 0.25 of the wall width for specimens subjected to 0, 0.1 and 0.2 of normalized vertical load, respectively. In fact, the depth of neutral axis can be even smaller at the cross–section including the tip of the inclined crack that eventually causes failure of the wall. In spite of its small depth the compressive zone is capable of sustaining a load significantly higher than that generally expected. This is because the compressive zone is subjected to a triaxial – not uniaxial – state of stress. A triaxial compressive state of stress can be developed due to both the occurrence of volume dilation in localized regions within the compressive zone, and the presence of stirrups as confinement reinforcement in this region. The development of such stress conditions is inevitable since it is essential for maintaining a compatibility of deformation in the compressive zone. A similar state of stress was observed in the experimental behaviour of reinforced concrete beams (Kotsovos, 1987a).

Figure 6.11 illustrates schematically the mechanism providing shear resistance to the lower part of the compressive zone of the wall. A part of the horizontal component of the triaxial compressive state of stress counteracts the tensile stresses that develop in the presence of shear forces. As a result, the compressive force within the compressive zone needs not to be significantly inclined in order to balance the shear force.

An indication of the causes of this behaviour can be obtained by assessing the average longitudinal and transversal stresses in the compressive zone of the walls. Using the measured values for the maximum horizontal load–carrying capacity of the wall, the amount of the applied vertical load and the strength of the longitudinal reinforcement both in tension and compression, the average longitudinal stress in the compressive zone at failure can be calculated by considering force and moment

equilibrium conditions. The calculated average longitudinal stress in the compressive zone of concrete was found to be for all the specimens much higher than the uniaxial cylinder compressive strength of the concrete. Information on the triaxial strength capacity of concrete (Kotsovos 1984a) indicate that for a concrete element to sustain such a longitudinal stress, surrounding concrete and stirrups must provide confinement which has been assessed to be a percentage of f_c' as shown in Figure 6.15. The combination of stresses due to bending with the stresses due to shear acting on the compressive zone is leading to the calculation of the combined principal stress conditions σ_1, σ_2, σ_3, which can also be transformed into their equivalent normal, σ_o and shear, τ_o octahedral stresses. Experimental data on the strength of concrete under triaxial stress conditions $\sigma_1 > \sigma_2 = \sigma_3$ have indicated (Kotsovos 1980) that the combinations of σ_o and τ_o causing failure can be expressed by

$$\frac{\tau_{o,ult}}{f_c'} = 0.944 \left(\frac{\sigma_o}{f_c'} + 0.05\right)^{0.724} \qquad \text{(Eq. 6.1)}$$

Therefore for given values of f_c' and σ_o equation 6.1 yields to the ultimate value of octahedral shear stress $\tau_{o,ult}$. In all the walls tested, the applied octahedral shear stress, following the previously described procedure, was always greater than the ultimate shear stress value. Table 6.5 summarizes the steps of the adopted procedure.

6.5. CONCLUSIONS

The main findings regarding the experimental behaviour of reinforced concrete structural walls with height to width ratio of one are as follows:

(a) The testing procedure adopted for the experimental investigation was proved to offer a valid experimental set-up. Out of plane displacement and base fixity values were negligible for all type I walls tested.

(b) Walls subjected to high levels of constant vertical load presented an increased horizontal load carrying capacity up to 1.3 times the measured horizontal load capacity of specimens subjected to no vertical load.

(c) The deformation response of all walls is distinctly non-linear. Vertical compression has been found to reduce the lateral displacement response.

Under high levels of vertical stress a reduction of the ductility ratio from 2.8 to 2.3 was observed.

(d) High vertical compressive stresses result in a smaller difference between the absolute elongation and shortening values of the wall edges, which in turn leads to greater depths of the neutral axis. Flexural displacement is responsible for most of the top lateral displacement. The higher the level of vertical force, the less shear deformation is responsible for the displacement at any level along the height of the wall.

(e) Initial flexural cracking, first inclined cracking and first yielding of tensile longitudinal bars appear at about 15, 40 and 70 percent of the ultimate horizontal load capacity of each wall respectively, i.e. they are independent of the vertical (axial) stress.

(f) The level of vertical force was found to affect strongly secant stiffness characteristics. The highest value of normalized vertical stress applied resulted to 100 percent enhancement of secant stiffness. The ultimate secant stiffness values of all specimens was equal to approximately 25 percent of the stiffness exhibited in the uncracked state of the wall.

(g) The amount of initially applied axial stress considerably affected secant and axial stiffnesses within the uncracked serviceability limit state. Measured stiffnesses were only a small percentage of their corresponding nominal values.

(h) Failure of the walls occurred due to nearly vertical splitting of the compressive zone in the region of the tip of the inclined crack, followed by splitting of the whole compressive zone. Splitting of the compressive zone and subsequent buckling of some of the longitudinal reinforcement bars is believed to be a post-failure phenomenon. It was observed that in walls subjected to higher vertical stresses it is due to the deeper neutral axis characterizing such specimens.

(i) A triaxial - not uniaxial - state of stress in the compressive zone is responsible for the high measured values of horizontal load carrying capacity of the walls and the subsequent resistance of the walls to high shear stresses. The triaxial state of stresses counteracts the tensile stresses due to shear forces. Such a behaviour might indicate that the wall resistance to high shear stresses, developed in walls with height to width ratio of one, is primarily provided by the compressive zone, and not the web, of the wall.

SPECIMEN	REINFORCEMENT PERCENTAGE				VERTICAL LOAD		ULTIMATE HORIZONTAL LOAD
	P_{hor} (%)	Pver (%)	P_{fl} (%)	Ps (%)	Fv (kN)	$\frac{Fv}{b l f_c'}$	F_H (kN)
SW11	1.1	2.4	3.1	1.2	0	0	260
SW12	1.1	2.4	3.1	1.2	230	0.10	340
SW13	1.1	2.4	3.1	1.2	355	0.20	330
SW14	1.1	2.4	3.1	1.2	0	0	265
SW15	1.1	2.4	3.1	1.2	185	0.10	320
SW16	1.1	2.4	3.1	1.2	460	0.20	355

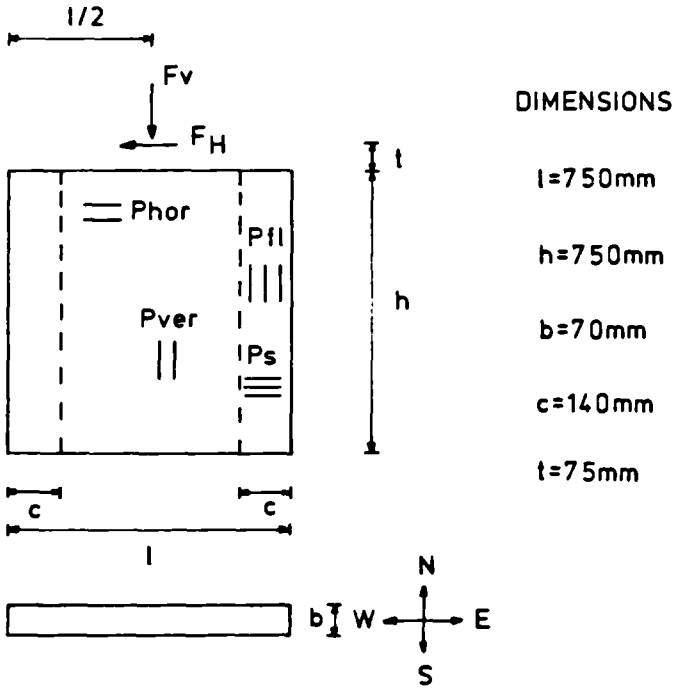


Table 6.1. Experimental data for type I walls.

SPECIMEN	TIME OF TESTING (days)	CUBE STRENGTH fcu (MPa)			CYLINDER STRENGTH fcyl (MPa)
		7 DAYS	28 DAYS	TESTING DAY	TESTING DAY
SW11	87	33.8	51.0	52.3	44.2
SW12	77	34.8	46.3	53.6	39.4
SW13	54	29.6	42.2	40.6	29.4
SW14	54	33.1	39.8	42.1	34.0
SW15	48	37.2	50.1	43.3	30.5
SW16	46	37.4	45.3	51.7	43.6
MEAN		34.3	45.8		
ST.DEVIATION		±2.65	±3.98		

Table 6.2. Concrete strength characteristics of type I walls.

SPECIMEN	LOADING LEVEL															
	INITIATION OF CRACKING				INITIATION OF INCLINED CRACKING				FIRST YIELD OF TENSILE REINF				ULTIMATE			
	F_H	δ	k	γ *10^{-2}	F_H	δ	k	γ *10^{-2}	F_H	δ	k	γ *10^{-2}	F_H	δ	k	γ *10^{-2}
SW11	35	0.34	104.3	0.046	100	1.77	56.6	0.232	170	3.59	47.3	0.468	260	at250 8.25	30.3	1.074
SW12	45	0.26	174.4	0.036	130	1.24	104.8	0.187	210	2.90	72.5	0.392	340	at335 8.86	37.8	1.178
SW13	50	0.37	135.3	0.051	150	1.45	103.4	0.188	250*	3.82	65.4	0.496	330	8.88	37.2	1.159
SW14	35	0.34	103.1	0.045	100	1.82	54.8	0.242	170	3.90	43.6	0.511	265	11.21	23.7	1.465
SW15	45	0.27	167.3	0.036	130	1.28	101.6	0.169	210*	2.89	72.6	0.381	320	at315 8.05	39.2	1.054
SW16	80	0.40	199.7	0.052	210	1.45	144.7	0.288	270*	2.50	108.1	0.339	355	5.78	61.4	0.775

*ersg

F_H in KN

δ in mm

k in KN/mm

$\gamma = \frac{\delta}{h}$ drift index

Table 6.3. Principal results for type I walls at various loading levels.

SPECIMEN	SHEAR STRESS (MPa)				SHEAR STRESS RATIOS				
	FLEXURAL CRACKING	INCLINED CRACKING	YIELDING OF REINF.	ULTIMATE	$\frac{V_{ult}}{\sqrt{f_c'}}$	$\frac{V_{ult}}{f_c'}$	$\frac{V_{cr}}{V_{ult}}$	$\frac{V_{ic}}{V_{ult}}$	$\frac{V_y}{V_{ult}}$
	V_{cr}	V_{ic}	V_y	V_{ult}					
SW11	0.67	1.90	3.24	4.95	0.743	0.112	0.14	0.38	0.65
SW12	0.86	2.48	4.00	6.48	0.959	0.142	0.13	0.38	0.62
SW13	0.95	2.86	4.76	6.29	1.070	0.182	0.15	0.45	0.75
SW14	0.67	1.90	3.24	5.05	0.841	0.140	0.13	0.38	0.64
SW15	0.86	2.48	4.00	6.10	1.005	0.166	0.14	0.41	0.66
SW16	1.52	4.00	5.14	6.76	1.019	0.154	0.22	0.59	0.76

Table 6.4. Shear stress values for type I walls at various loading levels.

SPECIMEN	DEPTH OF N.A. c (cm)	STRESSES DUE TO BENDING				STRESSES DUE TO SHEAR	COMBINED PRINCIPAL STRESS CONDITIONS			APPLIED STRESSES IN OCTAHEDRAL FORM		$\tau_{o,ult}$ (MPa)
		$\bar{\sigma}_x$	max σ_x *	max $\frac{\sigma_x}{fc}$	$\sigma_y = \sigma_z$	$\tau_{xy} = \frac{F_H}{cb}$	σ_1	σ_2	σ_3	σ_o	τ_o	
SW11	9	89.0	124.6	2.8	22.3	41.3	139.2	22.3	7.7	56.4	58.9	51.3
SW12	13	76.7	107.4	2.4	16.0	28.6	115.6	16.0	7.8	46.5	49.0	45.2
SW13	19	56.9	79.7	2.3	12.1	24.8	87.8	12.1	4.0	34.6	37.7	33.8
SW14	10	72.0	100.8	2.8	18.0	38.0	115.8	18.0	3.2	46.0	50.0	42.0
SW15	14	64.8	97.0	2.6	16.0	32.7	108.5	16.0	4.5	43.0	46.6	40.2
SW16	18	66.0	92.4	2.1	11.0	28.2	101.2	11.0	2.2	38.1	44.7	39.0

All stresses in MPa

* assuming a parabolic stress distribution

Table 6.5. Stress conditions causing failure of type I wall specimens.

Table 6.5 Cont'd

NOTATION

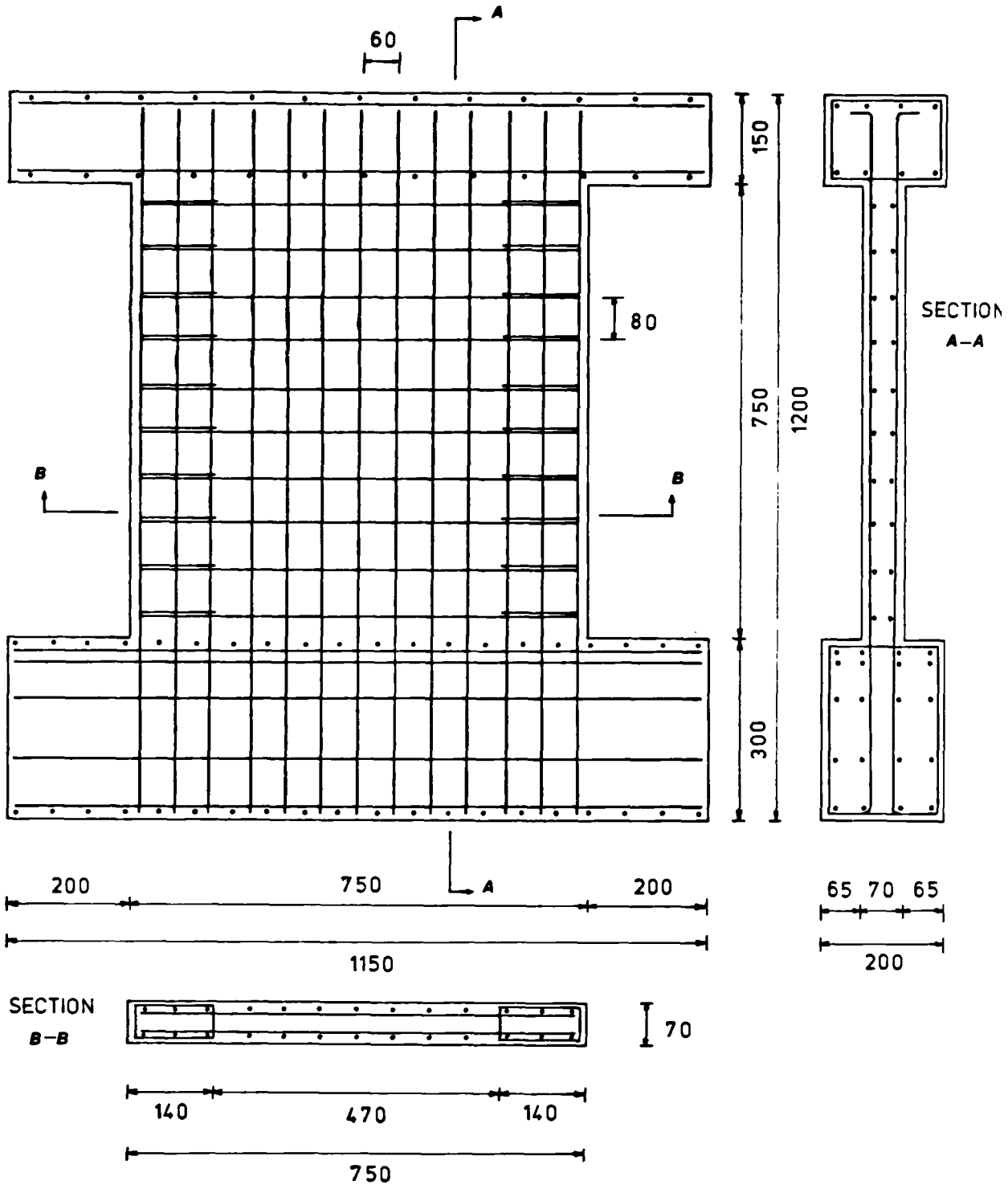
where $$\sigma_1 = \frac{\sigma_x + \sigma_y}{2} + \sqrt{\left\{\left(\frac{\sigma_x - \sigma_y}{2}\right)^2 + \tau_{xy}^2\right\}}$$

$$\sigma_2 = \sigma_z$$

$$\sigma_3 = \frac{\sigma_x + \sigma_y}{2} - \sqrt{\left\{\left(\frac{\sigma_x - \sigma_y}{2}\right)^2 + \tau_{xy}^2\right\}}$$

$$\sigma_{o,ap} = \frac{\sigma_1 + \sigma_2 + \sigma_3}{3}$$

$$\tau_{o,ap} = 1/3 \sqrt{\left\{(\sigma_1 - \sigma_2)^2 + (\sigma_2 - \sigma_3)^2 + (\sigma_3 - \sigma_1)^2\right\}}$$



All dimensions in mm

Fig. 6.1. Geometry and reinforcement details of type I walls.

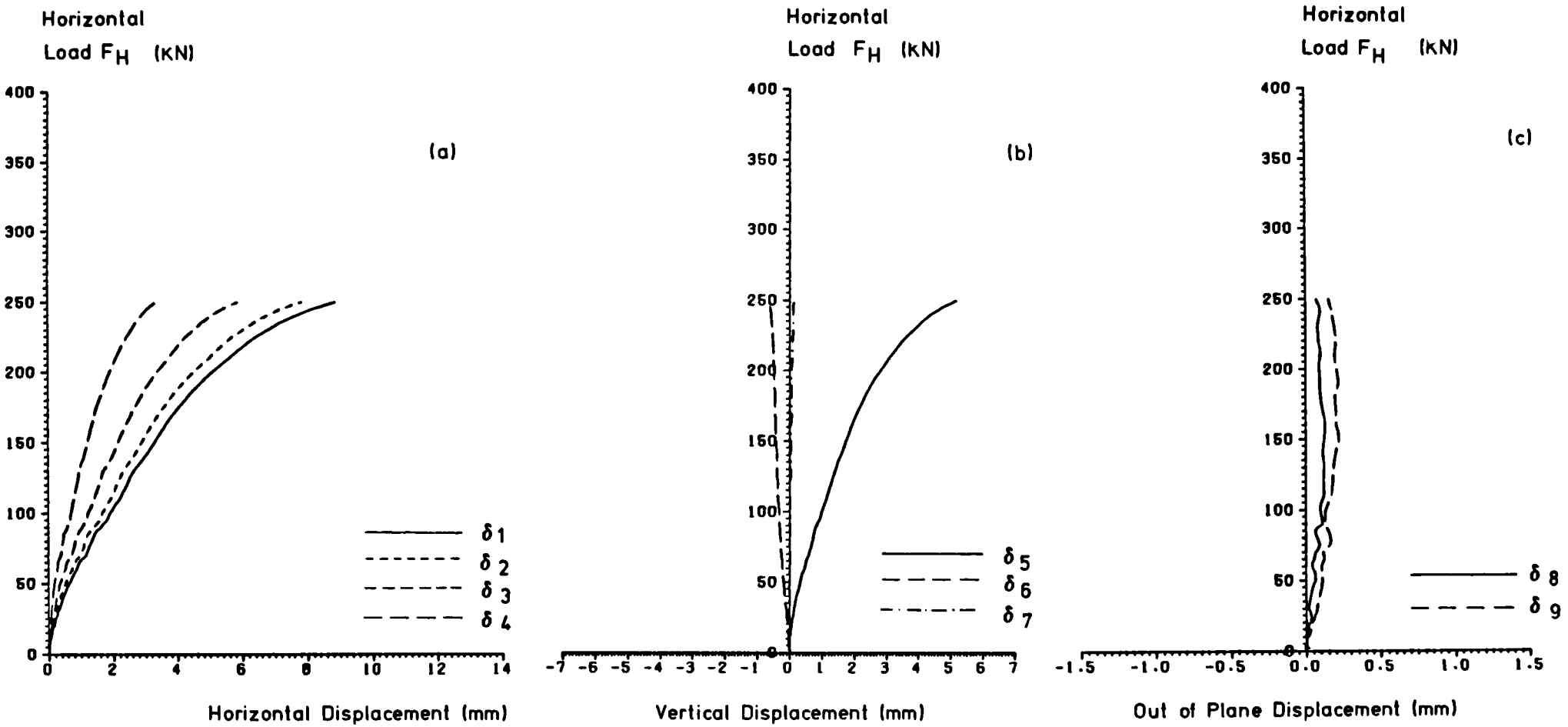


Fig. 6.2. Horizontal load-displacement curves of specimen SW11 constructed by using measurements of (a) horizontal displacement, (b) vertical displacement and (c) out of plane displacement.

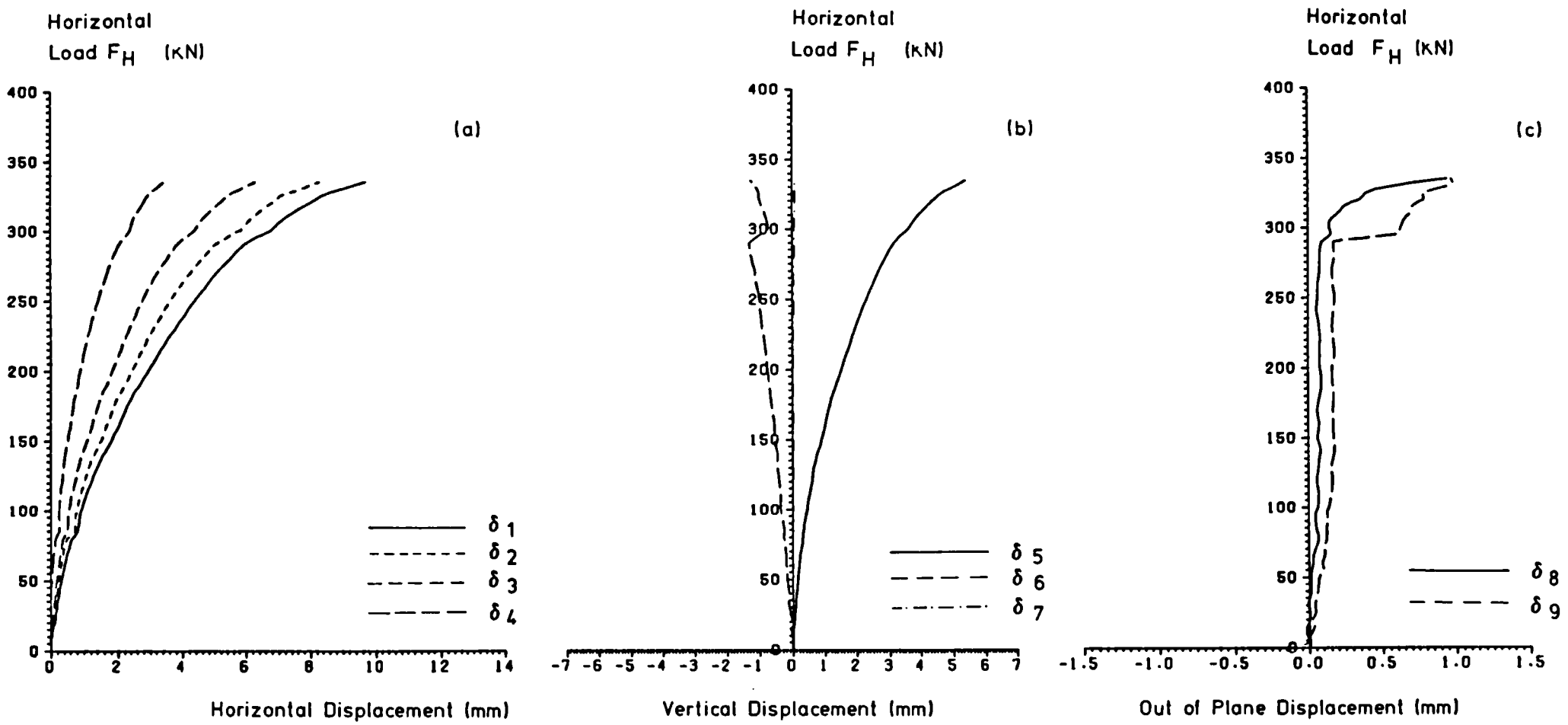


Fig. 6.3. Horizontal load-displacement curves of specimen SW12 constructed by using measurements of (a) horizontal displacement, (b) vertical displacement and (c) out of plane displacement.

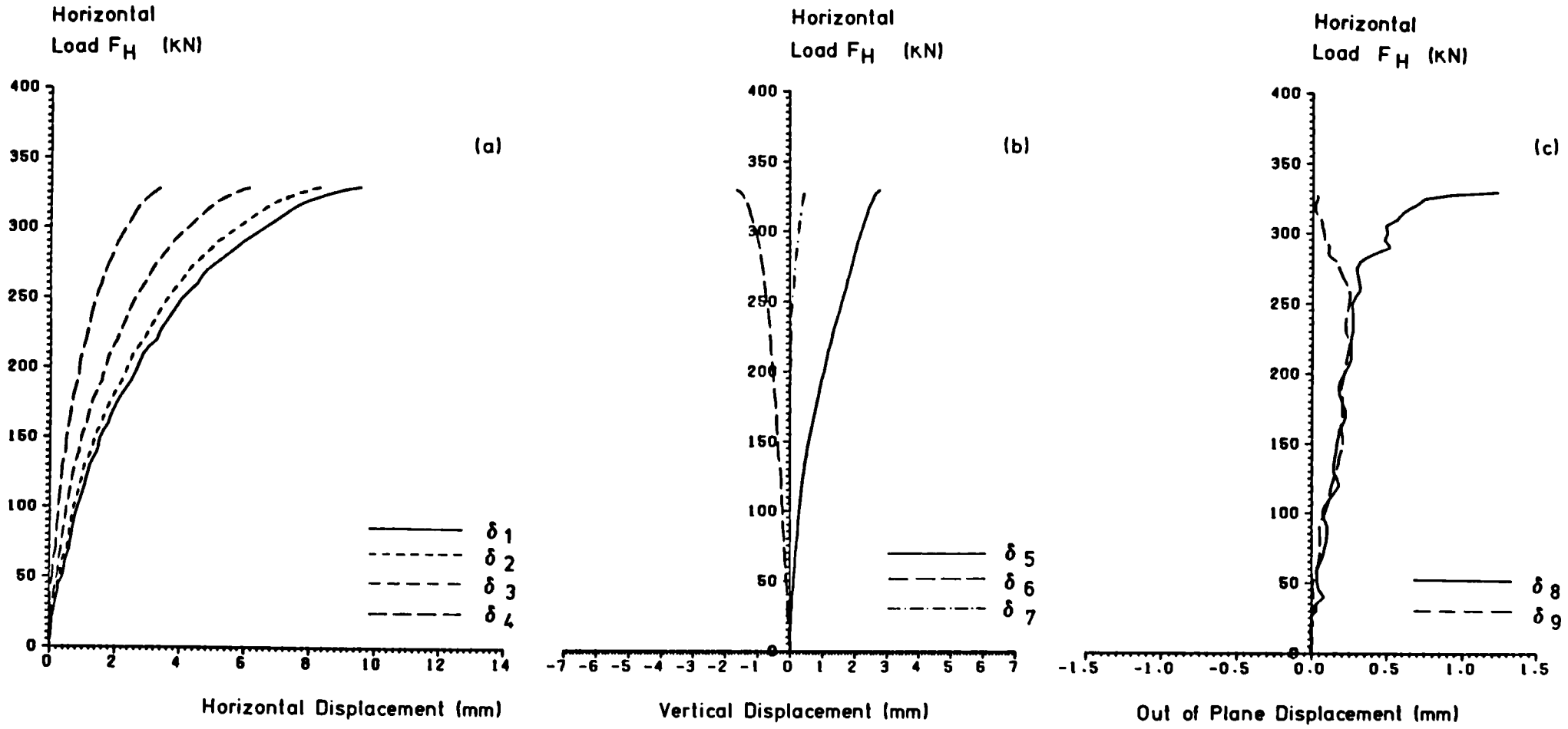


Fig. 6.4. Horizontal load-displacement curves of specimen SW13 constructed by using measurements of (a) horizontal displacement, (b) vertical displacement and (c) out of plane displacement.

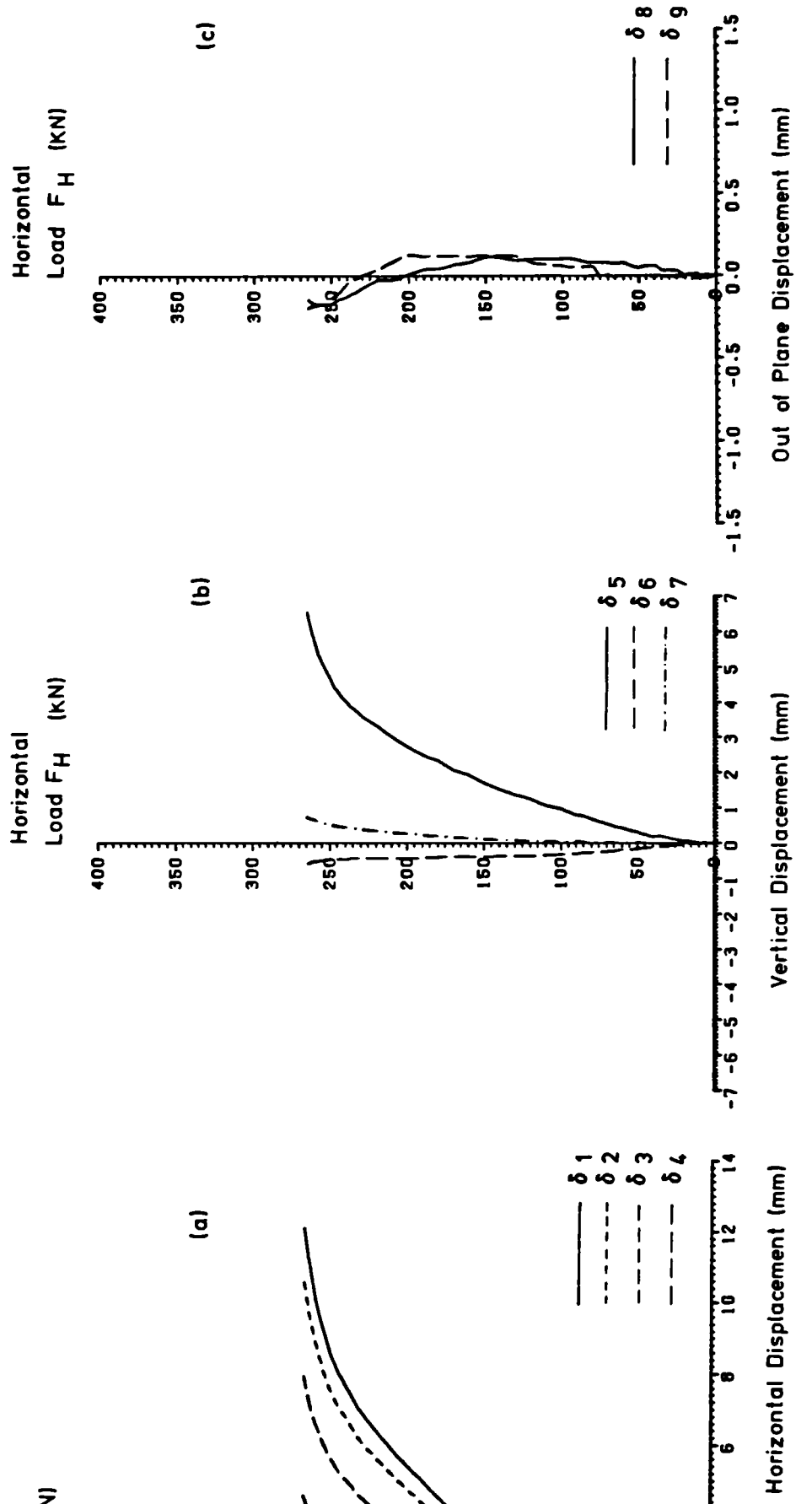


Fig. 6.5. Horizontal load-displacement curves of specimen SW14 constructed by using measurements of (a) horizontal displacement, (b) vertical displacement and (c) out of plane displacement.

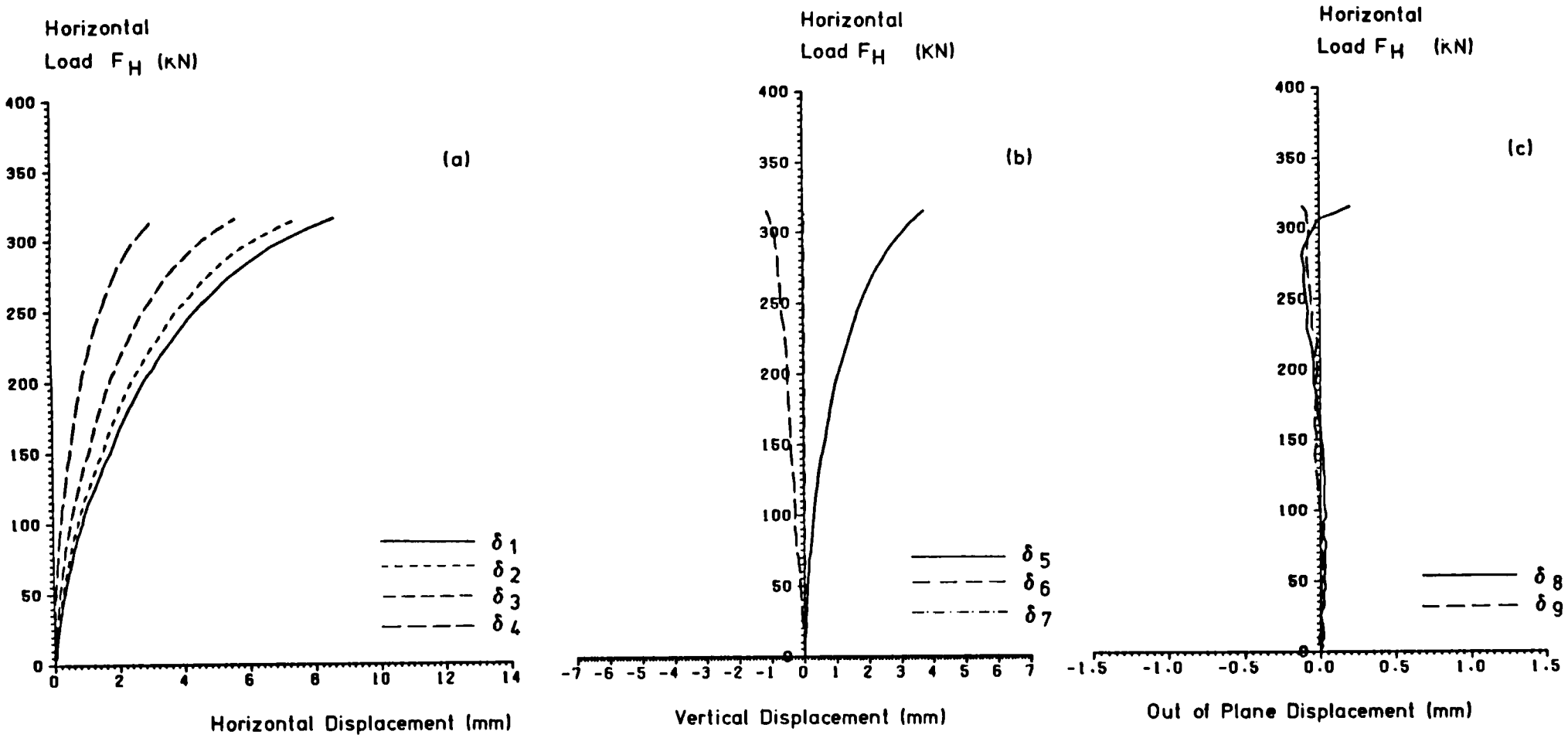


Fig. 6.6. Horizontal load-displacement curves of specimen SW15 constructed by using measurements of (a) horizontal displacement, (b) vertical displacement and (c) out of plane displacement.

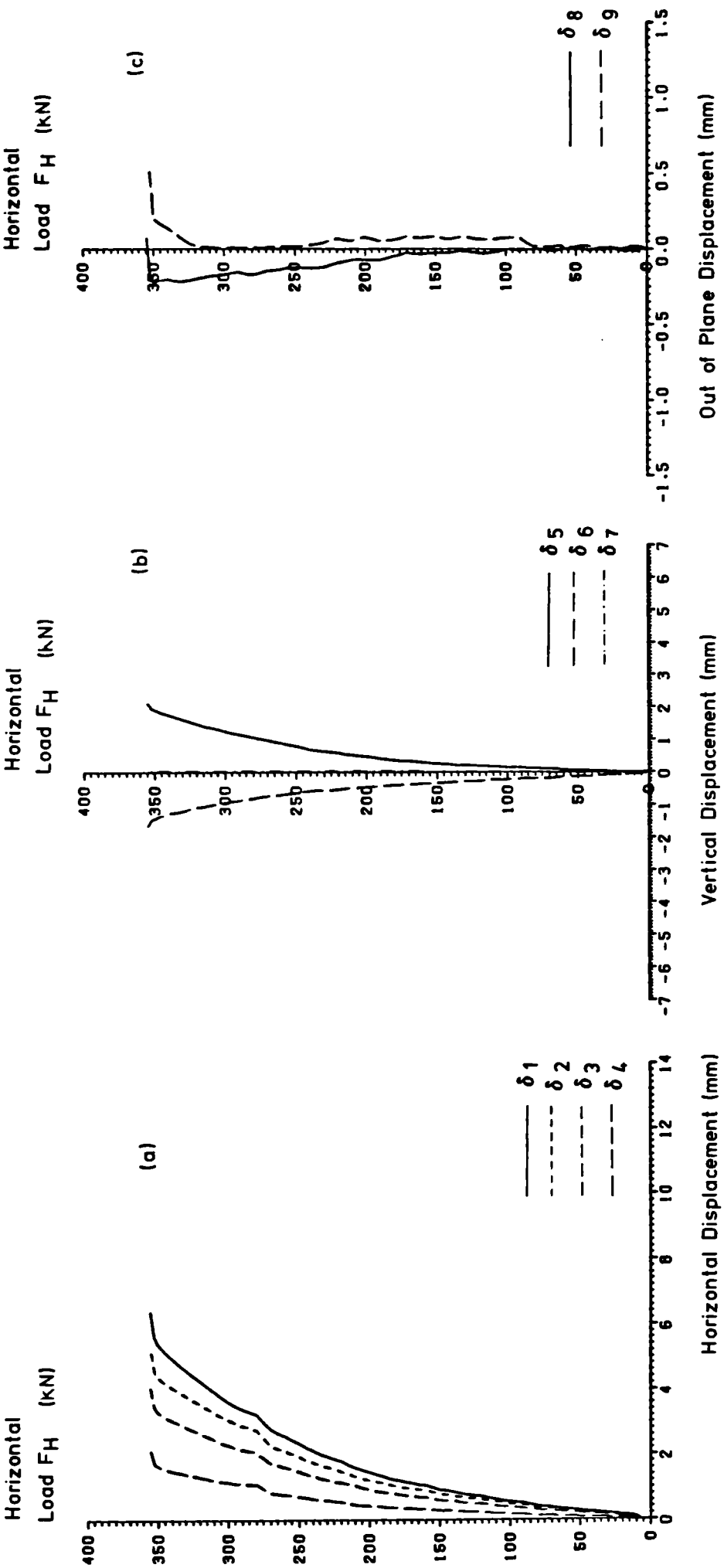


Fig. 6.7. Horizontal load-displacement curves of specimen SW16 constructed by using measurements of (a) horizontal displacement, (b) vertical displacement and (c) out of plane displacement.

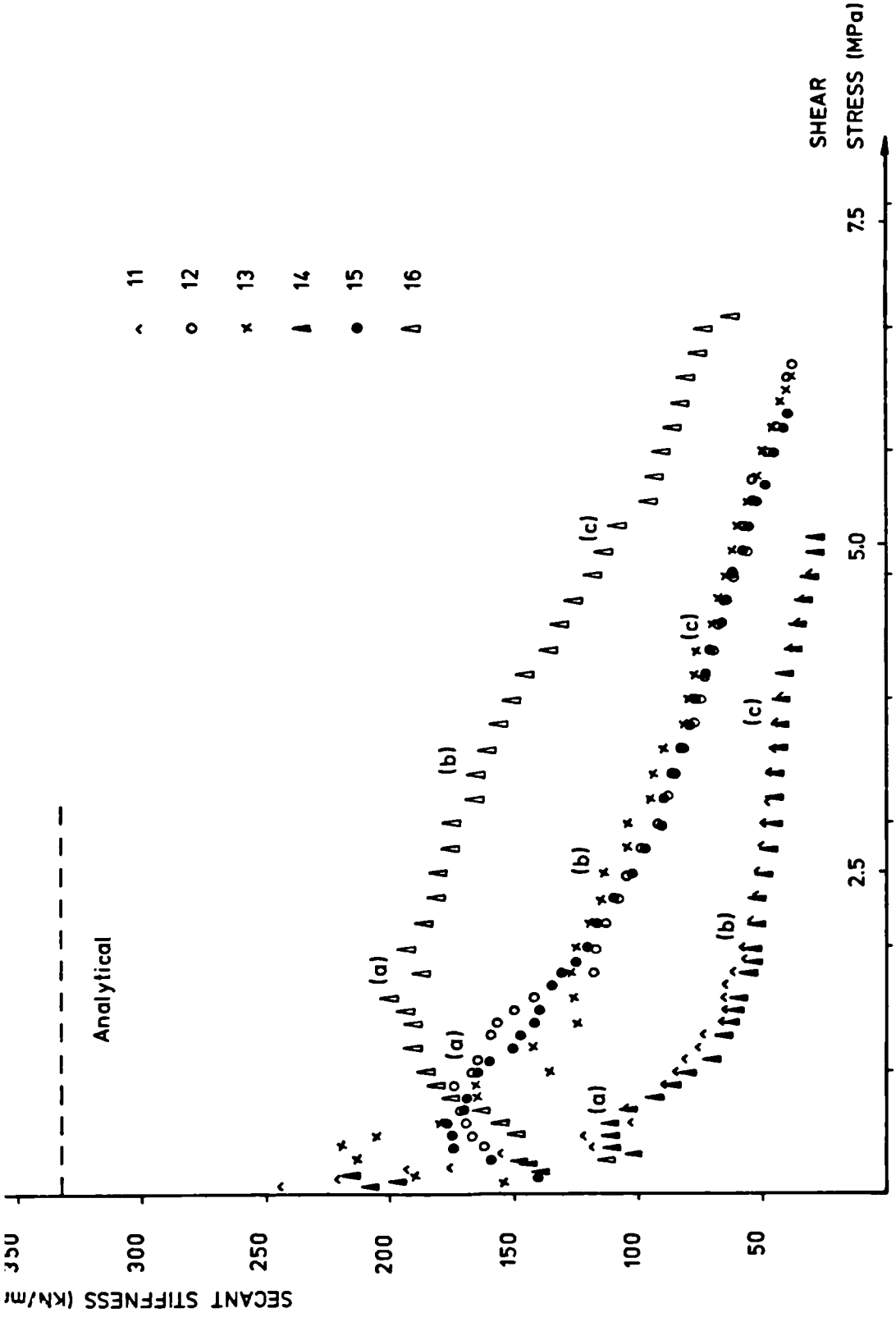


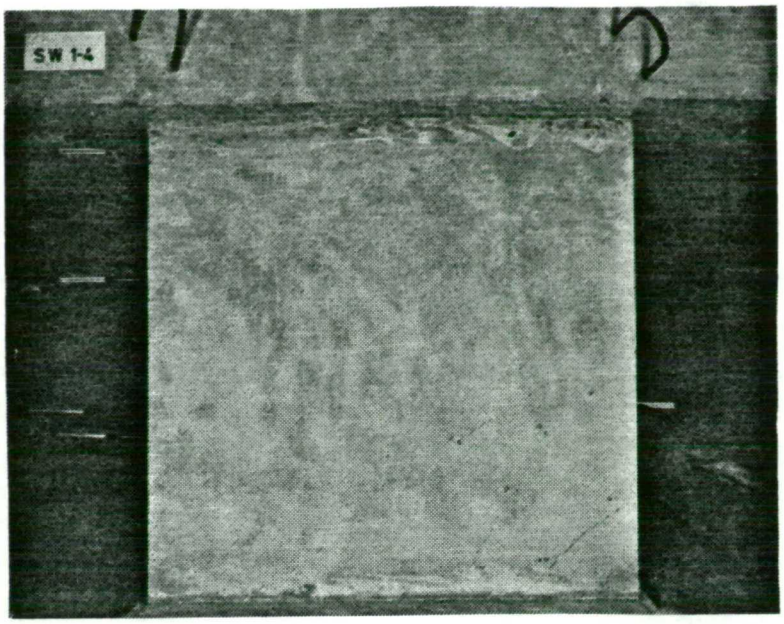
Fig. 6.8. Variation of secant stiffness with horizontal load expressed in terms of both force and stress units for type I walls.

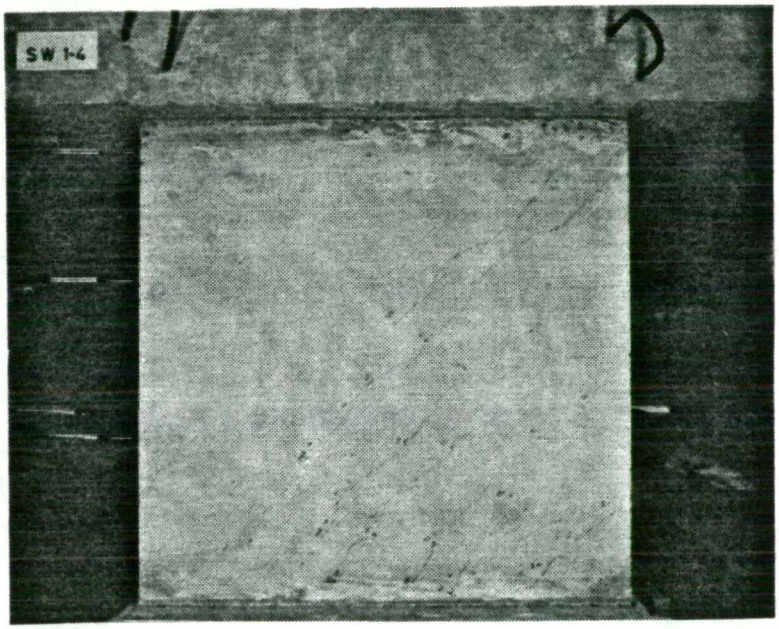
Fig. 6.9. Significant levels of cracking process exhibited by type I walls.

(a) Initiation of flexural cracking (upper plate),

(b) initiation of inclined cracking (middle plate) and

(c) crack pattern prior to failure (lower plate).


SW 1-4


SW 1-4

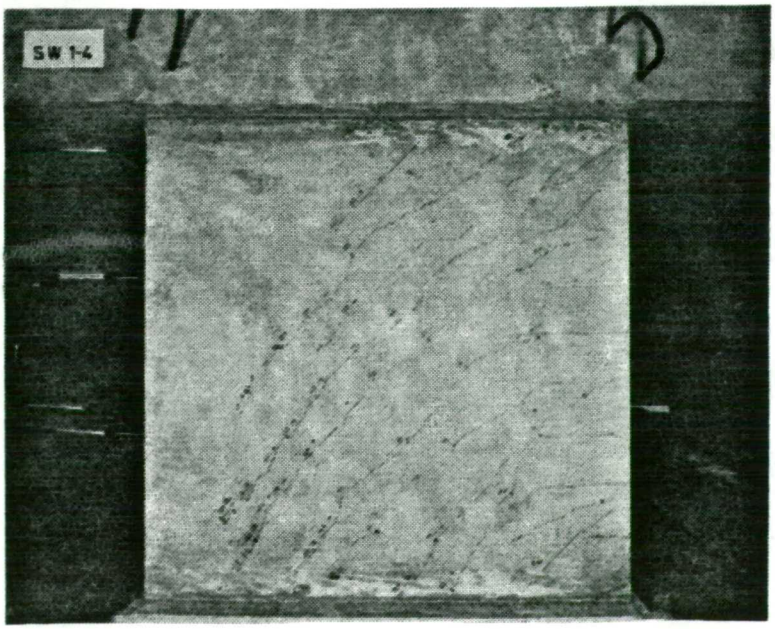
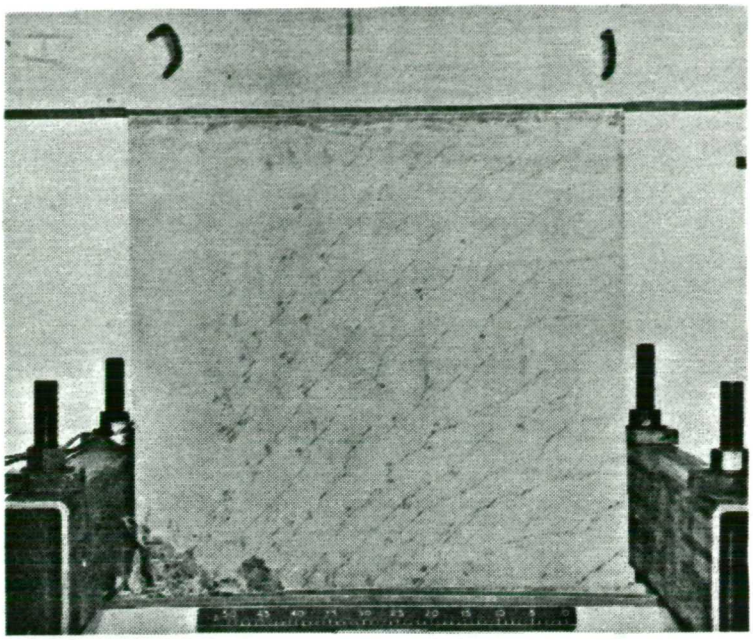
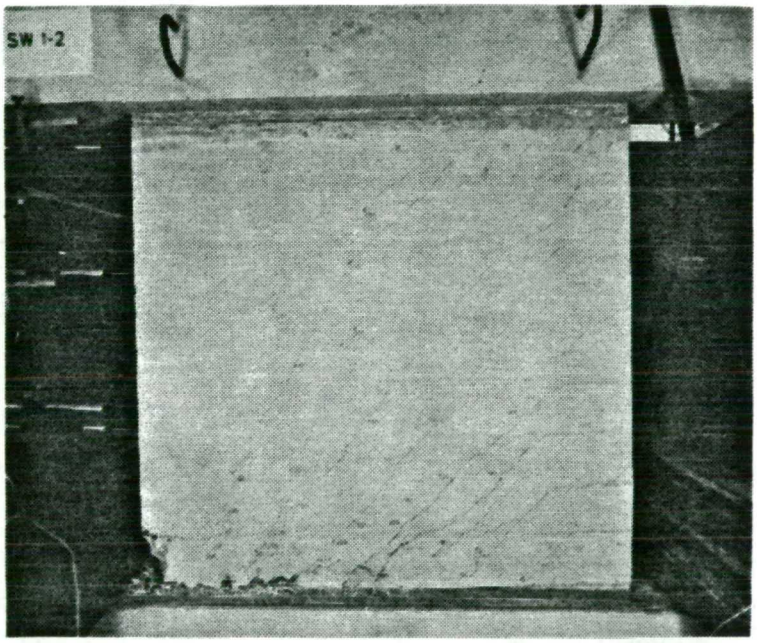
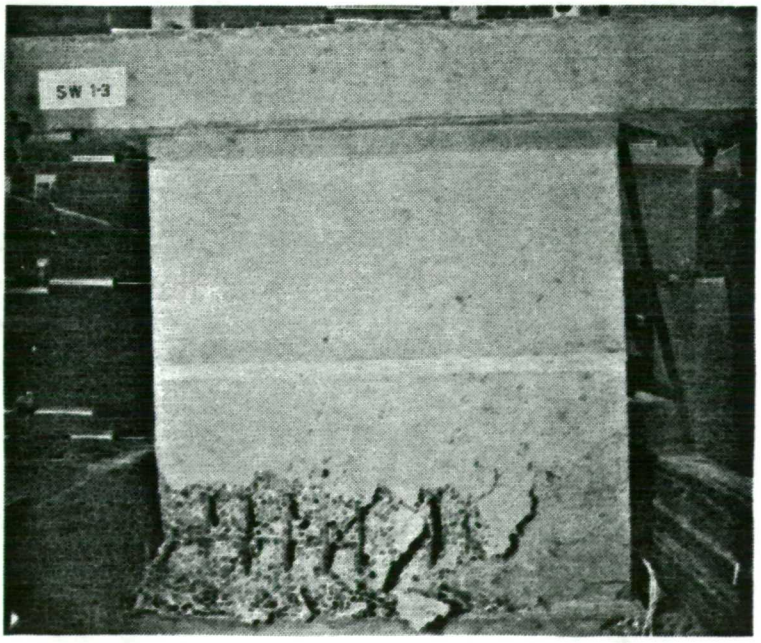

SW 1-4

Fig. 6.10. Modes of failure of type I walls subjected to normalized axial load (a) v=0 (upper plate), (b) v=0.1 (middle plate) and (c) v=0.2 (lower plate).




SW 1-2


SW 1-3

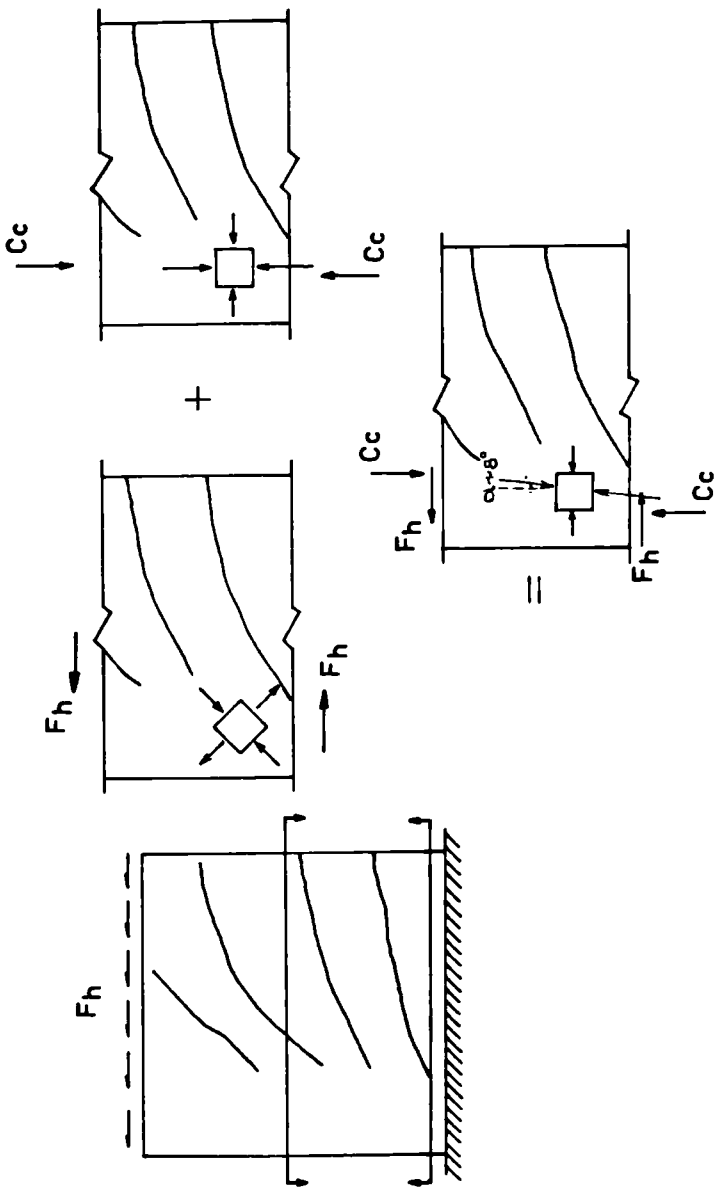


Fig. 6.11. Schematic representation of the failure mechanism of type I walls.

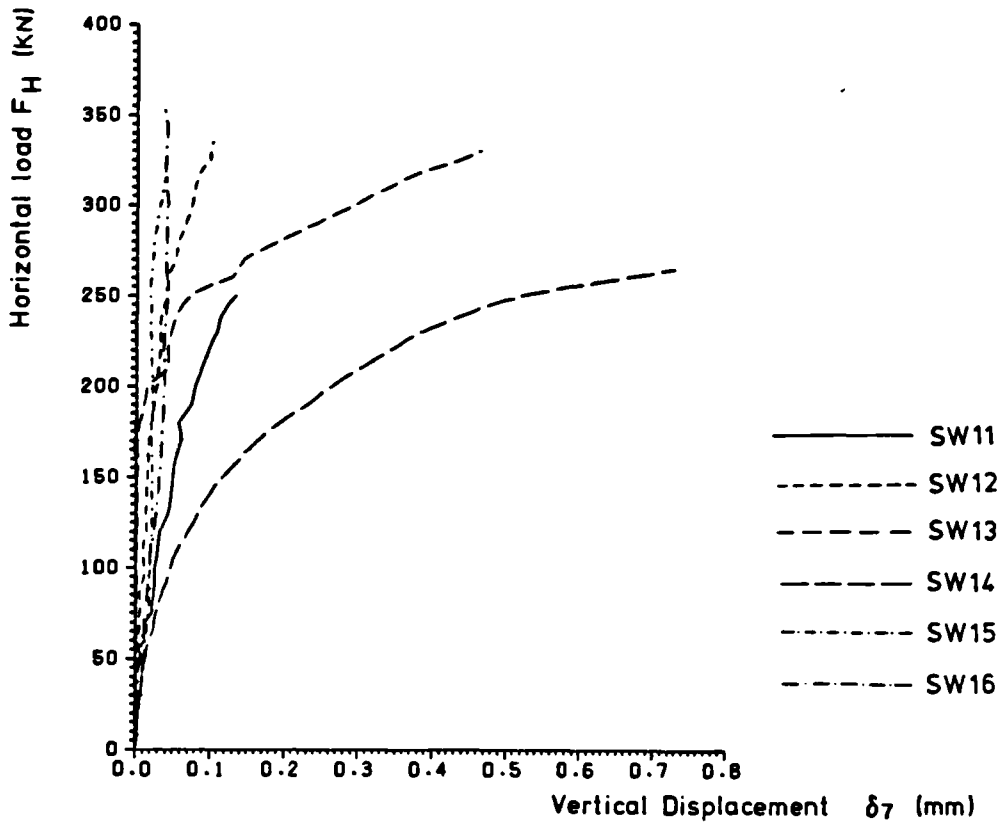


Fig. 6.12. Variation of horizontal load with base vertical displacement of type I walls.

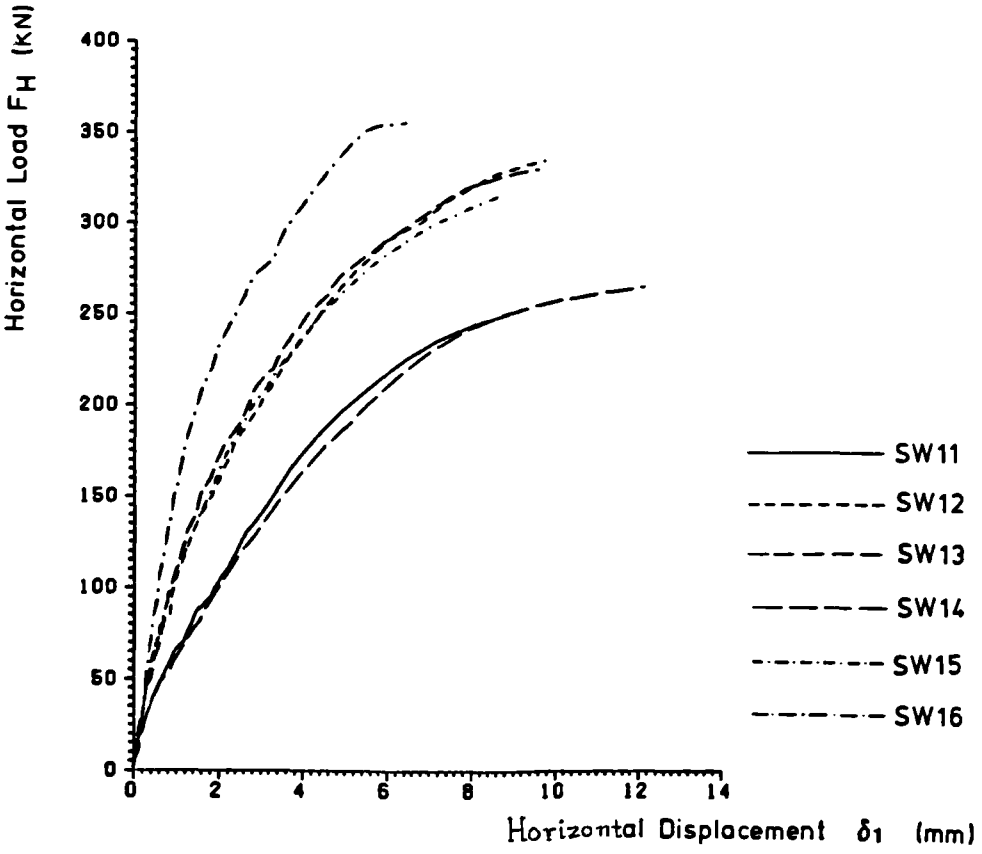


Fig. 6.13. Horizontal load versus top horizontal displacement curves for all type I walls tested.

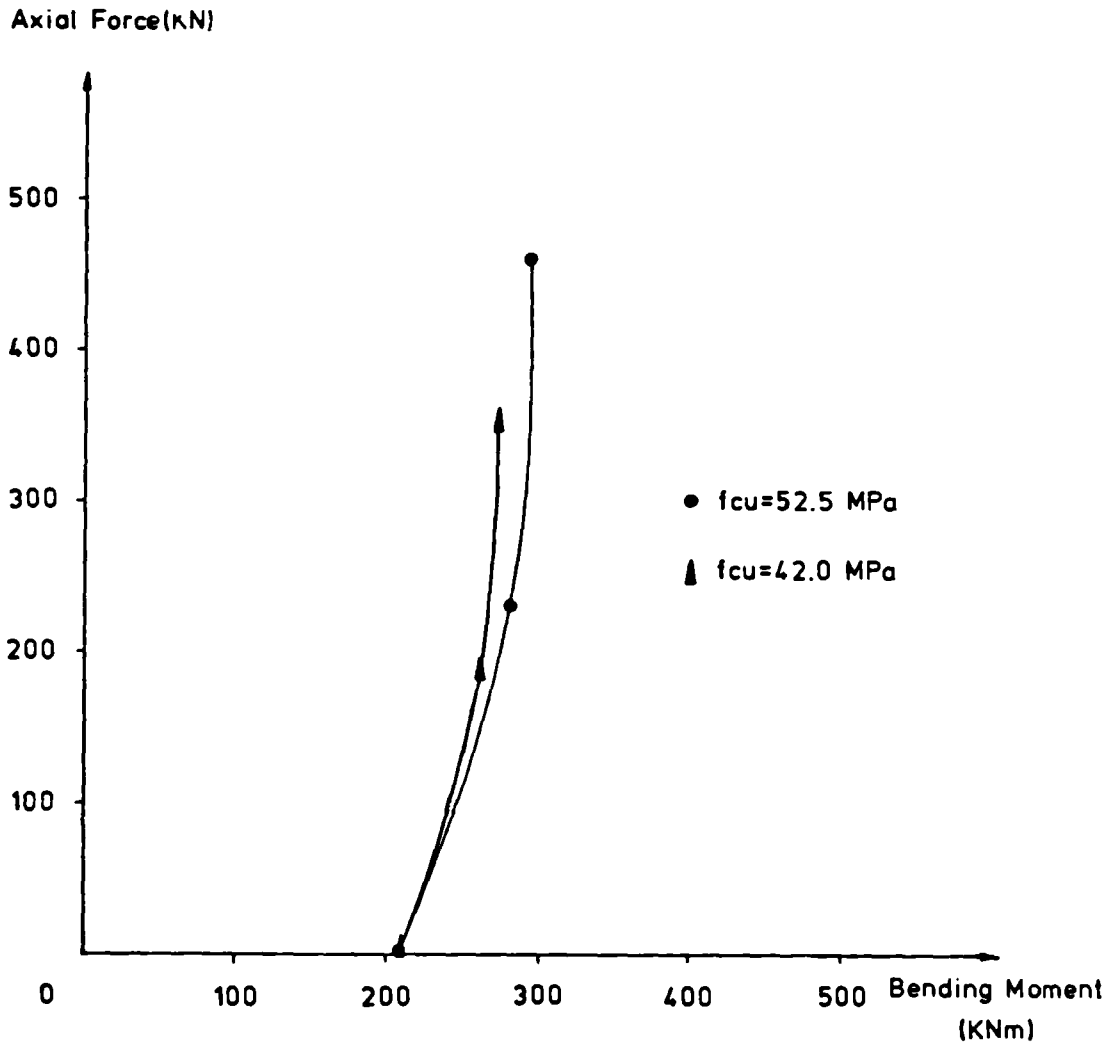


Fig. 6.14. Bending moment - axial force interaction diagram.

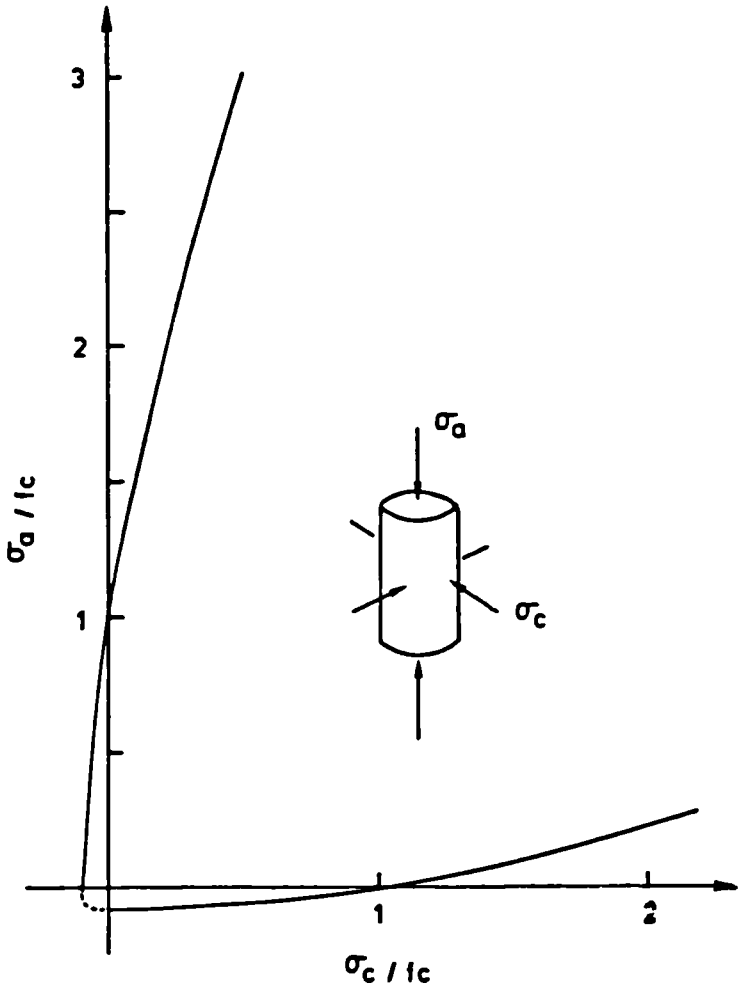


Fig. 6.15. Typical failure envelope of concrete under axi-symmetric triaxial state of stresses.

CHAPTER 7

EXPERIMENTAL INVESTIGATION OF THE BEHAVIOUR OF TYPE II WALLS UNDER MONOTONIC LOADING

7.1. INTRODUCTION

In this chapter, results of the six tests on reinforced concrete walls, with height to width ratio of two, subjected to constant vertical (axial) and monotonically increasing horizontal (lateral) loading are presented and discussed. Points of interest include strength and stiffness characteristics, deformational response and modes of failure of such walls. Attention is focused on the identification of causes and mechanisms of failure of slender walls. The effect of parameters such as the vertical loading, the concrete strength and the amount of horizontal (shear) reinforcement on wall behaviour was also investigated.

7.2. WALL DETAILS

Detailed information on the material properties (i.e. characteristics of reinforcement and concrete; mixing, casting and curing conditions) and the loading and instrumentation details used for the tests is given in Sections 5.2 and 5.3. Only additional information related to concrete strength and amount of reinforcement will be presented in this section.

Cross-sectional characteristics and reinforcement arrangement of a typical wall with height to width ratio of two together with design details of the upper (loading) and lower (foundation) beam are shown in Figure 7.1. Table 7.1 summarizes the average uniaxial compressive concrete strength values of the controls of type II wall specimens. The 28 day compressive cube strength was close to the specified value of 45 MPa.

The design of all specimens, except SW26, was based on the ACI Code of 1983. Since for specimens SW21 to SW25 the amount of vertical loading was the main variable, the percentage of vertical and horizontal wall reinforcement was kept constant for all these specimens. Specimen SW26 incorporates half the amount of horizontal (shear) reinforcement used in specimens SW21 to SW25. As the same reinforcing bar diameter was used throughout the investigation, this resulted in a larger spacing between the horizontal reinforcing bars. Furthermore, as shown in

Table 7.1 and discussed in Section 5.2.3, the concrete strength of specimen SW26 was designed to be significantly weaker than the corresponding strength of the other specimens. Table 7.2 includes data related to the amount of reinforcement used, the level of constant vertical (axial) load, both in terms of actual and normalized values, and the maximum horizontal (lateral) load sustained by the specimens. It should be noted that the levels of normalized vertical (axial) load applied to the specimens were identical to those applied on type I walls. A comparative study of the behaviour of type I and II walls subjected to the same level of normalised vertical load is included in Section 7.4.

7.3. PRESENTATION OF RESULTS

The principal results of the test specimens with height to width ratio of two, together with information useful for a better understanding of their behaviour, are given in this section.

The results obtained from load and deformation measurements are depicted in Figures 7.2 to 7.7. Three sets of graphs are included in each figure. They describe the variation with increasing horizontal load of:

(a) horizontal displacement at various heights along the wall;

(b) vertical shortening and elongation of the wall edges, as well as vertical upward displacement of the foundation beam;

(c) out of plane movement along the height of the wall.

Table 7.3 summarizes information on the horizontal (lateral) load, the top horizontal (lateral) displacement, the overall secant stiffness and the drift index of type II walls at (a) flexural cracking, (b) initiation of inclined cracking, (c) yielding of tensile reinforcement and (d) the maximum horizontal load level. These above levels which will be used regularly in the following sections are defined in Section 6.3. Most of the information on the tensile and compressive yielding of reinforcement is obtained from strain gauge readings. Figure 7.8 shows the variation of the tensile (positive) and compressive (negative) steel strains with increasing horizontal load. The strain readings were obtained by using gauges mounted on the lower part of selected tensile and compressive vertical steel bars.

Table 7.4 presents values of shear stress at various loading levels for all the

test specimens investigated. Shear stress is defined as the ratio of horizontal load to the gross cross-sectional area of the wall. The table also includes normalized values of the ultimate shear stress with respect to both cylinder concrete strength and the square root of the cylinder concrete strength. Normalized values were used to investigate expressions proposed by Oesterle et al (1984) and current Code provisions (ACI, 1983) which related the wall capacity to the concrete strength and the level of applied (axial) vertical compressive load.

Figure 7.9 illustrates the variation of secant stiffness with increasing horizontal load and/or shear stress, for all six test specimens. Significant stages of cracking process exhibited by type II walls are depicted in Figure 7.10. Modes of failure of type II walls subjected to the three levels of normalized vertical stress are shown in Figure 7.11, while a schematic representation of the failure mechanism of type II walls is presented in Figure 7.12.

7.4. DISCUSSION OF RESULTS

7.4.1. VALIDATION OF THE EXPERIMENTAL SET-UP

The main objectives in the design of the experimental set-up were

(a) to apply plane stress conditions to all test specimens;

and (b) to achieve fixed foundation conditions at the wall base.

Displacement transducers monitoring out of plane displacements were mounted at three levels along the wall height, at 100 mm from the wall base near the lower compressive edge of the wall, and at 700 and 1200 mm from the wall base, in the middle of the wall web. Figure 5.6 illustrates the position of the transducers and the sign convention of the displacement readings. As Figures 7.2(c) to 7.7(c) indicate, the maximum out of plane displacement, for the majority of the specimens, never exceeded 0.2% of the height of the wall. Furthermore, for walls subjected to an initial amount of constant axial compressive force, the measured values of out of plane movement were significantly smaller. The absolute maximum out of plane displacement was recorded during the testing of wall SW24 and corresponded to 0.28% of the height of the wall. It is apparent that such a displacement can only cause small secondary rotational and torsional moments to the wall. It would appear, therefore, that the experimental set-up designed for the tests is capable of subjecting the specimens to plane stress conditions.

Measurements of vertical upwards displacement at the top of the foundation beam of the wall were continuously recorded during testing. Since these values were negligible in comparison to the values of vertical shortening and elongation of the wall edges, included in Figures 7.2(b) to 7.7(b), Figure 7.13 was produced, in which the variation of horizontal load against vertical upwards displacement is plotted on an enlarged displacement scale. The maximum value was measured during testing of wall specimen SW26 and corresponded to a rotation of the foundation beam equal to 1.7 percent of a degree. Much smaller values were recorded during the testing process of the other wall specimens. Therefore, it can be concluded that the design of the experimental set-up succeeded in introducing almost perfect base fixity conditions to the wall specimens.

7.4.2. STRENGTH CHARACTERISTICS AND DEFORMATIONAL RESPONSE

An evaluation of the effect of axial load, concrete strength and amount of horizontal reinforcement on the behaviour of slender walls can be achieved by a comparative study of strength and deformation characteristics of such walls during testing.

As Table 7.2 shows the horizontal load carrying capacity of walls not subjected to axial load was similar. Despite the fact that wall SW26 incorporated half the amount of horizontal reinforcement used in specimens SW21 and SW24 and was significantly weaker than the other two with respect to concrete strength, no difference in ultimate horizontal (lateral) load capacity was observed. The ultimate horizontal load of specimen SW22, which was initially subjected to a normalized axial load of 0.1, was 22 percent higher than the ultimate strength of walls without axial load. An even higher enhancement in ultimate strength characterised specimen SW23, which was subjected to a normalized axial load of 0.2. The maximum horizontal load attained by this specimen was 45 percent higher than the average strength of walls SW21, SW24 and SW26. The variation of wall strength with the level of axial load was almost linear, in contrast to type I walls where a normalized axial load of 0.1 and 0.2 yielded an average increase of 26% and 30% respectively. An initial normalised axial load of 0.2 was also applied to specimen SW25. Unfortunately, an unexpected sudden movement of the spherical seating, through which the vertical (axial) load was applied to the spreader beam and through this to the specimen, resulted in the application of eccentric vertical loading when the increasing horizontal load reached 140 KN. The combination of the eccentric vertical loading and the horizontal load of 150 KN led to an early abrupt failure of specimen SW25.

The deformational response of walls SW21, SW24 and SW26 shown in Figures 7.2(a), 7.5(a) and 7.7(a) respectively indicates a ductile flexural behaviour for all three walls. A characteristic feature of the horizontal load against horizontal displacement family of curves is the non-linear pattern of the curves, even for the displacements recorded near the wall base. This is an indication that the wall specimens mainly deflect due to flexure.

Axial compressive load has been found to reduce not only the value of top horizontal displacement measured during testing, for a given horizontal load, but also the recorded values of horizontal displacement at the ultimate state. Top horizontal displacement readings at yield and at ultimate for specimens with strain gauges (see Table 7.3) show that a drop in displacement ductility ratio from 3.80 to 2.54 occurred as the normalized axial compressive load increased from 0 to 0.20. The rate of decrease in displacement ductility with increasing axial load for type II walls was higher than that for type I walls. However, with the exception of SW25, the deformational response of slender walls was non-linear, even under high axial compressive stresses.

Although the recorded values of ultimate top horizontal displacement differed significantly between type I and type II walls, small differences were observed between the drift indices at the ultimate load level. For both wall types normalized axial load levels of 0, 0.1 and 0.2 were related to drift indices of about 1.5×10^{-2}, 1.2×10^{-2} and 0.9×10^{-2} respectively. Differences were also noticed at the drift indices corresponding to wall serviceability limits. For type II walls first flexural cracks appeared at an early average drift index value of 0.031×10^{-2}, while for type I walls initiation of cracking occurred at an average value of drift index equal to 0.044×10^{-2} irrespective of the level of axial load.

Figures 7.2(b) to 7.7(b) indicate that the axial compressive load affects the vertical displacement of the wall edges. It is clear that the elongation of the wall tensile edge is smaller as the initially applied axial load increases, while the reverse is the case concerning the shortening of the wall compressive edge. Therefore, the difference between the absolute values of elongation and shortening drops as the level of axial compressive stress initially applied to the wall increases. Such behaviour implies that the higher the value of axial load, the bigger the depth of the wall neutral axis prior to failure.

Of course, it is very difficult to determine what proportions of the overall horizontal displacement along the wall height are due to pure bending and pure shear. A way of grossly assessing these terms based on vertical measurements was

described in Section 6.4.2. Following the same steps, it can be concluded that the ultimate flexural deformation measured at the top of walls not subjected to axial load was approximately 94 percent of the total lateral displacement. When an initial level of axial stress was applied to the walls the contribution of flexural deformation to the top lateral displacement increased to 98 percent. Since vertical displacement was not measured at intermediate heights along the wall, the top vertical displacements readings and the assumption that plane sections remain plane, were used to grossly assess the contribution of flexural deformation at the lower part of the wall. The calculations show that the level of contribution of flexural deformation to the lateral displacement measured at intermediate heights was independent of the location of the LVDT along the height of the walls in the present investigation.

Tables 7.3 and 7.4 indicate that the measured horizontal load and shear stress (i.e. horizontal load divided by wall cross-section), corresponding to the loading stages of cracking, yielding and ultimate, increases as the level of initially applied constant vertical (axial) load increases. As expected, the horizontal load required to cause flexural failure of the type II walls was smaller than that for type I walls. In fact for type II walls the ultimate boundary shear stress varied from 2.9 MPa to 4.3 MPa, while for type I walls the corresponding stress varied from 5.0 MPa to 6.5 MPa, for the same range of variation of axial load. The normalized values of shear stress with respect to the ultimate wall shear stress included in Table 7.4 indicate that, while axial stresses affect the normalized shear stress values at first observed cracking and first significant flexural cracking, they seem not to influence the normalized shear stress values at initiation of inclined cracking and first yielding of tensile reinforcement. Only for wall specimens subjected to high levels of axial load, top lateral displacement and drift index readings, at loading levels of initiation of cracking and first flexural cracking, showed a significant enhancement compared with values measured during testing specimens subjected to low levels of axial stress. No substantial differences were reported for the above quantities at the loading level of initiation of inclined cracking and yielding of tensile reinforcement. Such differences in behaviour may indicate inaccuracy in the identification of the loading levels.

The values of the ultimate boundary shear stress applied to the wall, (v_{ult}), normalized with respect to uniaxial cylinder compressive concrete strength, f'_c, and the square root of f'_c, are included in Table 7.4. It is obvious that, for the same level of normalized axial load, these values vary considerably. A comparison between the values corresponding to walls SW21, SW24 and SW26 indicate a decrease of the normalized shear stress ratio as the cylinder strength of concrete

(f'_c) increases. The drop is more significant when the values of ultimate boundary shear stress of the walls are normalized with respect to f'_c. This appears to indicate that the uniaxial strength characteristics of concrete are not the proper factor for the normalization of the ultimate boundary shear stress attained by slender walls. It is likely that uniaxial material characteristics are insufficient to describe the complex stress conditions exhibited in the failure zones of the specimens.

7.4.3. STRAIN MEASUREMENTS ON LONGITUDINAL REINFORCEMENT

Longitudinal reinforcement strains were measured by installing electrical resistance strain gauges (ersg) in wall specimens SW22, SW23, SW25 and SW26. In all specimens, except SW23, ersgs were mounted on the lower part of the tensile bars located at the corners of the tensile edge (concealed column) of the wall and on the lower part of the extreme bars of the compressive edge of the wall. In the case of wall SW23, four gauges were placed at the lower part of four corner bars at the compressive edge of the wall and two gauges were mounted on the two extreme tensile bars.

The first yield load of the specimens can be determined from the horizontal load versus longitudinal strain diagrams included in Figure 7.8. The yield load is reached when the average strain of the two reinforcing bars in the outer tensile steel layer exceeds 2500 microstrains.

Figure 7.8(d) illustrates that, for specimen SW26, the wall yielded when 55 percent of its ultimate strength was reached, while the compressive reinforcement yielded when 75 percent of the wall ultimate capacity was reached. The average strains recorded prior to failure were +28,000 and +20,000 microstrains for the outer and inner tensile steel layer respectively and −8,000 microstrains for the extreme compressive steel layer.

Figures 7.8(a) and 7.8(b) indicate that for walls SW22 and SW23, subjected to initial normalized axial loads of 0.1 and 0.2 respectively, yield of the extreme tensile steel layer occurred at horizontal levels corresponding to 72 and 77 percent of the ultimate horizontal load attained by the walls. The figures also show that first yield of compressive steel reinforcement occurred at a load equal to 83 and 92 percent of the ultimate horizontal load, for wall specimens SW22 and SW23 respectively. The average strains recorded prior to failure were +20,000 and +16,000 for the extreme tensile steel bars and −9000 and −7000 for the extreme compressive steel bars, for wall specimens SW22 and SW23 respectively.

Information related to the strain measurements on longitudinal reinforcement of specimen SW25, included in Figure 7.8(c), should not be considered representative of slender walls subjected to high levels of axial stress, since as discussed in Section 7.4.2, the wall failed prematurely.

A further look at the strain measurements of the wall specimens points to the fact that, for given wall reinforcement details, the presence of axial load does not alter the maximum compressive strain of the specimens, while it affects the maximum tensile strain measured prior to wall failure since wall failure is defined as the failure of concrete in the compression zone. An increase in the normalized axial load from 0 to 0.20 resulted in a drop of the maximum tensile strain from +28,000 to +16,000 microstrains. Nevertheless, the extreme maximum tensile strain was significantly higher than the yield strain for all the wall specimens, indicating that the walls exhibited considerable post yield deformations prior to failure.

An assessment of the variation of the wall neutral axis as increasing levels of horizontal load are applied to the wall can be based on the strain measurements recorded during testing. Figure 7.14 shows a schematic representation of the variation of neutral axis along the wall width against the strains as various levels of horizontal load are applied to wall specimen SW26. Two basic remarks can be made:

(a) The depth of neutral axis progressively decreases.

Up to half the ultimate horizontal load sustained by specimen SW26, half of the wall's width, at a cross-section near the base of the wall, is compressed and the remainder is tensioned. As significant yielding at tensile reinforcement occurs in the wall, the depth of neutral axis becomes smaller and smaller.

(b) The variation of localised strains along the wall cross-section near the base is non-linear.

As the ultimate horizontal load capacity of the wall is reached, the tensile edge of the wall elongates considerably more than the compressive edge of the wall shortens, resulting in a distinctly non-linear variation of strains. Of course, as discussed in Section 7.4.2, the above feature is less pronounced, but still in existence, when the wall is initially subjected to an axial load.

It is interesting to note that calculations of depth of neutral axis based on

strain measurements are in compliance with the depths of neutral axis observed as testing progressed. The latter information will be included in Section 7.4.5, where the fracture processes of the tested slender walls will be discussed.

7.4.4. STIFFNESS CHARACTERISTICS

The secant stiffness values, given in Table 7.3 for various loading levels, and the variation of stiffness with increasing horizontal load, illustrated in Figure 7.9 for various levels of vertical load, indicate that the applied level of constant vertical (axial) load has a significant effect on stiffness characteristics. The following significant features were observed :

(a) The application of a normalized axial stress equal to 0.1 results in an increase of secant stiffness values. A 20 percent increase was recorded for loads corresponding to first visible cracking, while a 70 percent increase in stiffness values was recorded at the levels of significant flexural cracking, inclined cracking, yielding of reinforcement and ultimate load.

(b) For a normalized axial load of 0.2 the values of secant stiffness were only slightly higher than those of the walls subjected to lower levels of normalized axial load. Only at the ultimate horizontal load level, significantly higher values of ultimate secant stiffness were measured. However the variation of secant stiffness values with increasing normalized axial load was less pronounced for type II walls than it was for the walls with the lower height to width ratio.

(c) For the first increments of horizontal loading, stiffness values exhibit a large variability since recorded values of load and displacement are very small and below the sensitivity of the instruments measuring them. Early cracking leads to a steep drop of secant stiffness during the early stages of the applied horizontal load. Since most of the flexural crack pattern develops during the above load steps the secant stiffness – horizontal load curves tend to become horizontal, indicating that a further increase in horizontal load results in insignificant changes in secant stiffness. As inclined cracking and yielding of the wall tensile reinforcement initiates the secant stiffness – horizontal load curves change curvature. With more vertical bars reaching their yielding strength, stiffness values decrease at a higher rate with the increasing horizontal load up to the ultimate horizontal load carrying capacity of the wall.

(d) The ratio of secant stiffness values at the ultimate level to stiffness values just before the first visible crack (representing the uncracked stiffness of slender walls) increases with the level of normalized axial load. Values of 0.2, 0.25 and 0.35 were measured for walls subjected to normalized axial load levels of 0, 0.1 and 0.2 respectively.

The above results show that the effect of vertical (axial) load on the secant stiffness characteristics of slender walls is apparent even at the uncracked phase of the wall response. Based on analytical force–displacement relations, obtained from the one–dimensional cantilever element theory, a horizontal displacement value equal to 18.4×10^{-6} mm/N is proposed in the literature for the walls investigated (see Appendix A for the theoretical calculations). This value implies that the theoretically predicted secant stiffness value for the uncracked phase is 60.6 KN/mm, independent of the applied level of vertical (axial) load. The experimental stiffness values for the uncracked phase, included in Table 7.3, are 55, 67 and 74 percent of the theoretical nominal stiffness values for levels of normalized vertical stress equal to 0, 0.1 and 0.2 respectively.

The analytical axial stiffness, (EA)/wall height, also included in Appendix A, is approximately 1.2×10^{6} N/mm. The corresponding experimental value, based on the axial force versus axial shortening relationship of the walls investigated, is almost ten times smaller. Table A.3 summarizes the analytically predicted and experimentally measured values of axial wall shortening with respect to the axial load applied to the wall specimens.

A comparison between theoretical and measured values of secant stiffness due to horizontal and vertical loads, points out to the fact that predictions of wall stiffnesses, even though not as bad as they are for walls with height to width ratio of one, are poor. The reason for the smaller measured values of wall stiffness should be the microcracking of concrete at the material level due to shrinkage and heterogeneity, and the oversimplified assumptions of the analytical procedure.

7.4.5. FRACTURE PROCESSES AND FAILURE MODES

Descriptions of the fracture processes and the failure modes of the six walls specimens with height to width ratio of two, subjected to constant vertical and monotonically increasing horizontal loads, are presented for three groups of specimens. Each group includes walls initially subjected to the same level of normalized axial load. Information on the fracture process of walls subjected to

normalized axial load of 0, 0.1 and 0.2 is presented in the following Sections.

Specimens SW21, SW24 and SW26

Early flexural cracks appeared at the bottom tensile edge of the concrete surface of the specimens after the application of 8% of the ultimate horizontal load. Up to about 25% of the maximum horizontal load, no more cracking was observed. Only after the above load level was reached did significant flexural cracks appear as shown in Figure 7.10(a). Their spacing varied from 90 to 120 mm. As the level of horizontal load was increased, new flexural cracks covered half the height of the tensile edge of the wall, while the early flexural cracks started to spread at a slight inclination towards the wall web. When almost 65% of the ultimate horizontal load was reached the initiation of significant inclined cracking was observed. It started from the top third of the wall tensile edge and was extended towards the wall web at an angle of 45 degrees. (See Figure 7.10(b)). As the horizontal load was further increased, inclined cracks not only increased in number, but also propagated deeper into the wall web. Inclined cracks crossing the bottom half of the wall almost reached the compressive edge of the wall. Their spacing was 80 to 100 mm. New vertical cracks were formed at the wall tensile edge in between the initial flexural cracks, decreasing the spacing between flexural cracks to 60 mm.

When 90% of the ultimate horizontal load was reached spalling of the concrete cover of the extreme compressive edge of the wall was observed. Thereafter, a nearly vertical crack was formed in the middle of the lower compressive edge of the wall, between the deepest flexural cracks. This finally led to the progressive failure of the compressive zone of the wall and the drop of the horizontal load carrying capacity of the wall as seen in Figures 7.10(c) and 7.11(a). It is interesting to note that the crack widths of the flexural cracks near the bottom quarter of the wall tensile edge were in the range of 0.8 to 1.5 mm when the ultimate load was reached, while only slight buckling of the extreme compressive reinforcement was observed at failure.

Despite the fact that for wall specimen SW26 the concrete strength was substantially lower and the amount of horizontal reinforcement was half the amount supplied to specimens SW21 and SW24, no major differences were noticed in the fracture process and the failure mode among the three specimens.

Specimen SW22

Although some early flexural cracks were detected in specimen SW22, when only 9 percent of the ultimate horizontal load was applied to the wall, significant flexural cracking initiated at a horizontal load corresponding to 37 percent of the wall capacity. Thereafter, flexural cracks covered two thirds of the tensile edge of the wall, at a spacing of 160 to 180 mm. When 75 percent of the ultimate horizontal load was reached, some of the flexural cracks had already started to branch almost diagonally into the wall web, while a number of independent inclined cracks were formed at the middle third band along the height of the wall reducing the crack spacing to 120 mm.

Further horizontal load increments resulted in the extension of the inclined cracks to the wall web. As the load increased to about 90% of the wall horizontal load carrying capacity, the tips of the deepest inclined cracks extended to a distance of 200 mm from the compressive face of the wall. No cracking was observed at the top third of the wall. Failure of the wall occurred when near-vertical cracks were formed at the lower compressive edge of the wall between the tips of the two most inclined flexural cracks (see Figure 7.11(b). Due to the presence of axial load the depth of the neutral axis was larger and the width of the concrete "crushed" band was more extensive.

Specimens SW23 and SW25

For wall specimens subjected to an initial normalized vertical load of 0.2, the observed crack formation was less extensive. Fewer flexural cracks were formed at the tensile edge, while inclined cracking penetrated a smaller area of the wall web. Not only was the spacing between the cracks larger but also crack extension ceased at a longer distance from the outer compressive face of the wall, indicating higher depths of neutral axis (see Figure 7.11(c)). Nevertheless, the higher value of axial load applied to specimen SW23 did not affect the mode of failure exhibited by the wall.

Wall specimen SW25 failed earlier than specimen SW23 for reasons discussed in detail in Section 7.4.2. It is interesting to note, however, that up to the application of a horizontal load of 130 KN, fracture processes exhibited by both specimens were similar. Only then, with the application of eccentric vertical and axial loading to specimen SW25, additional inclined cracking resulted which almost penetrated the lower compressive zone of the wall. Failure occurred when the deepest inclined crack propagated near-vertically to the lower part of the wall under

compression and was immediately followed by a sudden "crushing" of the lower compressive zone of the wall.

7.4.6. CAUSES OF WALL RESISTANCE AND FAILURE MECHANISM

The collapse of all slender walls tested occurred due to failure of the compressive zone of the walls. The presence of axial load increased the horizontal load carrying capacity but did not affect the failure mode of the wall. It is interesting to note that failure of the walls was preceded by complete separation of concrete from steel in localized regions adjacent to the vertical steel bars at the tensile edge of the wall.

One load increment prior to the failure load, the width of the flexural cracks at the lower tensile edge of the wall became considerable, resulting in an insignificant "shear" resistance of the concrete region of the wall below the neutral axis due to aggregate interlock. A small contribution to "shear" resistance at this region is also due to bond forces which develop between concrete and tensile reinforcement. Bond failure can change the equilibrium conditions of a wall element between the two deepest consecutive flexural cracks, as depicted in Figure 7.12.

Loss of the bond force results in an extension of the lower of the flexural cracks, which in turn reduces the depth of neutral axis and increases the intensity of the compressive stress block near to the base of the wall. Concrete in this region will be the first to reach the stage where volume dilation occurs (see also Figure 3.1). Such volume dilation will induce tensile stresses in the surrounding concrete and the lower compressive zone of the wall will be finally subjected to compression-tension stress conditions, i.e. compressive zone is subjected to a complex state of stresses. The wall will fail when the tensile strength of concrete is attained in these regions, leading to cracking in the direction of the maximum principal compressive stress. This may explain the presence of near-vertical splitting in th compressive zone of the wall, which characterizes the failure mode of slender walls (Figure 7.11).

The depth of neutral axis measured prior to failure was equal to 0.20, 0.26 and 0.29 of the wall width for specimens subjected to a normalized axial stress of 0, 0.1 and 0.2 respectively. This information, together with published information on the behaviour of concrete under triaxial state of stress (see Figure 6.15), may be used to assess the average longitudinal and transversal stresses in the compressive

zone of the walls. Using the measured values for maximum horizontal load-carrying capacity of slender walls, the existence of a complex state of stresses at the lower compressive zone of the wall can be verified. The steps of this procedure are described in detail in Section 6.4.5. Table 7.5 summarizes the steps of the adopted procedure for all wall specimens, except specimen SW25, that were tested.

7.6. CONCLUSIONS

The discussion of the behaviour of the reinforced concrete walls with height to width ratio of two subjected to monotonically increasing horizontal load led to the following conclusions:

(a) Out of plane displacements and base fixity values measured during testing of type II walls were too small to affect the ultimate horizontal load carrying capacity of the walls.

(b) Slender walls initially subjected to high levels of axial load showed a 45% enhancement in their horizontal load capacity compared with the capacity of walls not subjected to axial load. The lower strength presented by specimen SW25 was due to eccentric vertical and horizontal load applied to the specimen, when the spherical seating used to transfer the vertical loading to the wall moved unexpectedly.

(c) The horizontal load – horizontal displacement family of curves is non-linear even under high axial compressive load. Axial compression was found to reduce not only the horizontal displacements measured during testing, for a given horizontal load, but also the ultimate horizontal wall displacement.

(d) Strength and deformational characteristics of wall specimen SW26 incorporating half the amount of horizontal reinforcement included in specimens SW21 and SW24 and weaker concrete, were similar to the corresponding characteristics of the latter specimens.

(e) The application of axial compressive load results in a smaller difference between the absolute values of elongation and shortening of the wall edges. Higher depths of neutral axis were observed with increasing levels of axial compressive load applied to the wall specimens.

(f) The measured horizontal load corresponding to the loading stages of cracking (initial, flexural and inclined), yield and ultimate, increases with the level of initially applied vertical load.

(g) Strain gauge readings indicate that all walls tested, except SW25, exhibited considerable post yield deformations prior to failure. An increase in the normalized axial load from 0. to 0.20 did not alter the maximum compressive strain of the specimens while it led to a drop of the maximum recorded tensile steel strain from 28,000 to 16,000 microstrains.

(h) When a normalized axial load of 0.2 was applied to slender walls, the recorded secant stiffness values were slightly higher than the corresponding values of walls subjected to normalized axial stresses of 0.1. However, the secant stiffness values for both cases were much higher than the ones recorded from specimens not subjected to any axial load. Analytically predicted secant stiffness values of slender walls for the uncracked phase were higher than the experimentally obtained stiffness values. The differences were even higher when axial stiffness values were considered; measured axial stiffness values were only a small percentage of the corresponding analytical values.

(i) Failure of slender walls occurred due to near vertical splitting of the lower compressive zone of the wall between the two deepest consecutive flexural cracks. A possible failure mechanism for the development of such tensile stresses appears to be associated with the bond failure between tensile reinforcement and concrete when the bond stresses are critical.

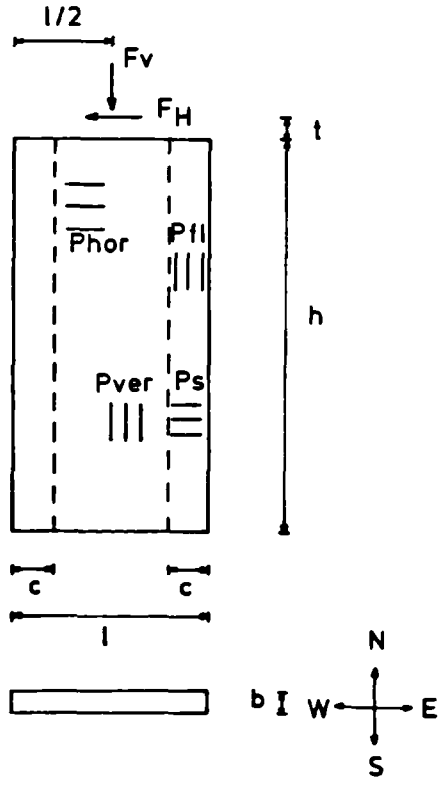
(j) A complex triaxial state of stress at the lower compressive edge of the wall is responsible for the horizontal load carrying capacity of the walls. A gross assessment of longitudinal and transversal stresses in the compressive region of the wall given in Table 7.5 verifies the validity of this statement.

SPECIMEN	TIME OF TESTING (days)	CUBE STRENGTH fcu (MPa)			CYLINDER STRENGTH fcyl (MPa)
		7 DAYS	28 DAYS	TESTING DAY	TESTING DAY
SW21	55	26.8	/	42.8	34.3
SW22	49	34.7	/	50.6	35.3
SW23	46	35.0	47.8	47.8	38.5
SW24	49	35.4	51.8	48.3	34.8
SW25	58	31.6	42.2	45.0	36.6
SW26 *	57	/	28.6	30.1	/
MEAN		32.7	47.3		
ST.DEVIATION		±3.24	±3.94		

*(different mix design)

Table 7.1. Concrete strength characteristics of type II walls.

SPECIMEN	REINFORCEMENT PERCENTAGE				VERTICAL LOAD		ULTIMATE HORIZONTAL LOAD
	P_{hor} (%)	Pver (%)	P_{fl} (%)	Ps (%)	Fv (KN)	$\frac{Fv}{blfc'}$	F_H (KN)
SW21	0.8	2.5	3.3	0.9	0	0	127
SW22	0.8	2.5	3.3	0.9	182.0	0.10	150
SW23	0.8	2.5	3.3	0.9	343.1	0.20	180
SW24	0.8	2.5	3.3	0.9	0	0	120
SW25	0.8	2.5	3.3	0.9	324.8	0.20	150
SW26	0.4	2.5	3.3	0.9	0	0	123



DIMENSIONS

l=650 mm

h=1300 mm

b=65 mm

c=140 mm

t=75 mm

Table 7.2. Experimental data for type II walls.

SPECIMEN	LOADING LEVEL																DUCTILITY
	INITIATION OF CRACKING				FLEXURAL CRACKING				INCLINED CRACKING & YIELDING OF REINFORCEMENT				ULTIMATE				
	F_H	δ	k	$\gamma *10^{-2}$	F_H	δ	k	$\gamma *10^{-2}$	F_H	δ	k	$\gamma *10^{-2}$	F_H	δ	k	$\gamma *10^{-2}$	
SW21	10	0.32	31.6	0.024	32	1.82	18.5	0.132	80	5.81	13.8	0.446	127	20.61	6.2	1.594	3.55
SW22	14	0.39	38.5	0.028	55	1.84	31.5	0.134	110*	4.91	22.4	0.375	150	15.30	9.8	1.183	3.12
SW23	20	0.52	38.4	0.041	70	2.54	29.4	0.185	120*	5.20	23.1	0.402	180	13.19	13.6	1.024	2.54
SW24	10	0.29	36.8	0.021	30	1.49	21.4	0.109	80	6.23	12.8	0.483	120	18.13	6.6	1.412	2.91
SW25	25	0.60	41.9	0.046	90	3.37	28.2	0.245	130*	5.87	22.2	0.450	150**	9.47	15.8	0.724	/
SW26	10	0.39	27.0	0.028	28	1.89	15.6	0.138	68*	5.51	12.4	0.423	123	20.94	5.9	1.620	3.80

*ersg

**prem.failure

F_H in KN

δ in mm

k in KN/mm

$\gamma = \frac{\delta}{h}$ drift index

Table 7.3. Principal results for type II walls at various loading levels.

SPECIMEN	SHEAR STRESS (MPa)				SHEAR STRESS RATIOS				
	FLEXURAL CRACKING		INCLINED CRACKING & YIELDING OF REINF.	ULTIMATE					
	Vcr	Vsf	Vic=Vy	Vult	$\frac{Vult}{\sqrt{f'c}}$	$\frac{Vult}{f'c}$	$\frac{Vcr}{Vult}$	$\frac{Vsf}{Vult}$	$\frac{Vy}{Vult}$
SW21	0.24	0.76	1.90	3.01	0.498	0.083	0.08	0.25	0.63
SW22	0.33	1.30	2.60	3.55	0.541	0.083	0.09	0.37	0.73
SW23	0.47	1.66	2.84	4.26	0.669	0.105	0.11	0.39	0.67
SW24	0.24	0.71	1.89	2.84	0.443	0.069	0.08	0.25	0.67
SW25	0.59	2.13	3.08	3.55	0.574	0.093	0.17	0.60	0.87
SW26	0.24	0.66	1.61	2.91	0.575	0.114	0.08	0.23	0.56

Table 7.4. Shear stress values for type II walls at various loading levels.

SPECIMEN	DEPTH OF N.A. c (cm)	STRESSES DUE TO BENDING				STRESSES DUE TO SHEAR	COMBINED PRINCIPAL STRESS CONDITIONS			APPLIED STRESSES IN OCTAHEDRAL FORM		$\tau_{o,ult}$
		$\bar{\sigma}_x$	$\max \sigma_x$ *	$\max \frac{\sigma_x}{f_c'}$	$\sigma_y=\sigma_z$	$\tau_{xy}=F_H/cb$	σ_1	σ_3	σ_2	σ_o	τ_o	
SW21	13	50.4	100	2.7	15	15.03	102.6	12.4	15.0	43.33	41.92	40.19
SW22	17	51.6	100	2.3	11	13.60	102.0	9.0	11.0	40.67	43.38	40.50
SW23	18	50.8	101.5	2.5	10.2	15.40	104.1	7.7	10.2	40.70	44.90	39.80
SW24	13	59.6	120	2.9	18.5	14.20	121.95	16.6	18.5	52.33	49.23	47.50
SW26	14	38.4	76.8	3.0	11.5	13.50	79.5	8.9	11.5	33.30	32.70	29.70

*assuming triangular distribution

All stresses in MPa

Table 7.5. Stress conditions causing failure of type II wall specimens.

Table 7.5 Cont'd

NOTATION

where $$\sigma_1 = \frac{\sigma_x + \sigma_y}{2} + \sqrt{\left\{\left(\frac{\sigma_x - \sigma_y}{2}\right)^2 + \tau_{xy}^2\right\}}$$

$$\sigma_2 = \sigma_z$$

$$\sigma_3 = \frac{\sigma_x + \sigma_y}{2} - \sqrt{\left\{\left(\frac{\sigma_x - \sigma_y}{2}\right)^2 + \tau_{xy}^2\right\}}$$

$$\sigma_{o,ap} = \frac{\sigma_1 + \sigma_2 + \sigma_3}{3}$$

$$\tau_{o,ap} = 1/3 \sqrt{\left\{(\sigma_1 - \sigma_2)^2 + (\sigma_2 - \sigma_3)^2 + (\sigma_3 - \sigma_1)^2\right\}}$$

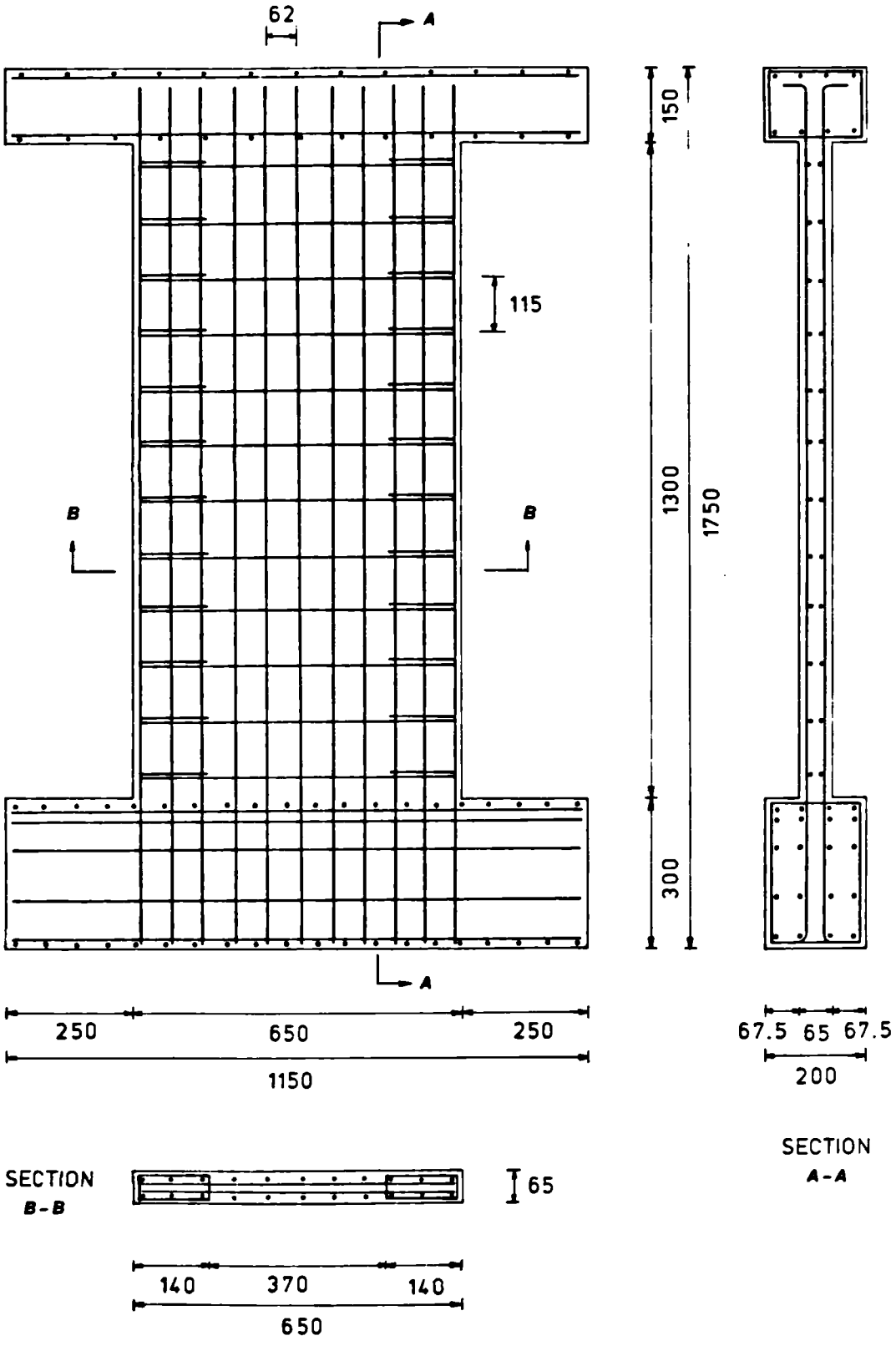


Fig. 7.1. Geometry and reinforcement details of type II walls.

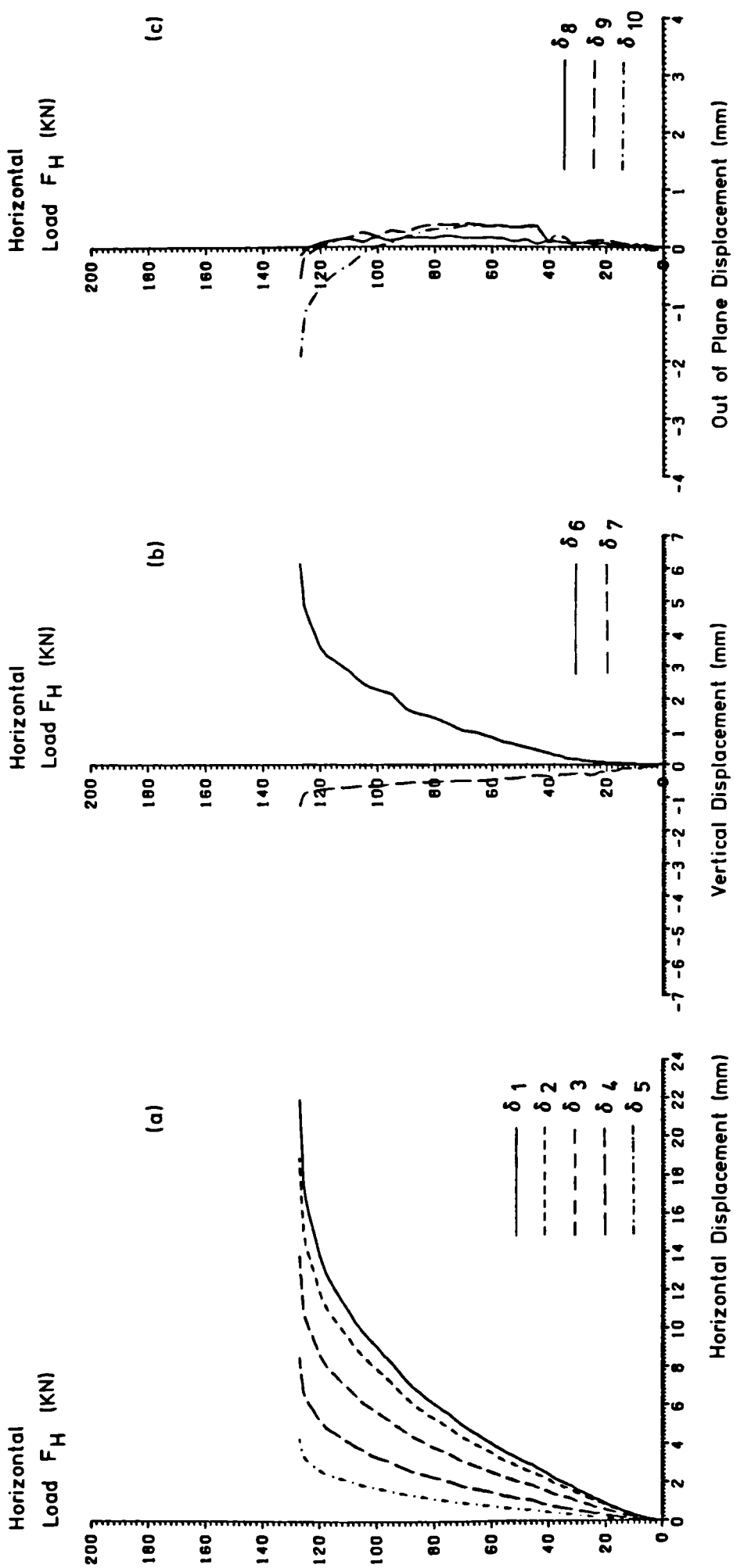


Fig. 7.2. Horizontal load-displacement curves of specimen SW21 constructed by using measurements of (a) horizontal displacement, (b) vertical displacement and (c) out of plane displacement.

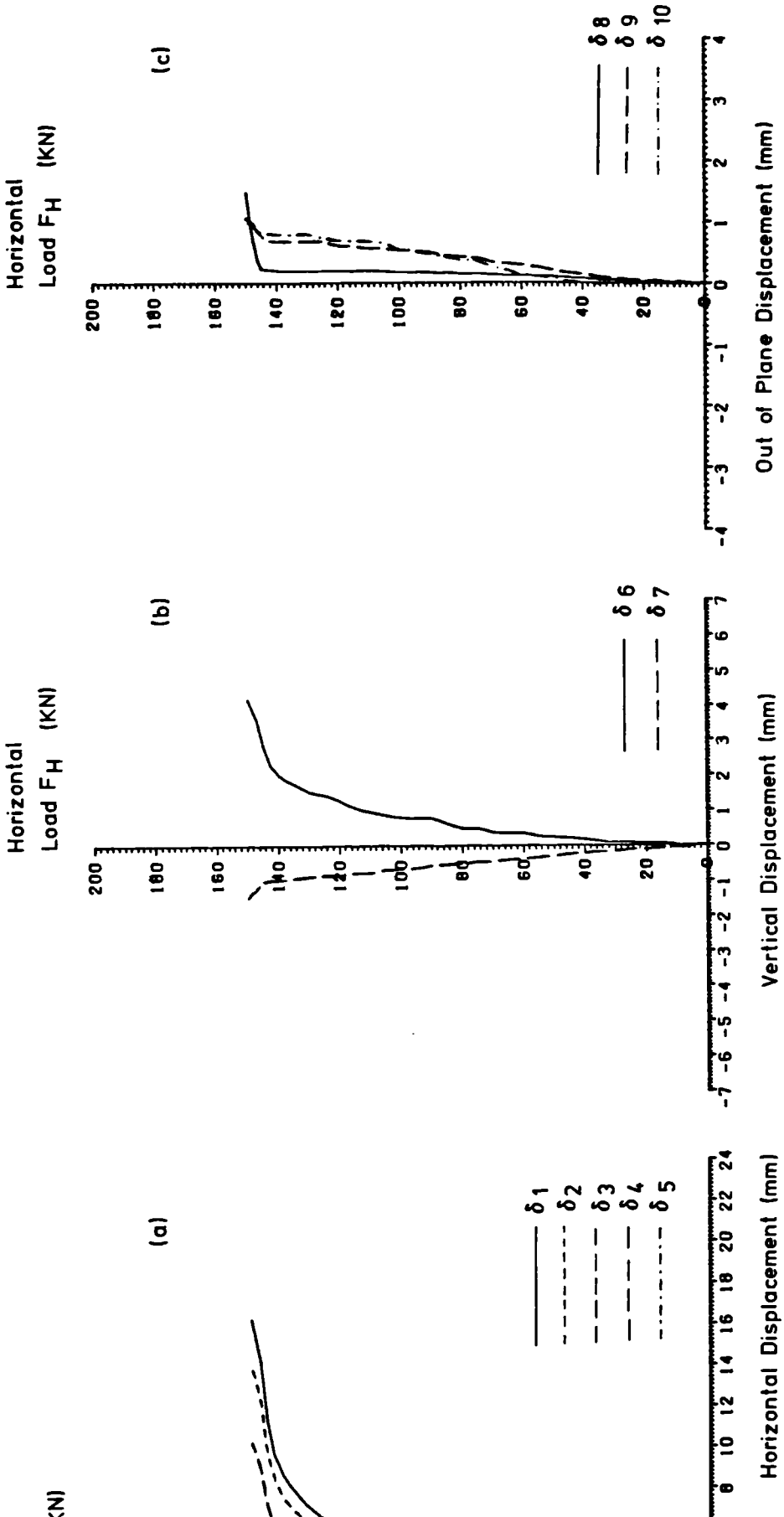


Fig. 7.3. Horizontal load-displacement curves of specimen SW22 constructed by using measurements of (a) horizontal displacement, (b) vertical displacement and (c) out of plane displacement.

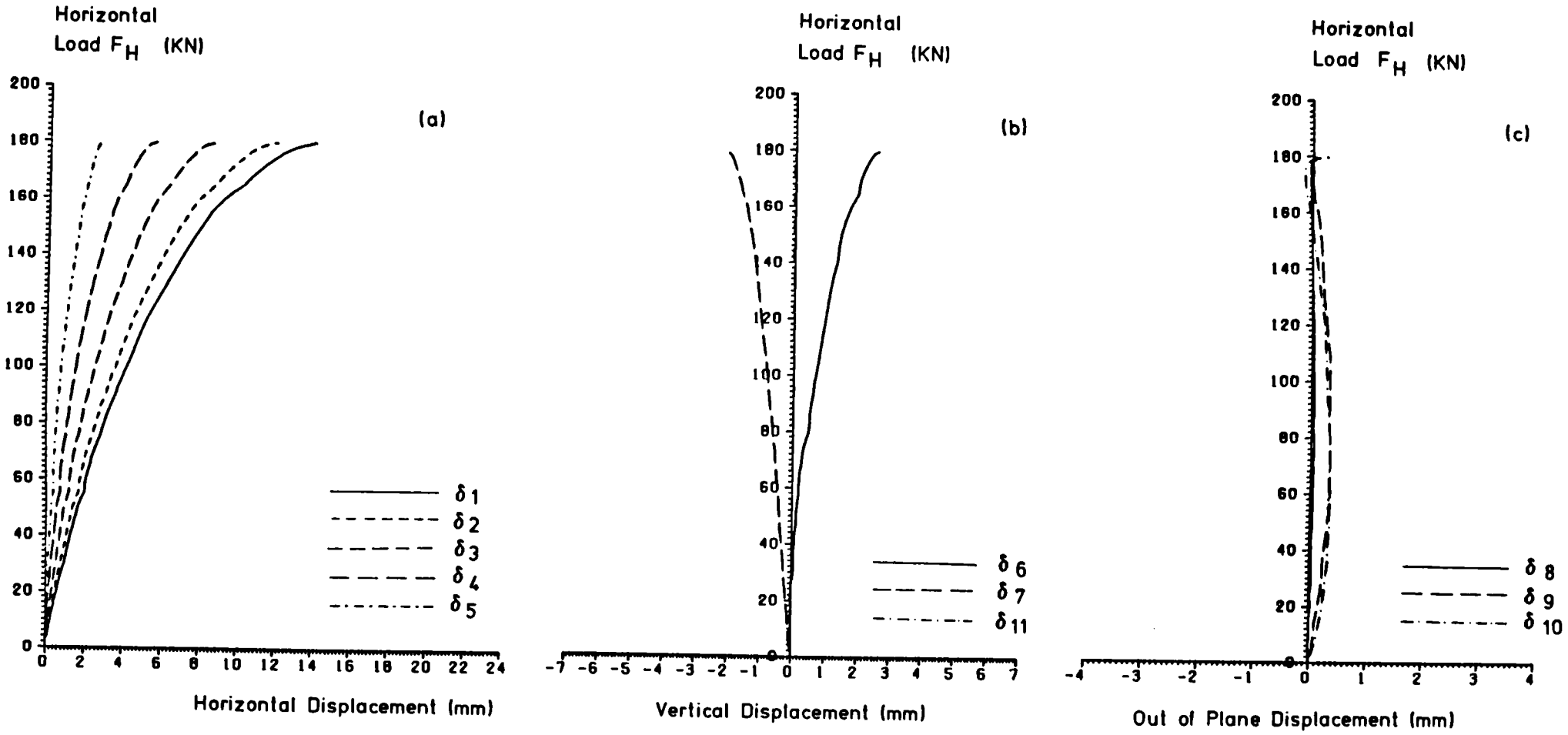


Fig. 7.4. Horizontal load-displacement curves of specimen SW23 constructed by using measurements of (a) horizontal displacement, (b) vertical displacement and (c) out of plane displacement.

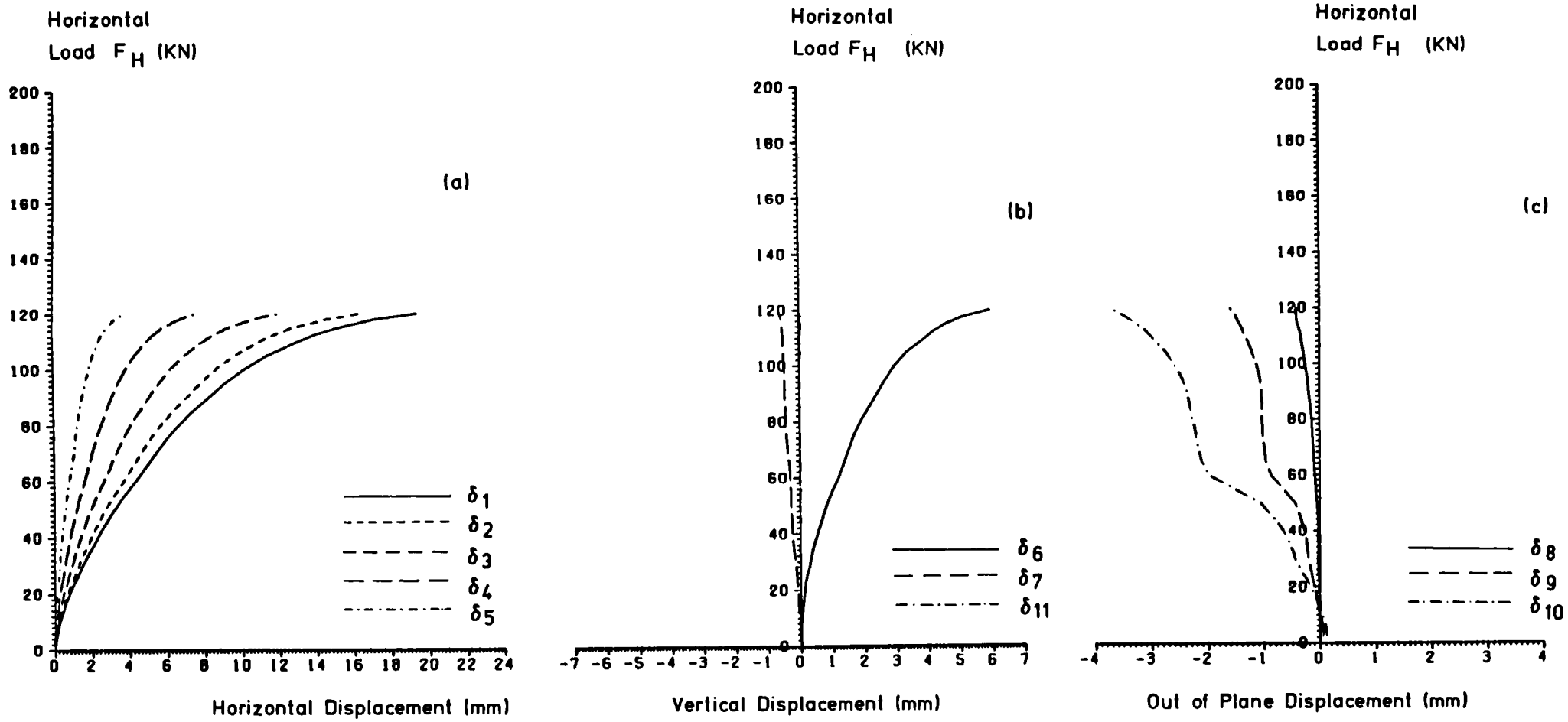


Fig. 7.5. Horizontal load-displacement curves of specimen SW24 constructed by using measurements of (a) horizontal displacement, (b) vertical displacement and (c) out of plane displacement.

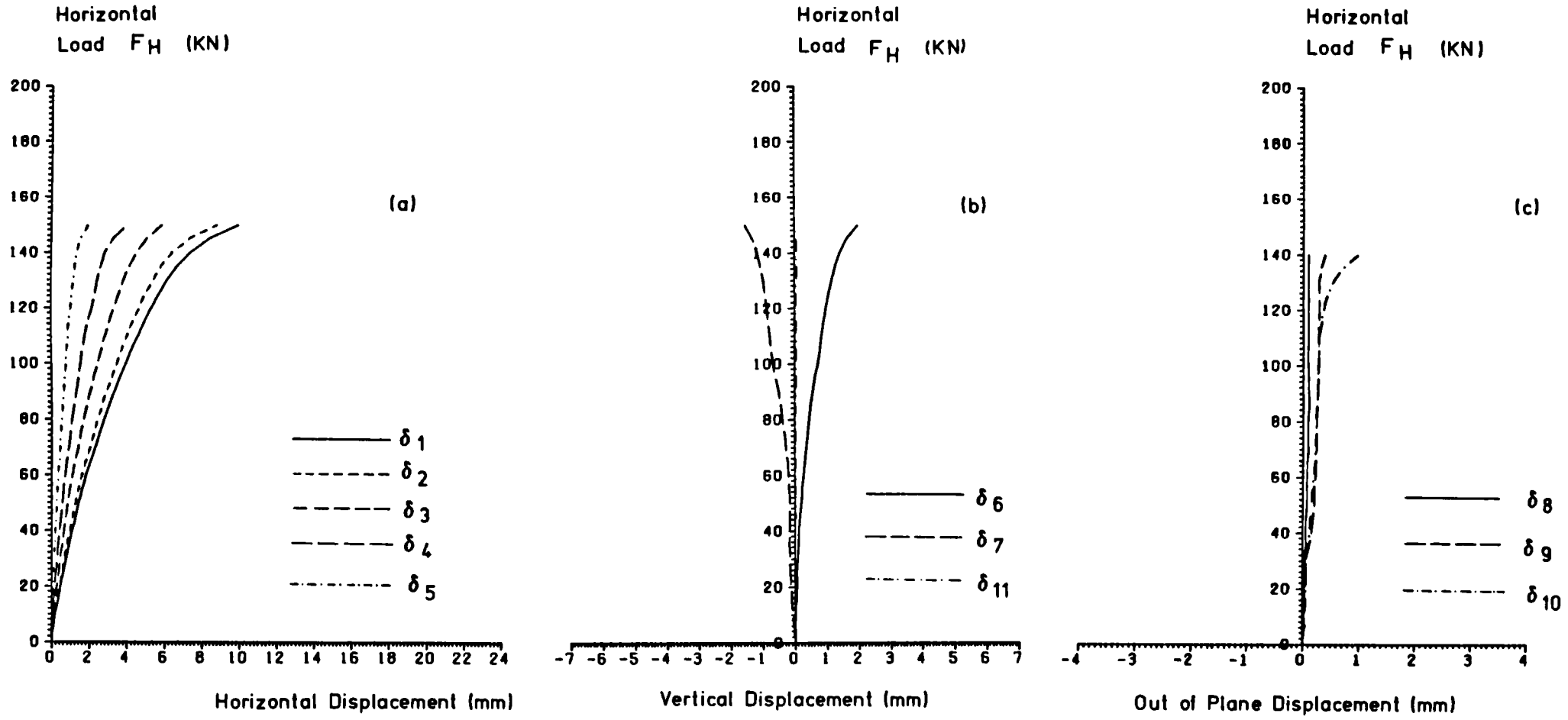


Fig. 7.6. Horizontal load-displacement curves of specimen SW25 constructed by using measurements of (a) horizontal displacement, (b) vertical displacement and (c) out of plane displacement.

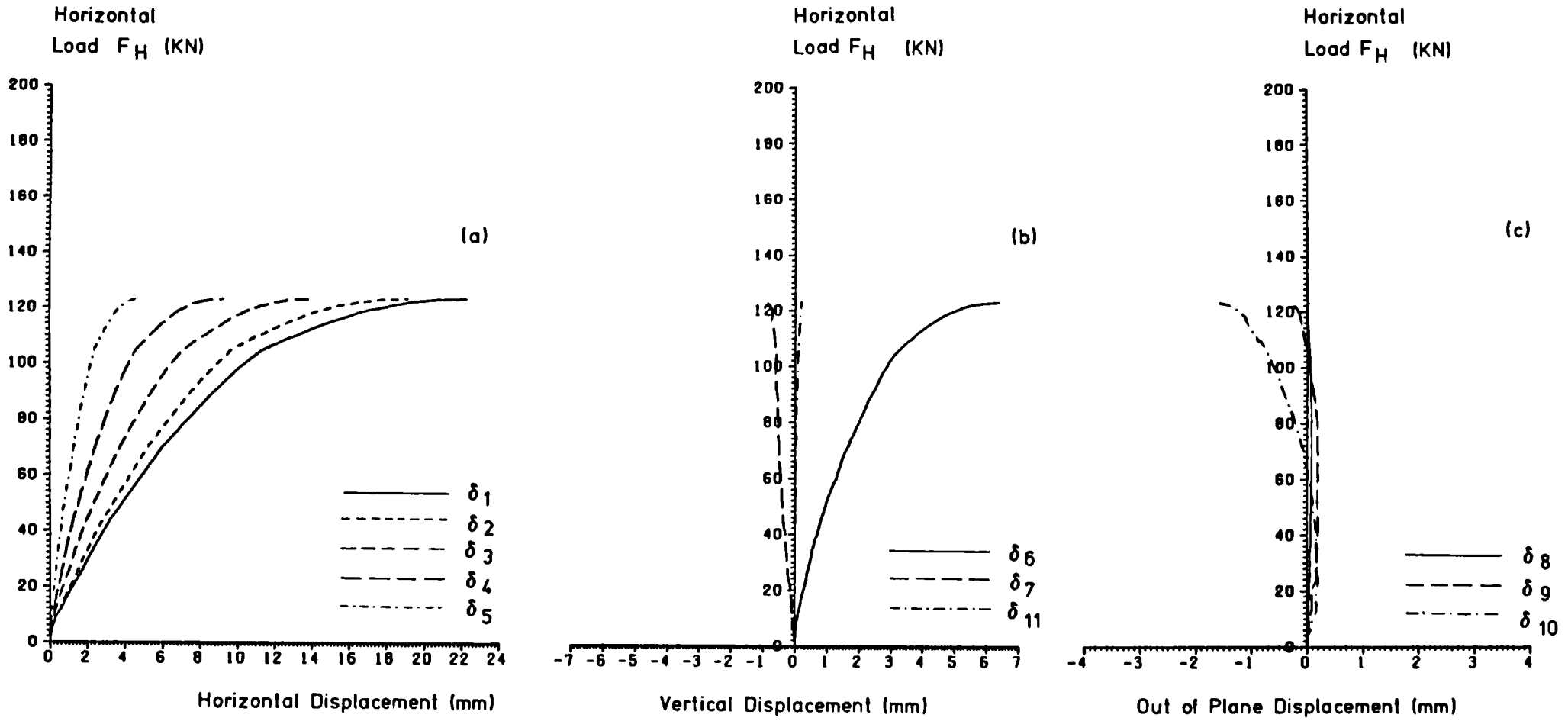


Fig. 7.7. Horizontal load-displacement curves of specimen SW26 constructed by using measurements of (a) horizontal displacement, (b) vertical displacement and (c) out of plane displacement.

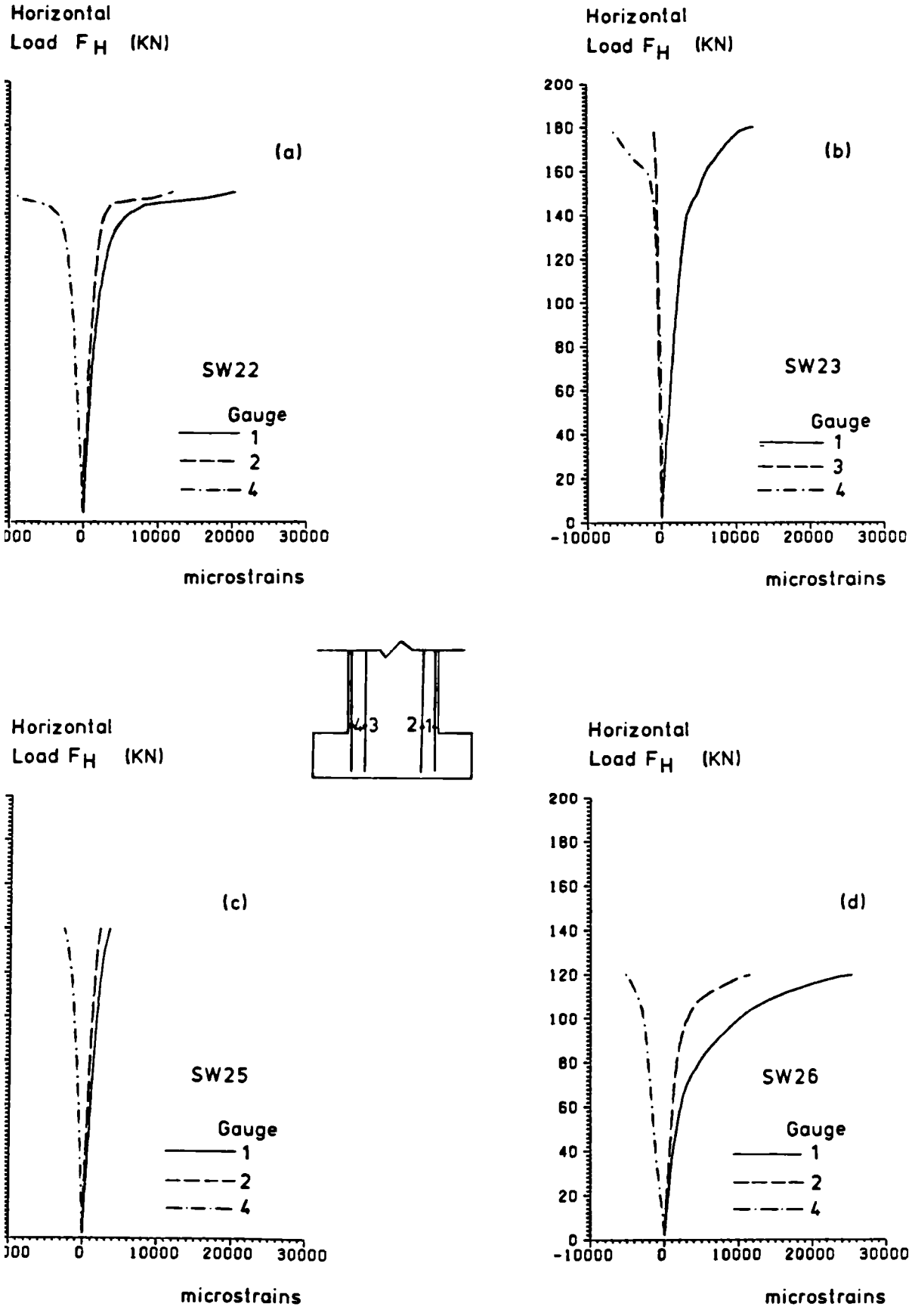


Fig. 7.8. Variation of the average strain of the longitudinal reinforcement with varying horizontal load for specimens (a) SW22, (b) SW23, (c) SW25 and (d) SW26.

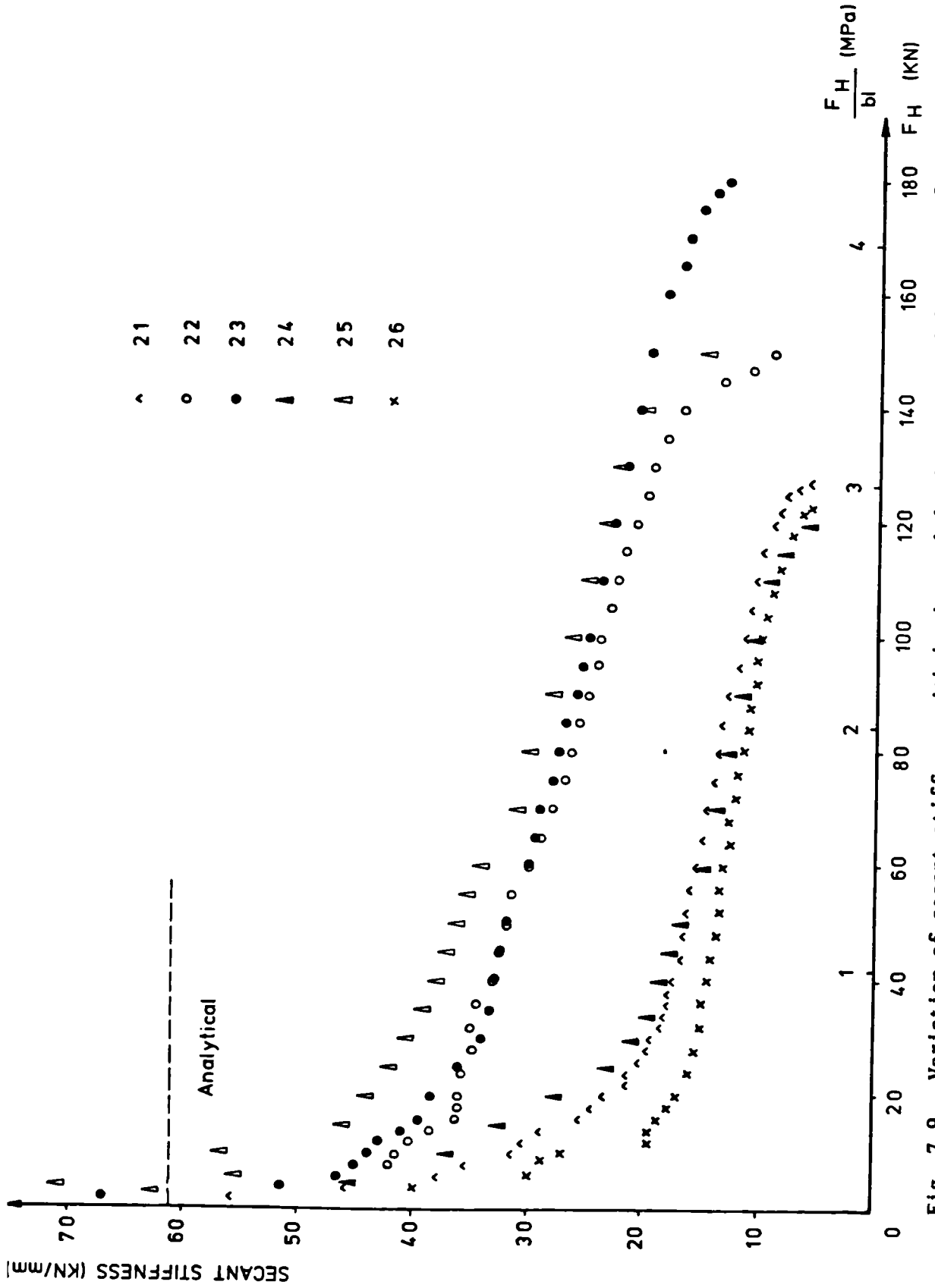


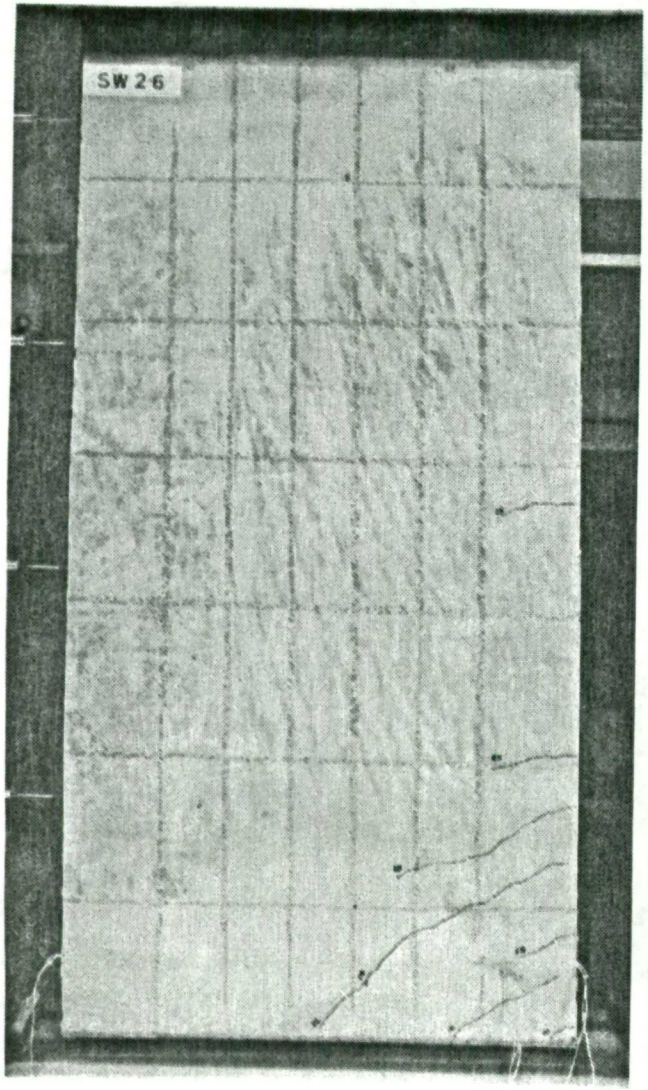
Fig. 7.9. Variation of secant stiffness with horizontal load expressed in terms of both force and stress units for type II walls.

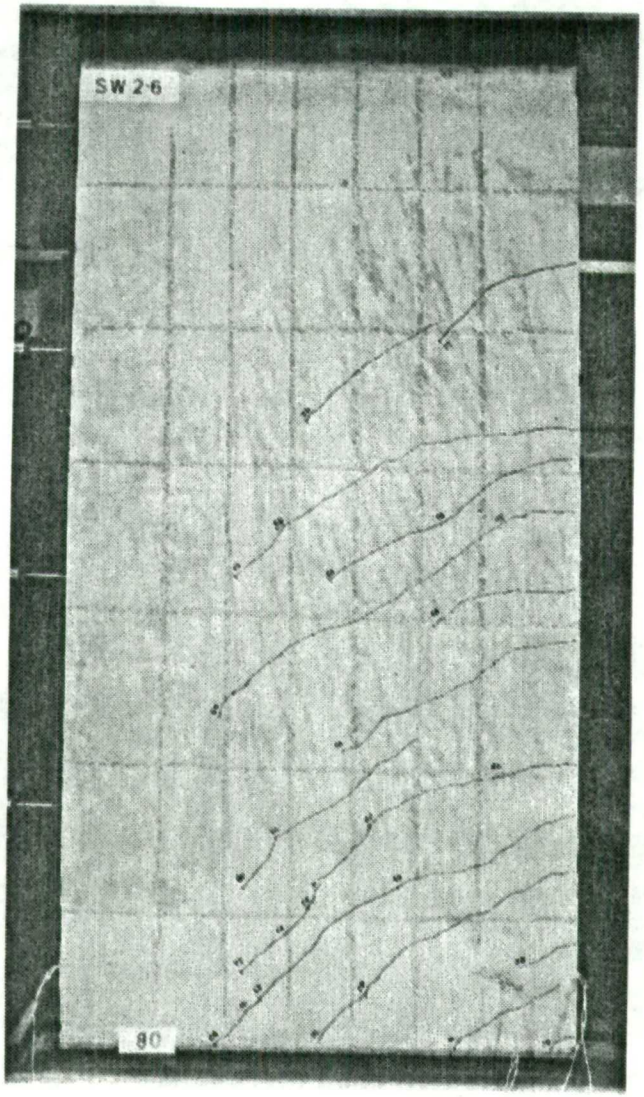
Fig. 7.10. Significant levels of cracking process exhibited by type II walls.

(a) Initiation of flexural cracking (left plate),

(b) initiation of inclined cracking (middle plate) and

(c) ultimate horizontal load (right plate).


SW 2-6


SW 2-6
80

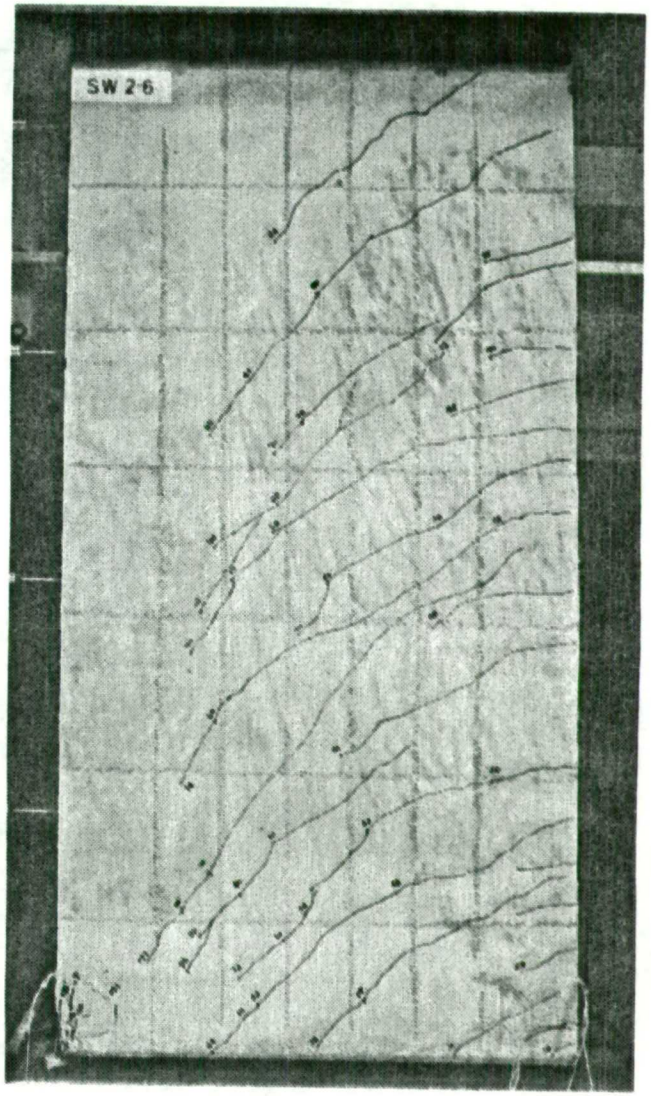
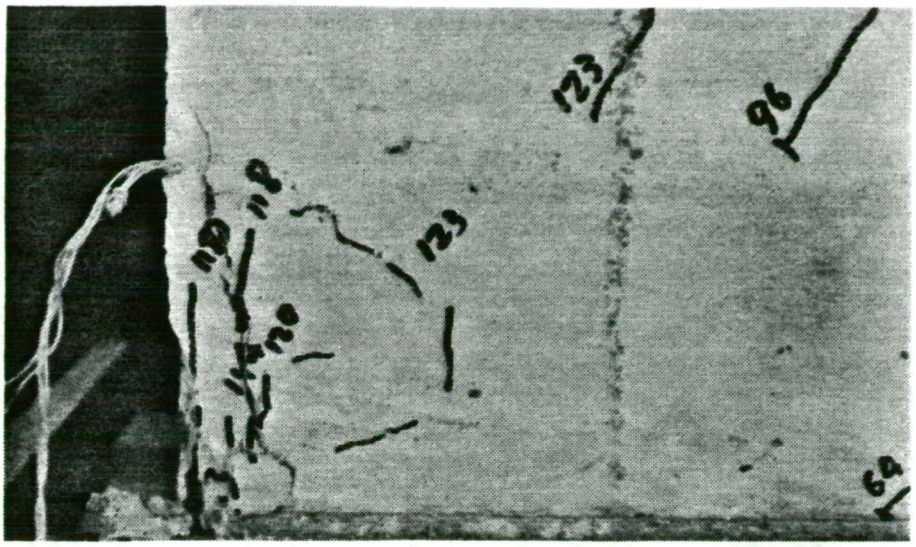
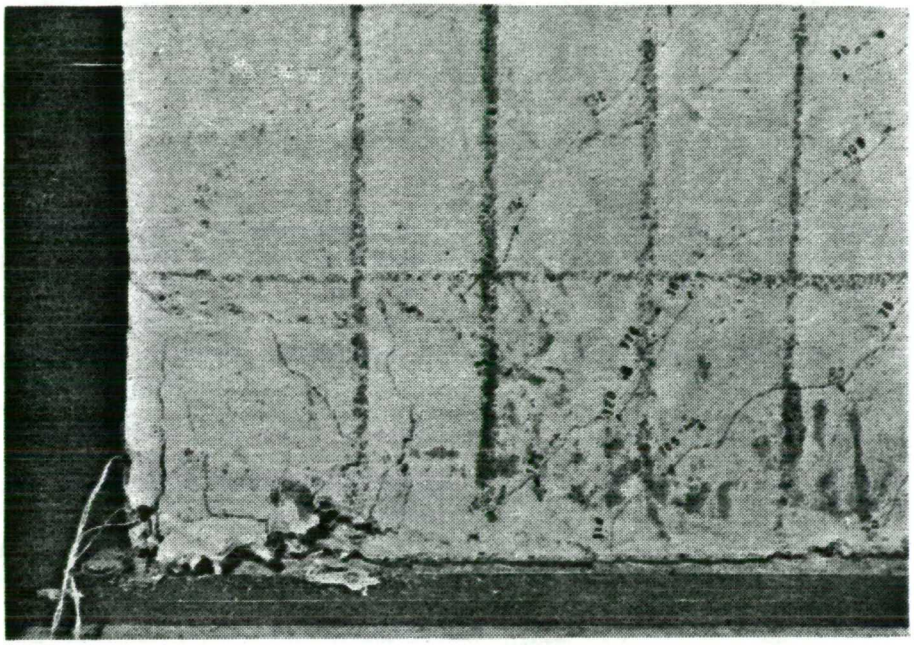
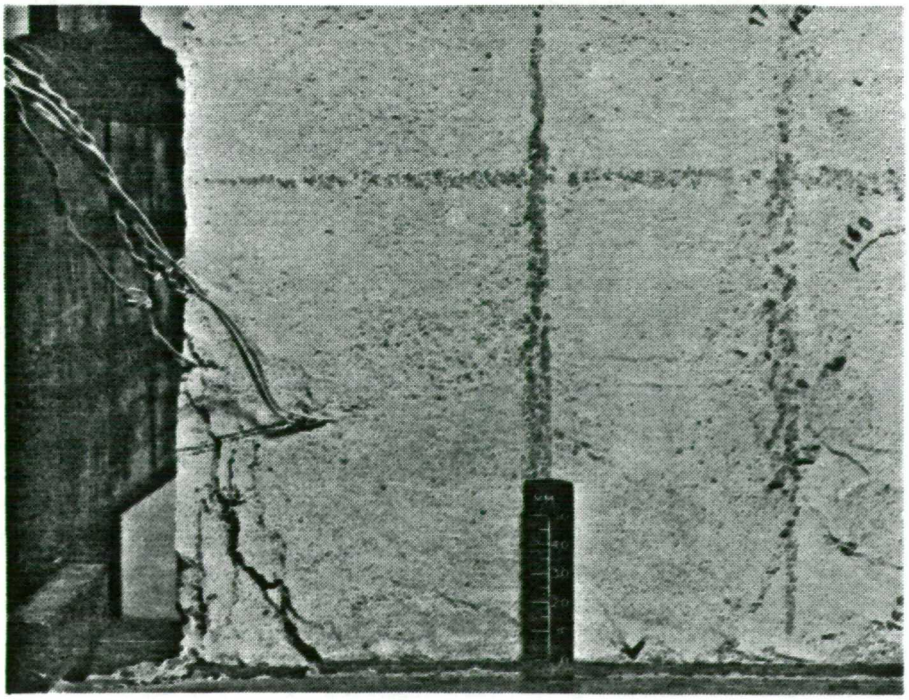

SW 2-6

Fig. 7.11. Lower compressive failure zone of type II walls subjected to normalized axial load
(a) v=0 (upper plate),
(b) v=0.1 (middle plate) and
(c) v=0.2 (lower plate).


123
96
123
64





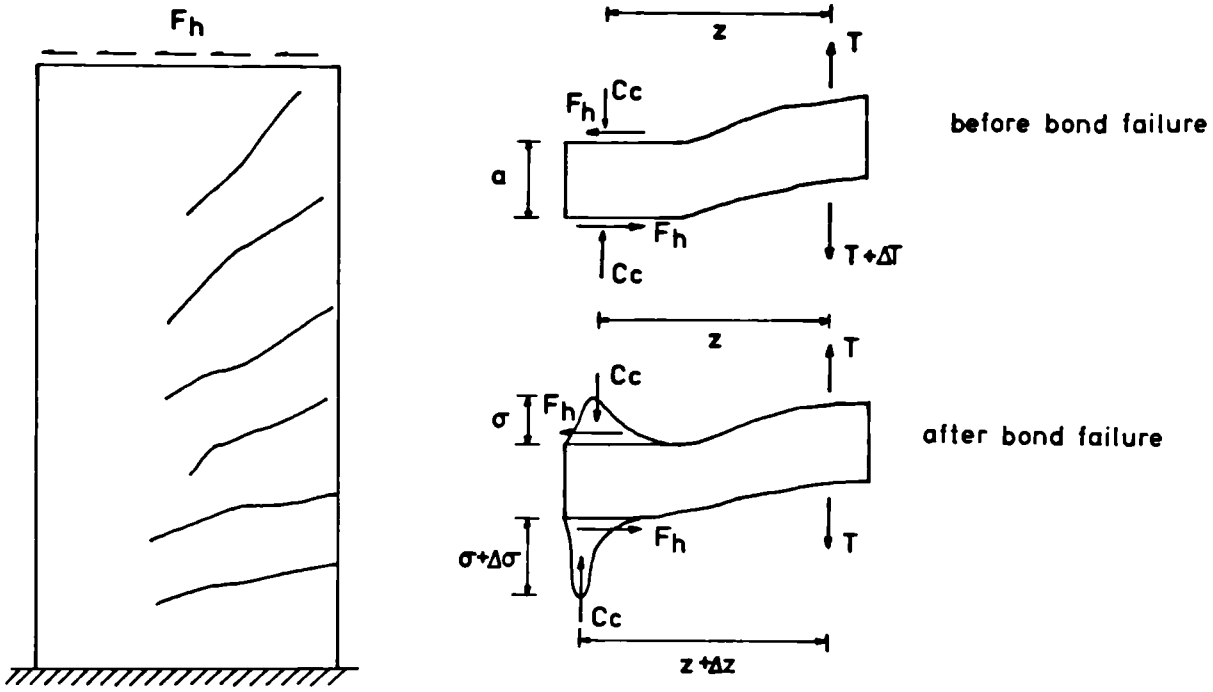


Fig.7.12. Schematic representation of the failure mechanism of type II walls.

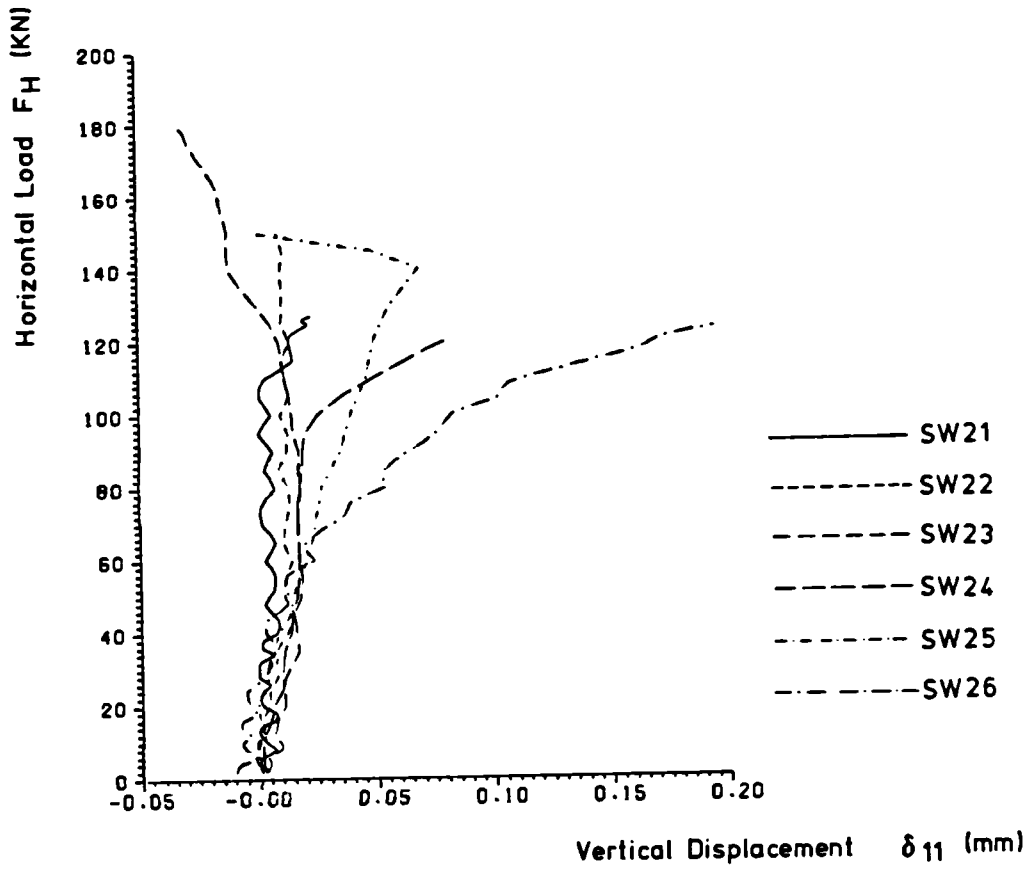


Fig. 7.13. Variation of horizontal load with base vertical displacement for type II walls.

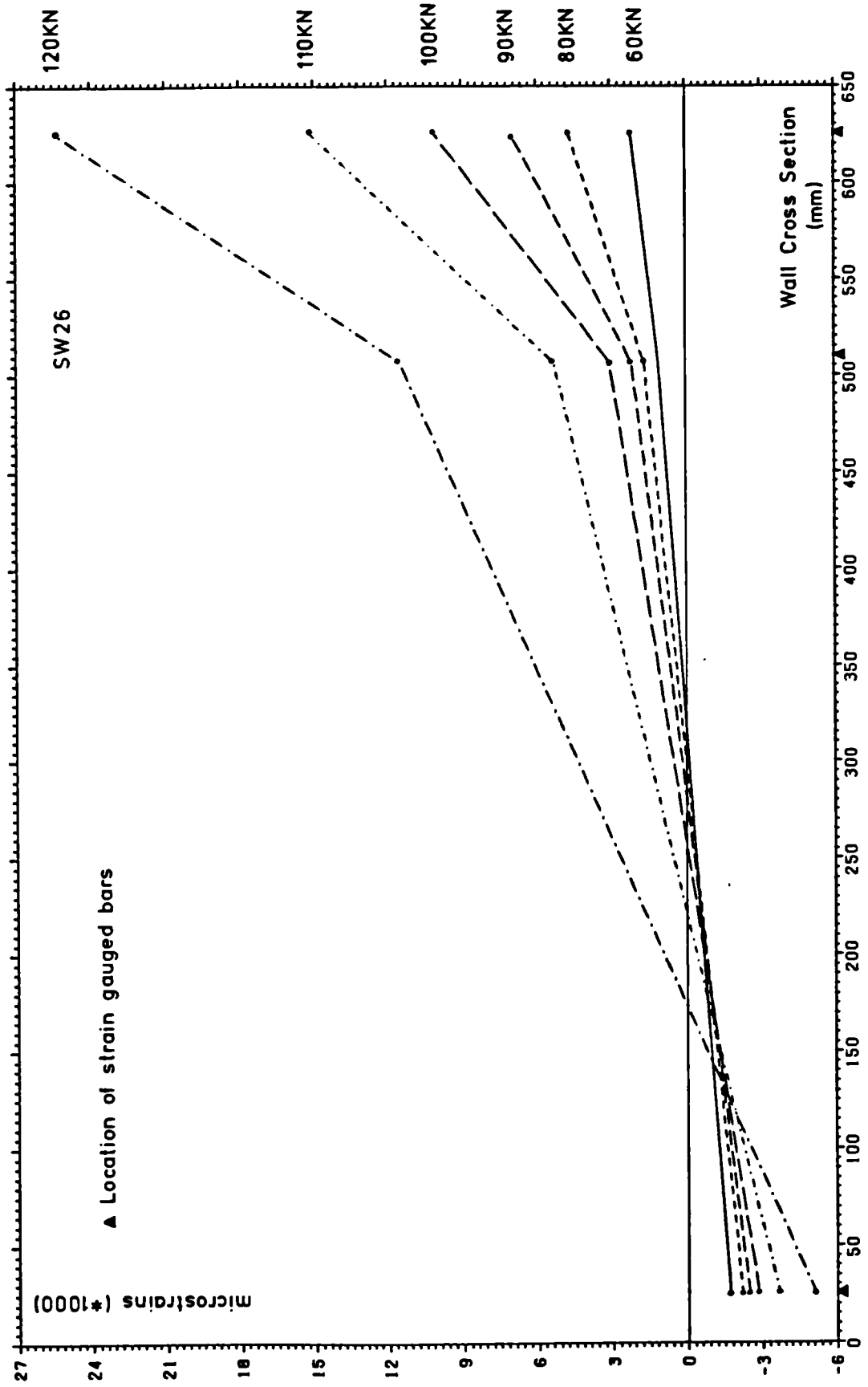


Fig. 7.14. Axial strain distribution along the lower wall cross-section for specimen SW26 under various levels of increasing horizontal load.

CHAPTER 8

EXPERIMENTAL INVESTIGATION OF THE BEHAVIOUR OF TYPE II WALLS UNDER CYCLIC LOADING

8.1. INTRODUCTION

A total of three tests were performed on large scale structural walls with a rectangular cross-section and a height to width ratio of two subjected to cyclic loading. The main objectives of the tests were to

(a) investigate the behaviour of high-rise walls under various cyclic loading regimes and in particular their structural deterioration characteristics;

(b) compare the above behaviour with that established from the monotonic tests discussed in the previous chapter.

8.2. WALL DETAILS AND LOADING CONDITIONS

The experimental set-up used for the tests was similar to that used for the monotonic loading tests described in Chapter 7. An additional jack was used to introduce horizontal forces on both sides of the loading beam. Figure 8.1 shows the cross-sectional characteristics and reinforcement details of the structural walls tested under cyclic loading. It should be noted that the percentage of horizontal web reinforcement of the walls was as low as 0.35 percent, which is almost the minimum amount specified by Code provisions (ACI 318-83), while the amount of vertical web reinforcement was 60 percent of that of corresponding walls subjected to monotonic loading. The reinforcement details of the wall edges (concealed colum·) were identical to those for monotonic loading. Table 8.1 lists the perce ages of reinforcement of the specimens, the maximum value of horizontal load · ıstained by the walls and the type of cyclic loading regime adopted for the tests. Information related to average uniaxial compressive strength of concrete used in the present series of tests is presented in Table 8.2.

It is well known that, under seismic loading conditions inertia forces develop due to the vertical and horizontal ground movements caused by the earthquake. Vertical movements will not be considered in these tests, since axial forces due to the vertical seismic accelerations have little effect on wall behaviour if compared

with horizontal forces due to horizontal seismic accelerations. Furthermore, the peaks of the structural response to vertical ground accelerations do not necessarily coincide with the peaks of the response to horizontal ground accelerations or to vertical accelerations arising purely from "overturning" response of a structure. Therefore, no other axial load than the gravity load of the specimen was applied to the walls.

In order to simulate the loading sequence that might be expected to occur in the field, three different simplified types of horizontal loading history were adopted. Loading history (a) is the pseudo equivalent of a field event which results in a base shear that mainly shakes the wall up to the first yield of the wall tensile reinforcement, before loading it up to failure. Loading history (b) is representative of an event with greater prefailure severity for the wall. It is associated with a number of prefailure cycles that cause yielding of all the vertical reinforcement of the tensile edge of the wall. Finally, cyclic loading regime (c) blends characteristics of the previous two case studies. After the horizontal load corresponding to either first or to complete yielding of the tensile reinforcement had been reached, the walls were subjected to load cycles to a given maximum displacement. Figure 8.2 provides a schematic representation of the loading programmes used for the tests. Diagrams presenting the variations of both horizontal load and top horizontal displacement with the number of cycles are included. Wall specimens were loaded and unloaded in both positive and negative direction at a rate of 0.04 KN/s, which was similar to that used for the loading tests discussed in previous chapters.

8.3. PARAMETERS OF STRUCTURAL DETERIORATION INVESTIGATED

The main results of the experimental investigation will be presented in Section 8.4 and discussed in Section 8.5. Horizontal load – horizontal displacement hysteresis curves were used to evaluate the structural degradation of the specimens. The main parameters considered to describe degradation are identified and discussed in the following sub–sections:

8.3.1. STIFFNESS DEGRADATION

The first loading of a structural element to a particular displacement or ductility ratio, referred to as virgin loading, is different in character from subsequent excursions to the same displacement level. As the number of cycles to

a particular displacement increases, the horizontal load corresponding to maximum displacement decreases.

The knowledge of the extent of degradation of a wall element after the n^{th} cycle to a displacement $\pm \delta$ (or ductility ratio μ) is significant for the aseismic design of this element. One of the principal aims in the design of structural elements subjected to cyclic loads is to ensure that the element will have the ability to offer a specified level of resistance against cyclic horizontal (lateral) loading.

For the case of monotonic loading, secant stiffness at a given load is defined as the ratio of the horizontal load to the corresponding horizontal displacement. When the wall specimen is subjected to cyclic loading from a positive displacement $+\delta_1$ to a negative displacement $-\delta_2$, the secant stiffness of the wall per cycle can be defined as the ratio of the sum of the two extreme absolute values of horizontal cyclic load to the sum of the corresponding absolute values of the lateral displacement (see Figure 8.3). As the wall is subjected to a particular range of lateral displacement, the secant stiffness of the wall decreases with increasing number of cycles.

8.3.2. ENERGY DISSIPATION AND EQUIVALENT VISCOUS DAMPING

Notwithstanding the fact that the primary aim of a wall element is to offer resistance against lateral cyclic loading, wall elements should also have the ability to dissipate large amounts of input energy. The energy dissipated by a wall specimen is defined as the area enclosed by the horizontal load – top horizontal displacement curve for a particular cycle. Usually, the amount of energy dissipated prior to first significant cracking of the wall is relatively small, but increases greatly once this level is exceeded. It is obvious that the energy dissipation capacity drops as the number of cycles increases for a given ductility ratio. However, load cycles after the first (virgin), and probably the second, cause insignificant additional cracking.

Figure 8.3 shows a typical horizontal load – horizontal displacement curve for the virgin and second loading cycles to the same displacement. The total energy imparted to the wall during virgin loading can be separated into three components, namely, the recoverable energy W_3, the damping energy W_2 and the damage energy, W_1. The energy dissipated by the wall is the sum of the damage energy, W_1, and the damping energy, W_2.

Another way of presenting the energy dissipated per cycle during a cyclic loading test is by using the concept of an equivalent viscous damping. This term has been used by investigators to correlate hysteretic energy dissipation to the standard concept of structural damping used for linear systems. In general, free decay tests cannot be used to determine a damping factor at amplitudes causing inelastic displacements. Therefore, the energy ratio method should be used to evaluate the equivalent damping ratio for the test cycles with post yield displacements. Jacobsen (1960) was probably the first who used this method to calculate the damping in composite structures. The equivalent damping ratio can be expressed by the ratio:

$$\zeta = \frac{W_D}{4 * \pi * W_S}$$

where W_D = the energy dissipated per cycle

W_S = the strain energy per quarter cycle of a corresponding linear system with the equivalent secant stiffness of the non-linear loop.

Based on the statistical analysis of experimental results on structural wall units subjected to cyclic lateral loading, Lefas et al (1982) proposed semi-empirical expressions for the decrease of horizontal load corresponding to given maximum displacement and hysteretic damping of reinforced concrete walls subjected to post yield cyclic deformations. The expressions are also included in the CEB, Bulletin No. 161 (1983). The above expressions will be validated with respect to the experimental results of the present investigation.

8.4. PRESENTATION OF RESULTS

This section includes the main results for reinforced concrete walls tested under cyclic loading, together with information useful for a better understanding of their behaviour.

Figure 8.4 presents the variation with horizontal load of (a) the top out of plane displacement and (b) the vertical displacement of the foundation beam for the three specimens tested. Figures 8.5, 8.6 and 8.7 present information related to the variation of horizontal and vertical displacements with increasing levels of horizontal load for the specimens SW31, SW32 and SW33 respectively. Each

figure consists of two subfigures; with subfigure (a) illustrating variations of top horizontal displacement and subfigure (b) presenting variations of alternate elongation and shortening of the wall edges.

Tables 8.3 and 8.4 summarize the experimental data on the strength and deformation response of the walls at loading levels corresponding to first visible cracking, significant flexural cracking, inclined cracking, yielding of tensile reinforcement and ultimate limit state. Values of horizontal load, top horizontal displacement, secant stiffness and drift index at the above levels are listed in Table 8.3, whereas Table 8.4 gives the boundary shear stress values at the above loading levels. Experimental and analytical values of the ratio of the wall horizontal load corresponding to maximum displacement with increasing number of cycles to the horizontal load corresponding to the same displacement during the first cycle are summarized in Table 8.5.

Variations of wall secant stiffness with horizontal load are illustrated in Figure 8.8, with Table 8.6 presenting data of secant stiffness deterioration with the number of cycles for various values of the ductility ratio. The amount of energy dissipated per cycle for each of the specimens tested is given in Table 8.7, while Table 8.8 shows experimental and analytical values of equivalent viscous damping of the wall specimens for different numbers of cycles and values of the displacement ductility ratio.

Figures 8.9 and 8.10 show the variation of the average strain of the longitudinal reinforcement with varying horizontal load for the specimens SW32 and SW33 respectively. The average strain was calculated from readings of the gauges mounted on the outer and inner reinforcing bars at both wall edges near the foundation beam of the wall specimens. Significant stages of the cracking process and the failure mode of type II walls subjected to cyclic loading are depicted in Figure 8.11.

8.5. DISCUSSION OF RESULTS

8.5.1. VALIDATION OF THE EXPERIMENTAL SET UP

As for the case of the monotonic tests, the application of plane stress conditions to the wall units and the achievement of wall base fixity were the basic aims of the design of the experimental set up for the cyclic loading tests. Since during cyclic loading test specimens deflected towards both the east and west

directions, an extra displacement transducer was mounted on the top side of the foundation beam to monitor the vertical displacement of the west side of the beam. The position of the displacement transducers used to record out of plane displacement during testing was the same as that of the transducers used for monotonic tests. Figure 5.6 illustrates the position of the new transducer and the sign of its reading.

The out of plane displacement measurements of the transducer mounted highest along the wall height, shown in Figure 8.4(a), indicate that very small values were recorded. The maximum out of plane displacement, monitored at the ultimate horizontal load stage was only 0.25% of the height of the wall. Therefore, even at the penultimate loading stage, such displacement values result in secondary rotational and torsional moments which cannot affect the primary moment applied to the wall. Out of plane displacement values recorded at a lower point along the wall height and at the lower compressive zone, reinforce the validity of the previous statement, since their readings were similar in trend but much smaller in absolute value.

Measurements of vertical displacement, on the east and west side of the foundation beam near the concealed columns of the wall were also small, as shown in Figure 8.4(b). The maximum vertical displacement of the foundation beam was measured during testing of wall specimen SW33, as the wall reached its horizontal load carrying capacity. It was equivalent to a rotation of the foundation beam of 2.0 percent of a degree.

It is interesting to note that the different cyclic loading histories have only slightly affected the absolute maximum values of measured vertical and out of plane displacements. A comparison between the displacement values shown in Figure 8.4 and the corresponding values, shown in Figure 7.13 and Figure 7.2(c) to 7.7 (c), indicates that there is not much difference between the absolute maximum values of out of pla: movement and foundation beam rotation recorded during monotonic and cyclic ' ading.

The above results lead to the conclusion that the original design of the experimental set-up for monotonic load conditions, was successfully extended to meet the requirements of slow cyclic loading tests on wall specimens.

8.5.2. STRENGTH AND DEFORMATIONAL RESPONSE

The horizontal load carrying capacity of the three walls tested under cyclic loading conditions was similar to that of the walls subjected to monotonic loading. Although the concrete strength of wall SW31 was 70 percent of the concrete strength of walls SW32 and SW33, the ultimate horizontal load attained by specimen SW31 was 4% higher than the maximum horizontal load of the other two specimens. Such small differences in strength reinforce the observation, made in Chapter 7 for wall specimens subjected to monotonic loading, that variations in concrete strength do not have a significant effect on the strength characteristics of slender walls. The slight drop in strength capacity of walls SW32 and SW33, might be attributed to the excitation of these walls to displacement cycles of higher post-yield severity. However, the differences are too small to suggest that wall strength was significantly affected by the variability of the cyclic loading regime.

The horizontal load - top horizontal displacement curves of walls SW31, SW32 and SW33, shown in Figures 8.5(a), 8.6(a) and 8.7(a) respectively, indicate a distinctly non-linear deformational response for all three walls. Walls SW32 and SW33, subjected to displacement cycles causing yielding of all tensile bars of the concealed columns of the wall, show a 10% increase of the top ultimate horizontal displacement recorded while testing specimen SW31. It is interesting to note that the horizontal load - horizontal displacement curves were flattened when about 95 percent of the horizontal load carrying capacity of the wall was reached. The same pattern of horizontal load-displacement curves was exhibited by the horizontal displacement measured at intermediate levels along the wall height. A comparison between the values of top horizontal displacement at yield and at ultimate, given in Table 8.3 for strain gauged specimens, show that the displacement ductility ratio of the slender walls subjected to cyclic loading varied from 4.4 to 5.6.

The variations of vertical displacement with horizontal load shown in Figures 8.5(b), 8.6(b) and 8.7(b), indicate that in all cases, a wall edge in tension underwent an elongation which was significantly larger than the shortening occurring under compression. When the specimen was unloaded, after being subjected to a given ductility ratio, a residual vertical displacement was observed at the wall edges. The values of residual vertical displacement increased, as the wall was subjected to horizontal displacement cycles of a higher maximum displacement. Another interesting feature of the recorded vertical displacements was that their absolute values were identical as wall edges were subjected to alternate compression and tension during full cycles.

The information given in Tables 8.3 and 8.4 indicates that the measured horizontal load and the corresponding boundary shear stress, at the loading levels of cracking, yielding and ultimate, was nearly the same for all the walls tested and was independent of the concrete strength. The normalized values of boundary shear stress with respect to the relevant ultimate value indicate that:

(a) first visible cracks appeared on the wall when 17 percent of the ultimate horizontal load was reached;

(b) significant visible flexural cracks occurred when the horizontal load applied to the wall reached 30 percent of its ultimate value;

(c) first yielding of tensile reinforcement was recorded and first inclined cracks were observed when about 60 percent of the wall capacity was reached.

As the horizontal load-carrying capacity of the walls appears to be independent of the concrete strength, it is apparent that normalized values of ultimate shear stress with respect to concrete strength do not provide a realistic indication of wall strength. In fact this is indicated in Table 8.4, which shows that while the ultimate shear stresses are similar for all the walls tested, the corresponding normalized values differ considerably.

Wall specimens SW31 and SW32 were subjected to four full cycles corresponding to displacement ductility ratio $\mu = 1$ and $\mu = 2$, respectively, before being loaded horizontally to destruction. Wall specimen SW33 was subjected twice to a displacement ductility of 1, twice to a displacement ductility of 1.5 and once to a displacement ductility of 2.6 in the positive load direction and 1 in the negative load direction. The common feature of all these cycles was that, for the specimens subjected to a given displacement ductility ratio, the load corresponding to the maximum displacement of the load cycle decreased with the number of the cycles. This decrease became more pronounced as the ductility ratio of the load cycle increased. This is because load cycles to displacements corresponding to higher ductility ratio cause more extensive cracking of the wall. This is reflected in the shapes of the horizontal load - top horizontal displacement hysteresis loops of specimens SW31 and SW32, as shown in Figures 8.5 and 8.6 respectively. Furthermore, the above decrease in the load corresponding to the maximum displacement of the cycle does not vary linearly with the number of the cycles. As the values shown in Table 8.5 indicate usually most of the reduction took place during the first cycle. Subsequent cycles caused further reduction, but only for a few cycles. Table 8.5 also includes the analytical predictions of the semi-empirical

expression proposed by the author and colleagues for wall units subjected to post-yield excitation. It appears that the expression predicts realistically both the values and the trend of the wall post-yield response with the number of cycles, to a given maximum displacement. The mean value of the ratio of experimentally recorded values to the analytically predicted ones is 0.994, with a standard deviation within the population of 0.017.

8.5.3. STIFFNESS CHARACTERISTICS

The values of wall secant stiffness for various loading levels, summarized in Table 8.3, and the variation of the wall secant stiffness with horizontal load, illustrated in Figure 8.8, indicate that wall stiffness characteristics can be considered independent of the severity of the cyclic loading regime. The slightly lower values exhibited by wall specimen SW33, cannot be attributed to the cyclic loading regime, since the wall specimen exhibited lower secant stiffness values even in its uncracked state. It is interesting to note that the wall secant stiffness had been reduced to half its value corresponding to first visible cracking when first yielding of tensile reinforcement occurred, while at the ultimate level the wall stiffness was only 16% of its value prior to cracking.

During the first horizontal load increments, stiffness values show significant variability and are unlikely to reflect wall response since they are highly affected by the sensitivity of the instruments. As the horizontal load exceeded 5 KN the secant stiffness value of all specimens was around 45 KN/mm. However, this value dropped to about 30 KN/mm before the appearance of the first visible wall crack. The non-visible microcracking process of concrete must be responsible for the above reduction. Stiffness decreased further when significant flexural cracking was initiated, and reached a value of about 15 KN/mm when most of the flexural cracks developed (see Figure 8.8). When significant inclined cracking and yielding of tensile reinforcement occurred, the reduction accelerated and eventually the stiffness attained a value of about 5 KN/mm at the ultimate limit state.

The information provided in the Table 8.6 shows that, for a given number of cycles, increasing the maximum displacement of the loading cycle increases stiffness deterioration. Wall specimen SW31, subjected to four cycles at a ductility of one, showed a 7% percent decay of its secant stiffness, while wall specimen SW32, subjected to four cycles at a ductility ratio of two, lost almost 8.2% of its secant stiffness. Furthermore, after a number of cycles, the decrease in secant stiffness is smaller than the decrease during the first couple of cycles.

The experimental secant stiffness values of the uncracked wall phase are compared with the theoretically predicted stiffness values in Appendix A, where it is shown that the experimental stiffness values recorded prior to the initiation of cracking, and considered representative of the wall uncracked stiffness, are about 55% of the analytically predicted stiffness values. This indicates that values of wall secant stiffness provided by structural analysis and recommended by most of the Code provisions overestimate the stiffness characteristics of the wall at the uncracked phase. The main reasons for the observed overestimation should be attributed to the simplified assumptions of the analyses and mainly to the fact that (a) concrete is not a homogeneous material and (b) laboratory or field ambient conditions can result in microcracks due to shrinkage, even before any load is applied to the walls.

8.5.4. ENERGY DISSIPATION AND DAMPING MEASUREMENTS

Dissipated energy is represented by the area enclosed by the complete horizontal load – top horizontal displacement hysteresis loop for a given cycle. As Figures 8.5, 8.6 and 8.7 illustrate, the energy dissipated during the first cycle, to a given ductility ratio, was significantly larger than the amount of energy dissipated during the following cycles at the same ductility ratio. After the specimens had been cycled once to a given ductility ratio, a "pinching" effect could be noted in the hysteresis loop of the second and the following cycles. As Table 8.7 indicates, the energy dissipated during the second cycle of all wall specimens was 55% of the energy dissipated during the first cycle, since most of the wall cracking to a given imposed displacement appears to occur during the first cycle. After four load cycles to a given displacement the energy dissipated by wall specimens SW31 and SW32 dropped to 40% of the initial dissipated energy. Furthermore, the ratio between damage and damping energy (as these terms are defined in Section 8.3) drops from 0.4 to very small values as the number of cycles increases.

Experimental data included in Table 8.7, also point out that as the ductility ratio increases, the amount of energy dissipation is enhanced considerably. An increase in the ductility ratio by a factor of two, results in an enhancement of the amount of dissipated energy by a factor of three. This implies that the main source of the energy dissipation capacity of reinforced concrete structural walls is the yielding of the tensile reinforcement and not the concrete cracking of the wall elements. It is interesting to note that as most of web tensile reinforcement reached its yield strength, significantly larger amounts of energy were dissipated during the half cycle of specimen SW33 to a ductility ratio of $\mu = 2.63$. The corresponding horizontal load was 95% of the ultimate horizontal load capacity of

the wall.

Damping plays an important role in reducing the vibratory motion caused by seismic loading. Equivalent viscous damping, as defined in Section 8.3, was used to obtain a normalized energy parameter for the wall specimens. As shown in Table 8.8, equivalent viscous damping tended to increase more than linearly with an increase in the ductility ratio. Equivalent viscous damping ratios of 11.8% and 11.5% were recorded at the first loading cycle of specimens SW31 and SW33, respectively, to a ductility ratio of one. A damping ratio of 14% was measured when wall specimen SW32 was subjected to its first cycle to a displacement corresponding to a ductility ratio of two.

Damping ratios dropped with the increase of number of cycles to a given displacement ductility. Table 8.8 presents, in addition to the experimental data, the analytical results of the expression proposed by Lefas et al (1982) to assess the variation of equivalent viscous damping of structural walls with the number of cycles to a given displacement ductility ratio. The comparative study between analytical and experimental values indicates that there is a very good agreement for the damping values of the first cycle at any ductility ratio. The only exception to that is the damping value of specimen SW33 at a ductility ratio of 1.5. In this case, the experimental damping value was smaller than the analytically predicted value, since the first excitation to a ductility ratio of 1.5 was preceded by two displacement cycles to the ductility ratio of one which considerably reduced the damage energy component of the dissipated energy recorded at this stage. When the same specimen was subjected to a ductility ratio of 2.63, close correlation between analytical and experimental damping values was observed, since at this level the damage energy component was a small fraction of the dissipated energy. Although analytical predictions exhibited the right trend, they were found to overestimate the equivalent viscous damping values obtained experimentally with the increase of the number of cycles to a given ductility ratio.

8.5.5. STRAIN MEASUREMENTS ON LONGITUDINAL REINFORCEMENT

Each of the longitudinal reinforcing bars at the four corners of the wall edges (concealed columns) of specimens SW32 and SW33 were mounted with electrical resistance strain gauges. The gauges were located in the lower region of the wall at about 10 cm from the foundation beam. The yield load was considered to have been reached when the average strain monitored by the two extreme reinforcing bars exceeded +2500 microstrains, in either direction of loading.

Figure 8.9 shows that when specimen SW32 was loaded in the positive direction, the steel bars of the outer tensile edge yielded at a horizontal load corresponding to 58% of the wall capacity (+64.9 KN) while the steel bars of the inner tensile edge yielded at a horizontal load corresponding to 85% of the wall capacity (+94.9 KN). Similar values were monitored when the specimen was loaded in the negative direction. Yielding of outer and inner tensile bars occurred at −66.4 KN and −89.1 KN respectively. Figure 8.10 illustrates the corresponding yield load values of wall specimen SW33. They were +71.5 KN/−63.0 KN and + 86.4 KN/−88.8 KN for the positive/negative loading direction. The average strain values of the outer tensile and compressive steel bars of specimen SW33, recorded prior to failure, were +22,500 and −6,650 microstrains respectively. During testing of specimen SW32 both gauges at the outer and inner tensile wall edges were broken when 95% and 99% of the wall capacity was reached. The maximum compressive strain recorded prior the failure load of specimen SW32 was − 4,700 microstrains.

A closer look into the strain gauge readings of wall specimens SW32 and SW33, depicted in Figures 8.9 and 8.10, reveals the following:

(a) When wall specimens were unloaded − after being subjected to a given ductility ratio in the positive direction − a residual tensile strain was observed in both the outer and inner tensile bars of the wall edge. The value of the residual tensile strain increases with the increase of the displacement ductility ratio. This phenomenon implies that the flexural cracks near the bottom section of the wall tensile column had not closed during unloading. When wall specimens were thereafter loaded in the negative direction, the initially tensile strains of the outer steel bars became compressive when about half of the negative load of the full cycle was reached. The same pattern was followed by the inner initially tensile steel bars only for cycles to a ductility ratio of one. As the wall specimens were subjected to load cycles with maximum displacement ductility ratios larger than 1.5, the strains of the inner tensile bars dropped to very small tensile values, but never attained compressive values. This suggests that when 75% of the ultimate horizontal load is reached, the depth of the neutral axis is smaller than the width of the wall's concealed column.

(b) The strain readings of the outer initially compressive steel bars suggest that, when wall specimen SW33 was subjected to low ductility ratios, strains became compressive when the specimen was reloaded in the positive direction. Wall specimen SW32 was subjected to four load cycles to a ductility ratio of two.

The strain history, recorded by the gauges mounted at the outer initially compressive bars, indicates that strain readings regained their original compressive sense only when the horizontal load applied to the specimen exceeded 90% of the horizontal load carrying capacity of the wall. Strain readings of the inner initially compressive steel bars were always slightly tensile when the specimens were subjected to displacement ductility ratios larger than 1.5. It is interesting to note that the tensile strains recorded by those gauges prior to failure were equal to +800 and +550 for wall specimens SW32 and SW33 respectively, indicating a very small depth of neutral axis at failure load.

(c) It should be noted that the trend of the horizontal load – vertical displacement curves of wall specimens SW32 and SW33, depicted in Figures 8.6(b) and 8.7(b) respectively, are in compliance with the trend followed by the corresponding horizontal load–strain measurements curves for the longitudinal reinforcing bars, since the elongation/shortening of the tensile/compressive edge of the wall is basically due to the elongation/shortening of the tensile/compressive longitudinal bars positioned at the wall edges.

8.5.6. FAILURE CHARACTERISTICS

8.5.6.1 MODE OF FAILURE

The testing programme was planned in such a way so that after a number of displacement controlled cyclic reversals to given ductility ratios, the walls would be monotonically loaded up to failure.

For all specimens the first cracks appeared near to the bottom tensile edge of the wall, when only 15% of the wall capacity was reached. As the horizontal load approached 30% of its maximum value, significant flexural cracking of the wall tensile edge was observed. These cracks were uniformly spaced at about 100 mm and covered the bottom third of the wall. When 55% of the ultimate horizontal load was reached, flexural cracks traversed the middle third of the tensile edge of the specimens, while the first diagonal cracks with an inclination of approximately 45° covered almost half of the wall web (Figure 8.11(a)). The crack pattern up to this stage was similar for all specimens. What happened next was mainly dependent on the cyclic loading regime.

Specimen SW31

Specimen SW31 was unloaded at this stage and horizontally loaded up to the same load level in the opposite direction. As Figure 8.11(a) shows, a fracture process almost symmetrical with respect to the middle vertical wall axis was observed. The deepest inclined cracks of the wall were orthogonally crossing each other. Four load cycles at this particular displacement level did not cause additional visible cracking. Thereafter, when the horizontal load was monotonically increased and reached 85% of the wall capacity, new horizontal cracks were formed at the tensile edge of the wall, while inclined cracking propagated as deep as the compressive edge of the wall. The spacing of the flexural and inclined cracks reduced to 60 and 90 mm respectively.

Just prior to failure the concrete cover of the lower compressive edge of the wall spalled off and near vertical cracks were formed in the compressive zone of the wall between the deepest flexural cracks. This finally led to failure of the compressive zone of the wall.

Specimens SW32 and SW33

Specimens SW32 and SW33 were both subjected to higher displacement ductility ratios than specimen SW31. Therefore, significant inclined cracks commenced from either side of the wall, corresponding to each load reversal and penetrated deeply into the web near the compressive edge. These cracks formed an orthogonally criss-crossed crack pattern which had a higher intensity for specimen SW33, since this wall was subjected to an additional cycle with ductility ratio μ = 2.6 in the positive direction. In contrast with the behaviour of wall specimen SW31, the higher ductility ratios caused additional cracks within wall specimens SW32 (see Figure 8.11(b)) and SW33, during the second and third load cycles to the same maximum ductility ratio. The additional cracks were usually extensions of existing inclined cracks, new vertical cracks in between existing flexural cracks or secondary cracks deviating from primary inclined cracks. This resulted in a denser crack pattern particularly at the bottom half of the wall web.

Despite the above differences in the crack pattern, the specimens exhibited a mode of failure similar to that of wall SW31.

8.5.6.2. FAILURE MECHANISM

The crack width of the flexural cracks nearest to the lower tensile edge of the wall at failure varied between 0.4 and 0.8 mm, with the higher values measured for the wall specimens subjected to a more intense cyclic loading regime. As discussed in detail in Section 7.4.6, bond failure occurring between consecutive flexural cracks at the lower tensile edge of the wall causes stress redistribution at the lower compressive edge of the wall. The lower compressive edge of the wall finally fails when the state of stresses in this region changes from a triaxial compression to a state of stress with at least one of the principal stress components being tensile, the latter resulting in near vertical splitting of the compressive zone between the deepest flexural cracks of the wall (see Figure 8.11 (c)).

8.6. COMPARISON WITH MONOTONIC TEST RESULTS

Monotonic and cyclic loading tests were carried out to investigate the behaviour of reinforced concrete walls with a height to width ratio of two. The results describing the behaviour under cyclic loading were presented and discussed in the previous sections, while Chapter 7 covered the experimental results of the monotonic tests. Despite the differences in the amount of reinforcement of the wall web, indicated in Tables 7.2 and 8.1, it was found that wall specimens exhibited many similarities in strength and deformation characteristics. A detailed comparative study between the wall specimens loaded monotonically to destruction and those subjected to a number of postyield displacement cycles before loaded to failure indicates the following:

(a) The inclusion of less vertical reinforcement in the wall web of specimens tested cyclically should be considered responsible for the 9% lower strength of these walls compared with the wall strength of the monotonically tested counterparts. As will be discussed in detail in the following chapter, a smaller amount of ve :ical web reinforcement resulted in a lower flexural strength of the wall and si e both monotonically and cyclically loaded specimens failed in a ductile flexural manner, it can be concluded that displacement reversals in the inelastic range have not affected the strength characteristics of slender walls.

(b) The overall deformation (i.e. horizontal and vertical displacements) occurring under cyclic loading was slightly higher than that occurring under monotonic loading. This resulted in the higher ductility ratios observed during the cyclic loading tests. Part of the larger deformations should be attributed to the

smaller amount of vertical and horizontal web reinforcement of the cyclically loaded tests. In fact, the displacements at first yielding of the tensile reinforcement of the wall (see Tables 7.3 and 8.3) indicate that the average top horizontal displacement recorded under cyclic loading was 80% of the corresponding value monitored during monotonic testing. It is interesting to note that up to the loading level of first yielding of the tensile reinforcement, the loading history of both series of tests was identical. Comparing the displacement values given in Tables 7.3 and 8.3 indicates that cyclic loading has an insignificant effect on displacements at ultimate load level. Values included in Table 8.3 appear to indicate that loading cycles to a higher ductility ratio may lead to higher deformations.

(c) Based on the items (a) and (b) above, it can be concluded that the horizontal load – horizontal displacement curves of wall specimens subjected to monotonic loading form an envelope to the load–displacement curves of those subjected to cyclic loading.

(d) With regard to the strain exhibited by the longitudinal reinforcement, it was observed that the maximum tensile and compressive strains recorded during cyclic loading tests were similar to the corresponding values measured during monotonic tests. However, the following feature characterizes the outer, originally compressive, bars of the wall: When the wall specimen was subjected to load cycles of high displacement ductility ratio, the strain readings of the outer compressive wall bars regained their compressive sense a few load steps prior to the ultimate wall capacity. This implies that when a wall specimen is subjected to a number of cycles of load or displacement close to the ultimate level, the deepest open flexural cracks near the compressive edge of the wall close only under high levels of applied horizontal load.

(e) The only difference in the crack pattern between the slender walls tested under monotonic and cyclic load conditions is that in the case of cyclic loading, cracking of the walls is more extensive. Full cycles of loading to a given ductility result in an almost symmetric orthogonal crack pattern. Despite this, the mode of failure and failure mechanism of wall specimens subjected to monotonic and cyclic loading were found to be identical.

8.7. CONCLUSIONS

The experimental data on strength and deformation obtained from tests on reinforced concrete walls with height to width ratio of two subjected to a number of post-yield deformations lead to the following main conclusions:

(a) The measurements of out of plane displacement and vertical displacement of the foundation beam suggest that plane stress conditions and fixity of the wall base were satisfied throughout the testing procedure.

(b) The strength and deformational response of the walls were found to be independent of the cyclic loading regime and the concrete strength. Horizontal load - horizontal displacement curves were non-linear. When 95% of the wall capacity was reached the above curves were flattened showing a distinct flexural behaviour prior to failure.

(c) Residual horizontal and vertical displacements were observed when the specimens were unloaded after being subjected to a given displacement ductility ratio. The above displacements increased with increasing ductility ratio.

(d) When the wall was subjected to load cycles to a given ductility level, a reduction in average secant stiffness and horizontal load corresponding to maximum displacement occurred with increasing number of cycles, the reduction being the largest during the first to the second cycles and becoming smaller in subsequent cycles. This was observed at all ductility levels. A proposed semi-empirical expression appears to realistically predict the decrease of horizontal load corresponding to maximum displacement with the number of cycles at a given ductility ratio.

(e) The energy dissipated during the first load cycle to a given ductility was considerably higher than the amount of energy dissipated during the subsequent load cycles to the same displacement. The amount of energy dissipation was found to increase with the increase of the ductility ratio. Similar trends were exhibited by the normalized energy parameter of equivalent viscous damping. Analytical predictions based on a proposed expression overestimated the experimentally obtained values of equivalent viscous damping.

(f) The maximum values of tensile and compressive strain recorded prior to failure indicate that the slender wall specimens with nominal percentage of horizontal reinforcement subjected to cyclic loading fail in flexure and are characterised

by small depths of neutral axis at failure load. Horizontal load–strain curves follow the same trends as the horizontal load – vertical displacement curves of the wall loading beam.

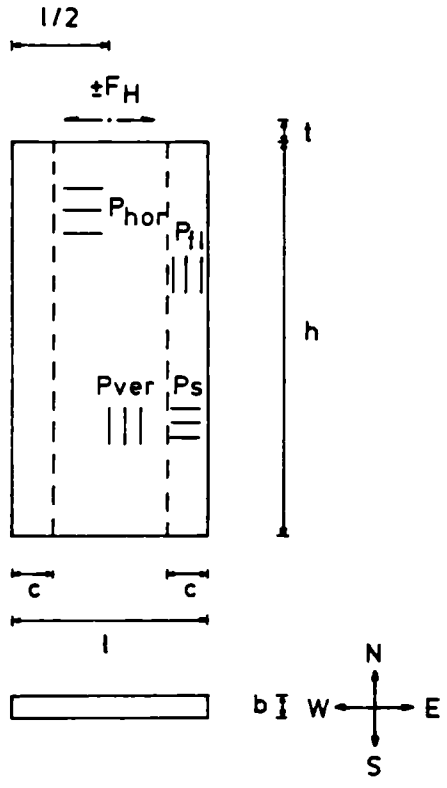
(g) An orthogonally criss–crossing crack pattern was observed when the wall specimens were subjected to load cycles to given post–yield displacements. Load cycles to low ductility ratio resulted in flexural and inclined cracks covering two thirds of the wall height. Cycles to high ductility ratios caused a criss–cross cracking pattern reaching the top third of the wall as well.

(h) Failure of all three specimens occurred when near vertical cracks were formed at the lower compressive zone of the wall between the deepest flexural cracks. Bond failure occurring between the flexural cracks of the lower tensile edge of the wall should have caused a stress redistribution at the lower compressive edge of the wall turning a triaxial compressive state of stress existing there prior to failure to a triaxial state of stress with one tensile component which resulted in the splitting of the compressive zone of the wall.

(i) Despite the fact that the amount of vertical and horizontal reinforcement provided to the web of walls subjected to cyclic loading was smaller than that subjected to monotonic loading, strength and deformation characteristics of both series of tests were similar, with monotonic load–displacement curves forming an envelope to the load–displacement curves of the cyclically loaded counterparts.

SPECIMEN	REINFORCEMENT PERCENTAGE				CYCLIC LOADING REGIME *	ULTIMATE HORIZONTAL LOAD
	P_{hor} (%)	Pver (%)	P_{fl} (%)	Ps (%)		F_H (KN)
SW31	0.35	1.5	3.3	0.9	a	115.8
SW32	0.35	1.5	3.3	0.9	b	111.0
SW33	0.35	1.5	3.3	0.9	c	111.5

* see Figure 8.2



DIMENSIONS

l=650 mm

h=1300 mm

b=65 mm

c=140 mm

t=75 mm

Table 8.1. Experimental data for type II walls subjected to cyclic loading.

SPECIMEN	TIME OF TESTING (days)	CUBE STRENGTH fcu (MPa)			CYLINDER STRENGTH fcyl (MPa)
		7 DAYS	28 DAYS	TESTING DAY	TESTING DAY
SW31 *	55	26.0	32.6	35.2	/
SW32	50	35.4	52.9	53.6	41.6
SW33	66	31.8	46.8	49.2	37.0

(*different mix design)

Table 8.2. Concrete strength characteristics of type II walls subjected to cyclic loading.

SPECIMEN	LOADING LEVEL																DUCTILITY
	INITIATION OF CRACKING				FLEXURAL CRACKING				INCLINED CRACKING & YIELDING OF REINFORCEMENT				ULTIMATE				
	F_H	δ	k	$\gamma * 10^{-2}$	F_H	δ	k	$\gamma * 10^{-2}$	F_H	δ	k	$\gamma * 10^{-2}$	F_H	δ	k	$\gamma * 10^{-2}$	
SW31	20	0.62	32.2	0.048	35	1.66	21.0	0.128	64.9	4.19	15.5	0.322	115.8	22.22	5.21	1.710	5.30
SW32	20	0.69	28.8	0.053	35	1.72	20.3	0.133	64.9*	4.40	14.7	0.339	111.0	24.51	4.53	1.887	5.57
SW33	16.4	0.67	24.4	0.052	31.5	1.88	16.8	0.144	71.5*	5.73	12.5	0.441	111.5	24.97	4.47	1.922	4.36

*ersg readings

F_H in KN

δ in mm

k in KN/mm

$\gamma = \frac{\delta}{h}$ drift index

Table 8.3. Principal results for type II walls at various cyclic loading levels.

SPECIMEN	SHEAR STRESS (MPa)				SHEAR STRESS RATIOS				
	FLEXURAL CRACKING		INCLINED CRACKING & YIELDING OF REINF.	ULTIMATE					
	Vcr	Vsf	Vic=Vy	Vult	$\frac{Vult}{f'c}$	$\frac{Vult}{\sqrt{f'c}}$	$\frac{Vcr}{Vult}$	$\frac{Vsf}{Vult}$	$\frac{Vy}{Vult}$
SW31	0.473	0.828	1.536	2.742	0.091	0.498	0.17	0.30	0.56
SW32	0.473	0.828	1.536	2.626	0.058	0.389	0.18	0.32	0.58
SW33	0.388	0.746	1.692	2.639	0.063	0.408	0.15	0.28	0.64

Table 8.4. Shear stress values for type II walls subjected to cyclic loading.

DUCTILITY RATIO	NUMBER OF CYCLES	$F_{H,n} / F_H$						
		ANALYSIS	EXPERIMENTS					
			* SW31 **		* SW32 **		* SW33 **	
1.0	2	0.968	0.993	0.944			0.963	0.960
	3	0.962	0.964	0.915			0.929	/
	4	0.958	0.934	0.914			/	/
	5	0.955	0.931	/			/	/
1.5	2	0.958					0.968	0.945
	3	0.950					0.939	/
2.0	2	0.949			0.958	0.945		
	3	0.939			0.927	0.928		
	4	0.932			0.916	0.916		
	5	0.927			0.911	/		
2.6	2	0.937					0.952	/

*positive load direction
**negative load direction

MEAN $\frac{EXP}{ANAL}$ =0.994

ST.DEVIATION=0.017

Table 8.5. Experimental and analytical values of wall horizontal load relaxation with increasing number of cycles to a maximum displacement.

SPECIMEN	DUCTILITY RATIO	NUMBER OF CYCLES	SECANT STIFFNESS	
			K(KN/mm)	K_n/K_1
SW31	1	1	14.63	1
		2	14.16	0.968
		3	13.75	0.940
		4	13.61	0.930
SW32	2	1	11.30	1
		2	10.74	0.950
		3	10.49	0.929
		4	10.37	0.918
SW33	1	1	12.93	1
		2	12.40	0.959
	1.5	1	10.98	1
		2	10.51	0.957

Table 8.6. Experimental values of secant stiffness reduction with the number of cycles for various values of the ductility ratio.

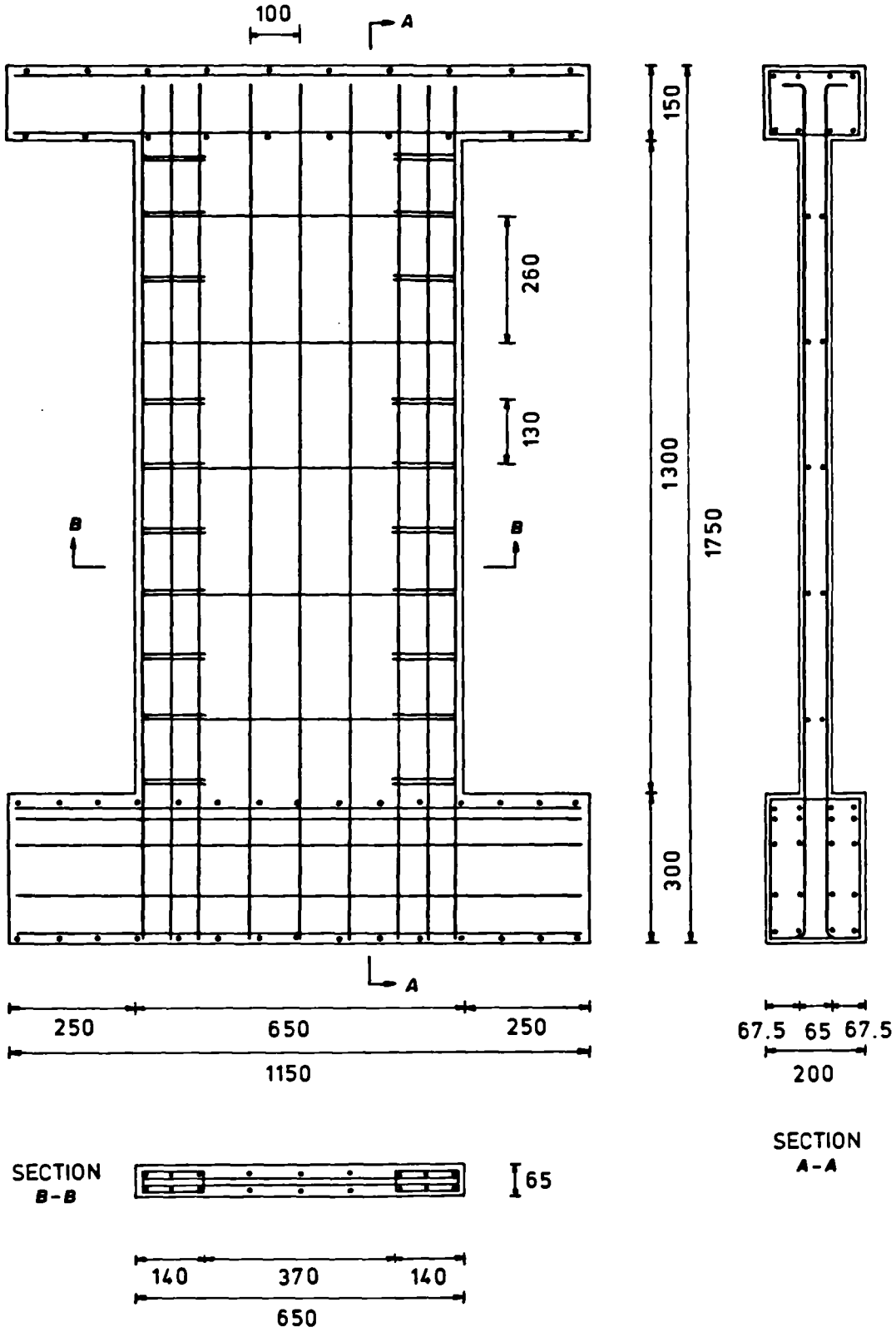
SPECIMEN	DUCTILITY RATIO	ENERGY DISSIPATION PER CYCLE Ei(Joules)			
		n=1	n=2	n=3	n=4
SW31	1	216.5	115	92	85
SW32	2	659.5	368	290.3	253.2
SW33	1	254.8	145.6	/	/
	1.5	477.1	302.9	/	/
	2.63	846*	/	/	/

*per half cycle

Table 8.7. Energy dissipation per cycle for wall specimens subjected to cyclic loading.

DUCTILITY RATIO	NUMBER OF CYCLES	EQUIVALENT VISCOUS DAMPING			
		ANALYSIS	EXPERIMENTS		
			SW31	SW32	SW33
1.0	1	12.0	11.8	/	11.5
	2	8.4	6.2	/	6.6
	3	7.0	5.0	/	/
	4	6.0	4.6	/	/
1.5	1	13.8	/	/	10.2
	2	9.7	/	/	6.5
2.0	1	15.2	/	14.0	/
	2	10.8	/	8.2	/
	3	8.8	/	6.6	/
	4	7.6	/	5.8	/
2.6	1	16.8	/	/	17.0
				MEAN $\frac{EXP}{ANAL}$ =0.812	
				ST.DEVIATION=0.114	

Table 8.8. Analytical and experimental values of equivalent viscous damping for wall specimens subjected to cyclic loading



All dimensions in mm

Fig. 8.1. Geometry and reinforcement details of type II walls subjected to cyclic loading.

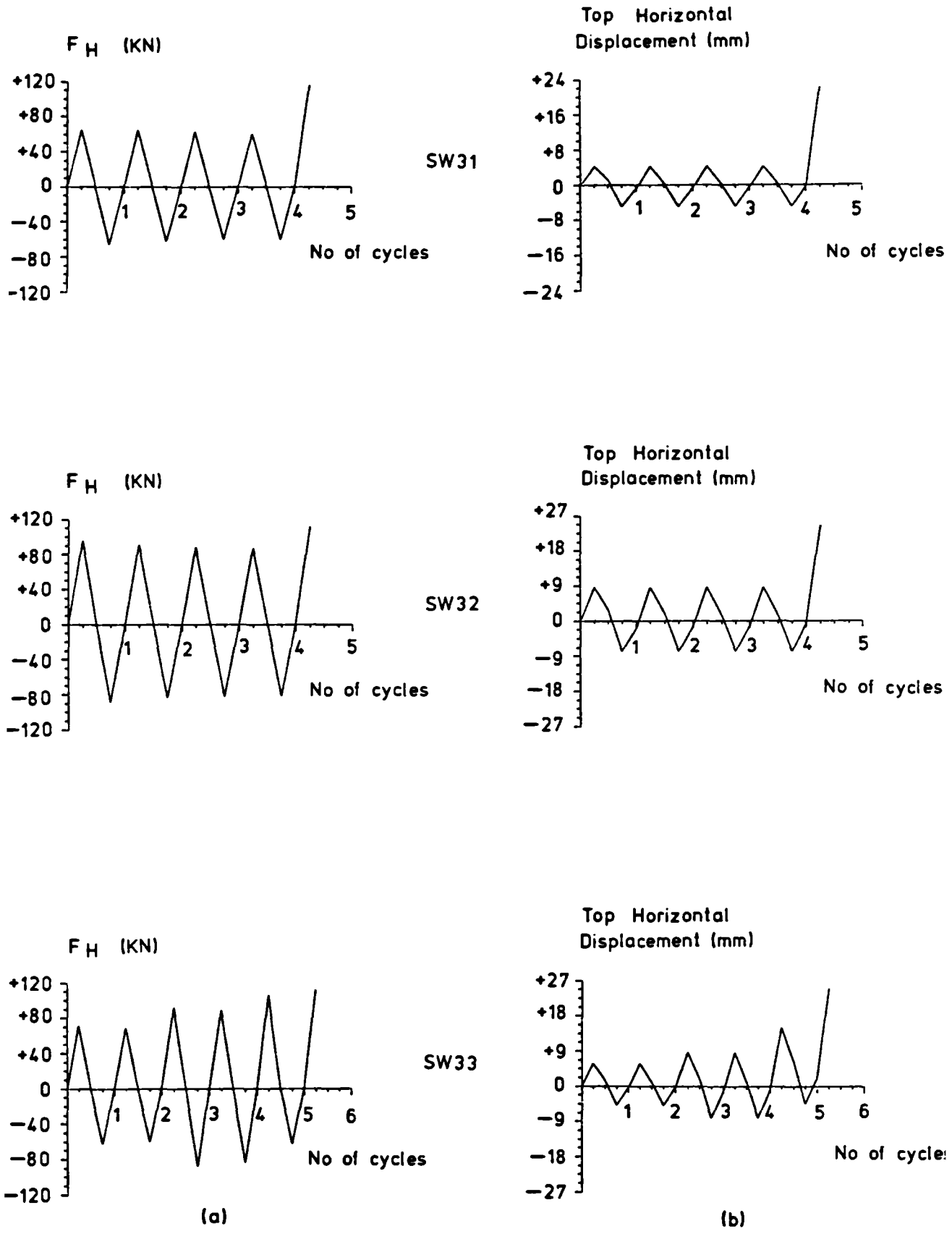


Fig. 8.2. Schematic representation of the loading history adopted for the cyclic tests in terms of (a) horizontal load and (b) top horizontal displacement.

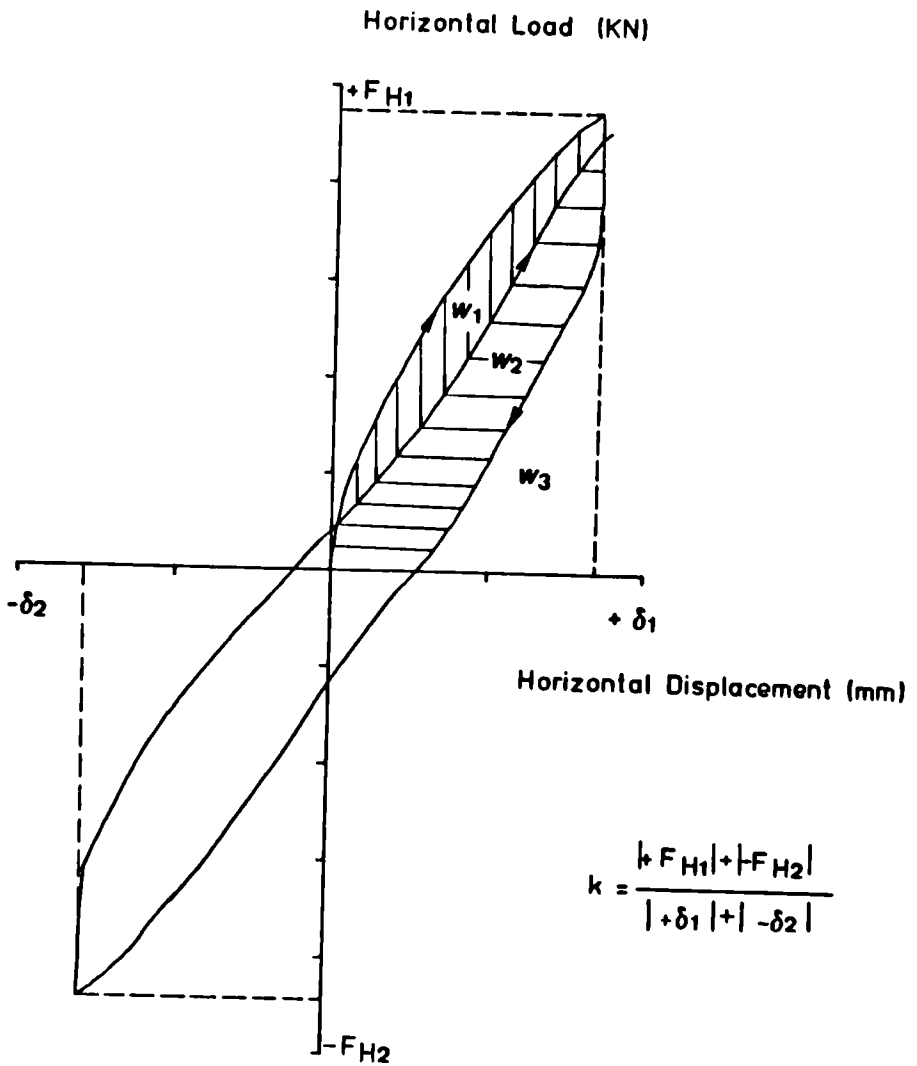


Fig. 8.3. Typical horizontal load-horizontal displacement curve and definition of the energy components and secant stiffness.

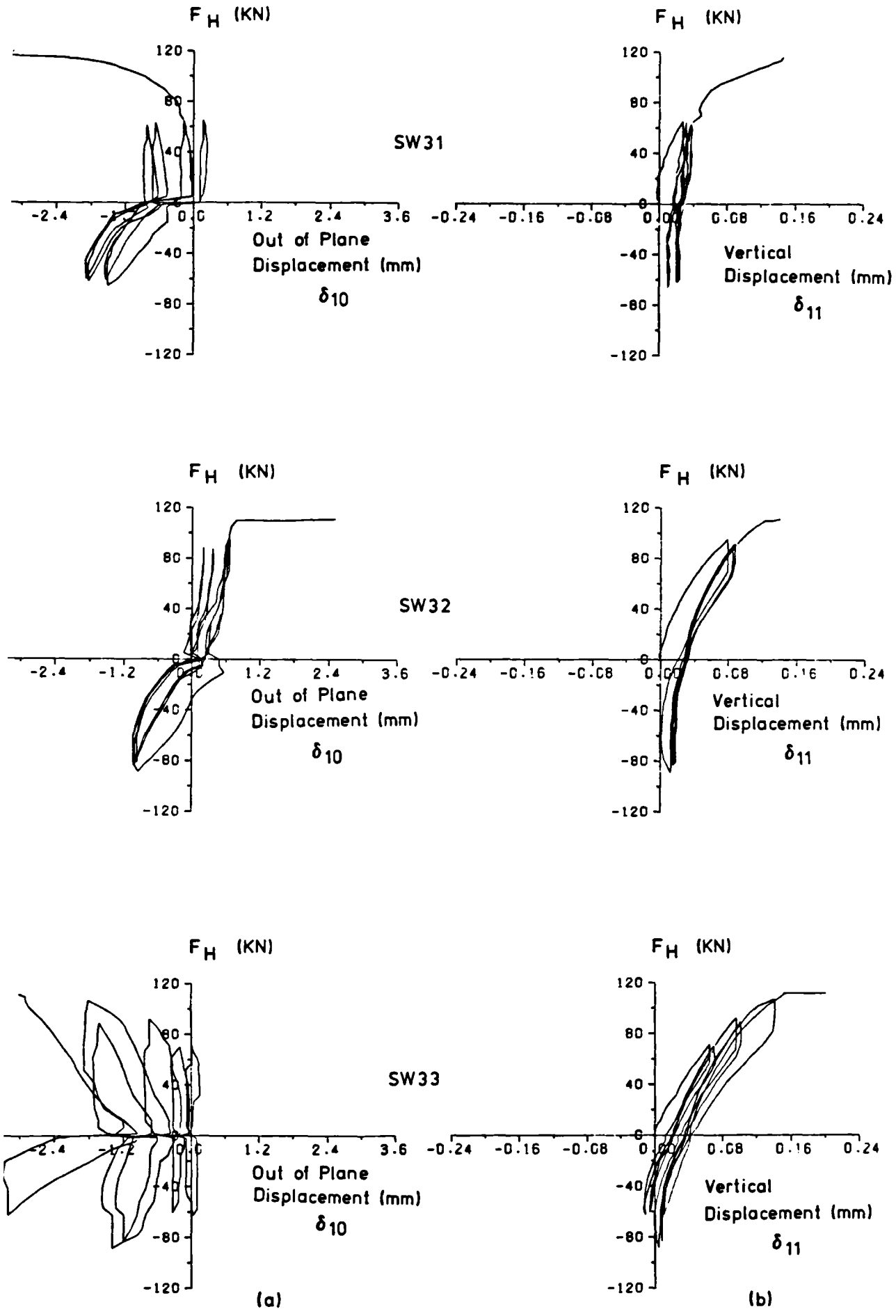


Fig. 8.4. Variation with horizontal load of (a) top out of plane displacement and (b) vertical displacement of the foundation beam.

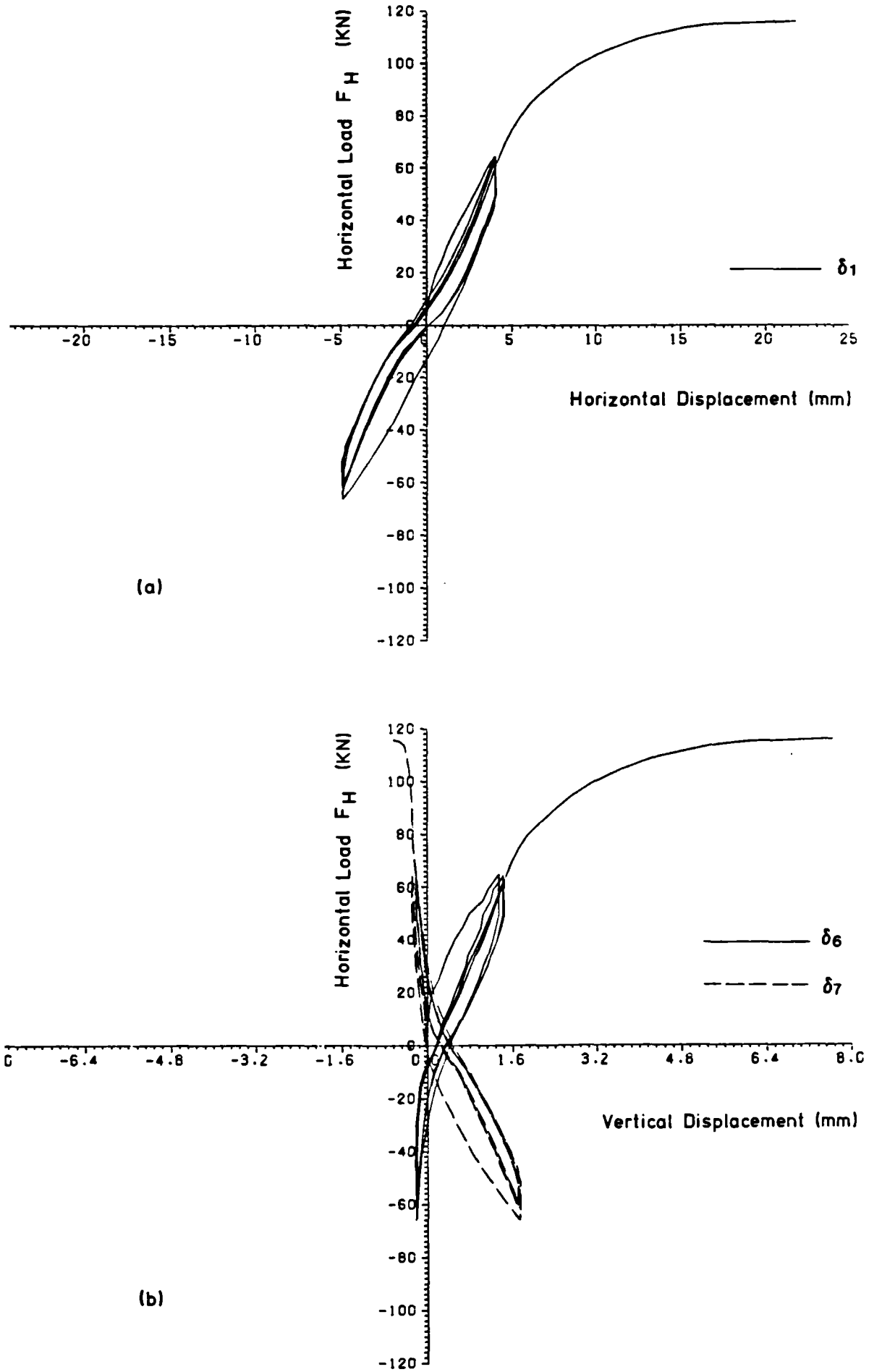
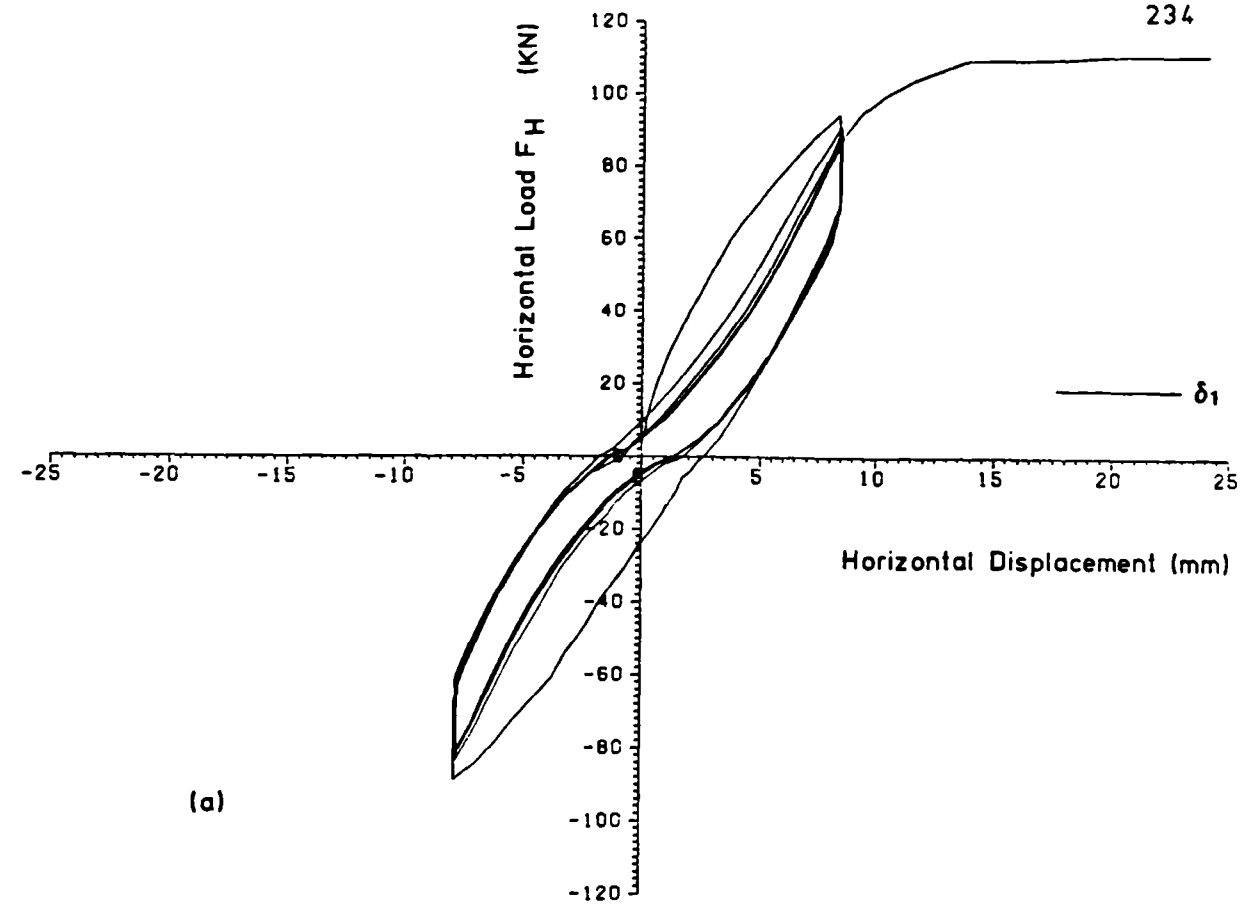


Fig. 8.5. Horizontal load-displacement curves of specimen SW31 constructed by using measurements of (a) top horizontal displacement and (b) vertical displacement of the wall edges.



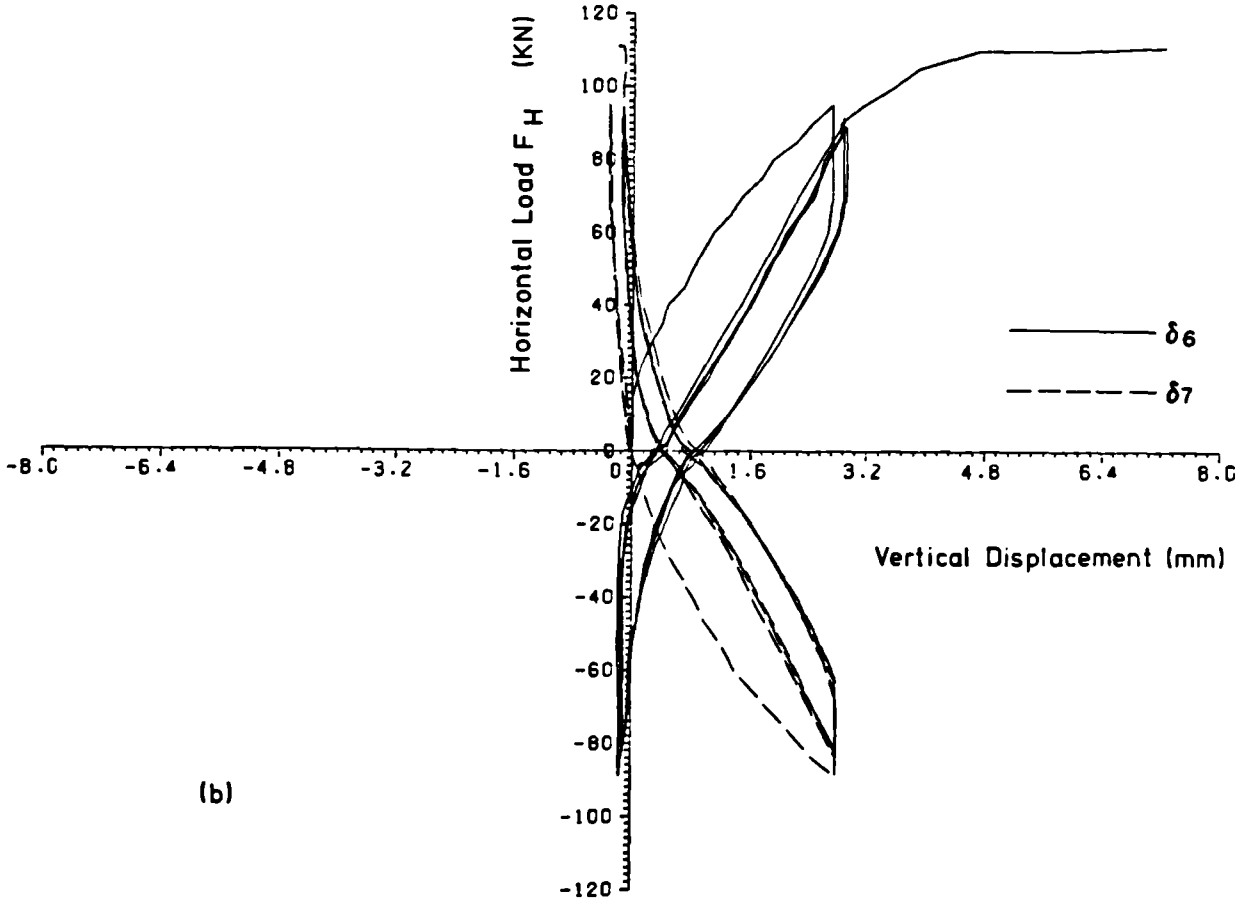
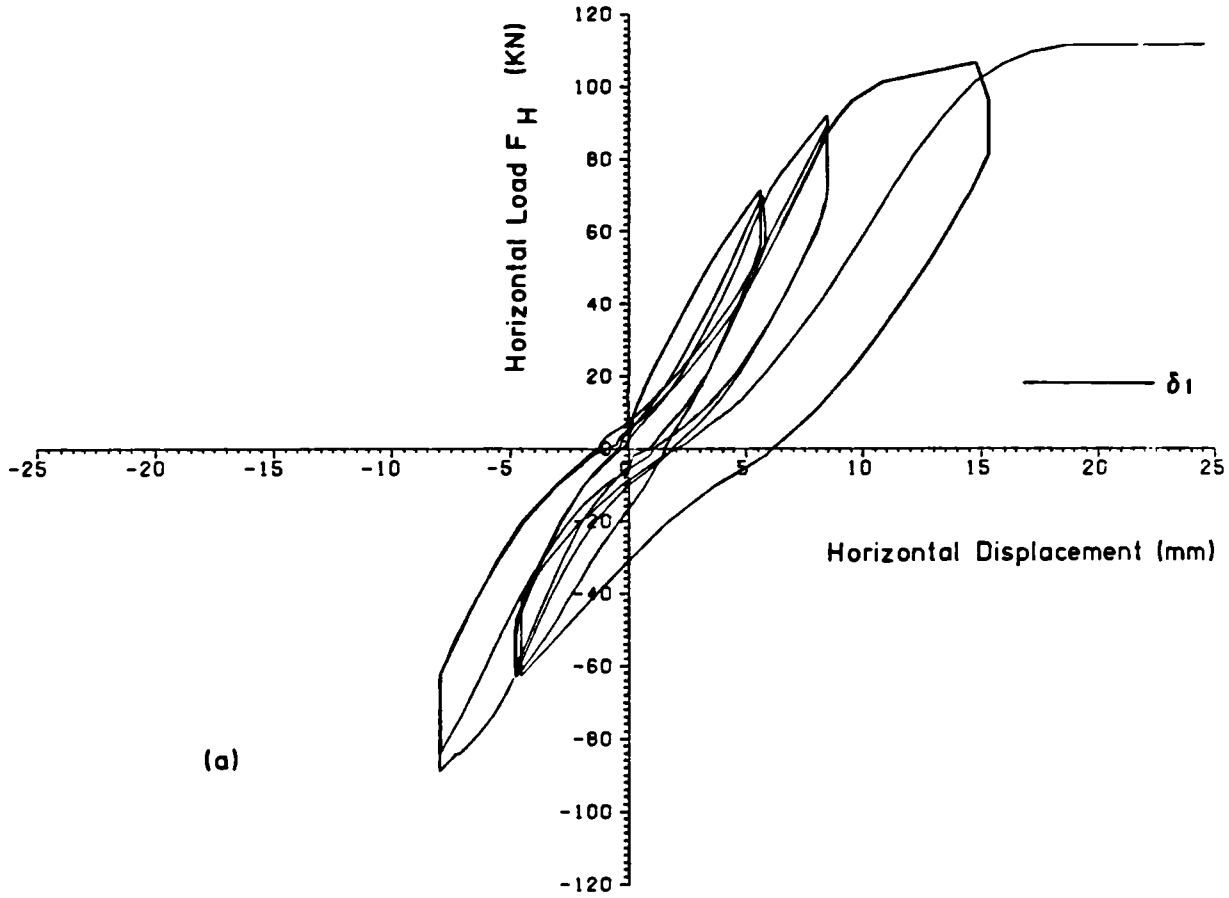


Fig. 8.6. Horizontal load-displacement curves of specimen SW32 constructed by using measurements of (a) top horizontal displacement and (b) vertical displacement of the wall edges.



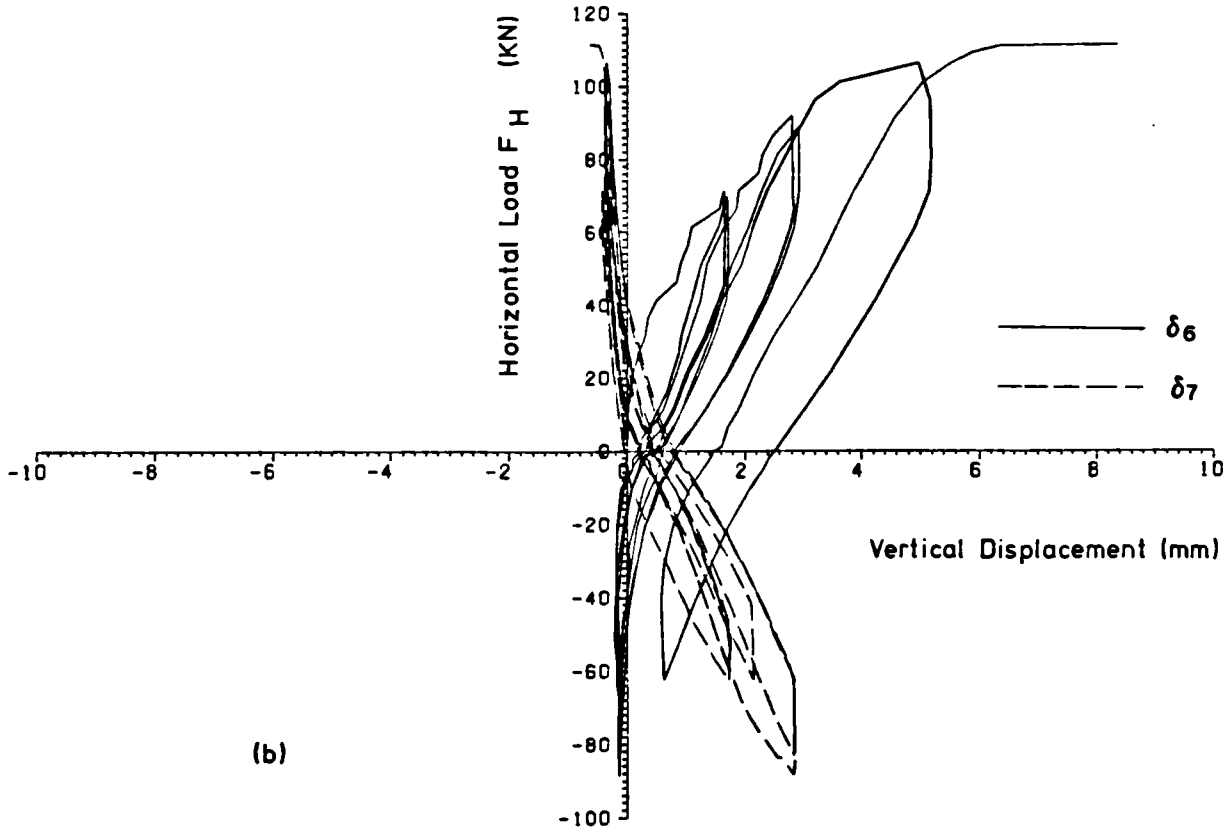


Fig. 8.7. Horizontal load-displacement curves of specimen SW33 constructed by using measurements of (a) top horizontal displacement and (b) vertical displacement of the wall edges.

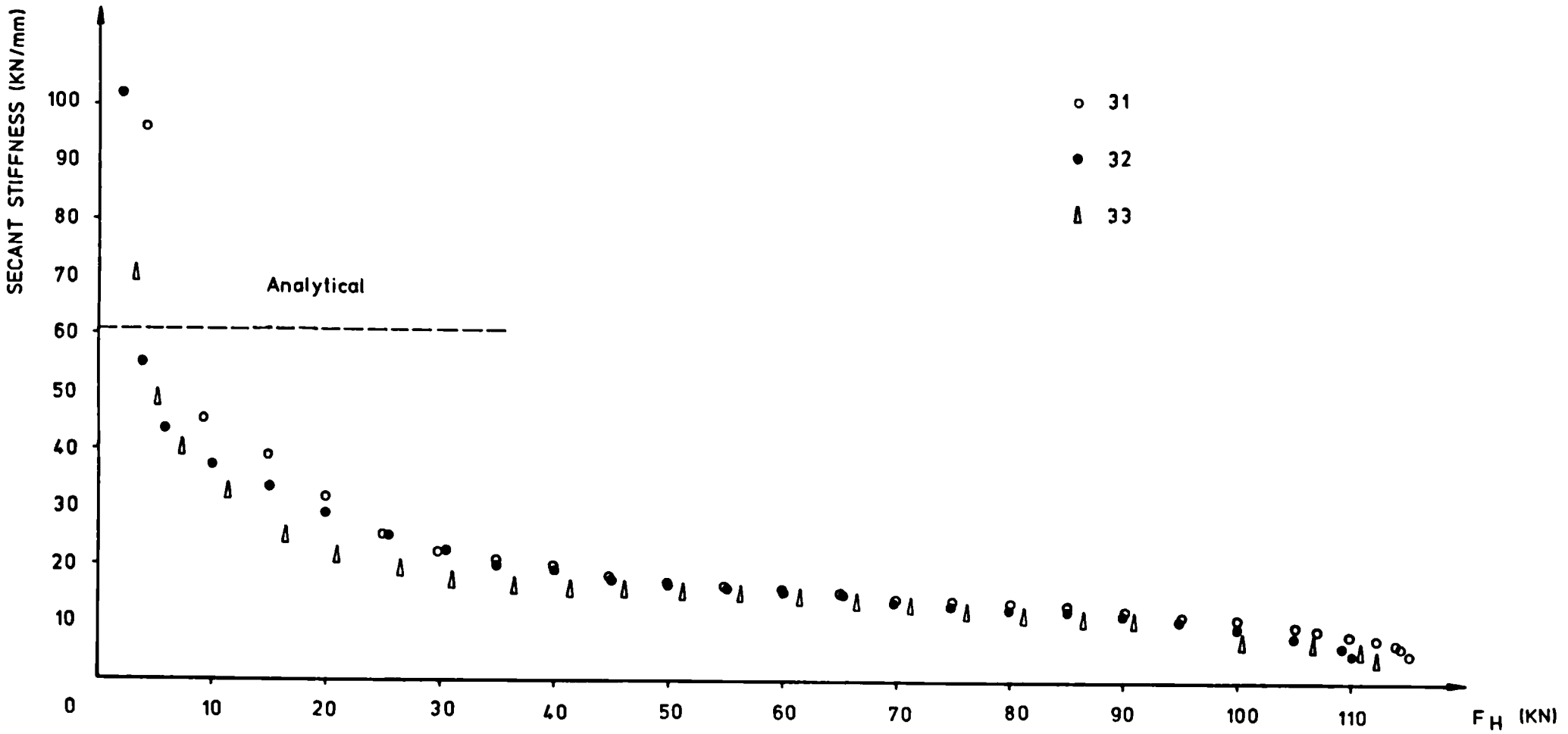


Fig. 8.8. Variation of secant stiffness with increasing horizontal load for type II walls subjected to cyclic loading.

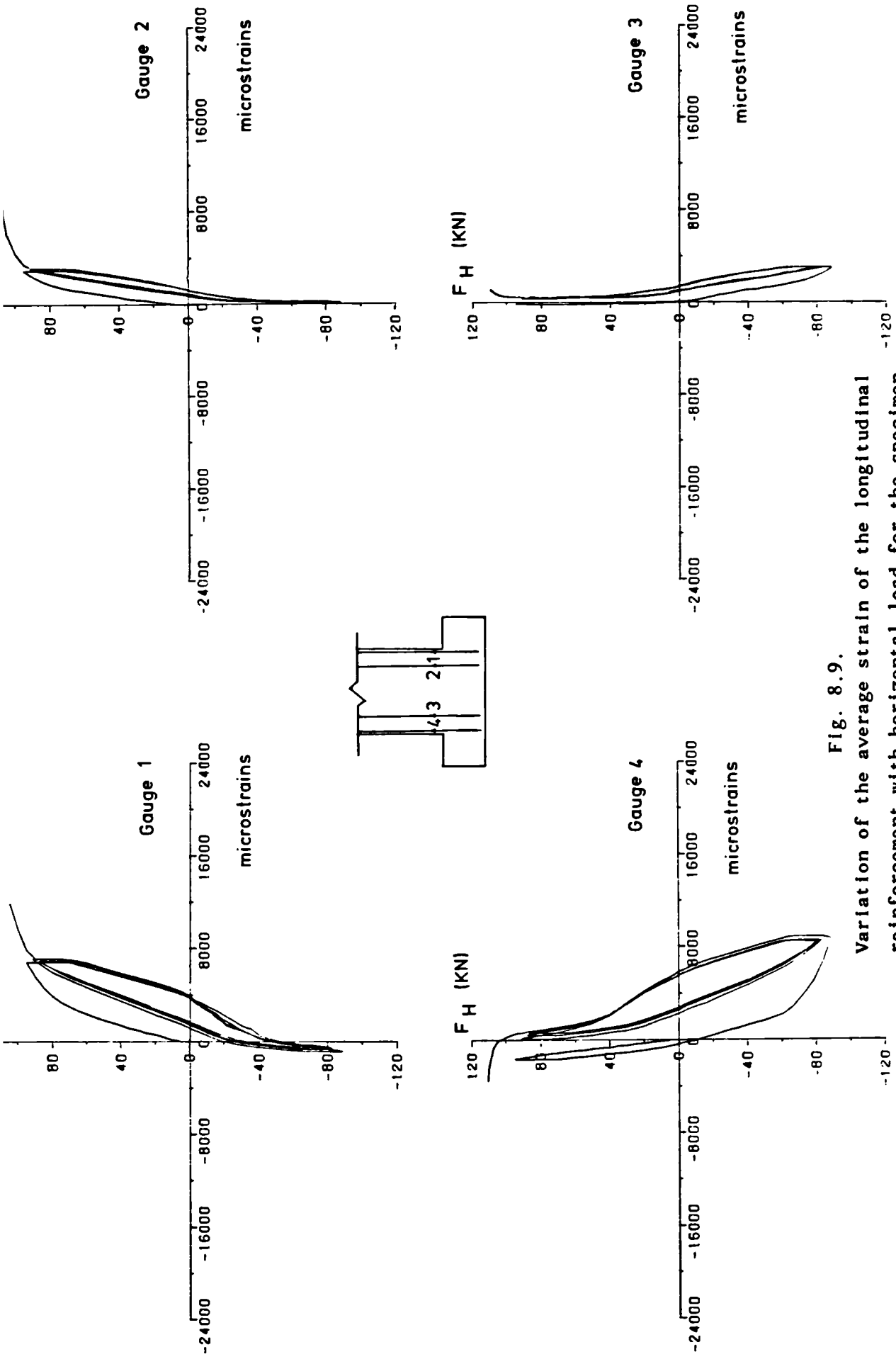


Fig. 8.9.
Variation of the average strain of the longitudinal reinforcement with horizontal load for the specimen

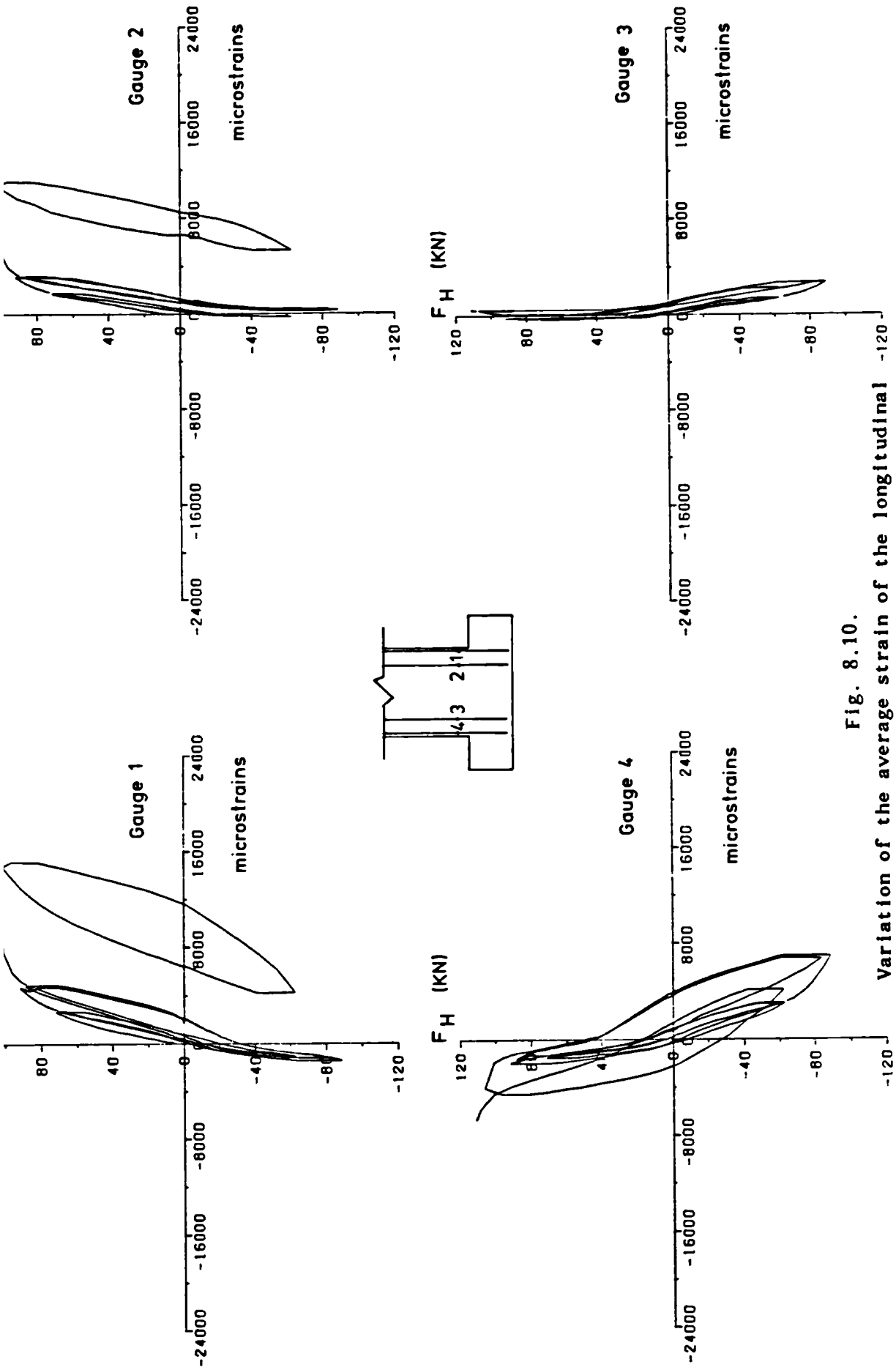


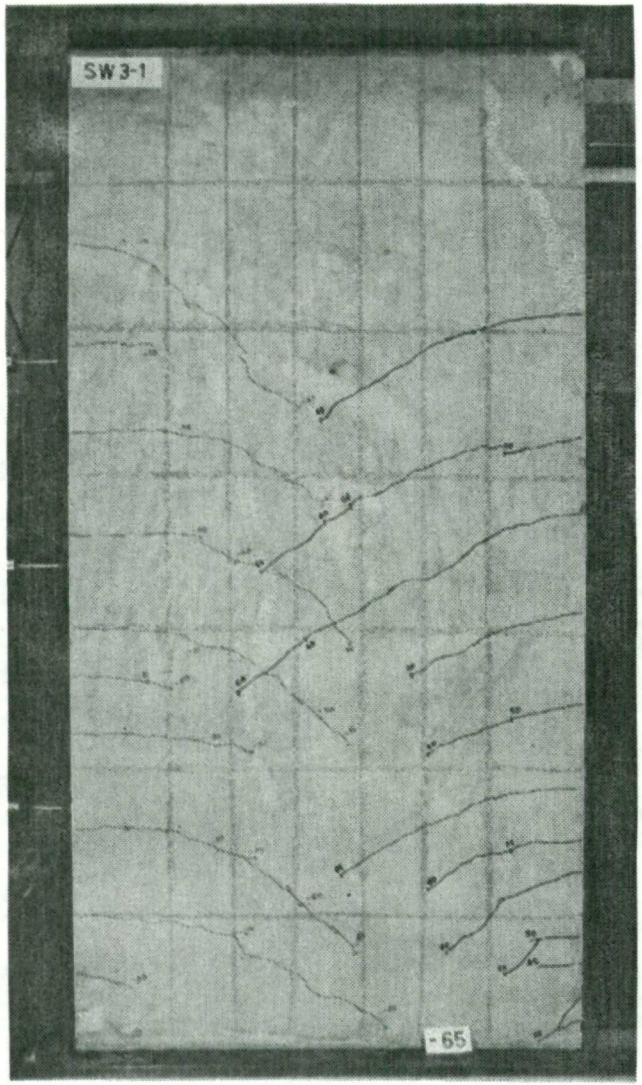
Fig. 8.10. Variation of the average strain of the longitudinal reinforcement with horizontal load for the specimen SW33.

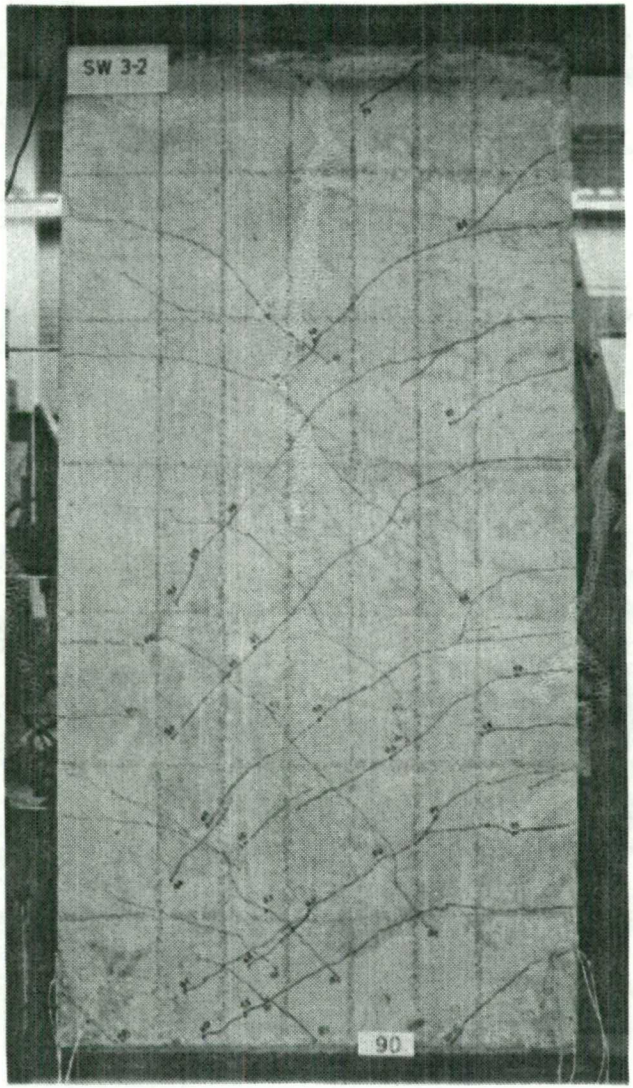
Fig. 8.11. Significant stages of the cracking process for type II walls subjected to cyclic loading.

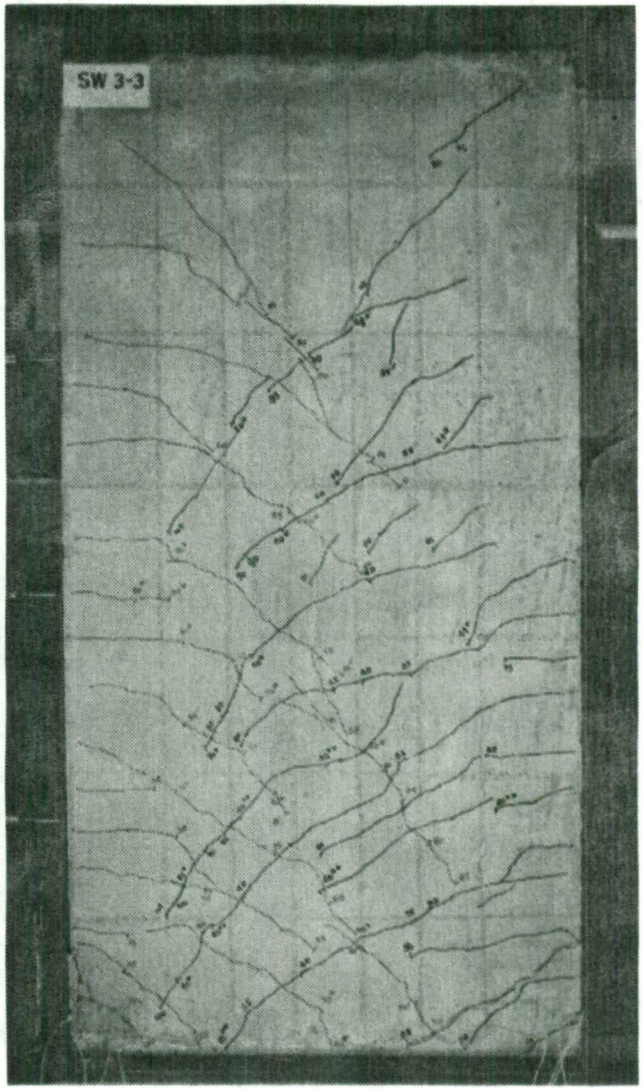
(a) At displacement ductility ratio of 1 (left plate),

(b) at displacement ductility ratio of 2 (middle plate) and

(c) at ultimate horizontal load level (right plate).


SW 3-1
-65


SW 3-2
90


SW 3-3

CHAPTER 9

COMPARISON OF EXPERIMENTAL AND ANALYTICAL WALL RESPONSES

9.1. INTRODUCTION

The present chapter is concerned with a comparative study of the experimental results presented in Chapters 6 and 7 with analytical predictions obtained by using the finite element programme discussed in Chapter 3. This study is focused on the main aspects of wall behaviour, i.e. strength and deformation characteristics, fracture process and mode of failure. The finite element programme was also used to predict the ultimate limit state behaviour of the walls tested under cyclic loading since the experimental results discussed in Chapter 8 indicate that strength, and corresponding deformation characteristics, and mode of failure obtained from the cyclic tests were similar to those obtained from the monotonic tests.

9.2. ANALYTICAL MODELLING

The finite element mesh adopted to represent both types of wall specimens tested is a simplified grid of 7 x 7 concrete elements. Figures 9.1(a) and 9.1(b) illustrate the mesh subdivision adopted in the analysis for walls of type I and II respectively. The equivalent steel area of the vertical reinforcement and confinement of the concealed wall columns was placed at the two extreme columns of concrete elements which extended to a distance of 125 mm from each side of the wall. In order to simplify the finite element discretization of the walls the concrete cover of the extreme tensile and compressive steel bars was ignored. The steel area corresponding to vertical and horizontal web reinforcement was arranged at the boundaries of the concrete elements. The presence of a loading beam is allowed for by simply including the appropriate stiffness of this element at the top layer of reinforcing steel. "Fixing" the element nodes along the lower boundary of the wall provided a realistic description of the boundary conditions imposed on the walls investigated experimentally. The analytical model was loaded with uniformly distributed edge pressure and traction along the upper boundary of the wall. Constant traction simulated the initially applied constant vertical (axial) load, while edge pressure simulated the incrementally applied horizontal load. Fifteen to twenty load steps were applied to each wall specimen, before the horizontal load carrying capacity of the wall was reached. The concrete strength used for the analysis was taken to be equal to 85% of the average cube concrete

strength of the control specimens whereas the strength values used for the reinforcement were those obtained from tensile tests.

The correlation between analytically predicted and experimentally obtained values of wall response was based on the following aspects of structural behaviour:

(a) the maximum horizontal load carrying capacity of the walls (i.e. ultimate horizontal load sustained by the wall);

(b) the change in crack pattern with load increasing to the ultimate level and the mode of failure of the wall;

(c) the trend of the horizontal load–top horizontal displacement curve of the wall.

9.3. WALLS OF TYPE I

Strength and deformation characteristics

The analytical predictions of ultimate horizontal load capacity of all type I walls are grouped and compared with the corresponding experimental data in Table 9.1. As the values in the above table indicate, the analytical model has yielded realistic predictions of the ultimate horizontal load of the walls. Furthermore, it appears that for wall specimens with high values of cube concrete strength (i.e. specimens SW11, SW12, and SW16), the analysis underestimated the experimental ultimate wall capacity by less than 10%, while for the rest of the specimens, predicted values were 18.5% smaller than experimental. Since any triaxial compressive stress conditions that may develop when the ultimate strength capacity is approached (see causes of wall resistance described in Section 6.4.5) are ignored by the plane stress analysis employed, the level of accuracy of maximum horizontal load provided by the analytical model must be considered satisfactory. It is interesting to note that for the case of walls with weaker concrete the presence of the vertical compression bars and the confinement reinforcement of the wall concealed column, resulted in higher (normalized with respect to cylinder concrete strength (σ_2/f_c' and σ_3/f_c') transverse stresses. As Figure 6.15 indicates, the value of normalized longitudinal stress σ_1/f_c' increases with increasing normalized transverse stresses. Thus the dependence of the wall load–carrying capacity on the triaxial stress conditions at the lower compressive edge of the wall is higher, with lower concrete strength. This may explain the lower values predicted by the plane stress analysis for wall specimens with weaker concrete.

It should be mentioned that for the sake of simplicity and generality no attempt was made to influence the accuracy of the ultimate horizontal load predictions by using a finer finite element mesh or different load step sizes.

Since it is not feasible to predict by plane stress analysis the near plastic deformation of the wall for horizontal loads increasing to a level close to the maximum load-carrying capacity of the wall, the triaxial stress conditions, appear to affect more the deformation rather than the strength characteristics of walls with a height to width ratio of one. Furthermore, the analytically predicted deformation values correspond to the maximum sustained load and not to the analytically predicted failure load which actually lies between the sustained load and the next load stage. Indeed the analytically obtained values of top horizontal displacement prior to the analytical ultimate load stage varied between 3.1 mm and 3.7 mm, while the measured experimental value at the same horizontal load level as the analytical ultimate horizontal load varied between 4.8 mm to 7.6 mm. Despite triaxial conditions-which are mainly responsible for differences between the analytical and experimental wall deformation responses near the ultimate load - there are two more factors which have to be taken into consideration in order to explain the inadequacy of the analytical model to match the displacement profiles obtained from the experiments:

(a) The modulus of elasticity assigned in the analysis for concrete was evaluated from stress-strain relationships on 100 mm x 250 mm cylinders cured in water. The ambient laboratory curing conditions of the wall specimens and the corresponding controls resulted in microcracks due to shrinkage within the concrete even before any loading and certainly reduced the modulus of elasticity of concrete. It should be also noted that the analysis ignores the heterogeneous nature of concrete. Furthermore, the analysis adopts higher values for modulus of elasticity of the steel bars (see Figure 3.2) compared with the corresponding measured value of the reinforcing bars incorporated in the wall specimens (see Table 5.1). The combination of the previous features resulted in the stiffer wall response predicted by the analysis for loading stages up to the initiation of inclined cracking and yielding of the tensile reinforcement of the wall specimens.

(b) The differences between analytical and experimental values of displacement beyond yielding of the tensile reinforcement are mainly due to the "long term" (creep) displacements recorded per load step during the testing procedure. As the horizontal load was maintained constant for a time at each increment, long enough to allow crack detection and marking, the displacement values

recorded at the start and the end of the above time span differed. These differences further increased when the tensile reinforcement of the concealed column reached the yield strength. For walls with height to width ratio of one, these differences were almost 30% of the recorded horizontal displacement values at the ultimate load level. In the analytical system, time dependent effects are ignored and thus the displacement values per load step represent "short term" response.

Figure 9.2 shows the horizontal load–top horizontal displacement curves of specimens SW15 and SW16 which are representative of walls with different concrete strengths. The figures include the analytically predicted load–displacement curve together with the corresponding experimental curves with and without the contribution of time dependent effects. The load–displacement curves included in the figure show that when time effects are excluded from the experimental displacement values, the analysis predicted realistically the experimental load–displacement profile. Nevertheless, the analytical curve shows a stiffer response during the first load steps. However such small differences may be attributed, as discussed in item (a) of the present section, to the higher values of the moduli of elasticity adopted in the analysis.

Crack Patterns and Modes of Failure

The experimentally obtained and analytically predicted crack patterns of wall specimen SW11 are compared in Figure 9.3. The distribution of cracking within the wall web and concealed columns is presented for horizontal load levels corresponding to :

(a) initiation of flexural cracking
(b) initiation of inclined cracking
(c) yielding of tensile reinforcement
(d) ultimate sta .

The horizontal load s ep adopted for the analysis of the particular case was 13.5 KN, while the displacement magnification factor of the analytical representations of the deformed shape of the wall was 20.

Figure 9.3(a) shows the typical flexural cracking of type I walls at load step 3 (40.5 KN). Inclined cracks were formed at a higher horizontal load level (load step 6, 81.0 KN) and are shown in Figure 9.3(b). For both load steps close agreement is observed between the analytical plots and the corresponding

experimental crack patterns. Load step 13 (175.5 KN) is associated with the first yielding of the tensile reinforcement of the wall (see Figure 9.3(c)). The obvious feature of the analytical plot and the corresponding experimental crack pattern at this loading level is that most of the diagonal cracking of the wall has been formed. However, analytical cracking covers a more extensive area of the wall, since

(a) during testing microcracking of concrete is difficult to detect by the unaided eye;

(b) the analysis uses the smeared crack approach and thus spreads the effect of cracking over a larger region than that observed experimentally;

(c) the analysis assumes a uniform distribution of horizontal loading at the top of the wall. In fact, after significant inclined cracking, the experimentally applied horizontal load is distributed non-uniformly along the top of the wall.

Figure 9.3(d) shows the typical close correlation between analytical and experimental crack patterns at the ultimate horizontal load level (load step 18, 243 KN). It is interesting to note the near vertical cracking of the lower compressive edge of the wall nearest to the deepest inclined crack prior to incipient failure. Similar agreement between analytical and experimental crack patterns was observed for all the wall specimens tested.

Figures 9.4 and 9.5 present the analytical deformed shape plots of wall specimens SW15 (wall subjected to low axial load) and SW16 (wall subjected to high axial load), respectively, one load step prior to the failure load and at the ultimate horizontal load step. The horizontal load step of the analytical runs was 16 KN, while the displacement magnification factor of the plots was 20. The following features can be observed in these figures:

(a) The presence of high values of axial loading resulted in larger depths of neutral axis prior to the ultimate horizontal load step. The above characteristic is in compliance with the corresponding experimental observations described in detail in Section 6.4.4.

(b) The macrocracking pattern predicted for both walls under the maximum sustained horizontal load indicates that walls failed when they could not sustain the near vertical extension of diagonal cracking into the compressive zone towards the wall support. In both cases a number of new almost vertical

cracks (indicated in figure by double parallel lines) was formed at the lower compressive edge of the wall at the last analytical load step. Such cracking eventually transformed the adjacent wholly compressive state of stress into a state of stress with at least one stress component being tensile.

(c) It is interesting to note that the higher the axial load the larger the area of concrete that fails in compression when the horizontal load leading to failure is reached. A similar behaviour can be observed from the photographs of typical experimental modes of failure of type I walls, tested under various vertical load conditions, included in Figure 6.10.

9.4. WALLS OF TYPE II

Strength and Deformation Characteristics

Table 9.2 lists and compares analytical predictions and experimental values of ultimate horizontal load of all type II walls tested. As the relevant values indicate there is a close agreement between numerical and experimental wall capacities for both monotonic and cyclic loading tests. For only two cases, an underestimation of wall capacity greater than 10% was observed. In wall specimen SW23 high levels of axial load obviously resulted in extremely intense triaxial conditions in the region of the wall above the neutral axis and therefore the plane stress conditions employed in the analysis could only yield a lower bound solution for the wall capacity. The same amount of confining reinforcement results in higher normalized (with respect to concrete strength, f'_c) values of transverse compressive stresses within the lower compressive zone of the wall for lower values of concrete strength. Such a state of stress enhances the vertical load carrying capacity of the compressive zone. Since only plane stress conditions were considered in the analysis, this reasoning appears to explain the lower level of ultimate horizontal load predicted analytically for wall specimen SW26.

Figure 9.6 illustrates the predicted and experimental horizontal load–top horizontal displacement curve of wall specimen SW21. The figure also includes the experimental load–displacement curve with "long term" deformations ("creep") removed. During testing of type II walls the cumulative second order deformation at the ultimate horizontal load level reached 35% of the top horizontal displacement for specimens not subjected to axial load, while the value decreased to 25% for specimens subjected to either low or high levels of axial load. As Figure 9.6 shows, the experimental load–displacement curve, with "long term" deformation

effects removed, is similar to the analytically predicted curve. Reasons for the slightly stiffer analytical load–displacement curve during the early load steps are discussed in detail in Section 9.3. A similar close agreement between analysis and experiment characterizes the load–displacement curves of all type II walls.

Crack Patterns and Modes of Failure

Features of the analytical cracking process of wall specimen SW22 are illustrated in Figure 9.7. The figure also includes the corresponding experimentally obtained crack patterns. Each horizontal load increment of the analytical run corresponds to 9.75 KN, while the displacement magnification factor of the deformed shape of the wall is 20.

At load step 6 (58.5 KN) significant flexural cracking initiated (indicated in the figure by double parallel lines), while some early flexural cracks (indicated by single lines) had already been formed during the previous load steps. The appearance of inclined cracks was delayed till load step 11 (107.25 KN). Up until the above loading level, flexural cracks had been extended towards the middle of wall web with the deepest ones covering the bottom third of the wall. When load step 14 (136.5 KN) was reached most of the inclined cracks had diagonally crossed the middle third of the wall web towards the compressive zone of the wall. At the same time, the criterion for tensile cracking of concrete was satisfied in a number of Gauss points at the top third of the wall web. The above analytically predicted crack patterns are in compliance with the detailed description of experimental fracture process of specimen SW22 given in Section 7.4.5.2 and depicted in Figure 9.7. Similar close agreement between analysis and experiment was observed in all type II wall specimens tested under monotonic loading.

The experimentally obtained crack patterns of type II walls subjected to full cycles of a given maximum displacement was characterised by a symmetrical layout of cracks with respect to the vertical central axis of the wall (see Section 8.5.6). Therefore, the analytical predictions of wall crack pattern can be readily compared with the experimental wall crack formation during either the half cycle to a positive or a negative level of displacement ductility ratio. Figure 9.8 shows the deformed shape plots of specimen SW32 at a load level corresponding to ductility ratio $\mu = 1$ (load step 8, 62.4 KN) and at a load level corresponding to ductility ratio $\mu = 2$ (load step 11, 85.8 KN). It is obvious that the above crack patterns correlate closely with the relevant experimental crack pattern, included in Figures 8.11(a) and 8.11(b), for both ductility ratios, characterised essentially by the same uniform pattern of flexural and inclined cracks.

Figures 9.9 (a), (b) and (c) present typical analytical modes of failure of type II walls subjected to normalized axial loads of 0, 0.1 and 0.2 respectively. In all three sub-figures, the presence of almost vertical cracks (developed for the first time at the ultimate load step) in the lower compressive zone of the wall between the deepest flexural cracks, can be easily recognised. Since increased levels of axial load result in larger depths of neutral axis prior to failure, it is interesting to note that the area of near vertical splitting increased with the increase of axial load applied to the walls. The failure modes, shown in Figure 9.9, are in close agreement with the corresponding experimental modes of failure depicted in Figure 7.11. They illustrate the fact that analysis can realistically predict fundamental characteristics of experimentally observed wall behaviour at the ultimate limit state. An indication of the likely failure mode of walls subjected to a number of full displacement cycles before being loaded monotonically to failure, can be obtained by analysing a wall with given material and geometric characteristics subjected to monotonic loading. The analysis of type II walls subjected to cyclic loading indicated similar modes of failure to that shown in Figure 9.9(a). The full description of experimentally obtained failure modes given in Section 8.5.6 also applies to the analytically predicted failure modes.

9.5. CONCLUSIONS

The main conclusions of the comparative study of the analytical and experimental wall responses may be summarized as follows:

(a) The experimental response of both types of wall under monotonic loading was successfully simulated using the non-linear finite element analysis. The programme proved to be a reliable tool for analysing the strength, deformational properties and cracking processes of structural walls with rectangular cross-section.

(b) The typical accuracy of the analytical predictions in all aspects of behaviour was 5 to 10%, due to the fact that any triaxial conditions that may develop near the ultimate state were ignored by the plane stress analysis employed.

(c) Attention should be also drawn to the fact that the analysis also predicts accurately the experimental mode of failure which is initiated by the appearance of near-vertical tensile cracks at the lower compressive edge of the wall.

SPECIMEN	fcu (MPa)	ULTIMATE HORIZONTAL LOAD (KN)		AUL/EUL
		EXPERIMENT (EUL)	ANALYSIS (AUL)	
SW11	52.3	260	243	0.94
SW12	53.6	340	304	0.89
SW13	40.6	330	272	0.82
SW14	42.1	265	216	0.82
SW15	43.3	320	257	0.80
SW16	51.7	355	320	0.90

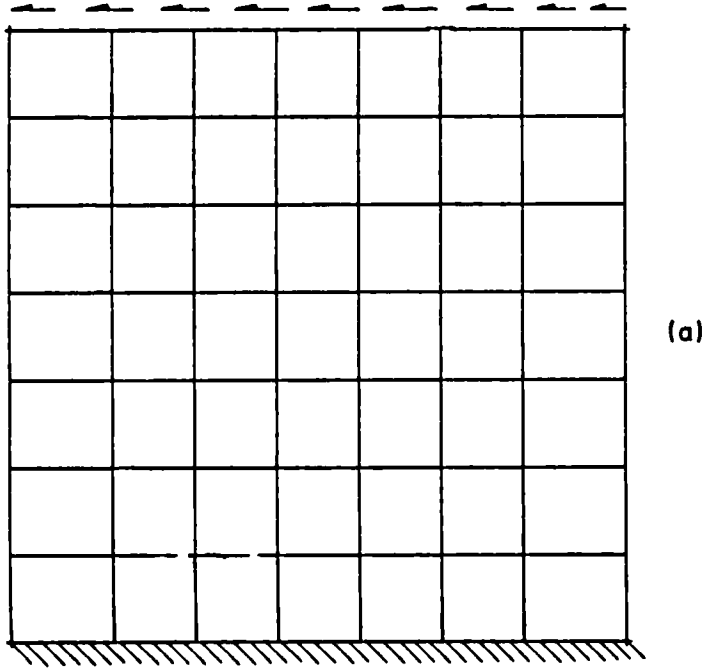
Table 9.1. Analytical predictions and experimental values of ultimate horizontal load for type I walls.

SPECIMEN	fcu (MPa)	ULTIMATE HORIZONTAL LOAD (KN)		AUL/EUL
		EXPERIMENT (EUL)	ANALYSIS (AUL)	
SW21	42.8	127	124.8	0.98
SW22	50.6	150	146.3	0.98
SW23	47.8	180	146.3	0.81
SW24	48.3	120	127.9	1.07
SW25**	45.0	150	146.3	/
SW26	30.1	123	96.0	0.78
SW31*	35.2	115.8	109.2	0.94
SW32*	53.6	111.0	124.8	1.12
SW33*	49.2	111.5	117.0	1.05

*cyclic loading tests

**premature failure

Table 9.2. Analytical predictions and experimental values of ultimate horizontal load for type II walls.



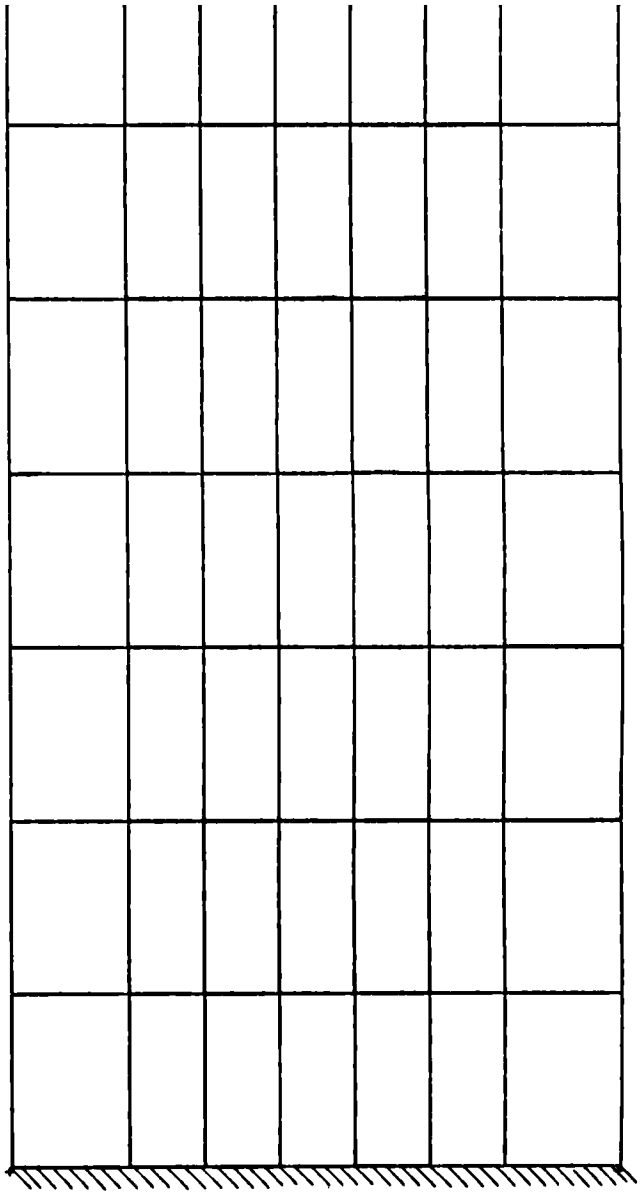


Fig. 9.1. Finite element mesh adopted for the analysis of (a) type I and (b) type II walls.

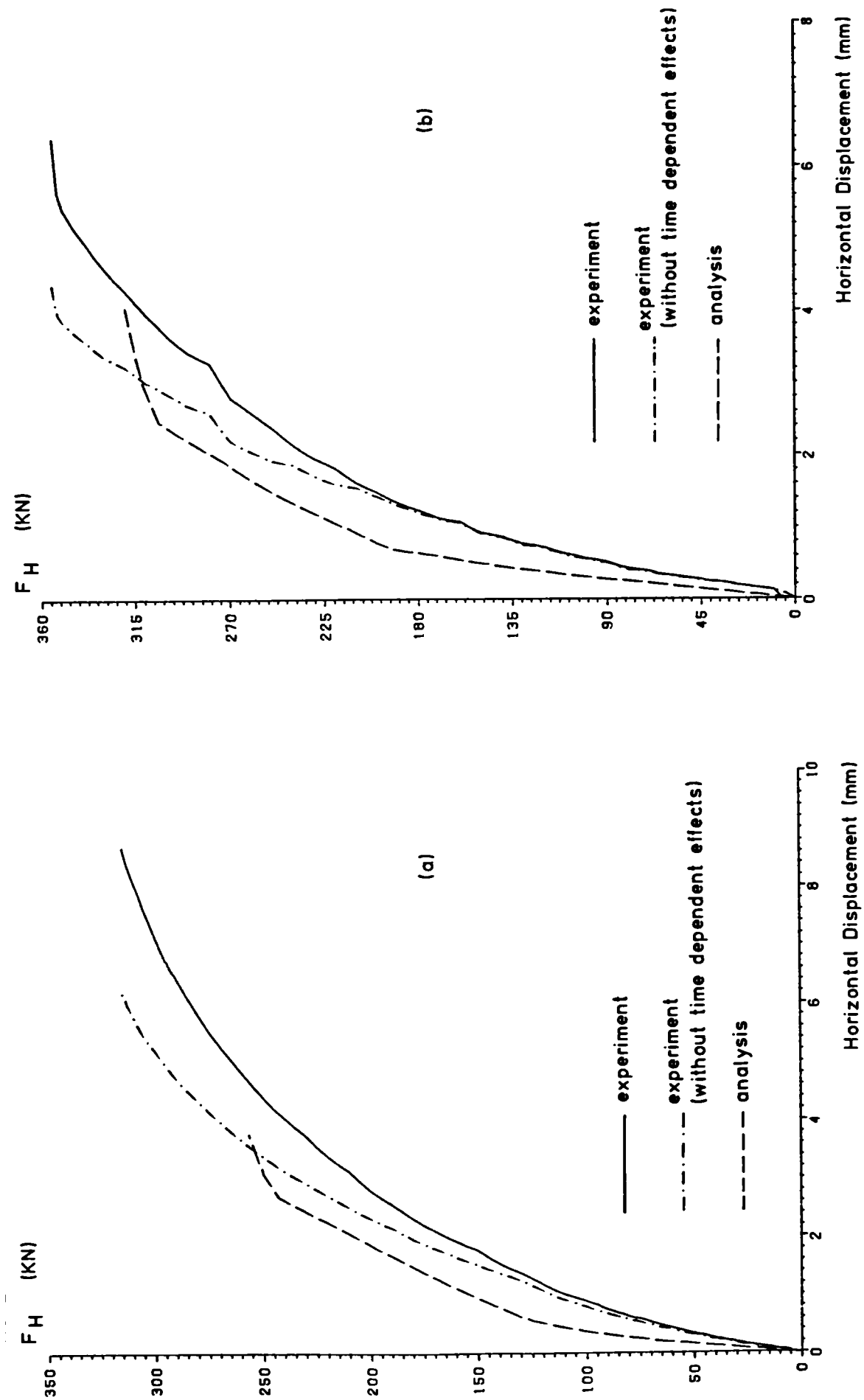


Fig. 9.2. Experimental and analytical horizontal load-top horizontal displacement curves for wall specimens (a) SW15 and (b) SW16.

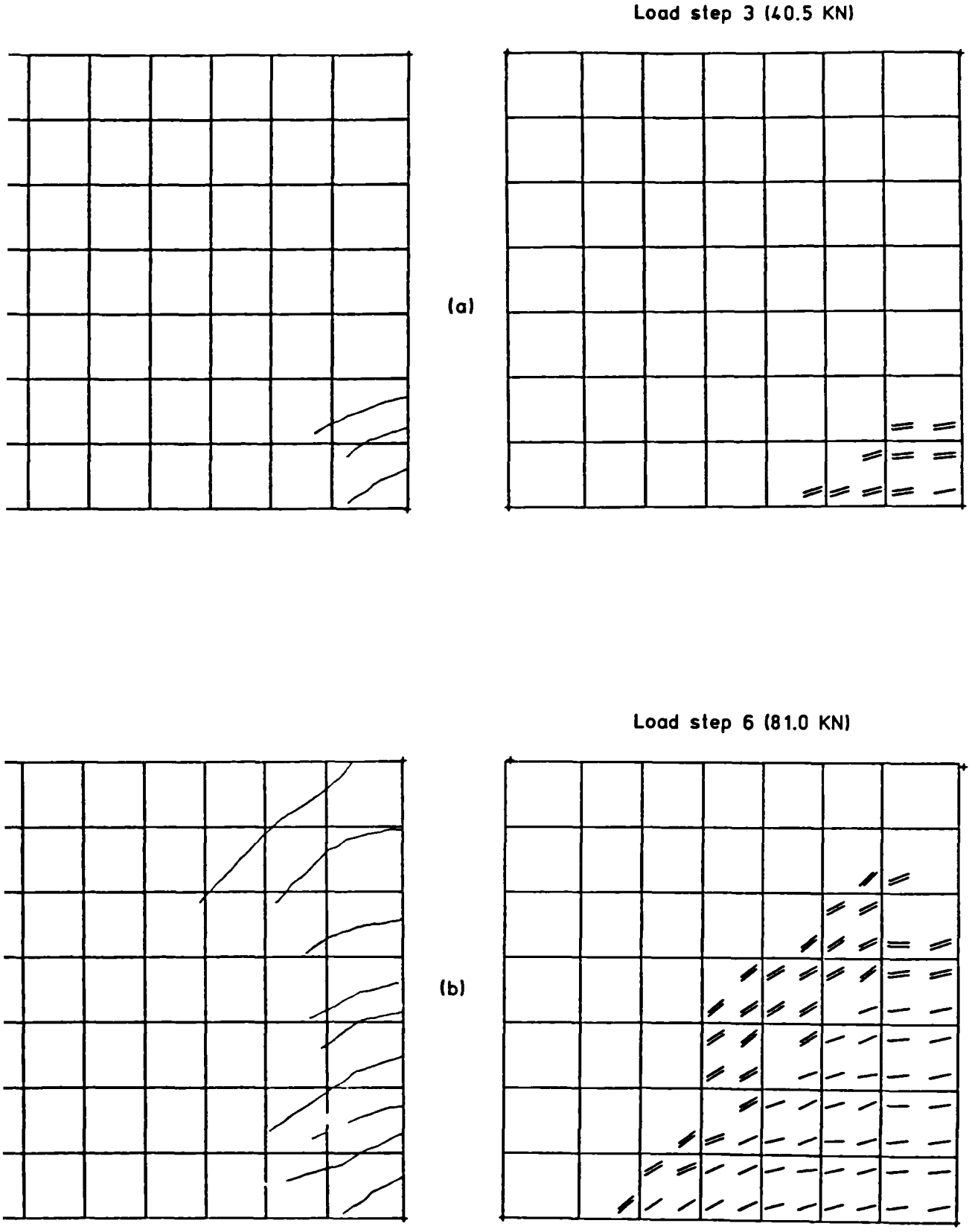
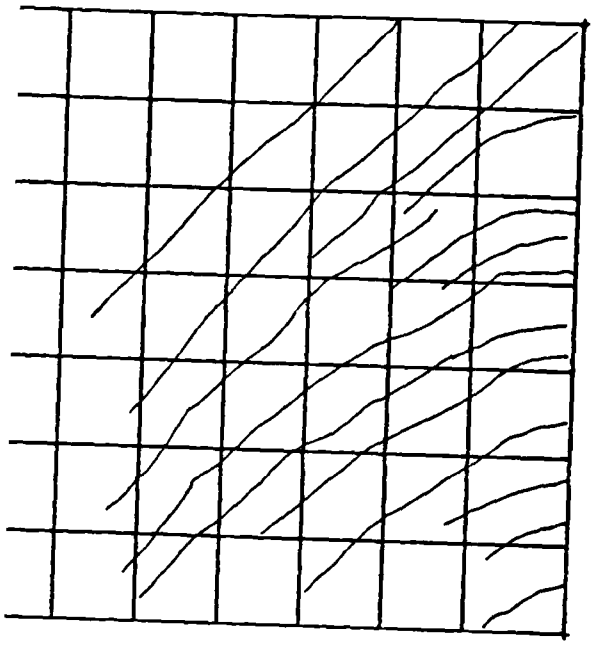
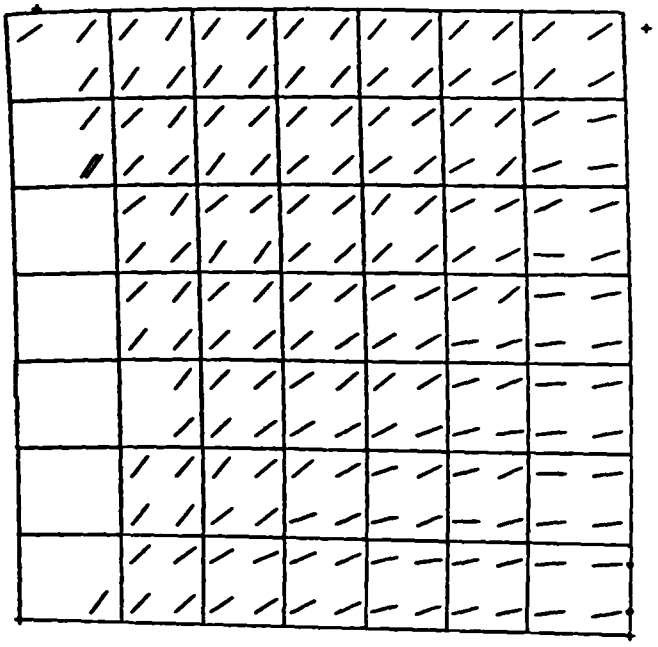


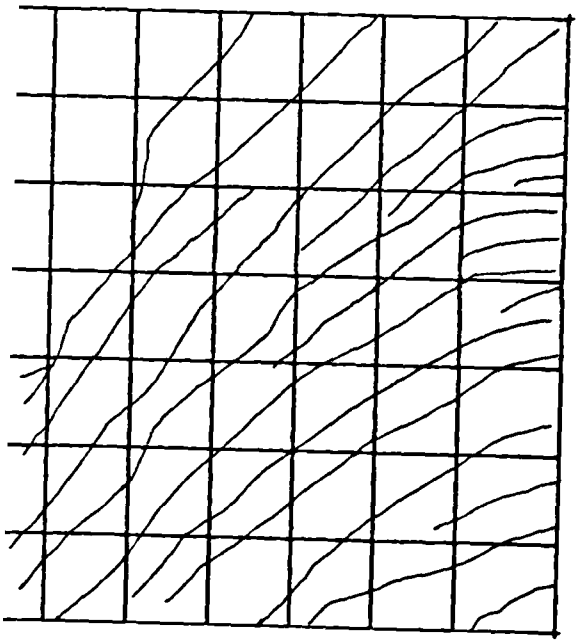
Fig. 9.3. Comparison of experimentally obtained and analytically predicted crack patterns for specimen SW11 at (a) initiation of flexural cracking, (b) initiation of inclined cracking, (c) yielding of tensile reinforcement and (d) ultimate state.



(c)

Load step 13 (175.5 KN)





(d)

Load step 18 (243.0 KN)

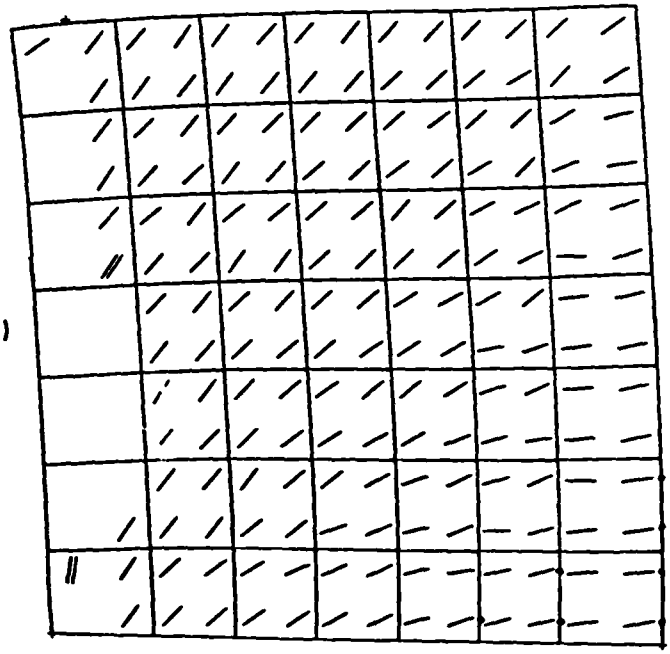


Fig. 9.3 Cont'd

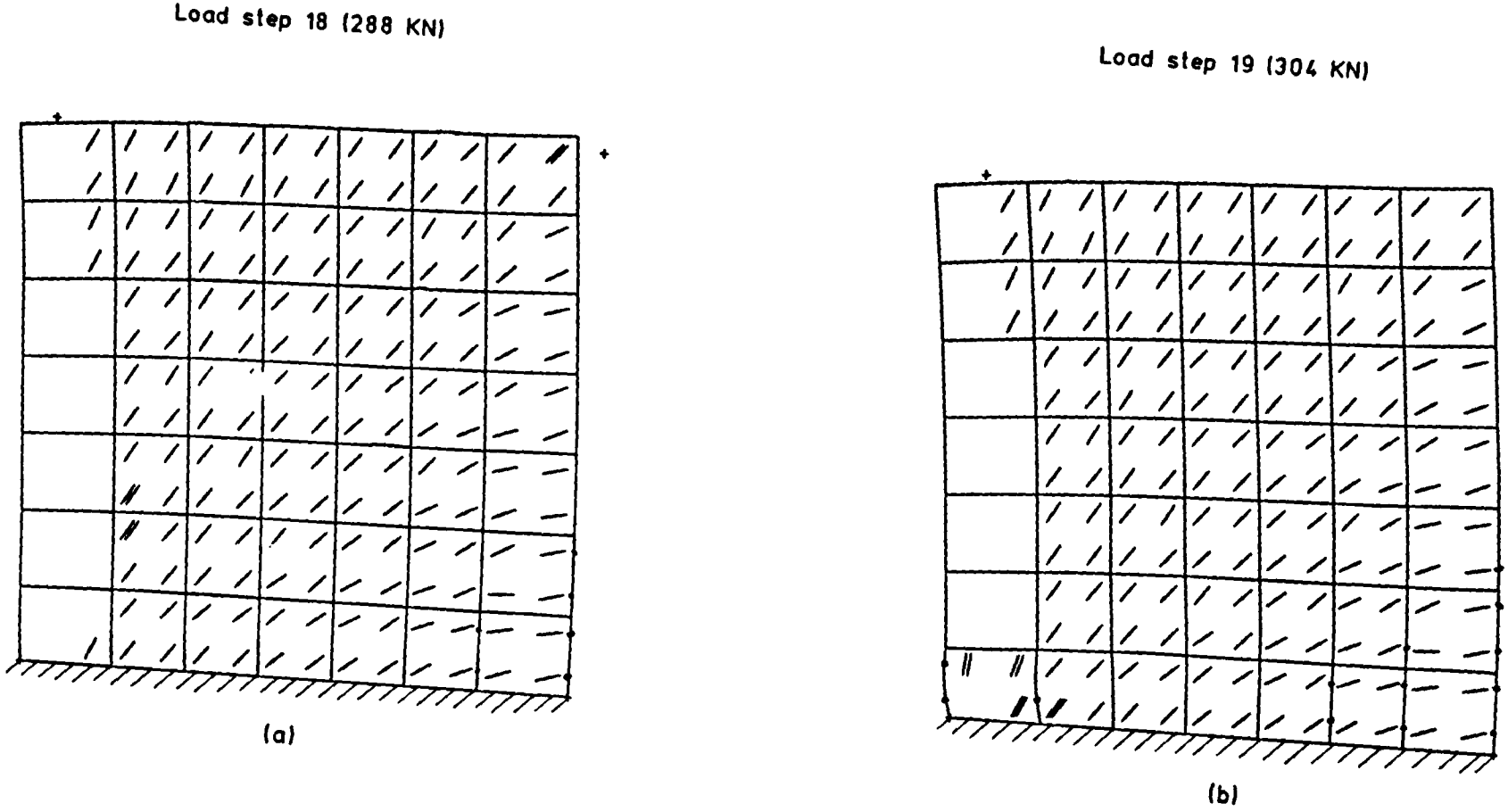


Fig. 9.4. Analytical crack patterns and deformed shape plots for wall specimen SW15 (a) one load step prior to failure and (b) at the ultimate load step.

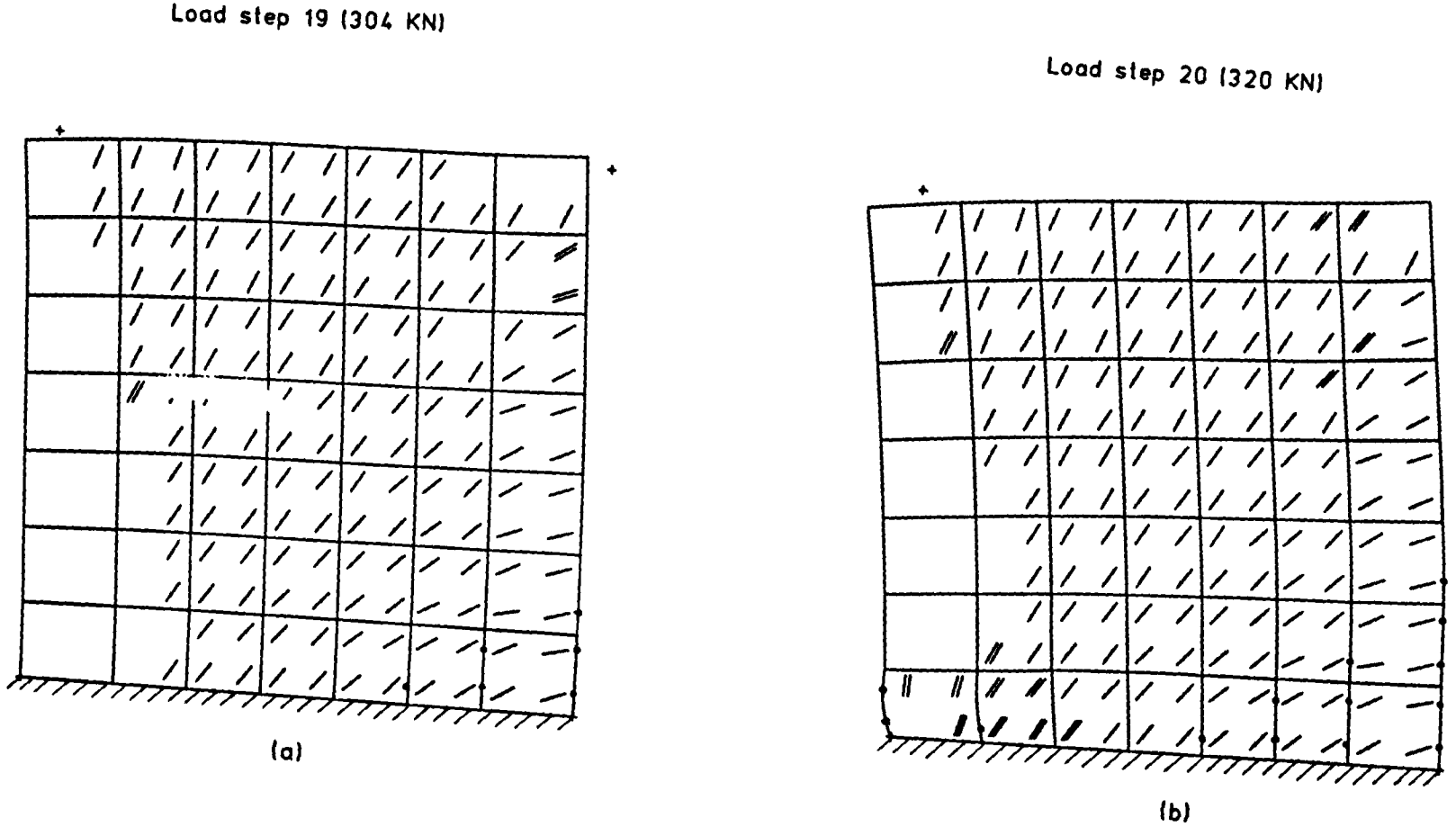


Fig. 9.5. Analytical crack patterns and deformed shape plots for wall specimen SW16 (a) one load step prior to failure and (b) at the ultimate load step.

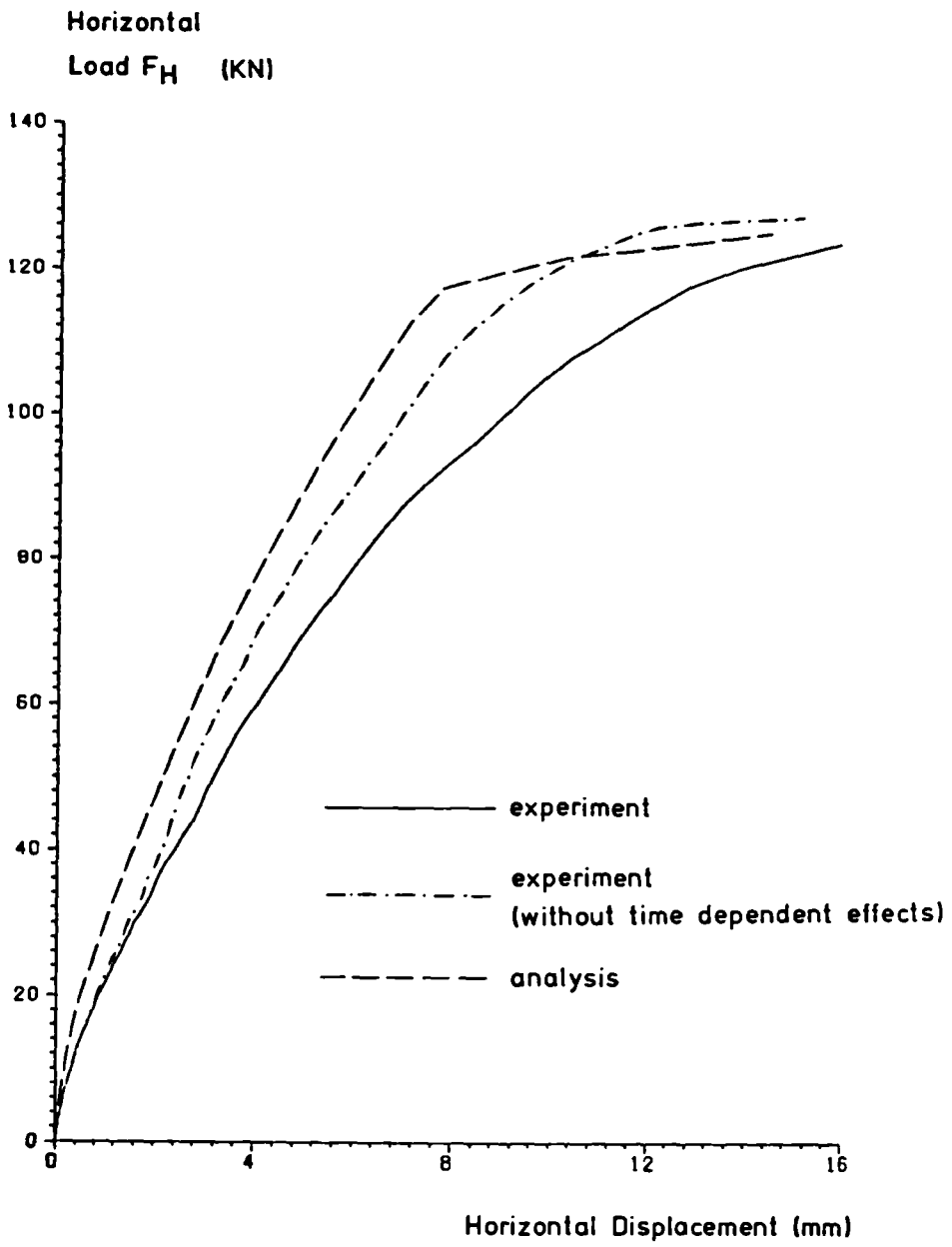


Fig. 9.6. Predicted and experimental horizontal load-top horizontal displacement curve for wall specimen SW21.

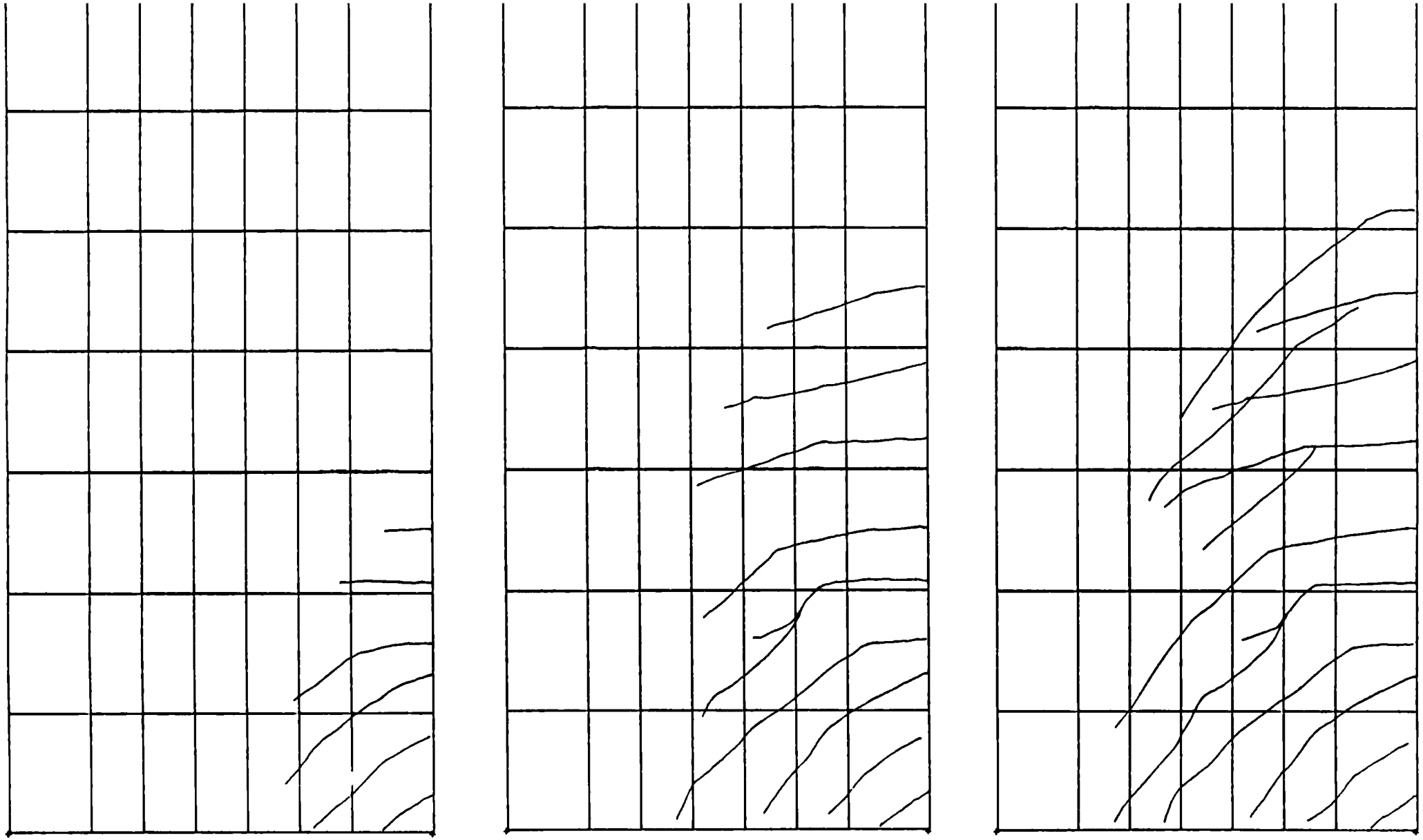


Fig. 9.7. Comparison of analytical and experimental cracking process for wall specimen SW22 at (a) initiation of significant flexural cracking, (b) initiation of inclined cracking and (c) prior to failure load.

Fig. 9.7. Cont'd

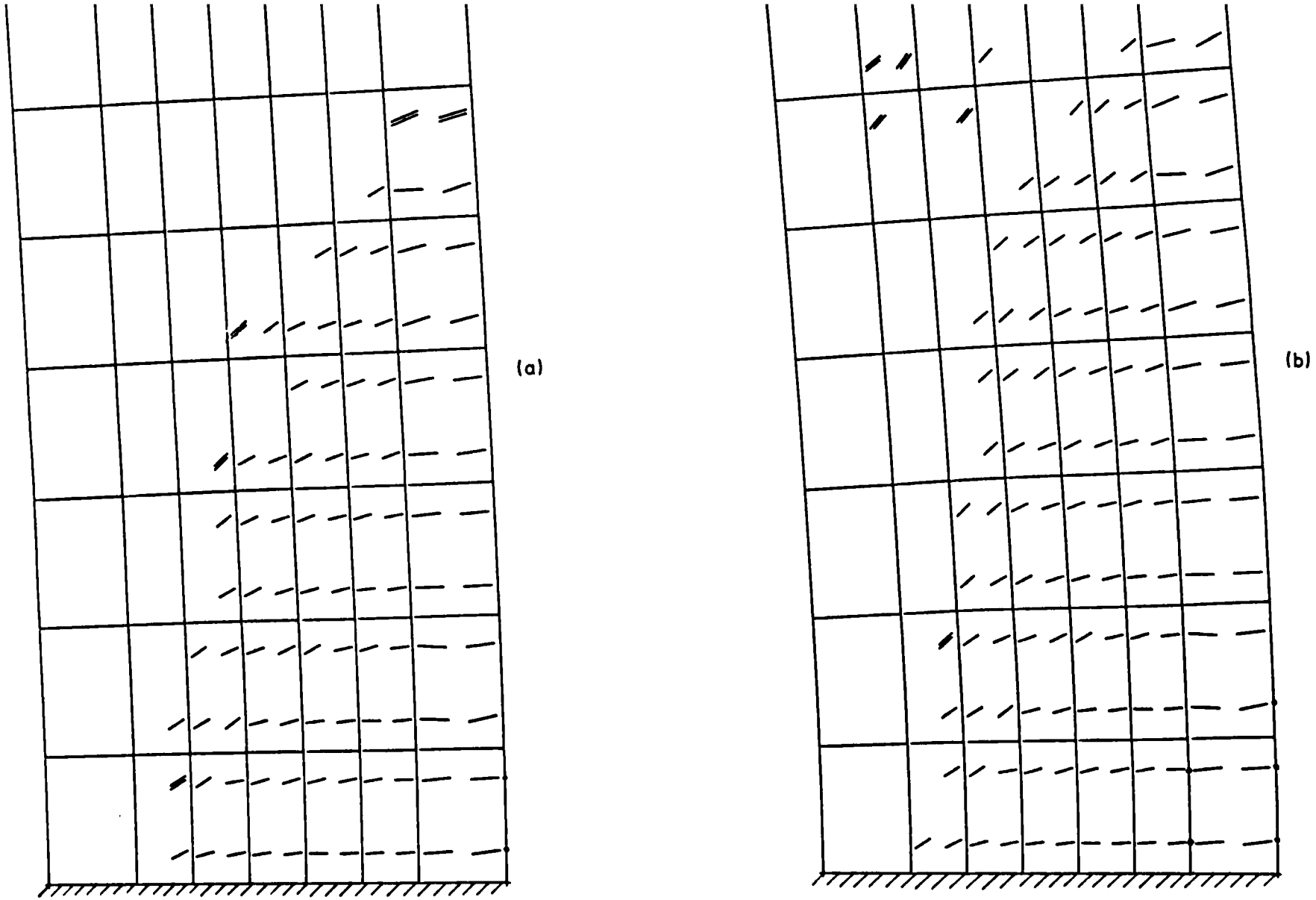


Fig. 9.8. Crack pattern and deformed shape plot for wall specimen SW32 at a load level corresponding to (a) ductility ratio $\mu = 1$ and (b) ductility ratio $\mu = 2$.



Fig. 9.9. Typical analytically predicted modes of failure for type II walls subjected to a normalized axial load of (a) $\nu = 0$, (b) $\nu = 0.1$ and (c) $\nu = 0.2$.

CHAPTER 10

DESIGN IMPLICATIONS

10.1. INTRODUCTION

The present chapter is concerned with a comparative study of the structural wall behaviour, established experimentally and discussed in previous chapters, with that predicted by current Code provisions. The study indicated that, while the concepts forming the basis of Code provisions cannot provide a satisfactory explanation of structural wall behaviour, a recently introduced concept, the compressive force path concept appears to provide a realistic description of the causes of the observed structural wall behaviour. This latter concept is used to develop a physical model which has been used as a basis for the development of a simple and rational design method for structural walls.

10.2. EVALUATION OF CODE PREDICTIONS

In the present section the experimentally measured wall strength is compared with the nominal strength computed by the expressions for flexure and shear recommended in BS 8110 (1985), UBC (1982), ACI (1983) as well as the expression for wall strength suggested by Oesterle et al (1984). Actual (measured) strengths of concrete and steel will be used in all expressions. A detailed discussion of design procedures recommended by the above Codes for the assessment of the flexural and the shear strength of reinforced concrete structural walls is included in Section 4.2.

Tables 10.1 and 10.2 summarize the Code predictions expressed in terms of horizontal load together with the experimentally obtained ultimate horizontal load for type I and II walls, respectively. It should be noted that in all specimens yielding of the vertical reinforcement controlled the wall response at the ultimate limit state, and hence it is interesting to see how accurately and effectively can Code recommendations predict the observed wall behaviour.

1982 UBC Expressions

The UBC predictions of the flexural strength of the walls are obtained by Equation 4.2. and take into consideration only the contribution of the vertical

reinforcement of the wall edges. As column (3) of Tables 10.1 and 10.2 indicates the UBC expression for flexure is overconservative when walls are subjected to a normalized axial load smaller than 0.2, and conservative for higher levels of axial load. Even for the case of type II walls subjected to cyclic loading, where less vertical reinforcement was supplied to the wall web, the predicted flexural wall strength was 60% of that obtained experimentally.

The smaller of the values included in columns (4) and (6) of both tables represents the wall shear strength as predicted by the UBC expressions. For type I walls these expressions indicate that specimens SW13 and SW16 should have failed in shear before attaining their flexural capacity, which was not in agreement with the experimental results. Wall specimens with height to width ratio of one sustained a much higher horizontal load than the UBC expressions for shear predict. The same holds for walls of type II containing less horizontal reinforcement (i.e. SW26 and SW31 to SW33). Furthermore, for type II walls subjected to cyclic loading, UBC provisions suggest that the contribution of concrete to shear strength should be neglected since yielding of flexural reinforcement bars is possible in both faces of the wall base. If this suggestion were correct, slender walls which incorporated almost nominal horizontal (shear) reinforcement and were subjected to cyclic loading should have failed due to shear at an early stage of 61.5 KN compared with the average experimentally measured wall strength of 112.8 KN (see columns (5) and (12) of Table 10.2). The main reason for these discrepancies should be attributed to the lack of an underlying theory describing the causes of "shear" failure.

ACI 318-83 Expressions

The ACI predictions of the flexural strength are obtained by Equation 4.1. Column (7) of Tables 10.1 and 10.2 includes flexural strengths predicted by using both the yield and the ultimate strength of steel. It should be noted that, for both types of wall tested measured wall capacities (column (12)) were higher than either of the predicted values. This indicates that Code provisions for flexure, incorporating uniaxial strength characteristics, are conservative even if higher values of steel strength are considered. However as the discussion in Section 4.5.1 pointed out, the assumption of uniaxial strength characteristics for the calculation of wall flexural strength does not appear to be realistic.

Since ACI defines the effective nominal shear area of the wall as b * l, rather than 0.8 * b * l as recommended by UBC, it yields 25% higher shear strength. ACI, like UBC, limits the nominal shear strength assigned to any wall unit.

Hence, the wall shear strength is the smaller of the values included in columns (8) and (10) of Tables 10.1 and 10.2 or columns (9) and (10) for walls subjected to cyclic post-yield displacements. ACI expressions predicted that (a) wall specimens SW13, SW15 and SW16 should have failed in "shear" due to "crushing" of the concrete struts of the "truss" model and (b) walls subjected to cyclic loading should have failed prematurely in "shear" before the yielding of the vertical reinforcement bars at a load equal to 70% of measured ultimate horizontal load. The experimental data of type I walls (see Chapter 6) indicate that not only these values were conservative (even though less conservative than UBC predictions) but also they do not describe realistically the wall behaviour at ultimate limit state.

PCA expression (Oesterle et al, 1984)

Based on a number of structural wall tests at PCA, Oesterle et al (1984) suggested that the ACI predictions of limiting shear stress requirements do not eliminate "web crushing" as a possible failure mode for walls subjected to high boundary shear stresses. The PCA expression was derived using the truss analogy and correlates wall shear strength with the cylinder concrete strength and the normalized level of axial load. The predictions of this expression are included in column (11) of Tables 10.1 and 10.2. Since for type II walls the predictions are higher than both the flexural and shear wall strength, the mode of failure will be either flexural or shear. However, for type I walls, the predicted values for wall strength were close to the experimental wall capacities for specimens with concrete cylinder compressive strength higher than 44 MPa, while they significantly underestimated the wall strength of the remaining specimens. Such results indicate that the PCA expression may have been by coincidence accurate in predicting the strength of some wall specimens since as discussed in preceding Chapters, uniaxial concrete strength characteristics do not appear to affect wall strength.

BS 8110, 1985 Expressions

The general ultimate limit state procedure recommended by BS 8110 was used to determine the design ultimate strength of the cross-section of the walls tested under combined bending and axial load. As discussed in Chapter 4, these predictions yield more realistic flexural strengths than the two versions of Equation 4.2 recommended by ACI, since unlike the ACI formulae they identify whether the wall cross-section is under-reinforced, balanced or over-reinforced. Column (2) of Tables 10.1 and 10.2 includes the BS 8110 predictions for type I and type II walls, respectively. It is interesting to note that :

(a) for the specific amount of vertical reinforcement used in the specimens, the BS predictions lie between the two ACI predictions,

(b) even on the basis of first principles, the predicted flexural strength is smaller than the experimentally obtained value, since triaxial stress state conditions existing in the lower compressive zone of the wall are not accounted for in the above expressions. It should be also noted, that the higher the level of axial load applied to the wall, the more conservative are the BS 8110 predictions for flexure.

10.3. ANALYTICAL AND EXPERIMENTAL SUPPORTING EVIDENCE

The results of the analytical investigation described in Chapters 4 and 9, and the comparison between Code predictions and experimental results, presented in the previous section, demonstrate the inadequacy of current Code provisions. Most current design methods have been developed on the basis of the assumption that it is sufficient for practical purposes to rely almost entirely on uniaxial stress–strain characteristics for concrete. Such a reasoning underestimates the considerable effect that small stresses have on the load–carrying capacity and deformational response of concrete in critical regions of a structural wall. Using the experimentally measured values for the horizontal load–carrying capacity of the wall it was shown, considering the equations of force and moment equilibrium, that the calculated average vertical stress in the compressive zone of the wall is much higher than f_c' for both types of wall tested. Such a large stress can only be sustained if the stress conditions in the compressive zone of the wall are triaxial compressive. Concurrently, the expanding concrete induces tensile stresses in adjacent regions and this gives rise to a triaxial state of stresses with at least one principal stress component being tensile. The latter state of stress reduces the strength of concrete and results in vertical splitting of the lower compressive zone of the wall. The above reasoning is in compliance with the analytical predictions of the fracture process and the mode of failure of the walls.

However the most significant shortcoming of the Code design provisions is not the conservative nature of the predicted flexural strength but the method used to assess the wall shear strength. The analytical work has shown, that the concept of truss analogy does not form a suitable basis for the shear design of reinforced concrete walls. The results obtained by the non–linear finite element analysis indicate that while Code predictions are conservative for the lower range of values of horizontal reinforcement, they may be unsafe for the upper range of these

values. For walls failing below their flexural capacity, the amount of horizontal reinforcement is not as important for shear resistance as the Code expressions assume.

The inadequacy of the above concept as the basis of current shear design methods has also been demonstrated in the experimental programme. For type I walls which were subjected to high boundary shear stresses, the maximum experimental horizontal load was, in most cases, much higher than the Code predicted value corresponding to "crushing" of the concrete struts of the "truss model" and the value representing the horizontal reinforcement contribution to shear assuming that the contribution of concrete is negligible. In fact, the concrete contribution to shear resistance is considered negligible by most current Codes when yielding of the vertical reinforcement occurs. Although specimen SW26 and type II walls subjected to cyclic loading incorporated almost nominal amount of horizontal reinforcement, they failed in flexure, exhibiting considerable post-yield deformations, under a horizontal load much higher than that the truss analogy concept predicted for an early "shear" failure.

The inadequacy of the truss analogy concept to form a rational basis for shear design methods has also been demonstrated in other experimental programmes reviewed in Chapter 2. Results obtained from these programmes showed that (a) walls without horizontal reinforcement had a horizontal load-carrying capacity significantly higher than that predicted by current Code provisions and (b) horizontal reinforcement was less effective in resisting shear than the Code provisions suggest.

The above evidence clearly indicates that failure of the walls cannot be described as a "shear" failure as defined by the truss analogy concept. Furthermore the large deflections exhibited particularly by type II walls led, in all cases, to large widths of the deepest flexural cracks prior to failure and thus considerably reduced the "aggregate interlock".

With aggregate interlock significantly reduced and the type II walls subjected to cyclic loading failing in flexure at a horizontal load much higher than the contribution of nominal horizontal reinforcement to shear, it is realistic to suggest that the main contributor to "shear" resistance of the reinforced concrete wall is the compressive zone, with the region of the wall below the neutral axis (in the tensile zone) making an insignificant contribution. A similar conclusion was drawn by Kotsovos (1987b, 1987c) during the experimental investigation of the behaviour of reinforced concrete beams with various arrangements of shear reinforcement subjected to two-point loading with various shear span to depth ratios.

The validity of the above view is also supported by the analytical evidence obtained in the present thesis. It was shown that the inclusion, near the extreme compression and tension fibres of additional reinforcement in both the compression and tension zones of the wall results in a significant increase of the horizontal load-carrying capacity. This occurs in spite of the considerable reduction of horizontal reinforcement to near nominal levels.

10.4. COMPRESSIVE FORCE PATH

The analytical and experimental information discussed in the preceding section leads to the conclusion that the "compressive force path" concept (Kotsovos, 1983b) can explain more realistically than the "truss analogy" concept the behaviour of reinforced concrete structural walls at the ultimate limit state.

On the basis of this concept the wall strength is associated with the strength of concrete in the region of the path along which the compressive forces is transmitted to the wall base. As Figure 10.1 depicts the path of the compressive force may be visualised as a "flow" of compressive stresses with varying section perpendicular to the path direction and with the compressive force representing the stress resultant at each section. It is considered that failure is related with the development of tensile stresses in the region of the path. Such stresses may develop due to a number of causes, the main ones being the following:

(a) Change in the path direction : A tensile stress resultant develops for equilibrium purposes at locations where the path changes direction. These locations are dependent on the height to width ratio of the wall.

(b) Varying intensity of the compressive stress field along the path : The compressive stress will reach a critical level at the smallest cross-section of the path where the stress intensity is highest. This level marks the start of an abrupt material dilation which will induce tensile stresses to the surrounding concrete.

(c) Tip of inclined cracks : It is well-known from fracture mechanics that large tensile stresses develop perpendicular to the direction of maximum principal compressive stress in the region of the crack tip.

(d) Bond failure : For slender walls bond failure at the level of the vertical reinforcement under tension between the two deepest consecutive flexural cracks can change the stress conditions in the lower compressive zone of the wall as described in Section 7.4.6 and illustrated in Figure 7.12.

An indication of the shape of the path of the compressive force may be provided by the experimentally obtained crack pattern of wall specimens just before failure. For rectangular walls with height to width higher than or equal to one, it is realistic to consider that the compressive force is transmitted from the loading beam to the wall base following a path consisting of two near-linear portions intersecting at a point lying at a distance of approximately 2l' from the loading beam, where l' is the distance of the point of application of the horizontal load resultant to the extreme compressive fibre of the wall.

Failure may occur either in the region where the compressive force path changes direction or within the near-vertical portion of the compressive force path closest to the wall base due to (a) development of tensile stresses caused by bond failure or (b) large tensile stresses in the region of the tip of inclined cracks. Such modes of failure can only occur if anchorage failure and failure due to poor detailing of the construction joints have been prevented by proper anchoring of the tension stel and adequate construction techniques, respectively.

It appears from the above, that wall failure occurs due to tensile stresses developing within the compressive zone beyond a distance of approximately 2l' from the loading beam. This indicates that horizontal reinforcement is required only within the above portion of the wall to prevent "shear" failure.

10.5. PHYSICAL MODELS

T: compressive force path concept may be introduced in design by developing physica' models capable of providing a realistic description of the features of struct ..l concrete behaviour. Such a physical model describing the behaviour of R.C. beams without transverse reinforcement has been proposed by Kotsovos (1988b). This model comprises a frame with inclined legs providing a simplified description of the shape of the compressive force path and a number of concrete cantilevers which form between consecutive flexural or inclined cracks occurring within the beam web under increasing load, as shown in Figure 10.2. The tensile reinforcement ties this "comb-like" structure. For the case of two-point loading the length of the horizontal projection of the inclined legs of the frame is

considered to be equal to either twice the beam depth for $a/d > 2$ or the shear span for $a/d < 2$. The distance between the concrete cantilevers is taken equal to half the depth of the horizontal member of the frame.

The part of the above physical model between the sections at the support and the load-point resembles the reinforced concrete walls investigated during the present experimental programme. Of course there are a number of distinct differences such as the manner in which loading is applied to the top beam of the wall, the fact that wall tensile reinforcement is distributed and covers a wider area than in the beam case, and in particular the way in which the compressive stresses "flow" from the loading beam to the wall base.

For the case of a reinforced concrete wall subjected to a uniformly distributed horizontal load at its top end face, a realistic physical model may have the form depicted in Figure 10.3. It can be seen in the Figure that, as for the model discussed earlier the compressive force path comprises two legs (one vertical and one inclined), while the flexural and inclined cracks occurring within the wall web under increasing load form a number of concrete "teeth" tied by the tensile reinforcement.

The vertical projection of the inclined leg may be given a value equal to a portion of the wall width. Since the slope of the inclined leg follows a slope of two to one and the experimentally measured distance of the point of application of the horizontal load resultant to the extreme compressive fibre varies with the height to width ratio, the length of the vertical projection may be considered to be equal to $^2/_3$ and $^3/_4$ of the wall width plus the depth of the neutral axis for $h/l = 1$ and 2, respectively. For walls with height to width ratio between one and two, the vertical projection of the inclined leg may be obtained from the above values by linear interpolation. When the wall height to width ratio is higher than two the wall is expected to exhibit a flexural mode of failure.

The depth of the horizontal leg may be considered equal to the depth of the neutral axis near the wall base at the ultimate limit state. It is possible to establish the depth of the neutral axis by considering force and moment equilibrium conditions, taking into account the triaxial state of stresses as it will be discussed in detail in Section 10.6. The depth of the inclined leg may be defined as described by either the Institution of Structural Engineers and the Concrete Society (1979) or Kotsovos (1988a).

In compliance with the compressive force path concept, wall strength is

predominantly provided by the tied frame with the concrete "teeth" between the cracks making a small contribution to wall load-carrying capacity through the bond forces which develop between concrete and tensile reinforcement. As discussed in Section 7.4.6, loss of bond between concrete and reinforcing bars at the lower tensile zone of the wall causes a significant stress redistribution within the compressive zone which may lead to wall failures.

10.6. FAILURE CRITERIA

In order to implement the above model in design, it is essential to complement it with a failure criterion. Such a failure criterion cannot be unique since wall failure may occur due to a number of causes. The analytical and experimental investigations discussed in preceding chapters have indicated two particular types of wall behaviour, each one characterised by a specific mode of failure.

Type I behaviour is characterised by a flexural mode of failure which occurs when the flexural capacity is attained. It should be noted that the flexural capacity predicted by analysis and established by experiment was higher than that predicted by the approach forming the basis of BS 8110 (1985), particularly for the case of underreinforced wall cross-sections. The main factor responsible for the higher wall flexural capacity was the higher strength and deformability of the concrete of the compressive edge due to the confinement provided by stirrups.

It is important to accurately establish the flexural strength of the wall since, as it will become clear later on, the wall "shear" resistance calculated by using the compressive force path concept is dependent on flexural strength. In order to assess the flexural capacity of the wall, the equilibrium conditions between internal and external actions may be formulated by assuming:

(a) A rectangular stress block with an increased concrete strength (kf'_c) due to the triaxial conditions. The factor k may be assessed by using the expression suggested by Park et al (1982)

$$k = 1 + \omega_t \qquad \text{(Eq. 10.1)}$$

where ω_t is the volumetric percentage of confinement reinforcement at the compressive zone given by the expression

$$\omega_t = \frac{\rho_s \cdot f_{su}}{f'_c}$$

where ρ_s is the percentage of confinement reinforcement.

Alternatively, k may be assessed by using the method developed by Tassios and Lefas, 1984 to calculate the transverse normalized compressive stresses, σ_2/f'_c and σ_3/f'_c, developing within the compressive zone due to lateral confinement. The normalized longitudinal compressive stress is then calculated by using the information included in Figure 6.15.

(b) The concrete strain at the ultimate limit state should have a more representative value than the conservative 0.003, since confining transverse stresses can increase the above value as suggested by Blume et al (1961).

An indication of the accuracy of the above design procedure for flexural strength is shown in Table 10.3, where the results of two typical walls are presented. Using the design details of type I and type II walls, described in Chapters 6 and 7 respectively, the flexural strength of both walls was calculated following a trial and error procedure (helped by a small computer programme). An average design compressive cube strength of 45 MPa was used. As the table indicates, the analytically predicted flexural wall capacities are in close agreement with the experimentally measured values.

Type II behaviour characterises walls which, due to the combined action of the bending moment and shear force, may fail before flexural capacity is attained. For this type of behaviour an analytical description of the stress conditions that cause "shear" failure is essential. This analytical description should be used not only as a failure criterion but also as a basis for the calculation of the tensile forces to be sustained by the horizontal reinforcement. Such an analytical description in which the stress conditions leading to failure are expressed in terms of internal actions (bending moment and shear force) that cause them, has already been derived empirically for R.C. beams by Bobrowski and Bardham-Roy (1969). The above formula has been validated for a wide range of reinforced concrete beams likely to be used in practice.

Figure 10.4 presents a modified version of the formula which takes into account the characteristics of the physical model adopted for the walls. Equation 10.2 has been found to yield realistic predictions of the horizontal load-carrying capacity of walls without horizontal reinforcement. An indication of such predictions

is given in Figures 10.5(a) and (b) which show the predicted values of horizontal load-carrying capacity of walls (expressed in terms of boundary shear stresses) with height to width ratio of one and two, respectively, for various amounts of vertical reinforcement. The figure also includes the wall flexural capacity (assessed by using the approach recommended by BS 8110, 1985) and the predicted values obtained by the non-linear finite element analysis. The figure indicates a close correlation between the values predicted by the analysis and those predicted by the empirical expression in all cases where the walls failed before attaining their flexural capacity. It is interesting to note in the figure that while the walls with height to width ratio of two fail in "shear" only for high values of vertical reinforcement ($\rho_v \geq 4\%$), the walls with height to width ratio of one without horizontal reinforcement fail in "shear" for vertical reinforcement ratios $\rho_v \geq 1\%$. Furthermore the figure shows that the predicted values obtained by using Equation 10.2 are 2 to 3 times larger than the values predicted by the Code provisions for "shear" design for the case of walls without horizontal reinforcement.

Besides the analytical supporting evidence, the modified version of the Bobrowski et al formula was also found to yield close predictions of experimentally measured strength of walls without horizontal reinforcement. The experimental data were those obtained from the tests of the walls S9 and SW10 carried out at the laboratories of Zürich and Portland Cement Association, respectively. Table 10.4 includes the predicted values of wall strength obtained by using Equation 10.2 and the ACI 318 Expression, together with the experimentally measured wall strength and information regarding the parameters involved in Equation 10.2. As the values of wall strength included in the table indicate, there is close agreement between the experimental value and the value predicted by using Equation 10.2, while in both cases the wall strength predicted by the ACI 318, 1983 expression was overconservative. The level of conservativeness increased with the amount of longitudinal reinforcement.

Equation 10.2 may be used for design purposes as follows:

(a) Design the wall to attain a given flexural capacity M_{fx}.
(b) Find the applied moment (M_{ax}) and shear (V_{ax}) at section x.
(c) Determine M_{cx} at section x by using Equation 10.2 and the ratio $a_{vx} = M_{ax}/V_{ax}$.

If $M_{cx} \geq M_{fx}$, only nominal horizontal reinforcement is needed in the wall web to safeguard against out-of-plane instability due to heterogeneity of concrete.

If $M_{cx} < M_{fx}$ a premature failure may be prevented by increasing either the area of the tensile steel or the area of wall cross-section. The other alternative is to provide horizontal reinforcement in accordance with the requirements discussed in the following section.

10.7. PROVISION OF HORIZONTAL REINFORCEMENT

As discussed in the preceding sections, for structural walls with height to width ratio less than two and depending on the amount of vertical reinforcement provided to the walls, significant internal tensile actions may develop for equilibrium purposes within either the region where the compressive force path changes direction or the vertical portion of the path, usually its section adjacent to the wall base where the flexural moment attains its maximum value.

Tensile Force in Region of Change of Path Direction

Figure 10.6 shows the region of intersection of the inclined and the vertical members of the physical model and indicates that the horizontal reinforcement not only sustains the action of the horizontal component of the inclined compression, but also subjects the shaded concrete block of the wall web, where it is anchored, to a compressive force. This force balances the shear force acting at the lower part of the above block.

It should be noted that the horizontal reinforcement will be activated only when the capacity of concrete to sustain alone the tensile stresses is exceeded. Hence, the horizontal reinforcement will sustain the excess tensile force $V_a - V_c$

where V_a is the horizontal component of the inclined compressive force, and

V_c is the portion of V_a sustained by concrete alone.

The amount of horizontal reinforcement required to sustain the excess tensile force will be

$$A_{sh} = \frac{V_a - V_c}{f_{su}} \qquad \text{(Eq. 10.3)}$$

where f_{su} is the characteristic strength of the horizontal reinforcement.

It is suggested that the area of horizontal reinforcement A_{sh} may be distributed over a length equal to the wall width, in the region where the compressive force path changes direction.

The spacing of the horizontal reinforcement may follow current detailing and be not more than b or 12 * d where b is the wall thickness and d the diameter of the horizontal reinforcement bar.

Tensile Force in Vertical Portion of Path

As discussed in the previous section, the vertical portion of the path is capable of sustaining significantly larger shear force than presently considered. The wall "shear" resistance can be destroyed if loss of the bond forces between concrete and tensile reinforcement causes stress redistribution as indicated in Figure 7.12. Bond failure can change the equilibrium conditions of a wall element between the sections including the deepest consecutive flexural (or inclined) cracks as discussed in Section 7.4.6.

The assessment of the tensile stresses developing beyond the region where the compressive force path changes direction is not a simple task since the triaxial stress conditions existing there prior to failure are complex. The presence of vertical and horizontal reinforcement within this region causes additional complications due to the complex interaction between steel and concrete. The data obtained in present work are insufficient for the development of a rational method suitable for the design of the reinforcement required to prevent failure due to causes discussed above. However, it should be noticed that the amount and spacing of confinement reinforcement specified by ACI 318, 1983, proved to be on the safe side, since in all tests of the present experimental programme the flexural wall capacity was achieved.

10.8. CONCLUSIONS

(a) Code predictions for flexural wall strength were conservative and, in cases where the distributed vertical reinforcement within the wall web was ignored, overconservative. In all cases, the walls tested failed under a horizontal load higher than that required for flexural failure and for type I walls, higher than the shear strength predicted on the basis of the truss analogy concept. Code predictions suggest that type II walls subjected to cyclic loading should have failed prematurely before the yielding of the vertical steel bars at a horizontal

load much lower than the experimentally obtained.

(b) Conclusion (a) indicates that the "truss analogy" concept does not form a suitable basis for the shear design of structural walls since it does not provide a realistic description of the actual "shear" resisting mechanisms of such structural elements.

(c) The validity of conclusion (b) is supported by the analytical evidence obtained in Chapters 3 and 4 and the experimental results of other investigators. In contrast to the truss analogy, the concept of the compressive force path suggests that wall "shear" resistance can increase by strengthening the concrete in the region of the path along which the compressive force is transmitted from the floor beam or slab to the wall base.

(d) Wall failure appears to be related with the development of tensile stresses in the region of the path due to a number of causes such as change in the path direction, varying intensity of the compressive stress field, stress concentrations on the tip of inclined cracks and loss of bond between tensile reinforcement and concrete.

(e) A physical model was developed capable of providing a realistic description of the main features of wall behaviour at the ultimate limit state. The model was complemented by failure criteria for the two types of wall behaviour observed.

(f) An analytical empirical expression, initially derived for beams, was used to describe the stress conditions leading to failure of walls without horizontal reinforcement under combined bending moment and shear force. Simple recommendations for the calculation of horizontal reinforcement, the latter being activated only when the capacity of concrete to sustain alone the tensile stre :s is exceeded, were proposed.

H/L=1

SPECIMEN	afterBS8110	UBC-82				ACI-83				PCA EXPRESSION	EXPERIMENT
	FLEX. STRENGTH	FLEX. STRENGTH	SHEAR STRENGTH			FLEX.STRENGTH fsy/fsu	SHEAR STRENGTH				
			Vc+Vs	Vs	UPPER LIMIT		Vc+Vs	Vs	UPPER LIMIT		
1	2	3	4	5	6	7	8	9	10	11	12
SW11	234.2	129.1	287.0	240.2	232.5	213.6/249.2	387.9	300.3	290.7	261.7	260
SW12	267.5	216.2	302.9	240.2	236.4	262.0/293.8	446.8	300.3	295.5	344.7	340
SW13	280.4	263.5	302.0	240.2	206.2	268.4/297.7	466.7	300.3	257.8	260.8	330
SW14	228.5	129.1	282.2	240.2	209.2	208.7/243.3	379.1	300.3	261.5	210.5	265
SW15	261.0	199.2	293.6	240.2	211.5	245.2/279.0	426.3	300.3	264.4	278.2	320
SW16	287.4	303.4	316.4	240.2	231.2	287.2/315.9	502.8	300.3	289.2	331.9	355

All forces in KN

Table 10.1. Code predictions and measured values of ultimate horizontal load for type I walls.

H/L=2

SPECIMEN	after BS 8110	UBC—82				ACI—83				PCA EXPRESSION	EXPERIMENT
	FLEX. STRENGTH	FLEX. STRENGTH	SHEAR STRENGTH			FLEX. STRENGTH fsy/fsu	SHEAR STRENGTH				
			Vc+Vs	Vs	UPPER LIMIT		Vc+Vs	Vs	UPPER LIMIT		
[1]	[2]	[3]	[4]	[5]	[6]	[7]	[8]	[9]	[10]	[11]	[12]
SW21	99.3	65.1	174.7	140.6	169.3	92.3/107.5	218.4	175.8	211.6	172.7	127
SW22	114.8	99.5	189.0	140.6	184.0	110.7/124.5	232.5	175.8	230.0	261.6	150
SW23	125.6	130.5	197.7	140.6	178.8	121.3/134.3	252.7	175.8	223.4	247.0	180
SW24	100.1	65.1	176.8	140.6	180.0	92.0/107.2	221.0	175.8	224.8	194.5	120
SW25	114.0	123.2	194.9	140.6	173.6	118.3/130.9	249.2	175.8	217.0	233.0	150
SW26	91.0	65.1	98.9	70.3	141.9	84.9/99.0	123.6	87.9	177.4	121.1	123
SW31	80.1	65.1	92.4	61.5	153.4	73.8/86.0	115.4	76.9	191.8	141.5	115.8
SW32	85.5	65.1	99.4	61.5	188.2	80.6/94.1	124.2	76.9	235.2	212.9	111
SW33	84.8	65.1	97.1	61.5	177.0	79.1/92.3	121.4	76.9	221.2	188.3	111.5

All forces in KN

Table 10.2. Code predictions and measured values of ultimate horizontal load for type II walls.

Wall Type	K	ε %	depth of neutral axis (mm)	M (KNm)	V (KN)
I	1.15	0.40	160.0	212.0	257.0
II	1.11	0.38	148.0	159.3	115.9

* design details in Chapters 6 & 7

Table 10.3. Assessment of flexural strength of two typical reinforced concrete walls.

Specimen	b (mm)	l (mm)	l' (mm)	a_{vx} (mm)	z (mm)	f'c (MPa)	fsu (MPa)	P(%)	Mfx (KNm)	Mcx (KNm)	Vcx (KN)	Vexp (KN)	Vc* (after ACI 318-83) (KN)
S9	100	1180	518	1200	590	31.3	762	0.23	470	404	306	342	165
SW10	76	1905	775	1905	953	40.3	560	0.82	950	661	347	305	230

* $V_c = 0.25 b l \sqrt{f_c'}$

Table 10.4. Measured and predicted values of wall strength for walls without horizontal reinforcement.

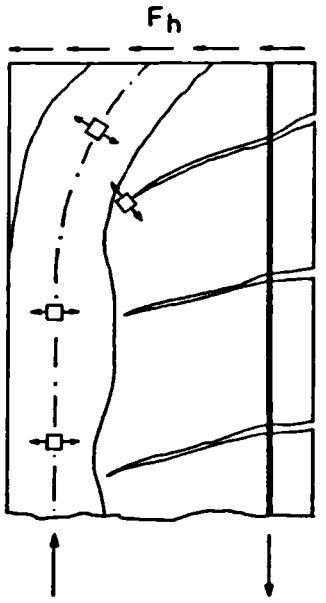


Fig. 10.1. Compressive force path.

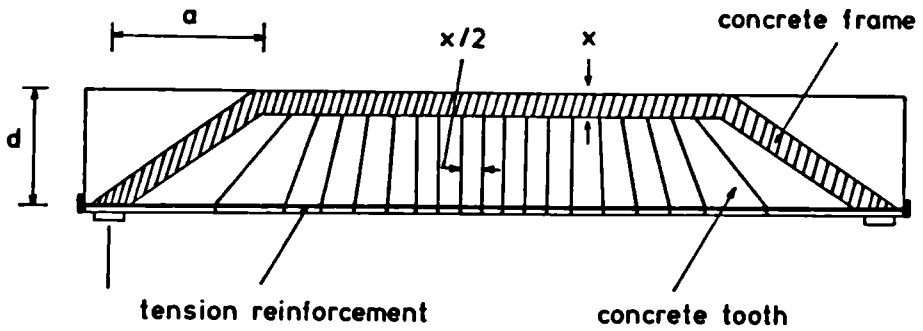


Fig. 10.2. Proposed "comb-like" model for R.C. beam.

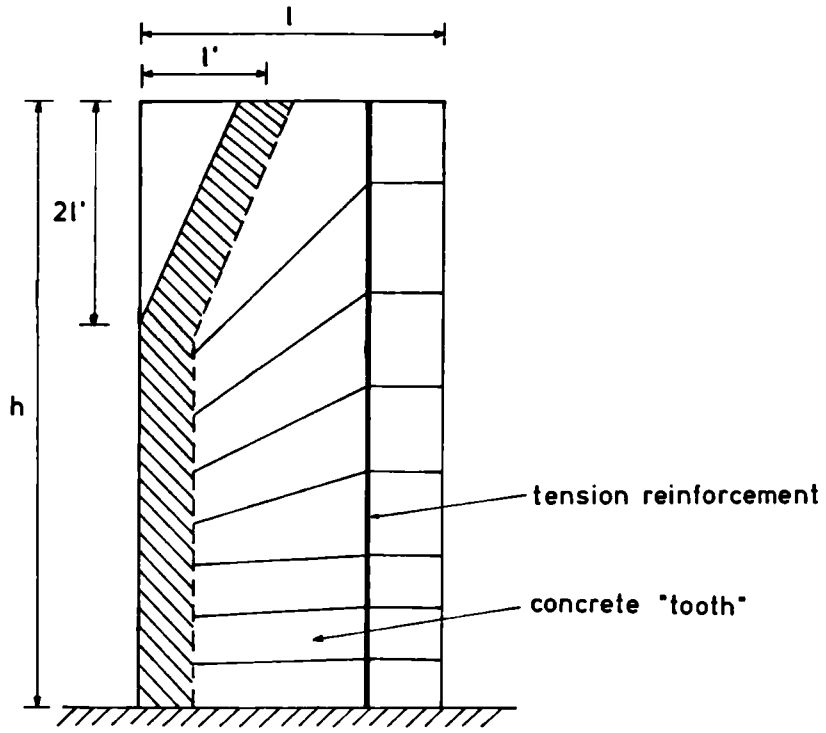


Fig. 10.3. Proposed physical model for R.C. wall.

$$M_{cx} = 0.875 * a'_{vx} * 1 * (0.342\ b + 0.3 \frac{M_{fx}}{1^2} \sqrt{\frac{z}{a'_{vx}}}) * \sqrt[4]{\frac{16.66}{\rho f_{su}}}$$

(Eq. 10.2)

where

M_{cx} is the moment corresponding to "shear" failure (Nmm)

M_{fx} is the flexural capacity (Nmm)

a'_{vx} is the expression $(1/1')\ a_{vx}$ (mm)

a_{vx} is the ratio M_{ax}/V_{ax} (mm)

M_{ax}, V_{ax} are the applied bending moment (Nmm) and shear force (N), respectively at a given section x

1 is the wall width (mm)

1' is the horizontal projection of the inclined portion of the path (mm)

z is the lever arm (mm)

ρ is the ratio $\frac{\text{area of tensile reinforcement of the concealed wall column}}{\text{gross concrete wall area}}$

f_{su} is the characteristic strength of the tension steel (N/mm^2).

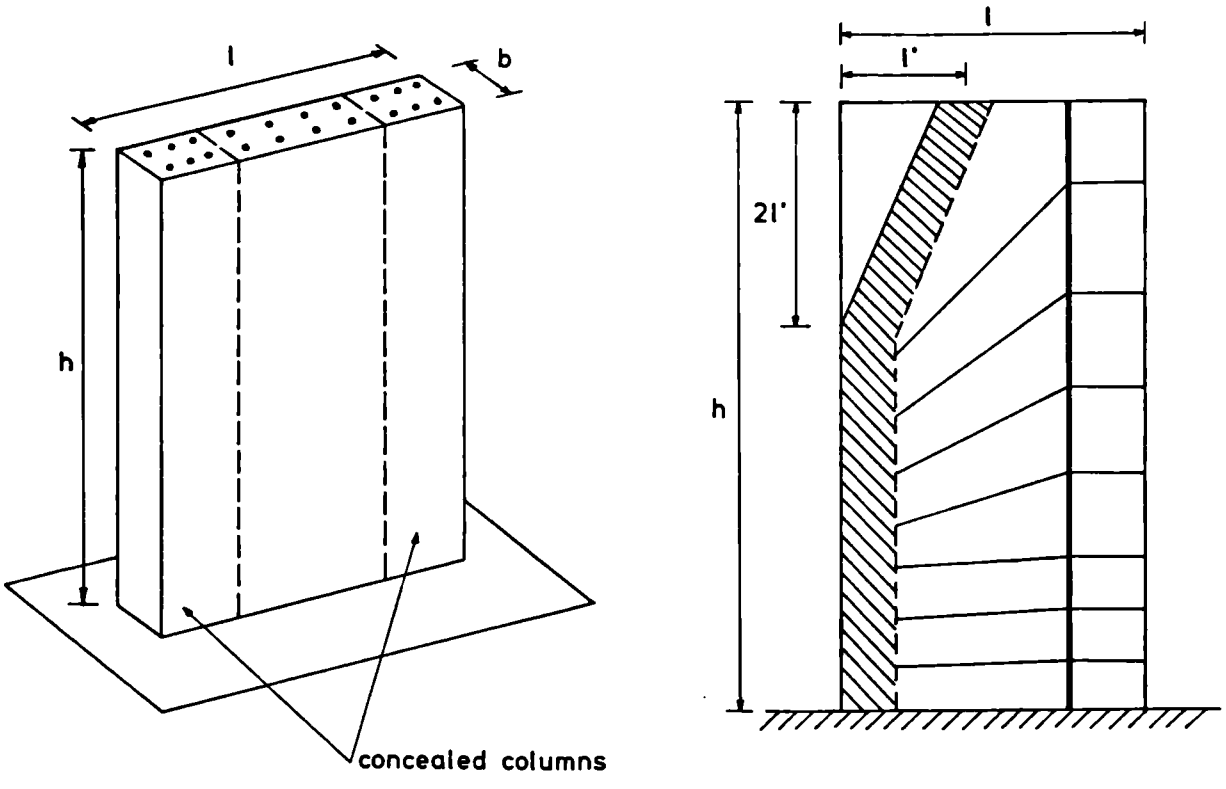
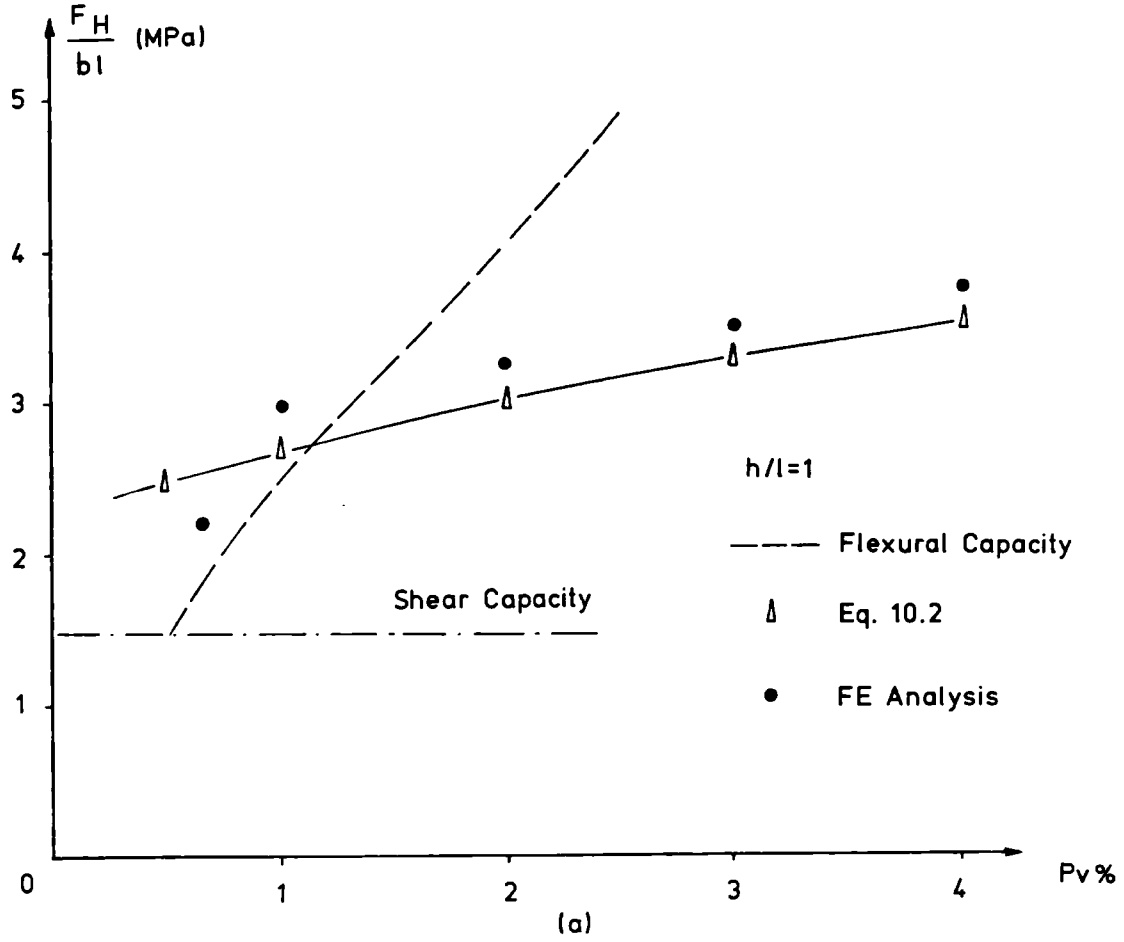


Fig. 10.4. Design equation for type II behaviour.



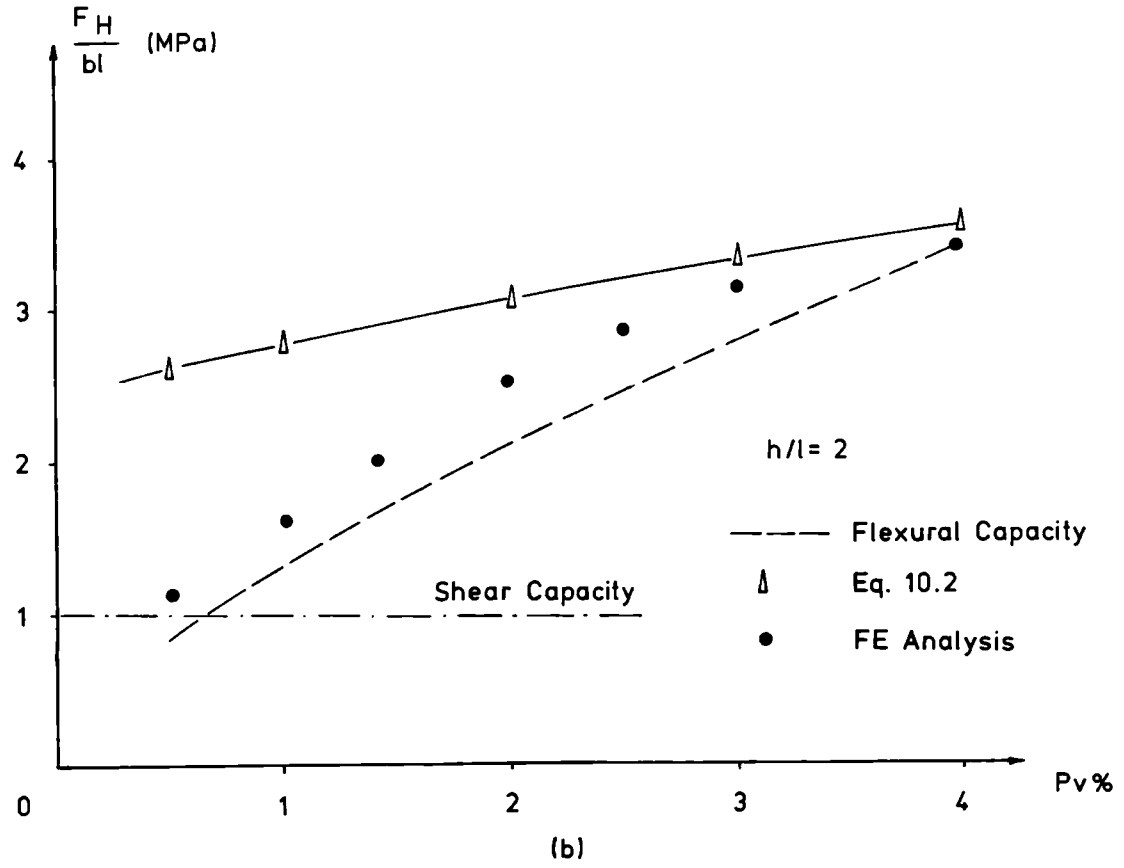


Fig. 10.5. Validation of Eq. 10.2 with values obtained from FE Analysis for walls without horizontal reinforcement and with height to width ratio of (a) one and (b) two.

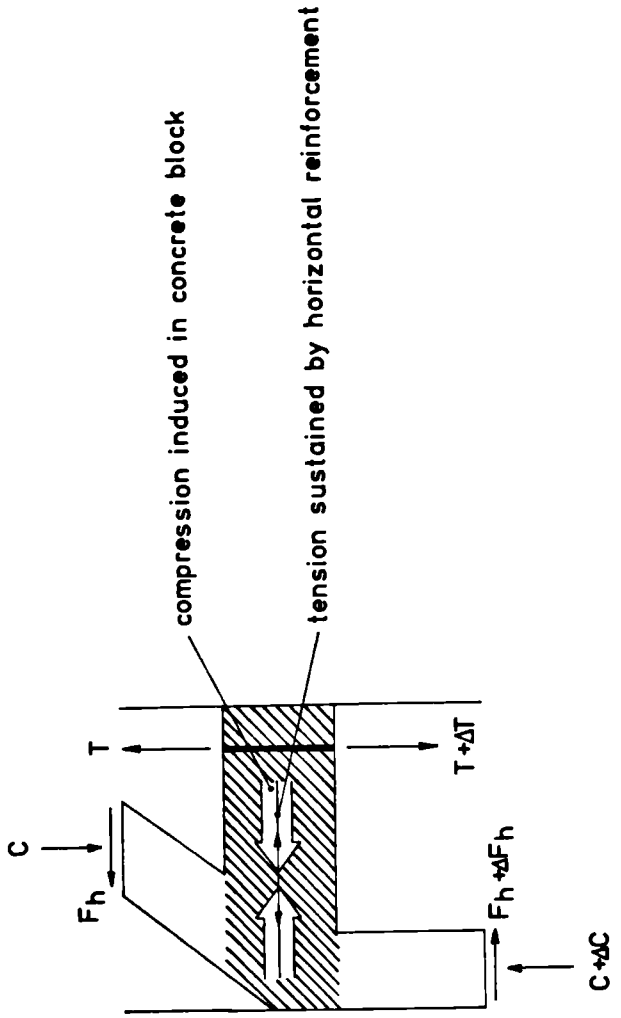


Fig.10.6. Effect of horizontal reinforcement on proposed model in the region where path changes direction.

CHAPTER 11

BEHAVIOUR OF STRUCTURAL WALLS DURING THE KALAMATA (GREECE) EARTHQUAKE OF 1986

11.1. INTRODUCTION

This chapter initially presents the source characteristics of the Kalamata earthquake of 1986 and a brief description of the damage caused by the event to masonry and reinforced concrete frame systems. It then concentrates on the performance during the earthquake of reinforced concrete buildings incorporating structural walls. The conclusions drawn from the analytical and experimental part of the work help to identify and explain the causes of the observed damage to structural walls in the town. Finally, the inelastic behaviour and structural damage experienced by the walls of a one storey school building are discussed and compared with the analytically predicted strength, deformation characteristics and mode of failure obtained using the non-linear finite element technique.

11.2. EARTHQUAKE SOURCE CHARACTERISTICS

In September 1986, two earthquakes of moderate magnitude occurred in Kalamata, southern Greece causing extensive damage to masonry and reinforced concrete structures and the total or partial collapse of seven large buildings. The death toll was twenty people while the number of injured was more than one hundred. As reported by Elnashai et al (1987), the main shock had a magnitude M_S of 5.7 (± 0.2) and the main aftershock, which occurred two days later, a magnitude M_S of 4.6 (± 0.2). The epicentral distance of the two events was approximately 10 and 8 km away from the town centre respectively, and the focal depth of both earthquakes was 8 km (see Papazachos et al, 1986). These features explain why the damage was concentrated in the town of Kalamata and in villages located on the East side, a short distance from the town.

The strong motion records, obtained at the basement of a seven storey and a three storey building in Kalamata, showed relatively large horizontal ground accelerations with maximum values of 0.27 g and 0.25 g, for the main shock and the main aftershock respectively. The great degree of similarity between the two records clearly indicates that soil conditions had an insignificant effect on the ground motion. Observed failure modes were not associated with foundation

problems. As expected, from a near field event, considerable vertical accelerations were also recorded. The recorded peak vertical ground acceleration values were 0.22g and 0.08g for the main event and the strongest aftershock, respectively. However, the peak vertical acceleration was out of phase with the peak horizontal acceleration, while the vertical component of vibration was of higher frequencies than the two horizontal.

The elastic horizontal spectral acceleration values were significantly high. The amplification factors for a 5% damping for the main event were 3.3 and 4.4 for the longitudinal and the transverse component respectively. The corresponding amplification values for the aftershock were 3.1 and 3.2 respectively. The characteristic fundamental period of the recorded horizontal ground motion ranged between 0.15 and 0.80 seconds. Despite the short duration of the event (approximately 6 seconds), such features are indicative of the nature of the ground motion and the severity of the shock, since the dynamic characteristics of most of the structures in the town were within this period range.

It should be noted that according to the 1959 Greek Earthquake Resistance Regulations for Building Construction the base shear coefficient implicit in the quasi–static design adopted by the engineers for the region of Kalamata varied from 0.06 to 0.12 depending on the subsoil conditions. The 1984 additional clauses of the Greek code recommended an increase of the coefficient by 50% only for buildings that should remain operational after the earthquake, thus introducing an importance factor. Thus, the ground motions recorded in Kalamata considerably exceeded the levels of acceleration anticipated by the Greek Codes. Even the reduced values of spectral acceleration, accounting for a ductility factor as high as 3 (typical for a well constructed R.C. building) were higher than the values of the base shear coefficient recommended by the Codes.

11.3. DAMAGE OBSERVATIONS IN THE EPICENTRAL AREA

Unreinforced Masonry Buildings

Most of the buildings in the old town were two storey high masonry structures and were mainly built before the Second World War. Unreinforced stone or brick masonry and mortar of low cement content were the materials most commonly used. Almost 60% (1700 of 3000) of the masonry structures experienced severe damage. Even crudely detailed framing, of any sort, gave considerable protection to the majority of the remaining 40% of the structures. Two typical damage

patterns were observed:

(a) For the poor quality unreinforced masonry structures, exterior walls (mainly of the second floor) partially collapsed, dragging down as a consequence in most cases parts of the roof.

(b) For the better quality masonry structures, the most significant damage was characterised by diagonal cracks in the load bearing walls of the ground floor and in the pillars of the first and second floors between consecutive openings, as well as by separation of the inadequate wall to wall connections at the corners or at the level of the lintel beams.

The above features, combined with the narrow streets of the old town, resulted in a number of casualties.

The majority of churches and monumental buildings of the town were built with unreinforced stones or bricks and suffered considerable damage during the earthquake. In some cases, the dome or the bell towers of churches collapsed.

Reinforced Concrete Frame Structures

After World War II, reinforced concrete multistorey structures became the popular building technique in Greece. The age of the reinforced concrete (R.C.) buildings of Kalamata is 5 to 10 years. This type of construction covered the area south of the old town, between the town centre and the coast, as well as the east suburbs of Kalamata. Multistorey R.C. buildings exhibited a wide range of responses during the earthquake, ranging from undamaged to damaged beyond repair.

There were many examples of severe damage of reinforced concrete frame structures with masonry infill panels. They were either three to six storey buildings of the new town or more recently built two to three storey buildings of the east suburbs of the town which were closer to the epicentre. In both cases the damage was confined to buildings with either a few or no infill panels at ground floor (known as "pilotis"). Open ground floors were designed for car parking and showrooms or shops with glazed fronts. In the case of "strong" ground floor the structural damage was minimal but the damage to the infill panels was widespread along the building height. The above type of construction together with poor building techniques and quality of materials were mainly responsible for the three total collapses during the earthquake.

Extensive damage was also observed in two or three storey buildings with lightly reinforced and inadequately confined short columns at the basement. In many situations, an opening left for ventilation at the top of the infill panel between consecutive columns of the ground floor resulted in a "short column" susceptible over its exposed length to severe damage. In contrast to the above cases of extensive damage, well constructed symmetrical buildings with "strong" ground floor suffered slight or no damage, resulting in a non-uniform distribution of damage to R.C. buildings in Kalamata.

The damage experienced by the structural elements of the R.C. frame structures was as follows:

(a) Extensive damage to beams was very limited. Only in a few cases flexural and shear cracks in the flexural and shear spans of beams were observed. The most common feature was the almost vertical cracks near the beam-column joint due to lack of proper anchorage of the beam reinforcement to the beam-column joint region, which sometimes led to full separation of the beam from the column. Usually these cracks were extended to the slab for a length equal to the effective width of the flanged beam. Lack of detailing of the corner beam-column joints resulted in shear failure of the joint. The constructional deficiencies in the detailing of the joint involved insufficient anchorage of beam reinforcement, lack of horizontal and vertical stirrups in the joint and inappropriate lap splicing of the vertical bars of the column in the joint.

(b) The majority of structural damage in Kalamata was concentrated in vertical elements (i.e. columns in frame structures), since in most cases the sum of the moment capacity of the columns above and below the joint was smaller than the sum of the moment capacity of the beams converging to the same joint (i.e. violation of the weak beam - strong column concept). When the confinement of the column with closely spaced stirrups was adequate, but the confinement was not continued into the beam-column joint, flexural failures were observed. They were characterised by horizontal cracking at the top or bottom of the column combined with crushing of concrete and buckling of bars which was more extensive and widespread for ground floor columns where the level of axial force was high. Brittle failures were observed in cases where confinement and lapping of reinforcement were inadequate. In improperly designed elongated columns (i.e. columns with length to width ratio higher than 1.5 but less than 3) extensive inclined cracking covered the middle region of such elements, leading to failure in some cases. Criss-crossing diagonal

cracks were common in the short columns of the basement or in cases where lintel beams were constructed at the top of shop doors of the ground floor.

(c) Staircases, propped against intermediate heights of columns, caused short column conditions and led to similar crack patterns with those discussed before. The detrimental contribution of staircases to the seismic response of R.C. buildings was significant in 10 to 15 years old buildings. Such staircases were eccentrically placed and this fact together with the flexible ground floor columns resulted in significant mass and stiffness asymmetry and damage to the columns distant from centre of rotation.

11.4. BEHAVIOUR OF REINFORCED CONCRETE STRUCTURAL WALLS

The use of reinforced concrete walls in the buildings of Kalamata was not as widespread as the use of R.C. frame type of construction. The satisfactory performance of structures containing symmetrically placed reinforced concrete walls was convincingly demonstrated during the Kalamata earthquake. Furthermore, despite the fact that in some cases they exhibited inadequate behaviour for reasons which will be discussed later, they proved to be superior to frame structures in resisting the lateral forces induced by the earthquake. This was verified by the fact that none of the buildings incorporating walls suffered even partial collapse, while at the same time, walls were found to be very efficient in limiting non-structural damage.

Three types of structural walls were encountered in Kalamata representing three distinct stages of reconstruction of the urban areas of Greece with multistorey buildings after World War II. Structural walls were scarcely constructed in Greece before 1930 but it was the 1959 Code that first indicated the importance of structural walls to withstand the horizontal forces and to offer stiffness to the structure. This Code (Article 8) set a number of requirements concerning their symmetrical position in the plan view and their uniformity along the height. The presence of walls in both directions of the building with a total cross-section area of $^1/_{500}$ or $^1/_{800}$ (depending on the regional seismicity) of the total area of the above storeys was considered adequate. Their thickness should have been at least 150 mm when both ends joined columns or transverse walls, or otherwise 200 mm. The recommendations concerning the amount of reinforcement were for a grid of 8 mm bars per 250 mm at each face of the wall web and two vertical bars of 14 mm diameter at each end in case columns were not designed for the end regions.

Such design provisions resulted from 1959 to early 1970's in the wide use in construction of "pseudo walls" or extended columns with height to width ratio greater than or equal to one and width to thickness ratio between 4 and 6. It can be easily calculated that for this type of walls the percentage of uniformly distributed horizontal and vertical reinforcement of the wall web was as low as 0.15 or 0.2%. The purpose of these walls was to replace the old system of two columns connected with unreinforced masonry infill panels.

By the mid-1970's, R.C. wall core units were used around the perimeter of the space left for the lift, while in a number of cases these walls were extended around the staircase.

By the early 1980's, buildings with symmetrical layout of large walls were constructed. In most of these walls, adequate confinement of vertical reinforcement at the wall edges was provided. This type of construction became fashionable after 1984, when the additional clauses of the Greek Code were issued, after the earthquakes of 1978 and 1981, which had severely shaken Salonica and Athens respectively. The additional clauses increased the minimum horizontal and vertical reinforcement percentages of the wall to 0.25 and the minimum vertical reinforcement of the wall edge members to 4 bars of 14 mm diameter, while they suggested that the latter reinforcement should be well confined with 8 mm diameter stirrups spaced at half the wall thickness. The basic shortcomings of these clauses are as follows:

(a) Only the vertical reinforcement of the wall edges is considered in the calculation of the wall flexural capacity.

(b) The design of horizontal web reinforcement is based on the truss analogy concept while the influence of vertical reinforcement on the concrete contribution to the wall shear capacity is ignored. Furthermore, flexural and shear reinforcement are designed independently.

Most of the damage to buildings incorporating walls in Kalamata was due to the conceptually inappropriate presence of walls on the plan of the building. Eccentrically placed pseudo walls and core wall units were severely cracked during the earthquake since they were the stiffest elements of the structural system and thus attracted most of the lateral force (see Figure 11.1(a)). In addition, such wall construction resulted in undesirable torsional effects that damaged the top of the vertical elements (i.e. columns and infill panels) of the building furthest from the wall units particularly in cases where the open ground floor concept was

adopted. In a few cases, the poor overall structural configuration of buildings with isolated adequately reinforced walls resulted in moderate damage of structural and non-structural elements even though the walls in the buildings had suffered only hairline cracking.

The second cause for inadequate behaviour of walls in Kalamata during the earthquake was poor construction techniques and practices. The most common constructional deficiencies observed were:

(a) The inadequate preparation of the surface of the construction joint before the casting of the walls to the level of the next floor. Since the highest level of shear forces was developed at the ground level most of the observed failures due to cold construction joints were concentrated in this level (see Figure 11.1(b)). In a few cases waste material or pieces of the wooden mould were responsible for the slip of the wall at the construction joint.

(b) The insufficient length of anchorage and lap splicing of the vertical bars of the upper and lower parts of the wall between consecutive floors. Even in cases where the length was adequate, no special arrangement for the confinement of the area along the height of the splicing was considered.

Excessive confidence in the strength capacity of a structural system incorporating walls may have led to improperly dimensioned and inadequately detailed walls. Failures due to the above causes were more common in buildings between 5 and 10 years old. The two main modes of failure observed were as follows:

(a) Early shear failures before the yielding of the main vertical reinforcing bars. Such failures occurred at the ground floor and were characterised by a pair of inclined cracks at the top or mid-height of the wall depending on the height to width ratio, for the cases of inadequate anchorage of the vertical bars to the top beam or slab interface (see Figure 11.1(c)).

(b) Failure of the lower compressive zone of the wall usually accompanied by local buckling of the main compressive steel of the wall edge due to insufficient lateral steel restraint (see Figure 11.1(d)). For this type of failure extensive cracking of the wall web was observed in a number of cases, since the 1959 Code provisions recommended percentages of horizontal reinforcement lower than the nominal values generally specified by current Code provisions.

Such modes of failure are in compliance with the results of the analytical and experimental investigation of the present thesis which led to the design implications fully described in Chapter 10. The backbone of such implications is the concept that wall "shear" resistance is associated with the development of tensile stresses in the region of the path along which the compressive stresses are transmitted from the overlying storey to the wall foundation. Since most of the walls investigated by analysis and testing followed the crack pattern and the mode of failure described in item (b), it is interesting to discuss the analytically predicted deformed shape and mode of failure of walls with height to width ratio of 2 and 1 presented in Figure 11.2. In both cases, the wall unit was reinforced with adequate vertical reinforcement to withstand the combined action of bending moments and axial load while the amount of horizontal reinforcement was below the nominal (for the 1984 Codes) value and also due to the assumption of inadequate anchorage of the vertical bars to the beam or slab, a low value of stiffness was provided to the top steel elements. As this figure shows, both walls presented local distress and deterioration of the stress transfer mechanism in the region where the compressive force path changes direction (see physical models, Section 10.5) before the occurrence of any yielding of the vertical reinforcement. Such a failure is similar to early shear failures observed in Kalamata and can be explained by the concept of the compressive force path.

The satisfactory performance of buildings with symmetrical layout of well designed and detailed walls, as well as the 30% of the buildings that suffered no damage, during the Kalamata earthquake indicate that the earthquake resistant design of structural systems may depend less on the concepts of base shear coefficient and linear elastic spectra and more on the proper insight of the mechanisms of resistance of various structural elements to the ultimate limit state.

11.5. CASE STUDY : WALL FAILURES IN THE 18th PRIMARY SCHOOL OF KALAMATA

Back-analysis of structural elements or systems damaged during an earthquake require a detailed knowledge of the structural design and the construction details of each case, since the measurement of the dimensions of the building on site and the approximate estimate of the reinforcing details and the properties of the materials used in the building can only lead to a crude assessment of the actual hysteretic behaviour of the building during the earthquake. Fortunately, the complete structural design of a damaged one-storey primary school of Kalamata incorporating two structural walls in its plan view was available to the author through colleagues

of the National Technical University of Athens (P. Plaines, 1986), who had undertaken the repair of the school. The observed damage of the building will be described and discussed in the following sections while the analytical investigation will be focused on the strength, the crack pattern and the mode of failure of the two walls.

11.5.1. DESCRIPTION OF THE BUILDING

The 18th Primary School is a one storey building situated approximately 1 km East of the town centre near the main road linking Kalamata with the east suburbs. As the drawing of the plan view of the building included in Figure 11.3 shows the building presents an unusual architectural design, which was mainly responsible for its severe but repairable damage during the earthquake. In fact the building consists of two individual regions (region A and region B in the figure) with a cold joint between them filled with neopren. The joint is formed in the area where the 41 m x 41 m square configurations of the two separate buildings overlap each other.

In each square an 8 m diameter centrally positioned circle opening interrupts the slab of the top floor for natural illumination. A structural system of nine radially expanded series of columns and inverted beams covers like a fan three quarters of each building. The circular columns of the square perimeter have a diameter of 0.3 m, the columns nearer to the opening are 0.3 m wide and 0.5 m long, (lying on the circumference of a 6 m diameter circle), while the intermediate columns are 0.3 m wide and 0.8 m long (lying on the circumference of an 18m diameter circle). Masonry partitions formed nine classrooms in the region between the nearer to the square centre columns and the intermediate columns of each buildings. A ribbed top slab with a total depth of 0.35 m covers the above region and results in a considerable dead weight for the vertical elements of the building.

The structural system of the remaining quarter of each building consists of three frames 4.5 m apart from each other. The frames are 16 m long and two of them end in 0.4 m x 0.5 m columns. A similar column stands at one end of the third frame while at the other end a thinner 0.3 m x 0.4 m column is extended in the EW direction towards the nearest frame and forms a structural wall 2 m wide. An inverted beam, 0.5 m wide and 1.5 m deep, forms the top of the frame. Unreinforced masonry panels were constructed between the columns of adjacent frames in the EW direction. A top flat slab of 0.12 m covers this

region. The clear height of the buildings is 3.2 m throughout. The ground floor consists of a 0.15 m flat slab resting on the connecting beams of the footings of the vertical elements resulting in a shallow foundation.

Wall Details

A closer look at the walls with height to width and thickness to width ratios of 1.6 and 0.15, respectively, reveals the following:

(a) The vertical reinforcement of the wall edge that forms the column of the frame consists of 14 deformed bars of 20 mm diameter and 2 deformed bars of 16 mm diameter. The vertical reinforcement of the other edge consists of only 2 deformed bars of 14 mm diameter.

(b) The vertical and horizontal reinforcement of the wall web consist of a double layered uniformly distributed grid of 8 mm mild steel bars per 0.25 m.

(c) The ultimate tensile strength of the steel bars is approximately 550 MPa for the deformed bars and 450 MPa for the plain bars. The average cube strength of concrete in the structure is 38 MPa. This value was determined using the average value of three different methods for in situ cast concrete. The methods adopted were the core testing, the rebound hammer test and the ultrasonic pulse velocity test.

Walls, instead of columns, were used in positions A_1 and B_1 (see Figure 11.3) in order to stiffen the structural system in the EW direction and minimise excessive horizontal displacements, as well as to eliminate pounding of the two buildings in EW direction.

11.5.2. DAMAGE TO THE BUILDING

Both regions of the building were severely damaged during the earthquake but the degree of damage of the vertical structural and non-structural elements of region B was more extensive. The distribution of damage showed the following characteristics:

(a) Most of the infill panels between the columns, and the partitions were extensively cracked in both EW and NS directions. In particular the EW infill panels crossing the cold joint area were pulled down while the central

heating main pipes were distorted indicating significant movement of the two regions and probably a restraint of the lateral movement of each region imposed by the other.

(b) Only light damage was observed in the peripheral circular columns and in the columns nearer to the centre of each "square". The damage was concentrated either at the top part of the columns due to eccentric horizontal loading or on the lower part of the columns due to excessive bending moment combined with high axial forces. However the intermediate columns, and in particular those with NS orientation, were severely damaged by the earthquake. The damage to these elements was due to the combined effect of high lateral forces imposed by the earthquake and torsional moments. Therefore, inclined cracks commenced at the top part of the columns and descended to the bottom part winding round the column. Some individual inclined cracks due to shear boundary forces were also observed.

(c) The top and bottom slabs were found intact and no differential settlement was noticed for any of the vertical elements. This implies that the bottom floor level may be considered as a fixed base for the seismic response of the vertical elements and that the hefty top slab moved as a rigid body plate transmitting the dead weight and the lateral forces due to the ground movement to the vertical members in proportion to the lateral stiffness characteristics of these elements.

(d) As Figure 11.4 illustrates, the post earthquake crack pattern of wall A_1 indicates less damage than the corresponding pattern of wall B_1. For wall A_1, two deep diagonal cracks with relatively small widths can be observed starting from the top west corner and heading towards to the lower east corner of the wall, stopping 15 cm away from the east side. A series of two flexural cracks near the wall base, the lower being quite deep, and two or three hairline diagonal cracks can also be observed starting from the East side and moving towards the west side, criss-crossing the previous cracks in the lower third of the wall web. These cracks, like the previous ones, did not manage to penetrate the corresponding wall edge. Spalling of the concrete cover at the top part of the west edge can be also observed.

While wall A_1 was moderately damaged during the event, wall B_1 failed in flexure due to fracture of the main vertical reinforcement of the west edge member accompanied by extensive near vertical splitting and concrete cover spalling of the lower east edge member. Also it should be noted that the

crack widths of the deepest criss-crossing inclined cracks and the primary flexural crack remained visibly open after the earthquake since the residual top horizontal displacement after the wall failure was approximately 3 to 4 cm.

11.5.3. ANALYTICAL RESULTS AND DISCUSSION

The analytical modelling of the walls is similar to that adopted in Section 9.2 for the comparative study of the experimental and analytical wall responses. A simplified mesh of 7 x 7 concrete elements and an equivalent steel area representing the vertical and horizontal reinforcement arranged at the boundaries of the concrete elements were used. The material properties employed for the analysis were those described in detail in Section 11.5.1. It is interesting to note that the walls were identically reinforced but lacked symmetry in the reinforcement arrangement which resulted in different strength and deformation characteristics when cycled in the east or west direction. Hence, two analytical runs were carried out, which made use of the same model incrementally loaded to the ultimate limit state with uniformly distributed edge pressure (in opposite directions for each run) along the upper boundary of the wall. Following this procedure an upper bound of the horizontal load capacity of the walls to either East or West direction was obtained.

Figure 11.5 shows the analytically predicted horizontal load-top horizontal displacement curve of both analyses. The figure indicates that only for the early load steps (up to a horizontal load of 200 KN, corresponding to the uncracked wall phase) the response of the wall to top horizontal loading is similar for both directions of loading. After the initiation of flexural cracking, the deflection of the wall with the smaller amount of reinforcement in the tensile edge began increasing faster than the deflection of the wall with the higher amount of tensile reinforcement for the same increment of horizontal load. At a horizontal load of 400 KN first yielding was observed of the outer tensile reinforcement and the vertical web reinforcement, nearer to the tensile edge, while after 520 KN the wall started behaving "plastically", with almost half of the tensile reinforcement and some of the horizontal reinforcement having reached its yield strength. The analytically predicted ultimate horizontal load for this case was 720 KN and corresponded to a displacement of 8.2 cm. Such an ultimate displacement value is in compliance with the observed residual top horizontal displacement of wall B1, since after failure the magnitude of residual displacement is equal to about a third to a half of the ultimate value. The analysis also showed that at the above load level the outer tensile reinforcement was fractured, accompanied by vertical splitting of the lower compressive edge of the wall.

In contrast, the analysis of the wall with the higher amount of reinforcement in the tensile edge indicates that at a horizontal load level of 800 KN the wall experienced a top horizontal displacement of only 0.5 cm while the outer tensile reinforcement had just reached its yield strength. In fact, the analytically predicted ultimate horizontal load for this particular case was 1500 KN with a corresponding top horizontal displacement of 2.35 cm.

Figure 11.6 depicts the crack pattern and deformed shape plot of both walls (displacement magnification factor of 10) corresponding to the ultimate horizontal load level of the wall with the smaller amount of tensile reinforcement. This figure clearly illustrates the considerable differences in the crack formation and the amount of lateral displacement of the two walls. It is interesting to note that, while for wall B_1 (with smaller amount of tensile reinforcement) cracks are mainly flexural and cover two thirds of the wall height, in the case of wall A_1, the formation of two inclined cracks initiating from the top and extending through the web towards the lower compressive zone is evident as well as their inability to penetrate yet the latter zone. Another important feature of the crack pattern of wall B_1 is the complete loss of load-carrying capacity of the concrete (denoted in Figure 11.6 by crossed single and double lines) in the region of the deepest flexural macrocracks adjacent to the tensile reinforcement bars.

Based on the above analytical results, which verify the well accepted view that earthquakes always penalise the asymmetric reinforcement arrangement of vertical elements, it is possible to give a reasonable explanation of the different behaviour of walls A_1 and B_1 during the earthquake. After a number of pre-yield cycles which only slightly cracked both walls, the excitation of wall B_1 towards the east direction under the maximum horizontal acceleration of the event resulted in the flexural failure of wall B_1 and in the two significant diagonal cracks of wall A_1. Then, the maximum excitation to the west side (even though considerably smaller in acceleration content to that to the east side) had as a result the less deep series of flexural cracks of wall A_1 and the opening of a diagonal crack joining the failed in tension edge of wall B_1 with the top east corner of the wall. The distortion of the top west and east concealed columns of walls A_1 and B_1 respectively should be attributed to torsional effects due to the movement of the roof in the NS direction and to inadequate anchorage detailing of the vertical bars to the top beam.

The shear strength of these walls predicted by the Code, ignoring the concrete contribution (as recommended by Codes for high seismicity areas), is about 435 KN, which is only 65% of the ultimate horizontal load that wall B_1 withstood before failing in flexure and wall A_1 survived with just two diagonal cracks. Such a

performance once more points out how unsuitable (even though conservative in this case) is the truss analogy to form a reliable basis for "shear" design procedures. It also verifies the validity of the compressive force path concept as a practical design tool. It is interesting to note that even though the amount of horizontal reinforcement was below nominal, the wall elements did not fail early in shear at an intermediate height along the wall height since the concrete alone was sufficient to carry the tensile stresses developed in the region of the compressive force path (i.e. $M_{cx} > M_{fx}$; see Chapter 10).

11.6. CONCLUSIONS

The main conclusions drawn from the field observations in Kalamata and particularly the behaviour of buildings with R.C. walls may be summarized as follows:

(a) Although the Kalamata earthquake was near field event of moderate magnitude, it caused extensive damage to masonry and reinforced concrete structures whose dynamic characteristics were within the fundamental period range of excitation.

(b) Various types of damage to masonry buildings and R.C. frame structures with infill panels were observed. Much of the damage was concentrated on buildings with few or no infill panels at the ground floor. Beam–column joints, columns (long and short) and partitions were the areas of framed structures severely hit by the earthquake.

(c) Structures incorporating symmetrically placed R.C. walls as the principal means of resistance to loads caused by the earthquake ground movements were proved superior to R.C. frame structures and performed satisfactorily during the event.

(d) The damage to buildings with walls was mainly due to inappropriate presence of walls on the plan view. Eccentrically placed pseudo walls and core wall units resulted in the cracking of such elements as well as in general damage to the building. Other sources of inadequate behaviour included poor construction techniques and practices, and improperly dimensional and detailed walls. A share of the below par performance of such walls should be also attributed to 1959 design procedures of the Greek Code.

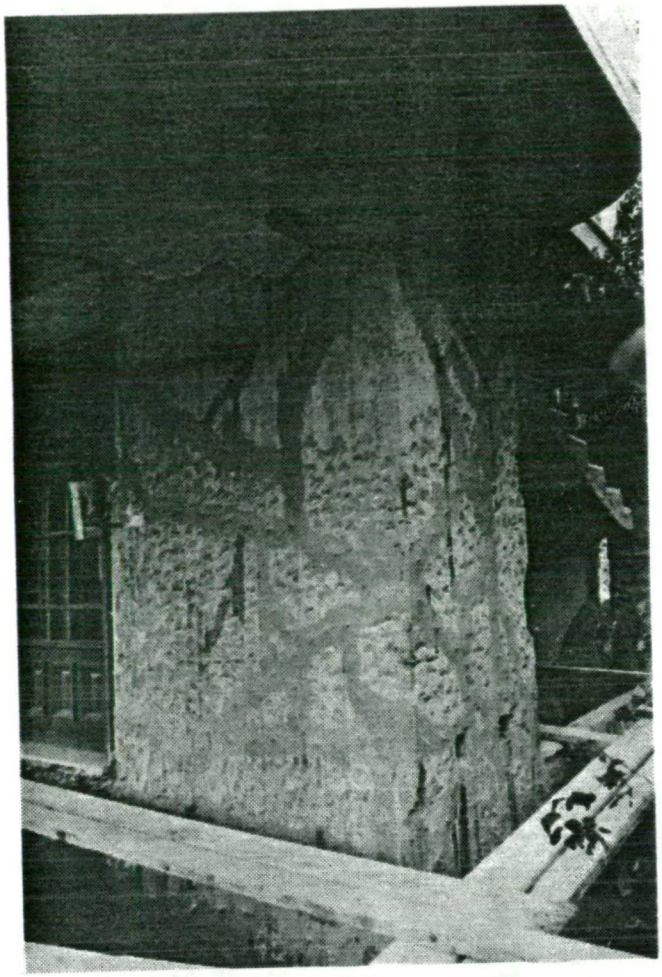
(e) Modes of wall failure observed in Kalamata are in compliance with the results of the analytical and experimental investigation of the present thesis which led

to design implications based on the concept of "the compressive force path". Walls with inadequate anchorage of the vertical bars to the top beam or slab and with amounts of horizontal reinforcement below the nominal level were found by analysis and in field surveys to fail within the region where the compressive force path changes direction. Otherwise, walls fail within the region of the lower compressive zone.

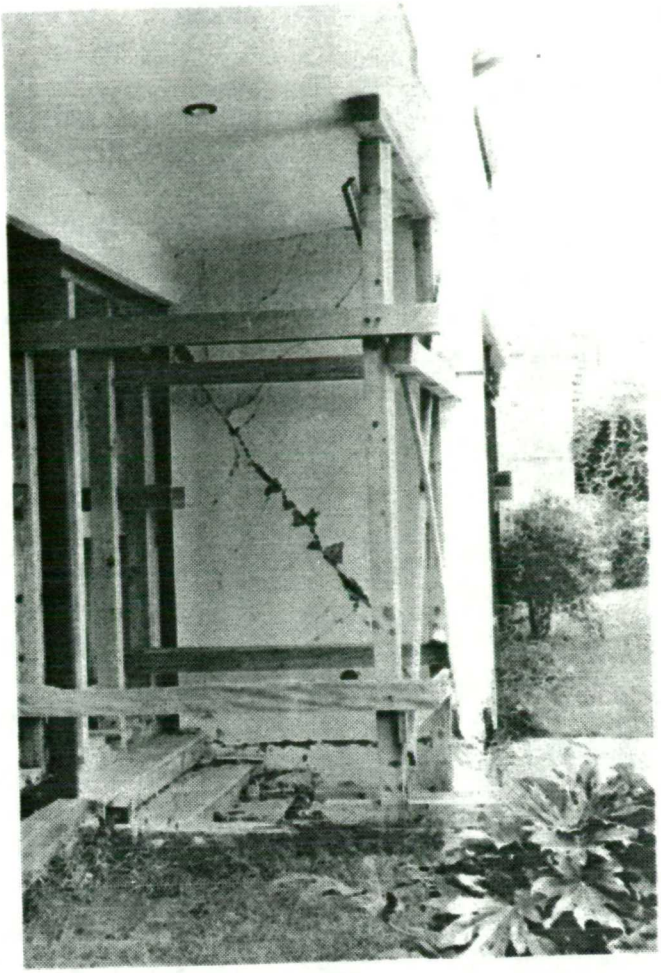
(f) The crack pattern and failure mode of the walls of a one storey school building, back analysed using the non-linear finite element technique, were in close agreement with the observed damage. The characteristics of the ground excitation and the asymmetric arrangement of vertical reinforcement at the wall edges were mainly responsible for the different extent of damage to the two walls of the structural system.

(g) The behaviour of the above walls subjected to a real earthquake input not only confirmed that the truss analogy cannot provide a safe and economic design solution but also verified that the compressive force path concept can form a suitable basis for a revision of shear design provisions.

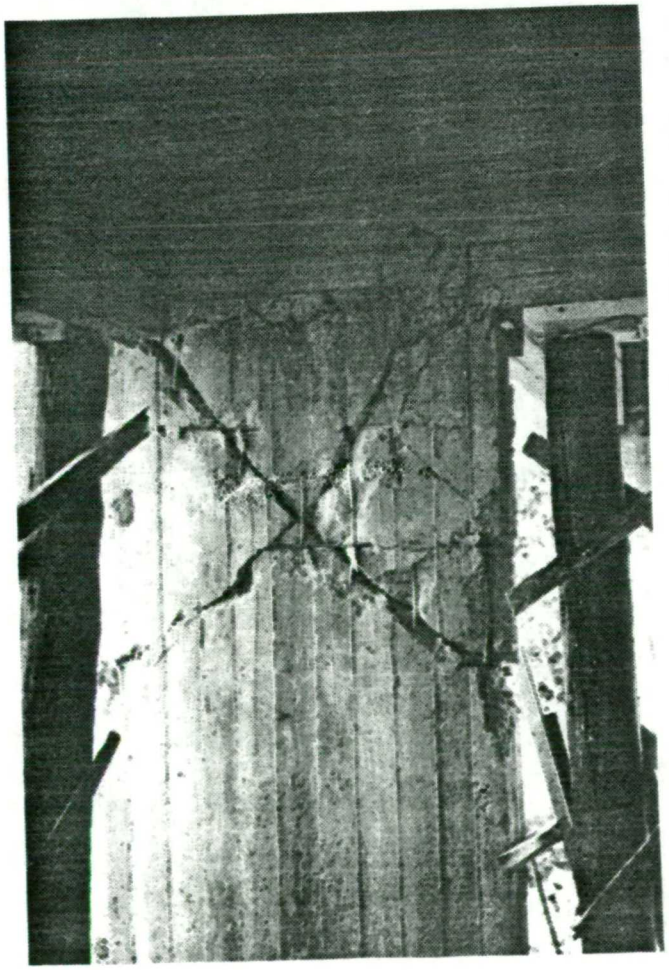
Fig. 11.1. Typical failures suffered by structural walls during the Kalamata earthquake
(a) Severely cracked core wall unit
(b) Failure of the wall at the construction joint
(c) Early shear wall failure
(d) Failure of the lower compressive zone of the wall.



(a)



(b)



(c)



(d)

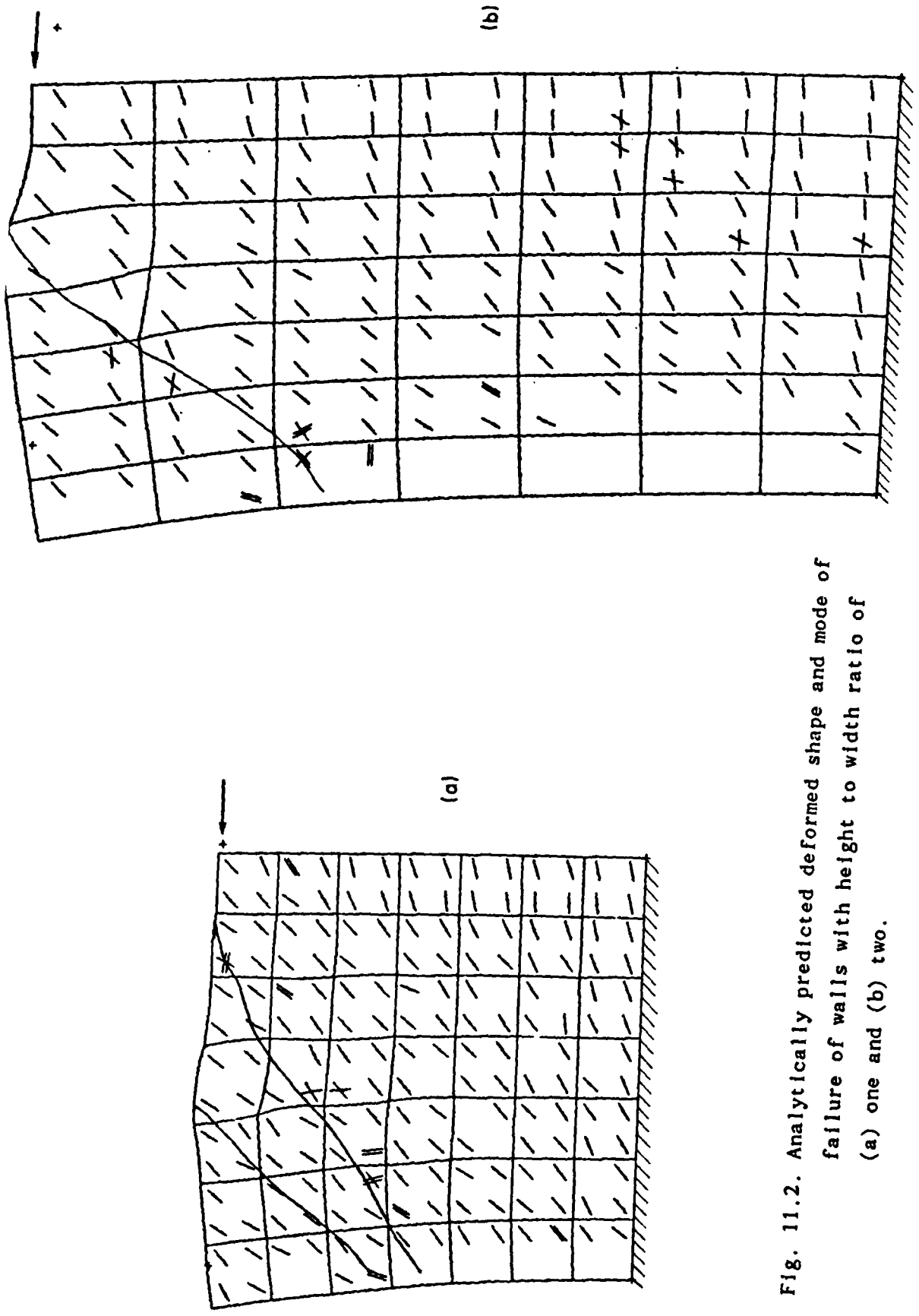


Fig. 11.2. Analytically predicted deformed shape and mode of failure of walls with height to width ratio of (a) one and (b) two.

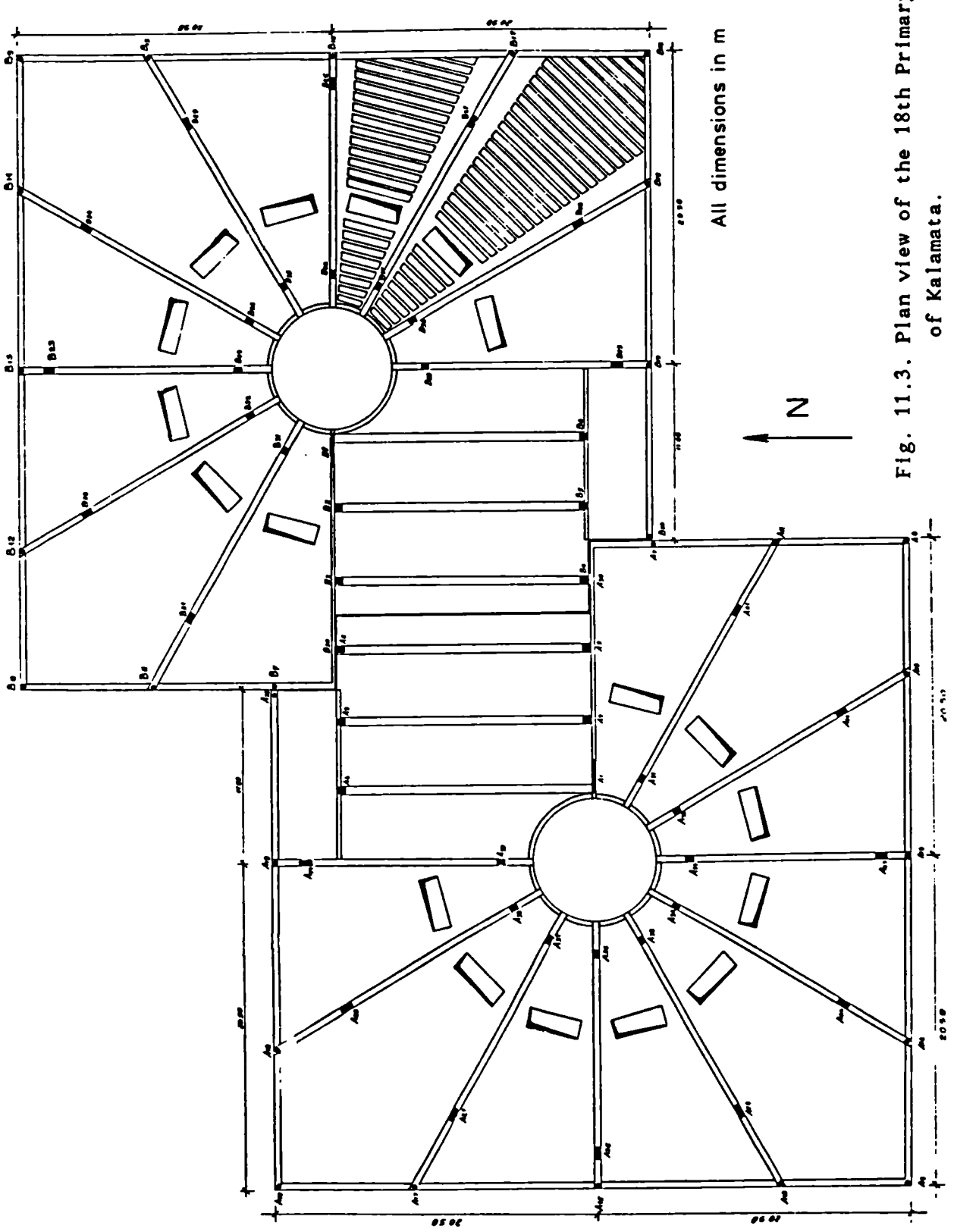
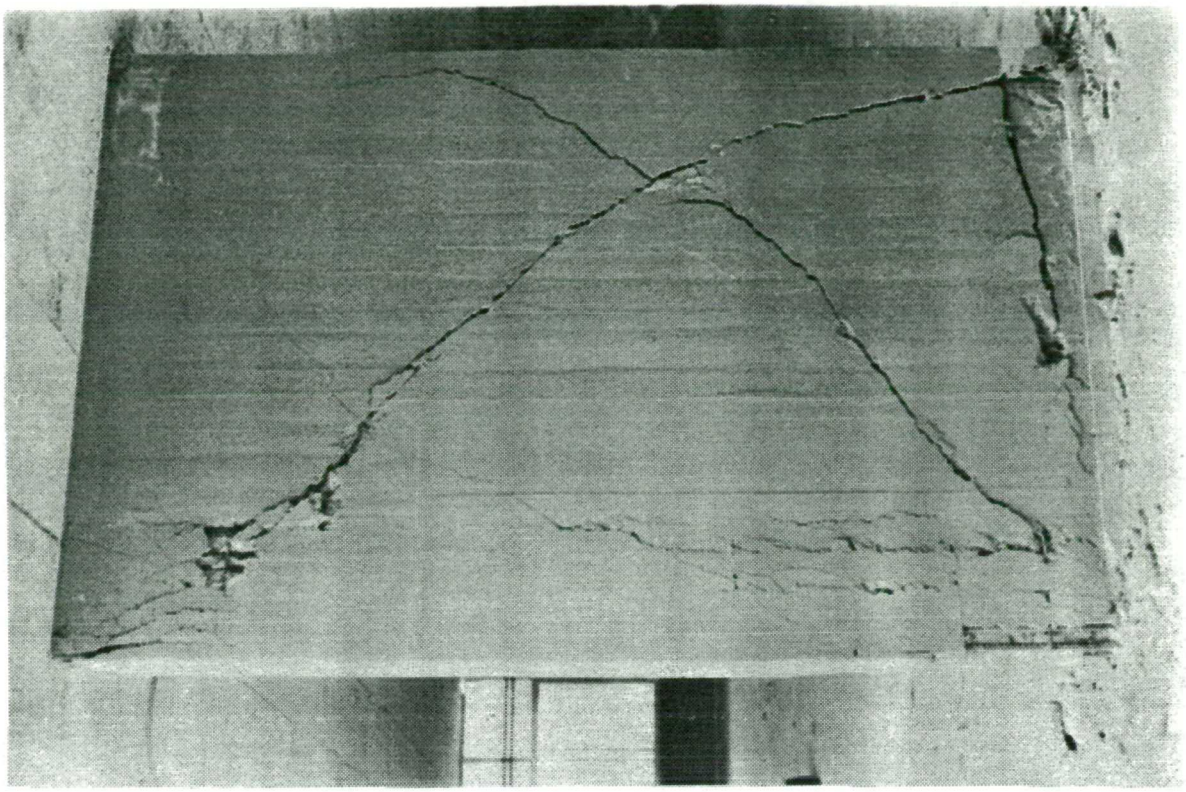
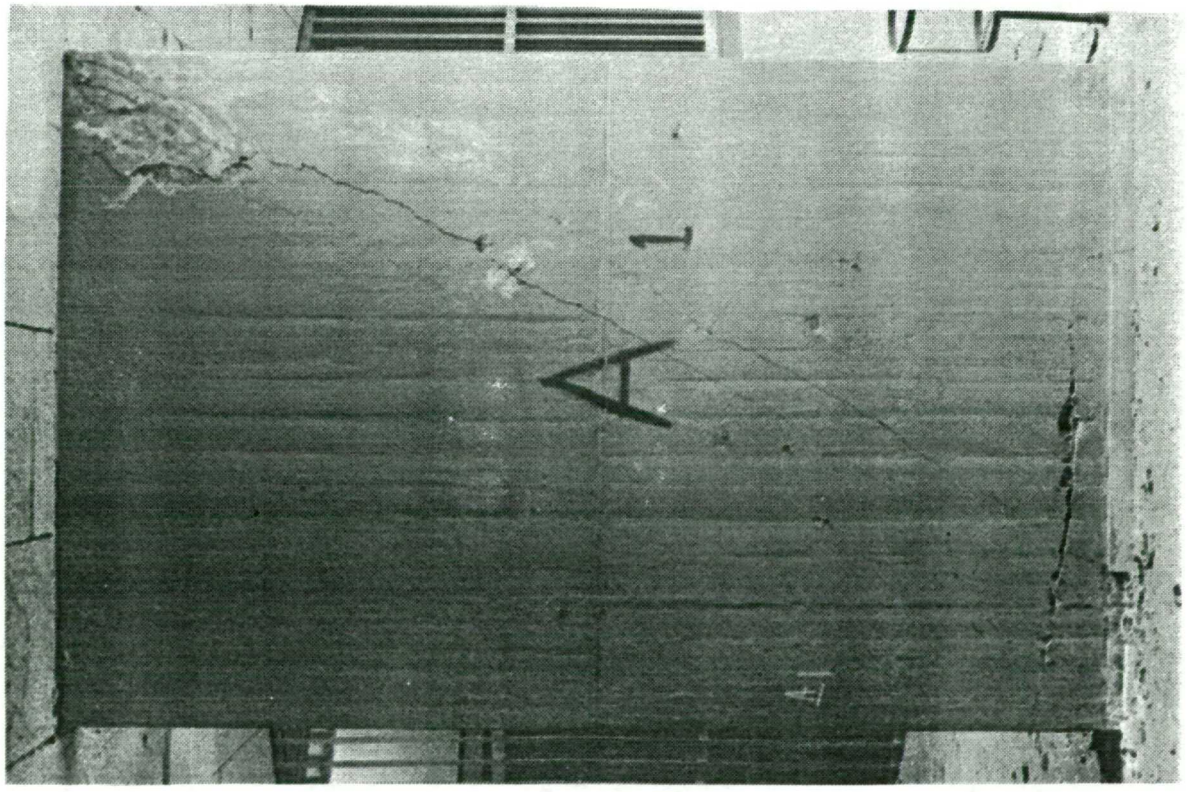


Fig. 11.3. Plan view of the 18th Primary School of Kalamata.

Fig. 11.4. Cracking suffered by walls A1 (left plate) and B1 (right plate) in 18th Primary School during the Kalamata earthquake.




A

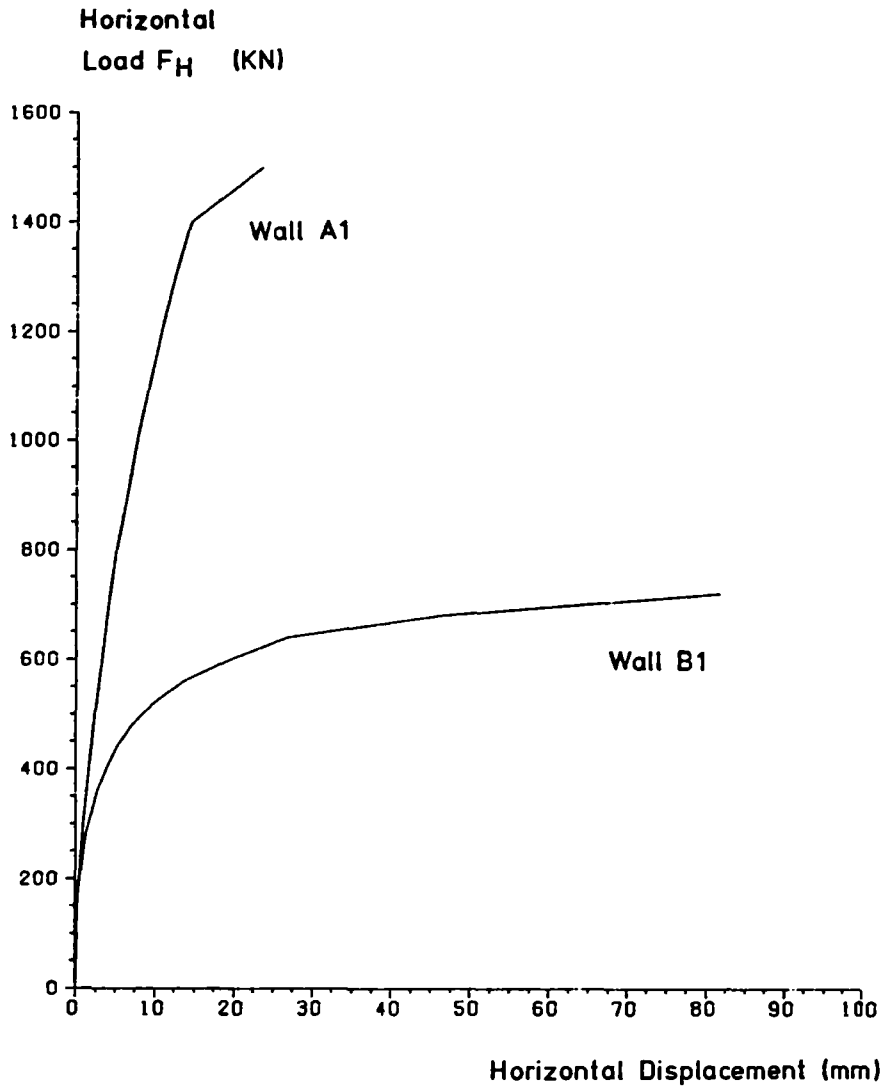


Fig. 11.5. Analytically predicted horizontal load-top horizontal displacement curve for walls A_1 and B_1.

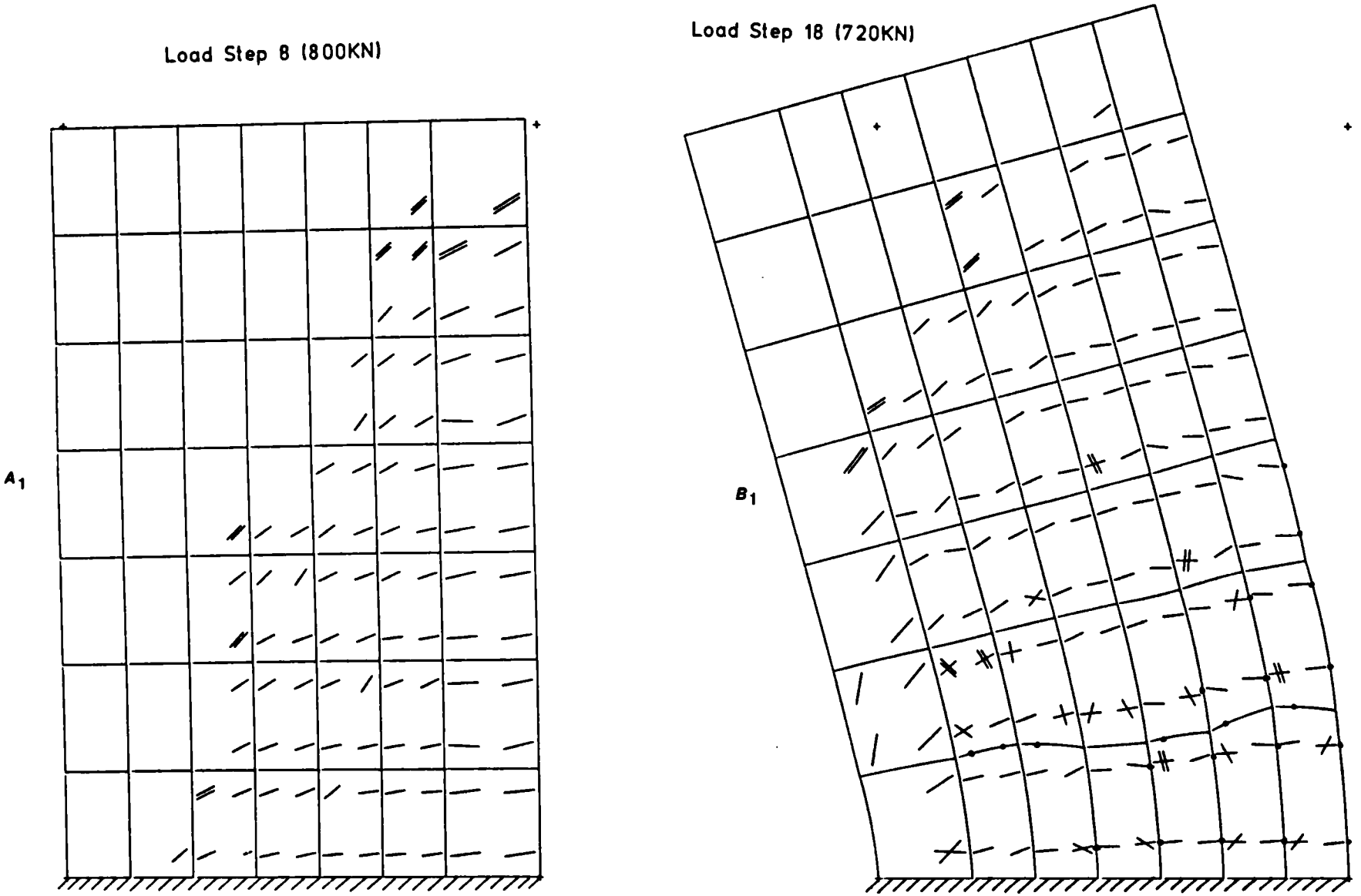


Fig. 11.6. Analytically predicted Crack pattern and deformed shape for walls A_1 and B_1 at the ultimate horizontal load level of wall B_1.

CHAPTER 12

PRINCIPAL CONCLUSIONS AND RECOMMENDATIONS FOR FUTURE WORK

12.1. PRINCIPAL CONCLUSIONS

The main analytical and experimental results presented in this thesis may be summarized as follows:

1. A literature survey indicated that it is the lack of a realistic description of the behaviour of concrete that has prevented well-established non-linear numerical techniques to realistically predict the behaviour of walls at the ultimate limit state. Furthermore, despite the fact that the behaviour of walls under different loading histories has recently been extensively studied by experiment, there remain uncertainties related to the influence of a number of parameters on the observed wall behaviour. Such parameters include the wall height to width ratio, the extent of the role of horizontal reinforcement in safeguarding against shear failure, the likelihood of vertical reinforcement - provided for axial-flexural demands - affecting the wall shear strength, the contribution of axial force to strength, ductility and energy dissipation characteristics and lastly the mechanisms of wall shear resistance. It would appear that due to inadequate provisions for both design and detailing, current Codes may have contributed to the severe damage and, in many cases, collapse suffered by structural walls during strong earthquakes. The lack of a realistic description of the underlying causes of shear failure in current design procedures is evident.

2. A non-linear finite element system, based on a realistic description of material characteristics such as failure criteria and deformational properties of concrete and steel, fracture processes of concrete, concrete-steel interaction has been found to provide a reliable analytical tool for the parametric study of the behaviour of structural walls up to their ultimate limit state. The system has been validated by comparing analytical predictions with published experimental information for a wide range of walls. A satisfactory correlation between analysis and experiment has been established for all aspects of structural behaviour investigated i.e. load-carrying capacity, deformational characteristics, crack patterns and mode of failure.

3. The extensive parametric study of the behaviour of reinforced concrete walls with rectangular cross–section at the ultimate limit state has shown that:

(a) A proper assessment of the influence of either distributed or concentrated vertical reinforcement on the ultimate strength of walls without horizontal (shear) reinforcement is lacking from current Code provisions. The likelihood of shear failure preceding flexural failure is dependent on both geometric and material wall properties. Shear strength is not a simple function of concrete strength.

(b) The expression for flexural design adopted by the ACI Code do not distinguish between "underreinforced", "balanced" or "overreinforced" wall cross–sections and hence they describe crudely the flexural capacity of the wall. Horizontal reinforcement, since it gives rise to triaxial conditions in the lower compressive zone, slightly increases wall flexural capacity.

(c) For walls failing at an ultimate horizontal load below their flexural capacity, Code predictions – based on the "truss analogy" model – are conservative for the lower range of values of the percentage of horizontal reinforcement, while they overestimate considerably the wall capacity for the upper range of these values. The inclusion of additional reinforcement in both the extreme compression and tension fibres of the wall results in a significant increase of wall capacity; this happens in spite of the considerable reduction in horizontal reinforcement.

(d) The presence of axial compressive force does not improve the effectiveness of horizontal reinforcement. The Code recommendations for omission of axial force in the calculation of wall shear strength can lead to uneconomical design, the problem becoming more severe with (a) decreasing wall height to width ratio and (b) increasing amount of vertical reinforcement.

(e) While current design is based on uniaxial stress–strain characteristics, the actual behaviour of walls at the ultimate limit–state can only be explained in terms of multiaxial effects. Hence, the uniaxial strength of concrete cannot realistically represent stress conditions of the wall failure zone and this should not be used as a normalizing factor of the wall strength.

(f) The analytically predicted mode of failure of walls is characterized by longitudinal cracking within the compressive zone near the base of the wall where the bending moment attains its maximum value.

4. The first two series of the tests have been concerned with the performance of large scale wall models with height to width ratio of one (type I) and two (type II) subjected to constant axial and monotonically increasing horizontal loading. The following principal conclusions have been reached:

(a) The experimental set-up used for tests has been found to cause insignificant out of plane displacement and base rotation, which does not affect the measured wall strength.

(b) Both types of wall, subjected to high levels of constant axial load, exhibit an increased horizontal load carrying capacity, the enhancement being higher for the type II walls. Although the recorded values of ultimate top horizontal displacement differ, small differences are observed between the ultimate drift indices.

(c) The deformational response of all walls is distinctly non-linear. Axial compression has been found to reduce not only horizontal and vertical displacement but also ductility. The rate of decrease in ductility with increasing axial load is higher for type II walls. Larger depths of neutral axis are observed with increasing levels of axial load applied to the walls.

(d) The level of axial force has a considerable effect on secant stiffness characteristics. However, the variation of secant stiffness values with increasing normalized axial load is less pronounced for type II walls. The ultimate secant stiffness of all specimens is a small portion of the stiffness exhibited in the uncracked state of the wall. Secant stiffness values for the uncracked phase predicted by currently used analytical expressions are higher than the corresponding experimental values.

(e) Wall failure starts with nearly vertical splitting of the compressive zone in the region of the tip of the inclined (type I) or the deepest flexural (type II) crack and is followed by multiple splitting of the whole compressive zone. The lower the height to width ratio and the higher the level of normalized axial load, the more extensive is the failure region within the compressive zone.

(f) A complex triaxial state of stress at the lower compressive edge of the wall is the cause for the wall resistance to high shear stresses. The triaxial compressive stresses counteract the tensile stresses due to shear forces. Such a behaviour indicates that the compressive zone rather than the wall web is the main contributor to wall resistance.

5. The third series of tests has been concerned with the performance of type II walls to horizontal cyclic loading increasing to a level close to but not beyond ultimate strength. The experimental results show that:

(a) The strength and deformational response of these walls is independent of the cyclic loading regime and the concrete strength. The monotonic load–displacement curves form an envelope to the load–displacement curves of the cyclically loaded walls.

(b) The provision of a near nominal percentage of horizontal reinforcement (far less than the amount Code provisions specify) has not affected the wall response, despite the fact that the wall was subjected to load cycles corresponding to post–yield displacements.

(c) The energy dissipated during the first load cycle is considerably higher than the amount of energy dissipated during subsequent cycles to the same displacement. The amount of energy dissipation is found to increase with the increase of the ductility ratio.

(d) Proposed semi–empirical expressions appear to predict adequately the decrease of horizontal load and the equivalent viscous damping with number of cycles at a given ductility ratio.

(e) The mode of failure and the failure mechanism of wall specimens subjected to monotonic and cyclic loading are found to be identical.

6. The comparative study of the analytically predicted and experimentally measured wall responses shows that the non–linear finite analysis programme can successfully simulate the experimental behaviour of any wall element. The typical accuracy of the analytical predictions of all aspects of wall behaviour is usually between 5 and 10%. It should be noted that the analysis accurately predicts the actual experimental mode of failure.

7. Both the analytical and the experimental results appear to indicate that the truss analogy concept does not form a suitable basis for the shear design of reinforced concrete walls, since it does not provide a realistic description of the actual "shear" resisting mechanisms of such elements. The multiaxial effects are those which govern load–carrying capacity in the region of the path along which the compressive force is transmitted from the floor beam or slab to the wall base. Wall failure is related to the development of tensile stresses in the region of the path due to a number of causes such as change in the path direction, varying intensity of the compressive stress field, stress concentrations at the tip of inclined cracks or loss of bond between tensile reinforcement and concrete. Based on these concepts a physical model, complemented by failure criteria, is proposed which realistically describes the main features of wall behaviour at the ultimate limit state. An analytical expression, initially derived for beams, is proposed to express the stress conditions leading to failure of walls without horizontal reinforcement under combined bending moment and shear force. When the capacity of the concrete to sustain alone the tensile stresses is exceeded, simple recommendations for the provision of horizontal reinforcement are proposed.

8. The inelastic behaviour and structural damage experienced by prototype walls during the Kalamata earthquake of 1986 are in agreement with the analytical findings as well as with the experimental results of the large scale wall models of the present thesis. The behaviour of prototype walls to a real earthquake input not only confirmed that the truss analogy cannot provide a safe and economic design solution but also verified that the compressive force path concept can form a suitable basis for a revision of current shear design provisions.

12.2. RECOMMENDATIONS FOR FUTURE WORK

The present work attempted to investigate analytically and experimentally the underlying causes of the observed behaviour and, in particular, the strength characteristics of reinforced concrete walls subjected to a wide range of monotonic and cyclic loading conditions. Furthermore it was attempted to illuminate pitfalls in current design procedures and to suggest a rational, safe and economic design solution for structural walls. However, the present investigation has neither exhaustively covered all the areas of wall behaviour nor uniquely answered all of the questions. In view of this, it would be highly desirable to extend the present work in the following areas:

1. Since the wall shear resistance can only be improved by strengthening the compressive force path rather than the portion of the wall below the neutral axis, additional monotonic and cyclic tests on large scale isolated walls with various cross-sections (i.e. rectangular, I-shaped, L-shaped, with openings), as well as coupled walls, are required. Such experimental programmes should be designed not only to enrich the knowledge of the influence of wall parameters on the strength of concrete within the region of the compressive force path, but also to verify and extend the present steps for the development of a sound theoretical basis for the design of reinforced concrete structures in shear.

2. Typical small and large scale wall models should be subjected to earthquake motions by using shake-table facilities driven by real earthquake records. The aim will be to establish the margin of safety of the proposed design method under actual seismic conditions. The well predicted response of prototype buildings with walls in recent major earthquakes and the encouraging pilot test of a small scale wall model on the shake-table facilities of Imperial College should form a firm foundation for such a test programme.

3. In order to alleviate any possible concern on size effects, full-scale monotonic and cyclic tests on selected properly designed wall cross-sections should be carried out. The results of these experiments should be compared with the corresponding results of large scale wall models.

4. It appears that for certain structural wall types (mainly tapered wall sections and walls with small height to width ratio), two dimensional approximations are not sufficiently realistic from a physical viewpoint and that three dimensional modelling (including full triaxial effects) must be used instead. Such a model has already been developed during a parallel research programme (Gonzalez Vidosa, 1988). Its application will be essential for an extensive parametric study of the ultimate behaviour of wall cross-sections for which the tensile stresses perpendicular to the plane of the structure cannot be neglected as too small. Such stresses often have a profound influence on the ultimate load and are likely to govern the mode of failure.

5. The existing non-linear finite element package should be extended to enable the analysis of structural walls subjected to cyclic and dynamic loading caused by earthquake motions. A parametric study of typical structural walls subjected to large load reversals should follow in order not only to provide realistic design information but also to identify critical situations which could then, in turn, be the subject of a few select experiments.

REFERENCES

ACI-ASCE Committee 326 (1962)
"Shear and Diagonal Tension",
Proceedings, American Concrete Institute, Vol. 59, Jan., Feb. and Mar., pp. 1-30, 277-334 and 353-396.

ACI-ASCE Committee 426 (1974)
"The Shear Strength of Reinforced Concrete Members",
ACI 426R-74, American Concrete Institute, Detroit.

ACI Committee 318 (1977)
"Building Code Requirements for Reinforced Concrete (ACI 318-77)",
American Concrete Institute, Detroit.

ACI Committee 318 (1983)
"Building Code Requirements for Reinforced Concrete (ACI 318-83)"
American Concrete Institute, Detroit, 111 pp.

ACI Concrete International Magazine (1986)
"In the Wake of the Quake",
Concrete International : Design and Construction, Vol. 8, No. 1, pp. 9-12.

ALEXANDER, C.M., HEIDEBRECHT, A.C. and TSO, W.K. (1973)
"Cyclic Load Tests on Shear Wall Panels",
Proceedings, 5th World Conference on Earthquake Engineering, Rome, pp. 1116-1119.

ANTEBI, J., UTKU, S. and HANSEN, R.J. (1960)
"The Response of Shear Walls to Dynamic Loads",
Department of Civil and Sanitary Engineering, Massachusetts Institute of Technology, Cambridge, 290 pp.

AOYAMA, H. and SHIOHARA, H. (1986)
"Plastic Analysis for Ultimate Strength of Reinforced Concrete Shear Walls",
Proceedings, International Symposium on Fundamental Theory of Reinforced and Prestressed Conctete, Nanjing, China, pp. 1406-1413.

APPLIED TECHNOLOGY COUNCIL (1978)

"Tentative Provisions for the Development of Seismic Regulations for Buildings",

ATC Publication ATC 3-06, NBS Special Publication 510, NSF Publication 78-8, U.S. Government Printing Office, Washington, D.C.

ARAKI, H. and SHIMAZU, T. (1986)

"Fundamental Study on Dynamic Behaviour of Multi-Storey Shear Walls",

Proceedings, International Symposium on Fundamental Theory of Reinforced and Prestressed Concrete, Nanjing, China, pp. 759-766.

ARCHITECTURAL INSTITUTE OF JAPAN (1980)

"AIJ Standards for Structural Calculation of Reinforced Concrete Structures",

3-2-19, Ginza, Chuo-Ku, Tokyo, Japan.

BARDA, F., HANSON, J.M. and CORLEY, W.G. (1977)

"Shear Strength of Low-Rise Walls with Boundary Elements",

Reinforced Concrete Structures in Seismic Zones, SP-53, American Concrete Institute, Detroit, pp. 149-202.

BÉDARD, C. (1983)

"Non-linear Finite Element Analysis of Concrete Structures",

PhD Thesis, Imperial College, London, 286 pp.

BÉDARD, C. and KOTSOVOS, M.D. (1985)

"Application of NLFEA to Concrete Structures",

Journal of Structural Engineering, ASCE, Vol. 111, No. 12, pp. 2691-2707.

BÉDARD, C. and KOTSOVOS, M.D. (1986)

"Fracture Processes of Concrete for NLFEA Methods",

Journal of Structural Engineering, ASCE, Vol. 112, No. 3, pp. 573-587.

BEEKHUIS, W.J. (1971)

"An Experimental Study of Squat Shear Walls",

Master of Engineering Report, Department of Civil Engineering, University of Canterbury, Christchurch, New Zealand, 132 pp.

BENJAMIN, J.R. and WILLIAMS, H.A. (1957)

"The Behaviour of One-Storey Reinforced Concrete Shear Walls",

Journal of Structural Division, ASCE, Vol. 83, No. ST3, pp. 1-49.

BENJAMIN, J.R. and WILLIAMS, H.A. (1958)
"Behaviour of One-Storey Reinforced Concrete Shear Walls Containing Openings",
ACI Journal, Proceedings, Vol. 55, No. 5, pp. 605-618.

BENJAMIN, J.R. and WILLIAMS, H.A. (1960)
"Reinforced Concrete Shear Wall Assemblies",
Journal of Structural Division, ASCE, Vol. 86, No. ST8, pp. 1-32.

BERTERO, V.V., MAHIN, S.A. and AXLEY, J.A. (1980)
"Lessons from Structural Damages Observed in Recent Earthquakes",
Proceedings, 7th World Conference on Earthquake Engineering, Istanbul, Vol. 4, pp. 257-264.

BLUME, J.A., NEWMARK, N.M. and CORNING, L.H. (1961)
"Design of Multistorey Reinforced Concrete Buildings for Earthquake Motion",
Portland Cement Association, Chicago, 318 pp.

BOBROWSKI, J. and BARDHAM-ROY, B.K. (1969)
"A Method of Calculating the Ultimate Strength of Reinforced and Prestressed Concrete Beams in Combined Flexure and Shear",
The Structural Engineer, Vol. 47, No. 5, pp. 197-209.

BOMMER, J. and LEDBETTER, S. (1987)
"The San Salvador Earthquake of 10th October, 1986",
Disasters, The International Journal of Disaster Studies and Practice, Vol. 11, No. 2, pp. 83-95.

BRITISH STANDARDS INSTITUTION (1985)
"Structural Use of Concrete : Part 1 : Code of Practice for Design and Construction" (BS 8110),
London, 154 pp.

CARDENAS, A.E. and MAGURA, D.D. (1973)
"Strength of High Rise Shear Walls - Rectangular Cross Sections",
Response of Multistorey Concrete Structures to Lateral Forces, SP-36, American Concrete Institute, Detroit, pp. 119-131.

CARDENAS, A.E., RUSSELL, H.G. and CORLEY, W.G. (1980)
"Strength of Low Rise Structural Walls",
Reinforced Concrete Structures Subjected to Wind and Earthquake Forces, SP–63, American Concrete Institute, Detroit, pp. 221–241.

C.E.B./F.I.P. (1978)
"Model Code for Concrete Structures",
English Edition, Cement and Concrete Association, London, 156 pp.

C.E.B. (1983)
"Response of Reinforced Concrete Critical Regions under Large Amplitude Reversed Actions",
Bulletin d'Information No. 161.

CONNOR, I.N. (1985)
"The San Antonio, Chile, Earthquake of 3 March, 1985",
Proceedings, Bulletin of the New Zealand National Society for Earthquake Engineering, Vol. 18, No. 2, pp. 128–138.

DANIEL, J.I., SHIU, K.N. and CORLEY, W.G. (1986)
"Openings in Earthquake Resistant Structural Walls",
Journal of Structural Engineering, ASCE, Vol. 112, No. 7, pp. 1660–1676.

DOWRICK, D.J. (1985)
"Preliminary Field Observations of the Chilean Earthquake of 3rd March, 1985",
Proceedings, Bulletin of the New Zealand National Society for Earthquake Engineering, Vol. 18, No. 2, pp. 119–127.

EEFIT Field Report (1986)
" e Mexican Earthquake of 19 September, 1985",
I olished by the Society for Earthquakes and Civil Engineering Dynamics,
l ndon.

EERI Report (1986)
"The Chile Earthquake of 3 March, 1985 – Performance of Structures",
Proceedings, Earthquake Spectra, Vol. 2, No. 2, pp. 293–371.

ELNASHAI, A.S., PILAKOUTAS, K., AMBRASEYS, N.N. and LEFAS, I.D. (1987)
"Lessons Learnt from the Kalamata (Greece) Earthquake of 13th September, 1986",
European Earthquake Engineering Journal, Vol. 1, No. 1, pp. 11–19

ENDO, T., ADACHI, H. and NAKANISHI, M. (1980)
"Force–Deformation Hysteresis Curves of Reinforced Concrete Shear Walls",
Proceedings, 7th World Conference on Earthquake Engineering, Istanbul, Vol. 6, pp. 315–322.

FINTEL, M. (1974)
"Ductile Shear Walls in Earthquake Resistant Multistorey Buildings",
ACI Journal, Proceedings, Vol. 71, pp. 296–305.

GALLETLY, G.D. (1952)
"Behaviour of Reinforced Concrete Shear Walls under Static Load",
Department of Civil and Sanitary Engineering, Massachusetts Institute of Technology, Cambridge, 123 pp.

GONZALEZ VIDOSA, F.M. (1988)
"Three Dimensional Finite Element Analysis of Structural Concrete under Static Loading",
PhD Thesis, University of London (to be submitted).

GREEK ASEISMIC CODE (1959)
"Aseismic Regulations for Building Construction",
Earthquake Resistant Regulations – A World List, published by the International Association for Earthquake Engineering, 1984 Edition, pp. 319–330.

GREEK ASEISMIC CODE (1984)
"Additional Clauses for the . eismic Design of Reinforced Concrete Buildings",
Text and Commentary, Mi· ·:y of Public Works, Greece, 34 pp.

GURLEY, C. (1987)
"Shear in Reinforced Beams",
Proceedings, The Institution of Engineers, Australia, Vol. CE29, No. 2, pp. 96–105.

HERNANDEZ, O. and ZERMENO, M. (1980)
"Strength and Behaviour of Structural Walls with Shear Failure",
Proceedings, 7th World Conference on Earthquake Engineering, Istanbul, Vol. 4, pp. 121–124.

HIRAISHI, H. (1984)
"Evaluation of Shear and Flexural Deformations of Flexural Type Shear Walls",
Proceedings, Bulletin of the New Zealand National Society for Earthquake Engineering, Vol. 17, No. 2, pp. 135–144.

HIRAISHI, H., NAKATA, S., KITAGAWA, Y. and KAMINOSONO, T. (1985)
"Static Tests on Shear Walls and Beam – Column Assemblies and Study on Correlation Between Shaking Table Tests and Pseudo–Dynamic Tests",
Earthquake Effects on Reinforced Concrete Structures, SP–84, American Concrete Institute, Detroit, pp. 11–48.

HITCHINGS, D. (1981)
"FINEL User's Manual",
Department of Aeronautics, Imperial College, London, 246 pp.

HSU, T.C.T. and MO, Y.L. (1985)
"Softening of Concrete in Low Rise Shearwalls",
ACI Journal, Proceedings, Vol. 82, No. 6, pp. 883–889.

ILIYA, R. and BERTERO, V.V. (1980)
"Effects of Wall Panel Reinforcement on Hysteretic Behaviour of Reinforced Concrete Walls",
Report No. UBC/EERC 80–04, Earthquake Engineering Research Centre, University of California, Berkeley.

INSTITUTION OF STRUCTURAL ENGINEERS and CONCRETE SOCIETY (1979)
"Design and Detailing of Concrete Structures for Fire Resistance",
Interim Guidance by a Joint Committee of the Institution of Structural Engineers and the Concrete Society.

JACOBSEN, L.S. (1960)
"Damping in Composite Structures",
Proceedings, 2nd World Conference on Earthquake Engineering, Tokyo, Vol. II, pp. 267–282.

JIANJUN, L. (1986)

"Shear Behaviour of Partially Prestressed Concrete Shear Walls",
Proceedings, International Symposium on Fundamental Theory of Reinforced and Prestressed Concrete, Nanjing, China, pp. 229–235.

KABEYASAWA, H., SHIOHARA, H., OTANI, S. and AOYAMA, H. (1982)

"Analysis of the Full-Scale Seven-Story Reinforced Concrete Test Structure : Test PSD3",
Proceedings, 3rd Joint Coordinating Committee Meeting of the U.S.-Japan Cooperative Research Programme, BRI, Tsukuba, Japan.

KANI, G.N.J. (1966)

"Basic Facts Concerning Shear Failure",
Proceedings, American Concrete Institute, Vol. 63, No. 6, pp. 675–692.

KOTSOVOS, M.D. (1974)

"Failure Criteria for Concrete under Generalised Stress States",
PhD Thesis, Imperial College, London, 284 pp.

KOTSOVOS, M.D. (1979)

"A Mathematical Description of the Strength Properties of Concrete under Generalised Stress",
Magazine of Concrete Research, Vol. 31, No. 108, pp. 151–158.

KOTSOVOS, M.D. (1980)

"A Mathematical Model of the Deformational Behaviour of Concrete under Generalised Stress based on Fundamental Material Properties",
Materiaux and Construction, RILEM, Vol. 13, No. 76, pp. 289–298.

KOTSOVOS, M.D. (1983 a)

"Effect of Testing Techniques on the Post-Ultimate Behaviour of Concrete Compression",
Materiaux and Constructions, RILEM, Vol. 16, pp. 3–12.

KOTSOVOS, M.D. (1983 b)

"Mechanisms of 'Shear' Failure",
Magazine of Concrete Research, Vol. 35, No. 123, pp. 99–106.

KOTSOVOS, M.D. (1984 a)
"Concrete: A Brittle Fracturing Material",
Materials and Structures, Research and Testing, RILEM, Paris, Vol. 17, No. 98, pp. 107–115.

KOTSOVOS, M.D. (1984 b)
"Behaviour of Reinforced Concrete Beams with a Shear Span to Depth Ratio Between 1.0 and 2.5",
ACI Journal, Proceedings, Vol. 81, No. 3, pp. 279–286.

KOTSOVOS, M.D. (1986)
"Behaviour of Reinforced Concrete Beams with a Shear Span to Depth Ratios Greater Than 2.5",
ACI Journal, Proceedings, Vol. 83, No. 6, pp. 1026–1034.

KOTSOVOS, M.D. (1987 a)
"Consideration of Triaxial Stress Conditions in Design",
ACI Structural Journal, Proceedings, Vol. 84, No. 3, pp. 266–273.

KOTSOVOS, M.D. (1987 b)
"Shear Failure of Reinforced Concrete Beams",
Engineering Structures, Vol. 9, No. 1, pp. 32–38.

KOTSOVOS, M.D. (1987 c)
"Shear Failure of R.C. Beams : A Reappraisal of Current Concepts",
CEB Bulletin 178/179, pp. 103–112.

KOTSOVOS, M.D. (1988 a)
"Design of Reinforced Concrete Deep Beams",
The Structural Engineer, Vol. 66, No. 2, pp. 28–32.

KOTSOVOS, M.D. (1988 b)
"Practical Design Utilising Multiaxial States of Stress",
Interim Report, CEB Task Group 24 (Personal Communication).

KOTSOVOS, M.D. and NEWMAN, J.B. (1978)
"Generalised Stress–Strain Relations for Concrete",
Journal of the Engineering Mechanics Division, ASCE, Vol. 104, EM4, pp. 845–856.

KOTSOVOS, M.D., PAVLOVIC, M.N. and ARNAOUT, S. (1985)
"Non-linear Finite Element Analysis of Concrete Structures : A Model based on Fundamental Material Properties",
Proceedings, Numerical Methods in Engineering : Theory and Applications Conference, NUMETA 85 (Ed. J. Middleton and G.N. Pande), A.A. Balkema, Rotterdam, Vol. 2, pp. 733-741.

LABIB, F. and EDWARDS, A.D. (1978)
"An Analytical Investigation of Cracking in Concentric and Eccentric Reinforced Concrete Tensions Members",
Proceedings of the Institution of Civil Engineers (Part 2), Vol. 65, pp. 53-70.

LEFAS, I.D. and LULURGAS, S.Z. (1982)
"Response Degradation and Hysteretic Damping of Reinforced Concrete Linear Elements and Shear Walls under Large Cyclic Post Yielding Deformations",
National Technical University of Athens, Diploma Dissertation, Supervisor T.P. Tassios, 172 pp.

MAIER, J. and THURLIMANN, B. (1985)
"Bruchversuche an Stahlbetonscheiben",
Institut fur Baustatic und Konstruction, Eifgenossishe Technische Hochschule, Zurich, 130 p.

MAU, S.T. and HSU, T.C.T. (1986)
"Shear Design and Analysis of Low-Rise Structural Walls",
ACI Journal, Proceedings, Vol. 83, No. 2, pp. 306-315.

MORGAN, B., HIRAISHI, H. and CORLEY, W.G. (1985)
"Medium Scale Wall Assemblies : Comparison of Analysis and Test Results",
Earthquake Effects on Reinforced Concrete Structures, SP-84, American Co ·ete Institute, Detroit, pp. 241-269.

ÓESTE ⌊E, R.G., FIORATO, A.E., ARISTIZABAL-OCHOA, J.D. and CORLEY, W.G. (1980)
"Hysteretic Response of Reinforced Concrete Structural Walls",
Reinforced Concrete Structures Subjected to Wind and Earthquake Forces, SP-63, American Concrete Institute, Detroit, pp. 243-273.

OESTERLE, R.G., ARISTIZABAL-OCHOA, J.D., SHIN, K.N. and CORLEY, W.G. (1984)
"Web Crushing of Reinforced Concrete Structural Walls",
ACI Journal, Proceedings Vol. 81, No. 3, pp. 231-241.

PAPAZACHOS, V. et al (1986)
"Surface Fault Traces, Fault Plane Solution and Spatial Distribution of the Aftershocks of the September 13, 1986, Earthquake of Kalamata", Publication No. 7, Geophysical Laboratory, University of Thessaloniki.

PARK, R., PRIESTLEY, M.J.N. and GILL, W.D. (1982)
"Ductility of Square Confined Concrete Columns",
Journal of the Structural Division, ASCE, Vol. 108, No. 4, pp. 929-950.

PAULAY, T. (1981)
"Design of Reinforced Concrete Ductile Shear Walls for Earthquake Resistance",
Research Report 81-1, Department of Civil Engineering, University of Canterbury, Christchurch, New Zealand.

PAULAY, T., PRIESTLEY, M.J.N. and SYNGE, A.J. (1982)
"Ductility in Earthquake Resisting Squat Shearwalls",
ACI Journal, Proceedings, Vol. 79, No. 26, pp. 257-269.

PAULAY, T. and GOODSIR, W.J. (1985)
"The Ductility of Structural Walls",
Proceedings, Bulletin of the New Zealand National Society for Earthquake Engineering, Vol. 18, No. 3, pp. 250-269.

PHILLIPS, D.V. and ZIENKIEWICZ, O.C. (1976)
"Finite Element Non-lin[illegible] Analysis of Concrete Structures",
Proceedings of the Instit[illegible]ion of Civil Engineers, Part 2, Vol. 61, pp. 59-88.

PLAINES, P. (1986)
Personal Communication

ROTHE, D.H. (1986)
"Experimental Studies of Non-linear Behaviour of Reinforced Concrete Structural Walls",
Darmstadt Concrete, Annual Journal on Concrete and Concrete Structures, Vol.

1, pp. 95–100.

SALSE, E.A.B. and FINTEL, M. (1974)
"Strength, Stiffness and Ductility Properties of Slender Shear Walls",
Proceedings, 5th World Conference on Earthquake Engineering, Rome, pp. 919–928.

SHIGA, T., SHIBATA, A. and TAKAHASHI, J. (1973)
"Experimental Study on Dynamic Properties of Reinforced Concrete Shear Walls",
Proceedings, 5th World Conference on Earthquake Engineering, Rome, Italy, pp. 1157–1166.

SHIRAI, N. and SATO, T. (1981)
"Inelastic Analysis of Reinforced Concrete Shear Wall Structures – Material Modelling of Reinforced Concrete",
Proceedings, IABSE Colloquium on Advanced Mechanics of Reinforced Concrete, Delft, pp. 197–210.

SHIRAI, N. and SATO, T. (1981)
"Inelastic Analysis of Reinforced Concrete Shear Wall Structures – Applications and Experimental Verifications",
Proceedings, IABSE Colloquium on Advanced Mechanics of Reinforced Concrete, Delft, pp. 687–700.

SMITH, B.S. and GIRGIS, A. (1984)
"Simple Analogous Frames for Shear Walls Analysis",
Journal of Structural Division, ASCE, Vol. 110, No. ST11, pp. 2655–2666.

SYNGE, A.J. (1980)
"Ductility of Squat Shear Walls",
Research Report No. 80–8, Department of Civil Engineering, University of Canterbury, Christchurch, 150 pp.

TASSIOS, T.P. and LEFAS, I.D. (1984)
"Concrete Ductility in Confined Columns",
Scientific Papers, Faculty of Civil Engineering, National Technical University, Athens, Vol. 8, No. 1–4, pp. 41–60.

THÜRLIMANN, B. (1987)
Personal Communication.

TOMII, M. and ESAKI, F. (1984)
"Design Method of Reinforced Concrete Framed Shear Walls to Sustain Vertical Loads after Shear Failure",
Proceedings, 8th World Conference on Earthquake Engineering, San Francisco, California, Vol. V, pp. 581-588.

UNIFORM BUILDING CODE (1982)
Chapter 23, Section 2312, Earthquake Regulations,
International Conference of Building Officials, Whittier, California.

VALLENAS, J.M., BERTERO, V.V. and POPOV, E.P. (1979)
"Hysteretic Behaviour of Reinforced Concrete Structural Walls",
Report No. UCB/EERC 79-20, Earthquake Engineering Research Centre, University of California, Berkeley.

VECCHIO, F.J. and COLLINS, M.P. (1986)
"The Modified Compression-Field Theory for Reinforced Concrete Elements Subjected to Shear",
ACI Journal, Proceedings, Vol. 83, No. 2, pp. 219-231.

VULCANO, A. and BERTERO, V.V. (1986)
"Non-linear Analysis of Reinforced Concrete Structural Walls",
Proceedings, 8th European Conference on Earthquake Engineering, Lisbon, Vol. 3, pp. 6.5/1-6.5/8.

WANG, T.Y., BERTERO, V.V. and POPOV, E.P. (1975)
"Hysteretic Behaviour of Reinforced Concrete Frame Walls",
Report No. UCB/EERC 75-23, Earthquake Engineering Centre, University of California, Berkeley.

WIRADINATA, S. and SAATCIOGLOU, M. (1986)
"Tests of Squat Shear Walls under Lateral Load Reversals",
Proceedings of 3rd U.S. National Conference in Earthquake Engineering, Charleston, Vol. II, pp. 1395-1406.

APPENDIX A : ANALYTICAL PREDICTIONS OF WALL STIFFNESS CHARACTERISTICS AT THE UNCRACKED PHASE

A.1. DEFINITION OF WALL ELEMENT STIFFNESSES

The force–displacement relations for one dimensional cantilever elements are presented in Figure A1. The cross–sectional parameters required to determine these relations are EA, EI and GA_v. In the analysis of reinforced concrete structural elements at the uncracked linear phase, parameters E, G, I and A_v are defined as follows:

(a) The secant modulus of elasticity of concrete at 45 percent of the cylinder strength is considered to represent an average value of E used for the evaluation of the response of uncracked R.C. walls. Codes suggest empirical expressions to determine E based on the nominal cube or cylinder strength of concrete. The expression adopted by BS 8110 is $E = 5500 \sqrt{f_{cu}}$ (in MPa), where f_{cu} is the cube strength of concrete in MPa.

(b) In practice the shear modulus of rigidity of concrete G is usually evaluated from the relation $G = E/2 * (1 + \nu)$. This relation is based on elastic, homogeneous and isotropic material properties. The value of the Poisson's ratio, ν, adopted for concrete is usually 0.20.

(c) The moment of inertia, I, of a reinforced concrete uncracked cross–section can be defined either as the moment of inertia of the gross concrete cross–section, including the transformed area of the longitudinal steel bars, or as the moment of inertia of the gross concrete cross–section only. For purposes of simplicity the latter definition will be used in the following calculations.

(d) The cross–sectional area A, used to compute the axial rigidity of the wall EA, may be evaluated either by considering the cross–sectional area of the gross concrete plus the transformed area of the longitudinal reinforcement or the area of the gross concrete cross–section only. Usually, the gross concrete area is considered.

(e) The effective shear area A_v of a R.C. wall cross–section is usually assumed to equal the nominal elastic shear area, which for the case of a rectangular cross–section is 80% of the area obtained by multiplying the web thickness of the wall by the distance between the extreme compression fibre and the

centroid of the tension reinforcement. Since this distance is suggested by Codes to be taken as 0.8 of the total depth, the effective shear area to be used in the analysis would be 0.64A, where A is the gross concrete area.

A.2. ANALYTICAL VALUES OF WALL RIGIDITIES IN THE UNCRACKED PHASE

Using the previous definitions, the formula for secant modulus of elasticity of concrete suggested by BS 8110 (1985), and an average cube strength of concrete equal to 45 MPa, Table A.1 is compiled. The table includes the analytical values of the parameters EI, GA_v and EA for both types of wall tested.

A.3. ANALYTICAL DISPLACEMENT VALUES

The analytical values of top horizontal displacement and axial shortening of both wall types can be extracted from the force–displacement relations included in Figure A.1., using the values of wall cross–sectional parameters listed in Table A.1.

For walls of type I and II, the above procedure leads to values of top horizontal displacement equal to 3×10^{-6} (mm/N) * F_H and 16.5×10^{-6} (mm/N) * F_H, respectively, while the relevant values of axial shortening are 3.9×10^{-7} (mm/N) * F_V and 8.3×10^{-7} (mm/N) * F_V, respectively. The former pair of values result in overall wall secant stiffness analytical values of 333.3 KN/mm and 60.6 KN/mm for wall types I and II, respectively.

Table A.2 summarizes analytical and experimental values of top horizontal displacement corresponding to horizontal load applied to the wall specimens prior to initiation of visible cracking. Table A.3 includes values of axial shortening recorded during testing of wall specimens subjected to constant vertical (axial) loading and equivalent values predicted by analysis.

Type of Wall	EI (KN m^2)	GA_V (MN)	EA (MN)
I	90,796.0	516.5	1,937.0
II	54,883.2	415.7	1,558.8

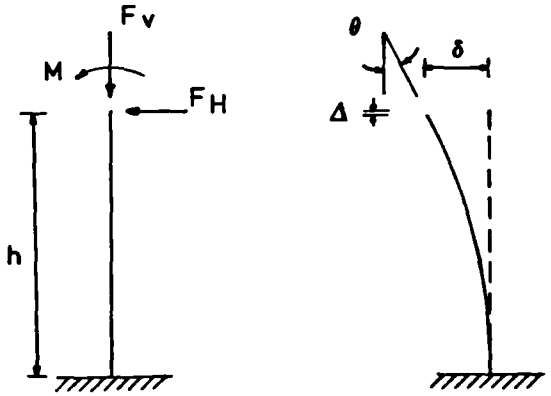
Table A.1. Analytical values of wall parameters EI, GA_V and EA.

h/l	Specimen	UNCRACKED WALL PHASE		
		F_H(KN)	δ_{exper}(mm)	δ_{analyt}(mm)
1	SW11	35	0.34	0.11
	SW12	45	0.26	0.14
	SW13	50	0.37	0.15
	SW14	35	0.34	0.11
	SW15	43	0.27	0.14
	SW16	80	0.40	0.24
2	SW21	10	0.32	0.16
	SW22	14	0.39	0.22
	SW23	20	0.52	0.32
	SW24	10	0.29	0.16
	SW25	25	0.60	0.40
	SW26	10	0.39	0.16
	SW31	20	0.62	0.32
	SW32	20	0.69	0.32
	SW33	16	0.67	0.26

Table A.2. Analytical and experimental values of top horizontal displacement of the uncracked wall phase.

h/l	Specimen	F_V(KN)	δ_{exp}(mm)	$\delta_{analyt.}$(mm)
	SW12	230	1.70	0.09
	SW13	355	2.87	0.14
1	SW15	185	1.50	0.07
	SW16	460	4.32	0.18
	SW22	182.0	1.49	0.15
	SW23	96.9	0.77	0.08
		193.8	1.69	0.16
2		290.7	2.69	0.24
		343.1	3.24	0.29
	SW25	98.3	0.83	0.08
		196.7	1.68	0.16
		323.5	2.87	0.27

Table A.3. Analytical and experimental values of wall axial shortening.



$$\begin{bmatrix} \Delta \\ \delta \\ \theta \end{bmatrix} = \begin{bmatrix} h/EA & 0 & 0 \\ 0 & h^3/3EI + h/GA_V & 0 \\ 0 & h^2/2EI & h/EI \end{bmatrix} * \begin{bmatrix} F_V \\ F_H \\ M \end{bmatrix}$$

Fig. A.1 : Force-displacement relationship for one dimensional cantilever element.